

Rapid Measurement and Estimation of Saturated Hydraulic Conductivity of Mineral Slurries

by

Yagmur Babaoglu

A thesis submitted to the Faculty of Graduate and Postdoctoral
Affairs in partial fulfillment of the requirements for the degree of

Doctor of Philosophy

in

Environmental Engineering

Carleton University
Ottawa, Ontario

© 2021, Yagmur Babaoglu

Abstract

Large strain consolidation (LSC) behaviour of mineral slurries regulates the performance of tailings management and reclamation plans. The hydraulic conductivity-void ratio relationship primarily influences this behaviour, dominating the long-term performance of fine-grained slurries with higher initial water contents. However, the determination of this function can be very challenging and time-consuming, considering the long duration of the conventional tests and significant variation in hydraulic conductivity values with the wide range of void ratios.

This study focuses on identifying or creating a rapid method to evaluate the large strain consolidation parameters, especially the k - e relationship, of fine-grained soils by (i) establishing a relationship between the consolidation parameters and more easily measured properties and (ii) designing a self-weight consolidation setup to evaluate the k - e relationship using Instantaneous Profiling Method (IPM). For part (i), a total of 79 k - e data sets of fine-grained soils are examined. Using some of the above innovations, equations are found that require only a single measurement of hydraulic conductivity at a single void ratio. When applying these new equations to the k - e data set, 94% of the predicted k values are within an order of magnitude of the measured data points. This is likely sufficient for this method to be used as a screening tool for tailings treatments. For part ii), the design of a prototype consolidometer is introduced, and the consolidation behaviours of various fine-grained soils are evaluated. The prototype is designed as an alternative experimental setup to conventional laboratory tests and aims to rapidly assess the k - e equation for fine-grained soils. The test column was instrumented with tensiometers and capacitance-based sensors

to determine pore water pressure and volumetric water content, respectively. Also, a robotic arm is connected to the sensor probe for more detailed profiling. The collected data are then utilized to determine the hydraulic conductivity of the tested fine-grained soils and polymer-amended fluid fine tailings using the IPM method. The compressibility curves of the tested materials were also determined using the measured data from the prototype consolidometer. The measured data and the predicted behaviour of the material are compared using a large strain consolidation software, UNSATCON, to tease out non-consolidation behaviours such as creep and to determine the applicability of the method in the proposed setup. The results demonstrated that the method could successfully determine the $k-e$ relationships in a shorter period of time compared to conventional laboratory tests. Finally, recommendations for modifications in the current experimental setup are discussed to improve the duration of the experiment.

Acknowledgements

First, I would like to thank my thesis supervisor, Dr. Paul Simms, for his support and guidance during the course of my thesis. He inspired, helped me in every step of my research with patience, and I would not be able to complete this work without him. I am also deeply thankful for the opportunity to be part of this research and this amazing research team.

I would also like to thank Mr. Stanley Conley, Mr. Jason Arnott, Mr. Pierre Trudel and Ms. Marie Tudoret Chow for their kindness in providing me hours and hours of technical support. Thank you for bearing with me and always come up with creative ideas when I needed help.

I would also like to express my gratitude to the members of my research team: Dr. Muhammad Salam, Dr. Shunchao Qi, Muhammad Hissan Khattak, Dr. Shabnam Mizani, Dr. Abdulghader Abdulrahman, Narges Gheisari, Dr. Amin Esmailzadeh, Arazoo Patel, David Igbinedion, Christopher Hey, Nadine Nasser Sallam, Étienne Parent and Oswaldo Hurtado. Thank you so much for your support and encouragement.

Finally, I would like to thank my family for encouraging and supporting me throughout this journey. My beloved friends Irem and Cagla, thank you so much for being there when I needed it the most. Lastly, I would like to thank my husband Burak; this work would not have been completed without you.

Table of Contents

Abstract.....	ii
Acknowledgements.....	iv
Table of Contents	v
List of Figures.....	xii
List of Tables.....	xix
List of Abbreviations and Symbols	xx
Chapter 1: Introduction	1
1.1 Background.....	1
1.2 Objectives	6
1.3 The novelty of the Research.....	7
1.4 The layout of the Thesis	8
1.5 Publications Related to Dissertation.....	9
Chapter 2: Literature Review	11
2.1 Alberta’s Oil Sands.....	11
2.2 Bitumen Extraction.....	13
2.3 Tailings Regulations	14
2.4 Basic Properties of Oil Sands Tailings	15
2.5 Problems Associated with Tailings	17
2.6 Dewatering Technologies and Reclamation Strategies	19
2.7 Dewatering Behavior of Soft Soils and Oil Sands Tailings	21
2.7.1 Sedimentation and Consolidation of Soft Soils and Slurries.....	21
2.7.1.1 Particulate Settling	22
2.7.1.2 Sedimentation.....	23

where S is the particle flux (number of particles crossing a horizontal section per unit area per unit of time), ρ is density, v is fall velocity, t is time, and x is the height.....	24
2.7.1.3 Segregation.....	25
2.7.1.4 Consolidation	27
2.7.2 Theories of Consolidation	29
2.7.2.1 One-dimensional Consolidation Theory.....	29
2.7.2.2 Two-dimensional Consolidation Theory	32
2.7.2.3 Three-dimensional Consolidation Theory.....	33
2.7.3 Thixotropy and Creep in Soft Soils and Slurries.....	33
2.7.3.1 Creep Compression	34
2.7.3.2 Structuration/ Ageing Effect	35
2.7.3.3 Thixotropy.....	37
2.8 Consolidation and Permeability Testing on Soft Clays and Slurries	40
2.8.1 Direct Methods to Determine the Consolidation Properties.....	40
2.8.1.1 Step-loading Test.....	41
2.8.1.2 Slurry Consolidometer	42
2.8.1.3 Constant rate of deformation (CRD)/ Constant rate of strain test.....	45
2.8.1.4 Controlled gradient test/ Constant hydraulic gradient test (CHG)	48
2.8.1.5 Constant rate of loading test.....	49
2.8.1.6 Continuous Loading Tests	50
2.8.1.7 Seepage-Induced Consolidation Test (SICT)	51
2.8.1.8 Centrifuge Tests.....	57
2.8.1.9 Hindered Settling and Self-weight Consolidation Tests	61
2.8.1.10 Relaxation Indentation Tests.....	65
2.8.1.11 Inter-connected Consolidometer Tests	65
2.8.2 Indirect Methods to Determine the Consolidation Properties.....	66

2.8.2.1	Soil Water Flow Theory.....	68
2.8.2.2	Non-destructive Measurement Techniques.....	69
2.8.2.2.1	Volumetric Water/Solids Content Measurement Techniques.....	69
2.9	Summary.....	75
Chapter 3: Tested Materials In This Study and Sample Preparation.....		77
3.1	Materials.....	77
3.1.1	Leda Clay.....	77
3.1.2	Kaolinite.....	78
3.1.3	Thickened Gold Tailings.....	78
3.1.4	Centrifuged Cake.....	78
3.1.5	Shell Fluid Fine Tailings.....	79
3.1.6	Syncrude Fluid Fine Tailings.....	80
3.2	Sample Preparation, including Flocculation of FFT.....	82
3.2.1	Preparation of Polymer-stock Solution.....	82
3.2.2	Preparation of Flocculated FFT.....	83
3.2.3	Optimized Mixing Technique.....	84
3.3	Summary of methods developed in the following chapters.....	85
3.3.1	Estimation of Consolidation Properties of Fine-grained soils using simple correlations.....	85
3.3.2	Determination of $k-e$ function from a prototype self-weight consolidation column.....	86
Chapter 4: Improving Hydraulic Conductivity Estimation for Soft Clayey Soils, Sediments, or Tailings Using Predictors Measured at High-Void Ratio.....		87
4.1	Introduction.....	87
4.2	Existing Hydraulic Conductivity Correlations.....	88
4.2.1	Clays.....	92
4.2.2	Dredged Materials.....	94

4.2.3	Oil Sands Tailings.....	95
4.3	Suitability of optimized equations for design	99
4.4	Predicting $k-e$ using the compressibility curve.....	101
4.5	Predicting void ratio – saturated hydraulic conductivity ($e- k$) relationship using a single measured data point k_{sat} at higher void ratios	105
4.6	Limitations	107
4.7	Summary and Conclusions.....	108
Chapter 5: Development of a Prototype Consolidometer and an Associated Analysis Method for Rapid Determination of the $K-e$ Curve		110
5.1	Introduction.....	110
5.2	Methodology: Instantaneous Profiling Method (IPM).....	112
5.3	Demonstration for IPM method with synthetic data.....	113
5.3.1	Description of synthetic experiments	113
5.4	Measurement of Pore Water Pressure Profiles	118
5.4.1	Pore water pressure measurements	118
5.4.2	Estimation of total potential measurements with depth within the column.....	120
5.4.3	Selecting the most appropriate method to fit pore water pressure measurement at various heights with time.....	122
5.5	Measurement of Volumetric Water Content Profiles within the Column.....	125
5.5.1	Electrical Conductivity (EC) Sensor Testing	126
5.5.2	Determination of Volumetric Water contents with SENTEK EnviroSCAN Sensors	130
5.5.2.1	Calibration of Volumetric Water Content Profiles with SENTEK EnviroSCAN sensors.....	132
5.5.2.2	Correction of Volumetric Water Content readings	138
5.6	The Design of a New Consolidometer.....	141

5.6.1	Wall-effect Testing	141
5.6.2	Automation Design	145
5.6.3	Final Design of the Column.....	148
5.7	Case study application of IPM.....	149
Chapter 6: Trials of New Consolidometer with Gold tailings, Kaolinite, and Raw FFT		
.....		153
6.1	Introduction.....	153
6.2	Summary of Conducted Experiments.....	155
6.3	Thickened Gold Tailings.....	157
6.3.1	Initial Conditions	157
6.3.2	Results and Discussion	161
6.4	Kaolinite	170
6.4.1	Initial Conditions	170
6.4.2	Results and Discussion	172
6.5	Unamended Fluid Fine Tailings	176
6.5.1	Initial Conditions	177
6.5.2	Results and Discussion	179
6.6	Conclusion	184
Chapter 7: Consolidometer Trials for Flocculated Fluid Fine Tailings		186
7.1	Introduction.....	186
7.2	Properties of Tailings and Initial Conditions	188
7.3	Amended Tailings with 800 ppm dosage using A3338	190
7.4	Amended Tailings with 1000 ppm dosage using A3338.....	196
7.5	Amended Tailings with 4000 ppm dosage using Polymer B	201
7.6	Discussion.....	206

Chapter 8: Discussion.....	208
8.1 When and how can practitioners use the different methods developed in this thesis?	208
Chapter 9: Summary and Conclusions	213
9.1 Summary.....	213
9.2 Novelty and Impact.....	217
9.3 Limitations	217
9.4 Future Recommendations	218
Bibliography	220
Appendix A Geotechnical Characterization Tests.....	252
A.1 Solid Content (C_s).....	252
A.2 Gravimetric (w) and Volumetric Water Content (θ).....	252
A.3 Specific Gravity (G_s).....	253
A.4 Atterberg Limits	253
A.5 Void ratio (e)	254
A.6 Particle Size Distribution	254
A.7 Total Bulk Density.....	255
A.8 Clay Content.....	255
A.9 Bitumen Content.....	256
Appendix B Dosage Optimization results for Polymer A3338 and Polymer B	257
B.1 Optimized Results using Shell FFT using A3338.....	257
B.2 Optimized Results using Syncrude FFT using Polymer B.....	265
Appendix C Estimating effective stress- void ratio equation for fine-grained soils using simple correlation relationships	270
C.1 Clays	273
C.2 Dredged Materials	275
C.3 Oil Sands Tailings.....	278

Appendix D Arduino and MATLAB Scripts	281
D.1 Cumulative Distribution Analysis – MATLAB Script.....	281
D.2 Automation System – Arduino Code.....	281
Appendix E Calculation of $k-e$ relationship from settlement curve for flocculated FFT at 800 ppm dosage.....	284

List of Figures

Figure 1-1: Satellite images showing the growth of surface mining over the Athabasca oil sands from 1984 to 2015 (pictures taken by the Earth Observatory at NASA).....	3
Figure 1-2: Solids content profile over time in a real deposit (modified from P. S. Wells (2011)).....	4
Figure 2-1: Current map of Canadian oil sands (Energy, 2017), and schematics of oil sands particles (Marcus, Tijseen, & Winkelman, 2017)	12
Figure 2-2: Diagram of CHWE process (R. J. Chalaturnyk et al., 2002)	13
Figure 2-3: the characteristics of the sedimentation process for clay-water mixtures (modified from Jeeravipoolvarn (2010) and Goro Imai (1981))	22
Figure 2-4: Tailings properties diagram of oil sands tailings (modified from Azam and Scott (2005))	27
Figure 2-5: The schematic diagram of slurry consolidometer – modified Pollock (1988)	43
Figure 2-6: Seepage Induced Consolidation testing apparatus (modified from Estepho (2014)).....	56
Figure 2-7: Schematic of centrifuge test setup (after Sorta, Segó, and Wilson (2012))	58
Figure 2-8: Schematics of TDR technique (from (Su et al., 2014)).....	72
Figure 2-9: Schematics of capacitance-based sensors (a) Capacitance sensors (b) FDR probe (after (Su et al., 2014).	73
Figure 3-1: Particle size distribution size of tested materials.....	82
Figure 4-1: The performance of predictive models to estimate void ratio-hydraulic conductivity relationship for clays.....	94

Figure 4-2: (a) Measured vs. predicted k values for dredged soils using various predictive models (b) Performance of $k-e$ functions for dredged materials	95
Figure 4-3: (a) Measured vs. predicted saturated hydraulic conductivity values for oil sands tailings (b-c) Performance comparison of predictive methods for estimating hydraulic conductivity for untreated and treated oil sands tailings, respectively	97
Figure 4-4: Best-fit $k-e$ models optimized to the data sets of (a) clay; (b) dredged material; and (c) oil sands tailings where coloured dots denote the predicted values.	99
Figure 4-5: Large strain consolidation analysis of hypothetical fluid fine tailings deposited at an original thickness and void ratio of 10 m and 4, respectively	101
Figure 4-6: The relationship between the hydraulic conductivity-void ratio-effective stress for untreated oil sands tailings	102
Figure 4-7: Improving the predictions of hydraulic conductivity when using a single measured data at a high-void ratio for both clays and dredged soils, also oil sands tailings (non-amended and amended), respectively.	105
Figure 4-8: Performance of Eq. (7) using k measured for points between 1 and 2 kPa for amended oil sands tailings.	106
Figure 4-9: Predictions of 10 m deposit $e_0 = 4$, assuming an order of magnitude difference of k at $e=1$ between the base case and either higher or lower case	107
Figure 5-1: The variation of total potential profiles at different elevations at selected days	115
Figure 5-2: The change in void ratio profiles at different elevations at selected days	116
Figure 5-3: Comparison with the calculated $k-e$ relationship with the input $k-e$ data using the second derivative of total potential values	118

Figure 5-4: The change of sign of the second derivatives of total potential values with depth for higher $k-e$ example	118
Figure 5-5: (a) The T5 Pressure Transducer by Meter Group and (b) the DL2e Data Logger by Delta-T devices utilized to measure pore water pressure measurements in this study	119
Figure 5-6: Calibration effort of pressure transducers prior to testing.....	120
Figure 5-7: Predicted PWP measurements for the amended FFT sample.....	121
Figure 5-8: Fitting of pore water pressure measurements to (a) Polynomial (third-degree) and (b) power equations for kaolinite tests.....	123
Figure 5-9: Fitted PWP measurements for Kaolinite experiment (a) Using power equation, and (b) using a polynomial fit	125
Figure 5-10: <i>on the left</i> : Three-electrode electrochemical cell used in EC experiments (Chow & Pham, 2019), <i>on the right</i> : 800 ppm FFT sample in the cell	127
Figure 5-11: Accumulation of finer particles at the positively charged rod observed during EC sensor testing.....	129
Figure 5-12: 7-day testing for 800 ppm sample on the duplicate cells	130
Figure 5-13: Potential readings vs. time for 800 ppm	130
Figure 5-14: SENTEK EnviroSCAN probe	131
Figure 5-15: (a) Volumetric water content vs. Scaled frequency relationship for an unamended FFT sample (b) Calibrated Parameters A and B for different types of soils	134
Figure 5-16: (a) A profile of VWC fitted with a best-fit polynomial curve and a compressibility curve (a power equation), (b) SF and VWC (from oven-drying)	

relationship from sensor testing of Leda clay, and (c) the continuous measurement test for Musselwhite gold tailings compared with final GWC from the oven-dried samples	137
Figure 5-17: Amended FFT sample, raw VWC reading at ten different locations (at every 1 cm intervals) from sensor 1	138
Figure 5-18: Amended FFT sample, raw scaled frequency reading from the sensor located in water ($z=34$ cm, sensor 3) and corrected reading.....	139
Figure 5-19: Amended FFT sample, corrected raw readings at ten different locations from sensor 1	140
Figure 5-20: Amended FFT sample, data is smoothed at every five reading points	141
Figure 5-21: 6" PVC, 12" PVC and 6" acrylic columns setup.....	143
Figure 5-22: Accumulation of Centrifuged FFT on the walls.....	144
Figure 5-23: Final weight profile at the end of the experiment for centrifuged FFT on a 12" PVC column	145
Figure 5-24: Different parts used in the automation of the sensors.....	146
Figure 5-25: Connection diagram for parts	147
Figure 5-26: Automation Testing of SENTEK EnviroSCAN sensors.....	148
Figure 5-27: Schematics of the self-weight consolidation column.....	149
Figure 5-28: Case Study- Settlement of the tailings water interface, with insert for the first 15 days	150
Figure 5-29: Case Study: Void ratio and pore-water pressure profiles.....	151
Figure 5-30: Comparison of predicted $k-e$ from IPM method	152
Figure 6-1: Total potential profiles for (a) Test #1, (b) Test #2 and (c) Test #3	159

Figure 6-2: Volumetric water content profiles for (a) Test #1, (b) Test #2 and (c) Test #3.	160
Figure 6-3: (a) Final gravimetric water contents from oven drying, (b) Water-tailings interface height versus time	161
Figure 6-4: $k-e$ relationships for (a) Test #1, (b) Test #2, (c) Test 3, and (d) Comparison of all models	163
Figure 6-5: (a) The compressibility curves determined from the final condition, (b-d) The compressibility curves determined from measured PWP and VWC measurements during Tests 1, 2 and 3, respectively	165
Figure 6-6: (a) Comparison of compressibility curves for all three tests (b) Settlement behaviour of thickened gold tailings at different volumetric water contents (Test #1: 53%, Test #2: 64% and Test #3: 61%) using Equation 5.	167
Figure 6-7: Comparison of predicted and measured volumetric water content profiles at different depths for Test #1.....	169
Figure 6-8: Measured total pore water pressure and volumetric water content profiles at selected times.....	171
Figure 6-9: (a) The settlement behaviour of Kaolinite (b) Final measured gravimetric water content profile in the column	173
Figure 6-10: The effective stress-void ratio relationship at different days	174
Figure 6-11: Calculated $k-e$ relationship for Kaolinite	175
Figure 6-12: Comparison of calculated $k-e$ to other published studies	175
Figure 6-13: The settlement modelling comparison with measured data for Kaolinite ..	176

Figure 6-14: (a) Total potential measurements, (b) excess pore water pressures, and (c) Volumetric water content profiles at selected times	178
Figure 6-15: (a)The settlement behaviour of unamended FFT, and (b) Final volumetric water content profile in the column determined with oven-dried samples	180
Figure 6-16: The effective stress-void ratio relationship at different days	181
Figure 6-17: Calculated $k-e$ relationship of unamended FFT	181
Figure 6-18: Comparison with independent measurements from LSC and Pane and Schiffman	182
Figure 6-19: The settlement modelling comparison of unamended FFT sample for (a) First 25 days and (b) until the end of the experiment.....	183
Figure 7-1: Measured pore water pressures and uncorrected volumetric water contents for fFFT tailings at 800 ppm dosage	191
Figure 7-2: (a) Settlement behaviour of the sample for 800 ppm fFFT, and (b) The final measured VWC profile in the column	192
Figure 7-3: The compressibility of 800 ppm FFT.....	193
Figure 7-4: (a) The $k-e$ relationship for 800 ppm fFFT tailings and (b) Comparison with independent measurements from LSC and Pane and Schiffman.....	194
Figure 7-5: Modelling of the height data from the 800 ppm fFFT experiment	196
Figure 7-6: Comparison of measured volumetric water contents at two different locations (two separate sensors).....	196
Figure 7-7: (a) The pore water pressure distribution and (b) uncorrected volumetric water contents from the first sensor for fFFT sample with 1000 ppm dosage	198

Figure 7-8: (a) The settlement behaviour for fFFT experiment at 1000 ppm dosage, and (b) The final measured VWC profile in the column.....	198
Figure 7-9: The compressibility curve using the measured data for 1000 ppm fFFT	199
Figure 7-10: (a) The $k-e$ relationship for 1000 ppm fFFT tailings, (b) Comparison of with 800 ppm test and Pane and Schiffman's equation	200
Figure 7-11: The settlement modelling comparison with measured data for 1000 ppm fFFT	201
Figure 7-12: (a) The pore water pressure distribution and (b) uncorrectd volumetric water for fFFT sample prepared using Polymer B	202
Figure 7-13: The settlement behaviour for fFFT experiment using Polymer B	203
Figure 7-14: The compressibility curve for (a) First 2 days and (b) Until Day 11	204
Figure 7-15: The $k-e$ relationship for 4000 ppm fFFT tailings and comparison of with initial $k-e$ data point (calculated using Pane and Schiffman's equation)	205
Figure 7-16: The settlement modelling comparison with measured data for 4000 ppm fFFT	206
Figure 8-1: Comparison of conventional tests with developed methods in this study	208
Figure 8-2: (a) Comparison of all methods applying to flocculated FFT sample (at 800 ppm dosage), (b) Comparison of settlement performance of a hypothetical analysis	212

List of Tables

Table 3-1: Geotechnical Properties of tested tailings (compared with other reported FFTs)	81
Table 4-1: Summary of correlation relationships for $k-e$ equation	89
Table 4-2: Reference list for all data used in this study	91
Table 4-3: Sensitivity analysis for proposed optimized $k-e$ relationships	103
Table 5-1: Specifications of six inches wall-effect experiments	144
Table 6-1: Initial and final conditions of tested materials	156
Table 7-1: Geotechnical Properties of Tailings and Initial conditions of the experiments	189

List of Abbreviations and Symbols

CHG	Constant Hydraulic Gradient Test
CHWT	Clark Hot Water Extraction
CRD	Constant Rate of Deformation
CST	Capillary Suction Test
DC	Direct Current
EC	Electrical Conductivity
FDR	Frequency Domain Reflectometry
FFT	Fluid Fine Tailings
GPR	Ground Penetrating Radar
ILTT	In-line Thickened Tailings
IPM	Instantaneous Profiling Method
LSC	Large Strain Consolidation
meq	Milliequivalents
MFT	Mature Fine Tailings
NMM	Neutron Scattering Technique
OSCA	Oil Sands Conservation Act
PAM	Polyacrylamide
PASS	Permanent Aquatic Storage Structure
PVC	Polyvinyl Chloride
SAGD	Steam Assisted Gravity Drainage
SDI	Serial Digital Interface

SF	Scaled Frequency
SICT	Seepage Induced Consolidation Test
TDR	Time-domain Reflectometry
TMF	Tailings Management Framework
TT	Thickened Tailings
<i>A, B, C, D, Z</i>	Material Coefficients
<i>act</i>	Activity
<i>c</i>	Velocity of light
<i>C</i>	Differential Water Capacity of the Porous Medium
<i>D</i>	Diffusion Capacity
<i>C_{KC}, C_P</i>	Kozeny-Carman Coefficient
<i>cP</i>	Centipoise (mPa.s)
<i>C_s</i>	Solids Content
<i>C_v</i>	Coefficient of Consolidation
<i>D_R</i>	Specific Weight
<i>Δm</i>	Percentage of mass
<i>e</i>	Void ratio
<i>e₀</i>	Initial Void Ratio
<i>F_a, F_w, F_s</i>	Raw count in Air, Water Bath, and Soil
<i>g</i>	Gravitational Acceleration
<i>G'</i>	Elastic or small-strain Shear Modulus
<i>G''</i>	Viscous Modulus

G_s	Specific Gravity
γ_c	Shear Strain
γ_w, γ_s	Specific Weight of Water and Solids
h	Pressure Head
H	Hydraulic Potential of Flow Domain
H_{ini}, h_0	Initial Height
h_{int}	Height at the interest point
k	Hydraulic Conductivity
k_a	Dielectric Constant
L	Length of the Probe
LI	Liquidity Index
LL	Liquidity Limit
m	Absolute Slope of the best-fit Line
M_b	Mass of Bitumen
M_s, M_w and M_t	Solids, Water and Total Mass of the Material
μ_w	Dynamic Viscosity of Water
η	Fluid Viscosity
η_c	Concentration
n	Porosity
p	Weight Portion of Clay Minerals
P_{atm}	Atmospheric Pressure
PI	Plasticity Index
PL	Plastic Limit

r	Stokes radius of Particle
R^2	Coefficient of Determination
ρ	Bulk Density
ρ_s, ρ_w	Solid and Water Density
ρ_p, ρ_f	Particle and Fluid Density
q	Applied Stress
S_s	Specific Surface
SI	Shrinkage Index
σ'	Effective Stress
u	Pore Water Pressure
v	Filtration Velocity
V_v, V_s and V_t	The volume of voids, solids and total material
v_s	The velocity of tailings-water Interface/ Initial settling Velocity
V_s	Particle Settling Velocity
v_{sp}	Tangential Velocity
w	Gravimetric Water Content
x, z	Coordinates
t	Time
τ_c	Shear Stress
θ	Volumetric Water Content
z	Gravitational Head

Chapter 1: Introduction

1.1 Background

This thesis is concerned with the measurement or estimation of hydraulic conductivity in soft clayey soils and tailings. Management of clayey tailings, dredged soils, and similar soft materials is dominated by their consolidation properties, which govern the magnitude and rate of settlement of such deposits (Carrier III, Bromwell, & Somogyi, 1983). The hydraulic conductivity varies with density and is on average low, which poses challenges for reliable and quick measurement or estimation.

This is particularly important with respect to the management of oil sands tailings generated by surface mining of bitumen in Northern Alberta. The oil sands are an unconventional oil source, where viscous oil (bitumen) is trapped in a matrix of sand particles. The oil sands formations are the third-largest proven deposit of crude oil in the world (approximately 13% of the world's oil reserve), and the industry contributes to Canada's gross domestic product (GDP) by \$108 billion in 2018, supporting more than 530,000 jobs across the country (CAPP 2019). These soil formations are composed of a mixture of bitumen, mineral content and water. The economic fraction, bitumen, contained in this formation within 200 m of the ground surface, is predominantly extracted through surface mining. Once recovered, bitumen is sent to refineries for upgrading and the waste product is hydraulically sent to dedicated disposal areas or impoundments.

This waste product of the mining operation is known as oil sands tailings, and it is a mixture of water, sands, clay and a small fraction of bitumen. While the sands largely segregate after deposition into the ponds, the coarser fraction settles and forms beaches,

whereas the finer fraction (clay and silt particles, 44 micrometres or less in diameter) remains in suspension and forms a layer. This finer fraction remains at gravimetric water contents (*mass of water/mass of solids*) greater than 200% for decades. At this stage, these tailings are also known as fluid fine tailings or FFT. Even though the footprint of these tailings ponds or dams are significant (which cover almost 300 km² and often exceed 80 m in height), this finer fraction doesn't settle or consolidate considerably afterwards and may not attain significant strength allowing for successful reclamation (Nicholas Beier, Wilson, Dunmola, & Segó, 2013; JC Sobkowicz, 2013). Figure 1-1 demonstrates the expansion of a single oil sands mining operation over the years. Out of all the disturbed areas, only about 0.1% of the land is fully reclaimed, whereas only 10% is currently undergoing reclamation work (R. J. Chalaturnyk, Don Scott, & Özü, 2002; Lothian, 2017).

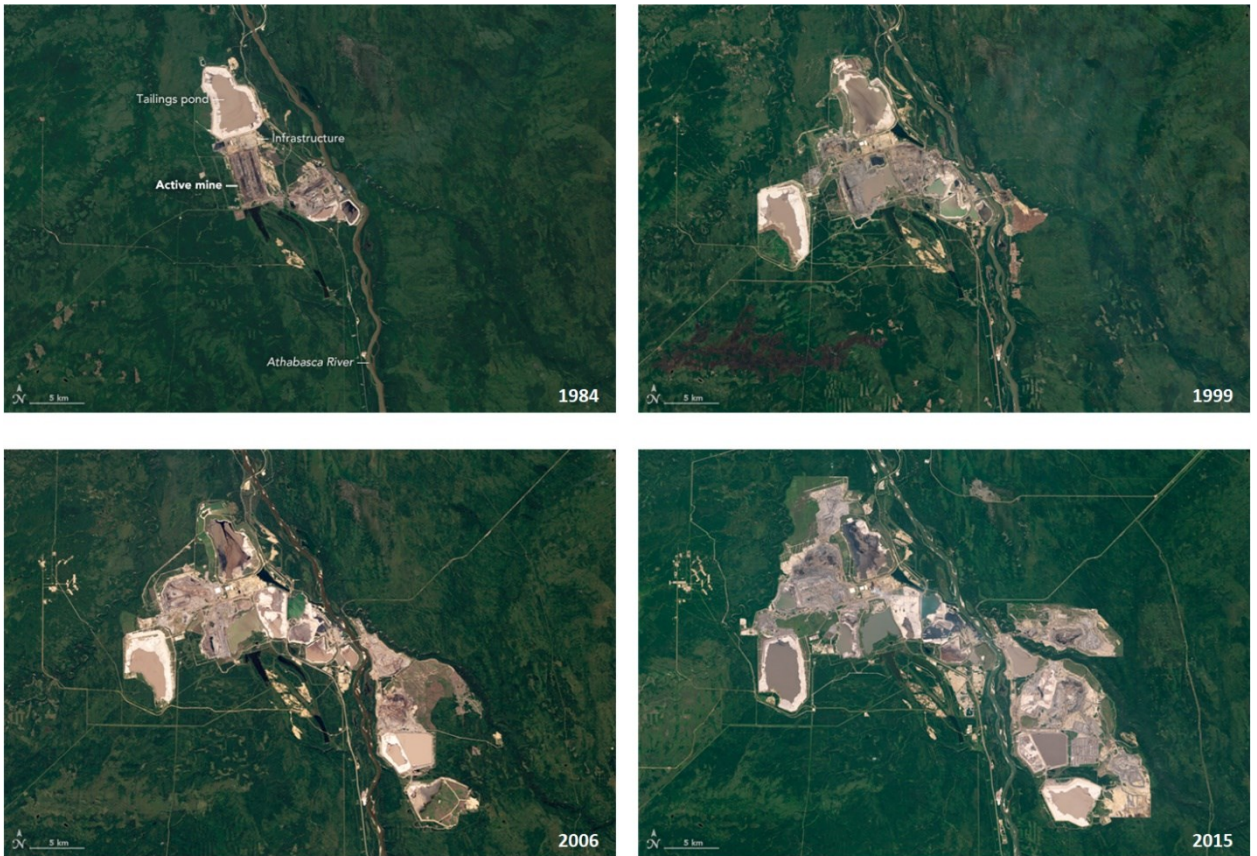


Figure 1-1: Satellite images showing the growth of surface mining over the Athabasca oil sands from 1984 to 2015 (pictures taken by the Earth Observatory at NASA)

The fine fraction of the tailings is composed of clays (40-70% kaolinite, 28-45% illite, and 1-15% montmorillonite) and other fines (R. J. Chalaturnyk et al., 2002). The clays are highly dispersed owing to the chemistry of the extraction process. As a result, the fine fraction is associated with poor consolidation properties such as low hydraulic conductivity and high thixotropic strength (Jeeravipoolvarn, 2005, 2010; W. G. Miller, 2010). This finer fraction stays in its loose wet state even after decades (a good example is illustrated in Figure 1-2) and poses environmental risks. Untreated, the fine materials do not gain significant strength or consistency to allow for land reclamation.

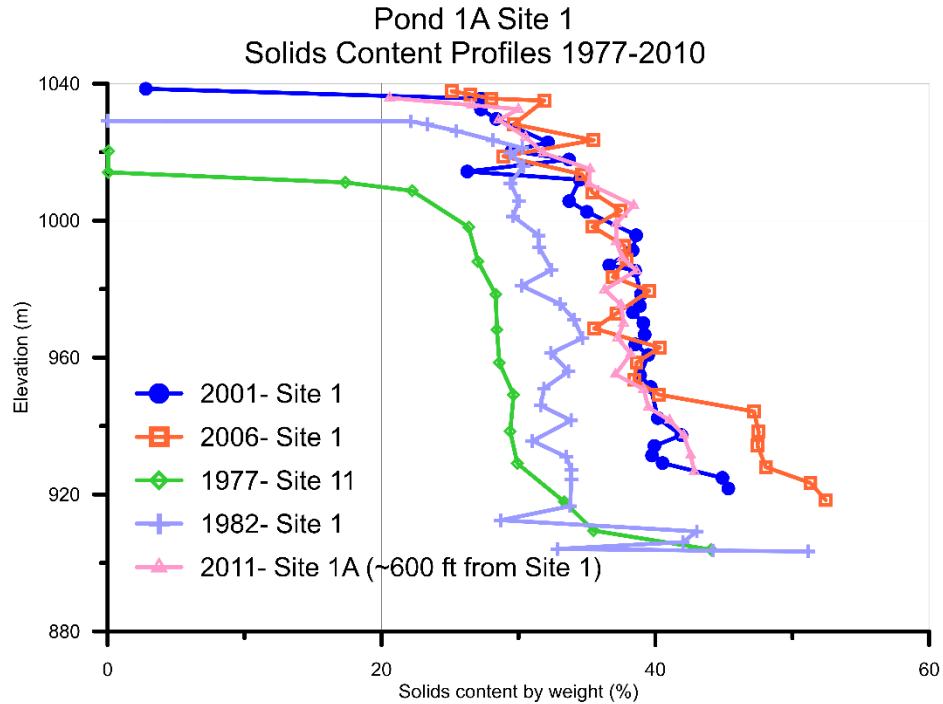


Figure 1-2: Solids content profile over time in a real deposit (modified from P. S. Wells (2011))

The Government of Alberta requires that companies remediate and reclaim 100 percent of the land after the oil sands have been extracted no later than ten years after mine closure. Reclamation means that land is returned to a self-sustaining ecosystem with local vegetation and wildlife, and no materials in above-ground impoundments should be left in their fluid state within the given time frame (Langseth et al., 2015). This restored topography is governed by multiple considerations, including surface water management, the susceptibility of cover soils to water and wind erosion, and water balance with supporting vegetation. All this requires that the tailings are strong enough to support reclamation activities and that the amount of long-term settlement will not be excessive (AER, 2017).

To meet these environmental regulations and to improve the settling process of tailings, the industry employs different strategies to treat this slurry material. The

objective of using tailing treatments is to increase the settling rate hence decreasing the time for liquid-solid separation in the pond and recovering the maximum volume of water possible. These strategies include recombination of FFT with the sands, using polymers to limit segregation (CT and NST), the use of polymers and coagulants to induce clay flocculation in the FFT, in combination with some dewatering technology (e.g. centrifuge, tank thickening, in-flocculation). These technologies generally achieve gravimetric water content of about 100%, which is still removed from the desired gravimetric water content of 35% (solids content about 75%) (JC Sobkowicz, 2013). Therefore, deposition strategies aim to increase dewatering in the deposit through combinations of desiccation and consolidation. Some of these dewatering technologies demonstrated promising results, but the innovations of these technologies are still progressing.

Prior to the implementation of these new technologies or strategies, each technology should be tested to discover the long-term performance of the tailings in the containment areas. For all technologies, the most important properties are those that govern consolidation, namely the hydraulic conductivity and compressibility functions. The former governs the rate of settlement, while the latter governs the final density profile of the tailings, which in turn regulates the strength of the deposit.

These two properties, especially the hydraulic conductivity-void ratio relationship of FFT, are highly variable, and the determination of the latter can be very time-consuming or expensive as it might need a large number of field or laboratory tests. Currently, the most commonly used experimental methods include slurry consolidometers (it can take up to a year to determine the full $k-e$ curve) and centrifuge tests (expensive to install and operate, also not commonly available in most of the research facilities and universities).

Therefore, there is a strong motivation in the oil sands industry to develop faster methods for evaluating the k - e relationship of potential tailings treatments. A rapid method could accelerate innovation in the oil sands industry by allowing quick evaluation of new technologies or improvements in the existing ones in terms of their long-term dewatering potential. This is of particular interest for planning deposition of clayey tailings, where polymer and other amendments are added to improve their consolidation characteristics, and a means to rapidly evaluate the influence of a candidate treatment (e.g. a new type of polymer, mixing strategy, change in grain size by adding sand, etc.), is highly desirable.

1.2 Objectives

The overall objective of this research is to identify or create rapid methods to evaluate the large strain consolidation behaviour of soft clayey soils and tailings. In order to achieve this goal, two separate lines of inquiry were pursued, associated with the following main objectives:

1. To establish a relationship between the easily measured index properties, i.e., Atterberg limits or grain size curves, and consolidation parameters of oil sands tailings and other soft clayey soils. This includes an evaluation of existing methods for estimating large strain consolidation properties of soft soils.
2. To design a prototype consolidation test that can determine the hydraulic conductivity-void ratio relationship rapidly that can be utilized as an alternative to conventional laboratory tests. The “Instantaneous Profiling Method” methodology is utilized in the

prototype column to determine the $k-e$ curve, and various fine-grained soils are tested to determine the applicability of the prototype design.

1.3 The novelty of the Research

The novel components of the research are:

Concerning objective i) There is substantial research available on the use of predictive models (using easily measured geotechnical properties) to estimate the consolidation parameters for both coarse and fine-grained soils. However, it is difficult to find a study comparing all the available methods on a large database to identify the most successful correlation relationships. The novelty of this research is to recognize the best performing predictive models for different types of fine-grained soils based on the statistical analysis, recognize the shortfalls of these models and consider the possible adjustments with the original formulation and/or come up with a new method to improve the deficiency of the correlation relationships. In particular, trying to come up with easily measured predictors that give information regarding the soil at a high void ratio well above the liquid limit.

Considering objective ii) Direct estimation from paired measurements of water content and pore-water pressure profiles have been used before. For example, in unsaturated soils, the Instantaneous Profile Method (IPM) was originally founded in 1966 and has been used by several researchers to determine k as a function of the degree of saturation. Similar techniques have been employed to estimate $k-e$ in soft saturated soils but at a low level of discretization (G Bartholomeeusen et al., 2002). The goal of the current study is to design an apparatus that provides data with sufficient resolution to enable

accurate direct measurement of the $k-e$ relationship, that is relatively inexpensive and safe: therefore, alternatives to high radiation-based techniques for measurement of density are explored, which have some safety issues and are relatively expensive.

1.4 The layout of the Thesis

This thesis is organized into nine chapters, and the outline is presented as follows:

Chapter 2: A literature review is presented, beginning with the general information on Alberta's oil sands tailings, including current dewatering and reclamation strategies, followed by the time-dependent behaviour of soft soils and oil sands tailings (consolidation, thixotropy, and creep). It is then extended to the consolidation and permeability testing on soft clays and slurries, direct (conventional testing), or indirect methods to determine the parameters of consolidation.

Chapter 3: The properties of the tested materials and methods utilized in this study to estimate or determine the consolidation parameters are discussed.

Chapter 4: An assessment of simple correlations to estimate consolidation properties for fine-grained soils is covered in this chapter. An extensive database of the properties for clays, dredged slurries and oil sands tailings are collected, and the performance of the existing correlations is evaluated. New prediction equations are proposed for each soil type based on the outcome of the study. Built on that work, an improved method is proposed to estimate the hydraulic conductivity of soft clayey soils using compressibility curves along with a measured data point.

Chapter 5: A prototype consolidometer design is presented in this chapter. The automation design and the system for the proposed experimental setup are explained. The application of the Instantaneous Profiling Method (IPM) using the proposed setup is discussed. A case study is examined for the application of the method.

Chapter 6: The applicability of the new prototype column along with the IPM method is tested for different slurry fine-grained soils. Self-weight consolidation tests were performed on thickened gold tailings, kaolinite, and FFT samples from two different operations. The results are analyzed and compared with numerical simulations using a large strain consolidation program (UNSATCON). For the convenience of readers, the results are separated into two chapters; this chapter discussed the results from different fine-grained soil tests, whereas the next chapter focuses only on amended oil sands tailings.

Chapter 7: Built on the knowledge from the previous chapters, the application of the setup is tested for amended oil sands tailings at different dosages. The necessary corrections on raw sensor readings are discussed. The results are then compared with the predicted values determined from UNSATCON.

Chapter 8: A general discussion and the application of both methods are presented in this chapter.

Chapter 9: Provides a summary of results and the limitations of both techniques presented in this research. For the future of this research, a set of recommendations are discussed.

1.5 Publications Related to Dissertation

Improving Hydraulic Conductivity Estimation for Soft Clayey Soils, Sediments, or Tailings using predictors measured at high void ratio, 2020, *ASCE Journal of Geotechnical*

and Geoenvironmental Engineering (This paper is presented as part of this thesis in Chapter 4)

Prototype Column Test to Estimate Hydraulic Conductivity of Slurry Tailings, 2020, *73rd Canadian Geotechnical Conference (GeoVirtual)* (This paper is presented as part of this thesis in Chapter 5 and 6)

A Rapid Measurement Method to Determine Hydraulic Conductivity of Tailings Under Self-Weight Consolidation, 2020, *Proceedings of the International Conference on Tailings and Mine Waste*, Keystone, Colorado (This paper is presented as part of this thesis in Chapter 5, 6 and 7)

Rapid Estimation of Hydraulic Conductivity for Fluid Fine Tailings, 2018, *International Oil Sands Tailings Conference*, Edmonton, AB (This paper is presented as part of this thesis in Chapter 4 and 5)

Estimating Saturated Hydraulic Conductivity from Compression Curves for Fluid Fine Tailings, 2018, *71st Canadian Geotechnical Conference*, Edmonton, AB (This paper is presented as part of this thesis in Chapter 4)

Estimating hydraulic conductivity from simple correlations for fine-grained soils and tailings, 2017, *70th Canadian Geotechnical Conference*, Ottawa, ON (This paper is presented as part of this thesis in Chapter 4)

Chapter 2: Literature Review

This chapter provides:

1. Background information on the formation and characterization of Alberta's oil sands tailings and the geotechnical behaviour of these materials after deposition.
2. A review of post-deposition dewatering behaviour of soft soils; i.e. sedimentation, flocculation, segregation, consolidation and time-dependent effects.
3. A review of methods for determining the consolidation parameters in laboratory conditions. Elements of these methods are adopted in the new estimation methods and new experimental setup described in Chapters 4 and 5.

2.1 Alberta's Oil Sands

Canadian oil sands are currently the third largest reserve of oil in the world. The oil sands deposits underlie an area of 142,200 km² with at least 165 billion barrels of crude oil extractable using current technologies (AER, 2019a). Produced crude oil sits on three central regions in Northern Alberta; Peace River, Athabasca and Cold Lake (Figure 2-1), and 20% of the total bitumen reserves are recoverable by surface mining (McEachern, 2009).

For shallow reserves (up to 75 m), surface mining is preferred for the recovery of the oil for economic reasons, whereas, for deeper deposits, the oil is recovered using methods such as steam-assisted gravity drainage (SAGD).

Oil sands consist of sand, water, clay and a heavy oil known as bitumen. Once bitumen is extracted, it needs to be heated or diluted in order to be pumped or flow. Oil

sands are mostly composed of uncemented quartz sands; each grain is surrounded by a light film of water and covered in heavy bitumen, as shown in Figure 2-1 (Zhu, 2013).

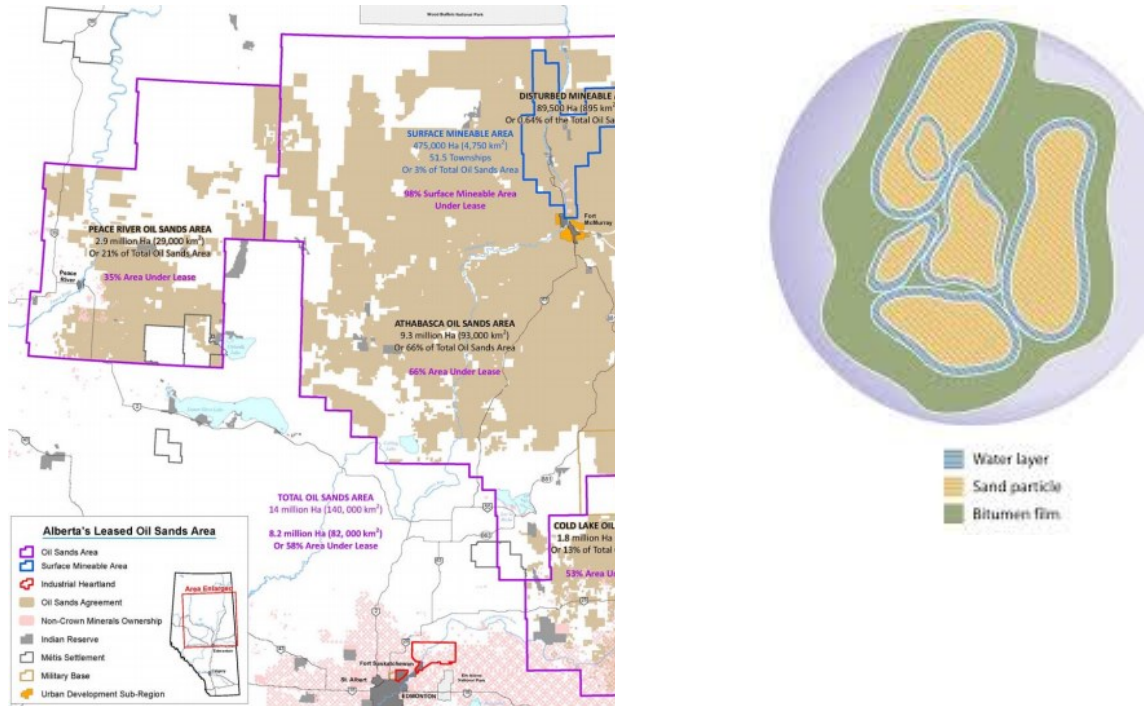


Figure 2-1: Current map of Canadian oil sands (Energy, 2017), and schematics of oil sands particles (Marcus, Tijseen, & Winkelman, 2017)

The origins of these sand deposits date back to approximately 100 years ago. It is believed that the streams flowing from the Rocky Mountains (in the west) and Precambrian Shield (in the east) filled between the ridges of Alberta and Saskatchewan brought sand and shale. The sand eventually spread into a larger area and became saturated with oil, which is originated at depth to the southwest but ended up flowing into these sand deposits (Jeeravipoolvarn, 2010; Mizani, 2017).

2.2 Bitumen Extraction

For commercial productions, oil sands are usually mined by a truck and shovel method and then transported by pipelines to extraction plants. In order to separate bitumen from oil sands, the ore components (sand, silt, clay particles, along with bitumen) should be disintegrated. All three major companies (CNRL, Syncrude, and Suncor) use Clark Hot Water Extraction (CHWT) process to separate bitumen by adding steam, hot water and sodium hydroxide (NaOH) to the mined oil sands. The elevated temperature reduces the viscosity of the bitumen, and the addition of NaOH promotes disassociation of the bitumen from the solids. The addition of NaOH changes the process water chemistry to facilitates the breakdown of clay-shale stringers releasing bitumen from the soils (R. J. Chalaturnyk et al., 2002). Figure 2-2 illustrates the general scheme for the CHWE process.

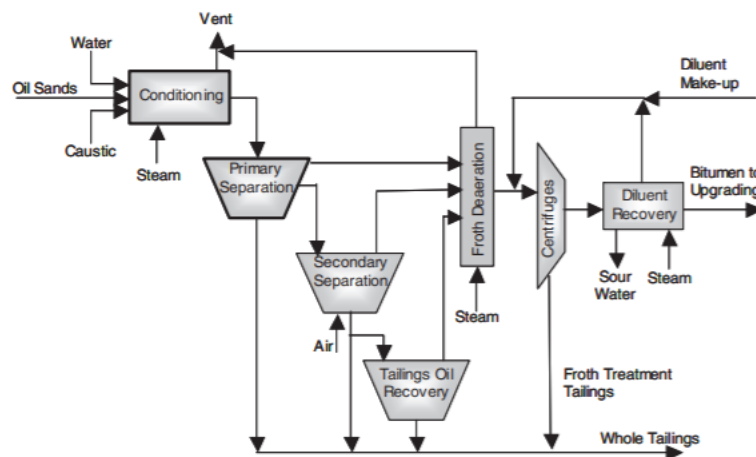


Figure 2-2: Diagram of CHWE process (R. J. Chalaturnyk et al., 2002)

The first step of the process is called conditioning, where NaOH is added to maintain the pH of the solution between 8-8.5 to separate the bitumen from the mineral

solids. The fine clay particles, which are in a thin water film layer around sand particles or as discontinuous thin beddings, will become dispersed and separated from bitumen at this stage. The next stage in this process will be the separation stage, which aims the separation of sand particles and promoting bitumen floating. Separated sand particles settle at the bottom of the large vessels and are removed as tailings streams, whereas the bitumen is separated as a froth floating to the surface of the vessel and collected. For the bitumen particles unobtained in the first two stages, the central portion of the slurry is moved to large deep cone vessels, known as scavenging cells, for additional bitumen recovery by injecting air to the stream. The produced bitumen froth at this stage has significant amounts of fine particles and water, and they must be separated prior to the upgrading process. After the separation of fine particles from bitumen in separation units, the underflow from this process is added with the coarse portion to be sent to the tailings ponds (Jeeravipoolvarn, 2010).

2.3 Tailings Regulations

Directive 085 was published in 2017 under the Oil Sands Conservation Act (OSCA) for managing fluids tailings volumes, establishing impoundment requirements, applications and processing reports for oil sands mining projects. The objective of the Tailings Management Framework (TMF) is to manage the tailings accumulation, ensure that the tailings are treated and reclaimed progressively throughout the life of the project, and minimize the liabilities and environmental risks associated with the accumulation of fluid tailings. One of the most important requirements of this directive is that all fluid tailings should reach *ready to reclaim* status ten years after the end of the mine life; however,

operators are required to reduce their volume of non-treated tailings progressively through mining operations. The operators must submit plans to the regulator that anticipate how the volume of untreated tailings will be reduced over time. The regulator must approve these plans and monitor each operator's progression towards these tailings' reduction goals.

2.4 Basic Properties of Oil Sands Tailings

McMurray Formation or Athabasca oil sands are composed of a mixture of bitumen, mineral content and water. The proportions of the components vary with location, but R. J. Chalaturnyk et al. (2002) reported the distribution as bitumen content ranging from 0-19%, mineral content (mainly quartz sands and silts with clay) from 84-86% and water from 3-6% by the total mass. Clays can be found as discontinuous clay layers in the McMurray bitumen-containing deposits.

Typically, the tailings are discharged into a containment area (also referred to as "dedicated disposal areas"). Upon deposition, tailings segregate in the pond; the coarser particles and about half of the total fine clay content settle at the bottom of the pit, whereas the remaining fine clays along with water and residual bitumen remain in suspension (~30% solids content and 230% gravimetric water content) for a significant amount of time. The reclaimed water at the ponds (with low solids content) can be reused in the extraction process. A portion of the entrapped water to be released from this suspension may take a few more decades (Vedoy & Soares, 2015), but even after many years, the material will not gain enough strength to meet requirements for successful terrestrial closures (Nicholas Beier et al., 2013; JC Sobkowicz, 2013).

The major clay formation in Athabasca oil sands is kaolinite (portion varies between 40% to 70%), then illite (30%-45%) with up to 10% mixed layer of smectite/illite. Active clays in this formation (illite and mixed-layer clays) may be responsible for poor processing and compaction issues in oil sands extraction and fine tailings disposal. It is believed that the “gel-like” structure (contains ultrafines and up to 90% water) formation in the tailings may be caused by the degraded active clays due to weathering or the action of caustic soda and the presence of bituminous residues around the particles (R. J. Chalaturnyk et al., 2002).

For efficient bitumen extraction by flotation, dispersion of the clay minerals is a necessity. To achieve that, caustic soda is utilized in the industry, which promotes several disadvantageous conditions regarding the fines content. The fine clay particles in fluid fine tailings originally form a stable colloidal system, but with the addition of caustic soda, these fine particles obtain an enhanced negative surface charge. As a result, these negatively charged particles repulse each other, creating a dispersed state of clay particles in the system (N. A. Beier, 2015). This dispersion process prevents rapid dewatering by sedimentation and consolidation of these fine minerals creating undesirable conditions for tailings disposal and storage (BGC Engineering, 2010). Also, residual bitumen content is believed to be a contributing factor to the poor consolidation properties of these materials (Jeeravipoolvarn, 2005).

Poor consolidation properties and water retention capacity of these fine minerals are governed by the surface properties of the minerals. Final settled volume, strength and hydraulic conductivity are dependent on forces (steric, electrostatic, hydration and Van der

Waals) affecting colloidal particles in suspension (Fine Tailings Fundamentals Consortium, 1995).

Some of the basic geotechnical properties of fluid fine tailings (FFT) are presented in Fine Tailings Fundamentals Consortium (1995) as;

- The mean particle size varies between 5 to 10 μm
- The average solids content and the void ratio are 31% and 5, respectively.
- The Atterberg limits of FFTs are; liquid limit ranges between 25-75% and plastic limit ranges from 10-38%
- Saturated hydraulic conductivity is responsible for the slow rate of consolidation and usually is presented in a power form ($k = Ae^B$) where A varies from 2×10^{-8} to 2×10^{-13} and B varies from 2.32 to 5.88.
- Time-dependent behaviour is present (thixotropy, creep and structuration)
- The viscosity of the materials is ranging from 0 to 5000 cP, increasing with time due to time-dependent changes
- The shear strength of FFT is typically less than 1 kPa

2.5 Problems Associated with Tailings

There are several challenges regarding tailings management and long-term storage; the accumulated amounts of tailings in containment structures, water management, the residual amount of bitumen in the ponds and the limitation of designated areas for disposal are simply a few of them (BGC Engineering, 2010).

Surface mining is the most economical method of extraction, even though only 10% of the total bitumen is mineable through this process. This operation has been continuing

over the past four decades, with large amounts of tailings accumulated and deposited in ponds occupying large extensions of lands that cannot be used for several decades. The treatment processes of these by-products were not really in effect until the introduction of regulations and by-laws (Vedoy & Soares, 2015). However, currently, the industry put significant effort in for research and commercial application in treating the FFTs upon deposition (i.e. the application of chemical or biological treatments, several stages of dewatering). The main objective of these treatment strategies is to remove the water from the tailings to obtain a trafficable load-bearing surface in a reasonable time frame. If achieved, this will lead to subsequent reclamation, and the tailings will no longer require dam-like containment for long-term storage (BGC Engineering, 2010). Surface disposal areas are limited for many of the mine leases, and considering the vast amounts of tailings, the out-of-the pit and in-pit spaces are restricted. A small amount of residual bitumen is also entrapped in tailings, which may affect the behaviour and characteristics of the tailings (J Sobkowicz & Morgenstern, 2009).

Aside from the management of tailings, the management of water is also very challenging for the mine sites. About 83% of water (by volume) is entrapped in FFTs and cannot be used, and recycling this entrapped water is challenging (Cymerman, Kwong, Lord, Hamza, & Xu, 1999). With the current treatment technologies, a significant portion of the water can be recovered from “fresh tailings,” reducing the amount of water and tailings deposited in the ponds. This reclaimed water is returned to the extraction plant (Vedoy & Soares, 2015). Currently, the mines are operating under a “zero-effluent discharge policy,” preventing the process-affected water from accumulating. However, the continual cycle of water recycling has induced the buildup of dissolved ions within the

recycled water. To decrease the level of dissolved ions and to keep up with the specified levels, freshwater may be added. This accumulation of dissolved ions may introduce several challenges not only for the operators (poor extraction recovery, challenges associated with equipment and piping) but it may also create future problems for water release and treatment (N Beier, Alstaz, & Segó, 2009).

2.6 Dewatering Technologies and Reclamation Strategies

The report published by Alberta Energy Regulator in 2018 titled “State of Fluid Tailings Management for Mineable Oil Sands” summarized all the current deposition and treatment plans for the oil sands tailings. There are currently six different treatments and deposit options are performed in the operating mine sites, which are thin-lift drying, thickening tailings as an initial treatment, non-segregating and composite tailings deposits, centrifugation of fluid tailings, permanent aquatic storage structure and water-capped tailings.

The thin-lift drying process involves the removal of fluid tailings from the ponds and mixes them with additives in order to bind the particles together. These tailings are later transported and spread over a large area facilitating further drying of the tailings (by gravity, capillary action, and ambient conditions such as evaporation, freeze/thaw cycles) within a couple of weeks. Once the drying process is complete, another layer or “lift” is poured on top of the existing layer, and the overall process is repeated. Currently applied by Suncor and referred to as “tailings reduction operation or atmospheric fines drying”. (AER, 2019b).

The thickening process of fluid tailings involves using a thickener where the flocculants are added to the material binding smaller particles, hence creating thickened tailings. This thickening process is an initial stage of treatment, and prior to deposition, additional treatment stages (co-depositing with whole tailings and/or coarse sand tailings and/or tailings solvent recovery unit in a single deposit, the addition of secondary polymer addition) are applied on the fluid tailings. Terrestrial closures are targeted for thickened tailings deposits with wetlands, and ready-to-reclaim trajectories and updated modelling for the deposits are required.

Non-segregating tailings are generated by mixing thickened tailings with sand from the extraction plant and added coagulant in a thickener, then deposited in a tailings pond. Similar to non-segregating tailings, composite tailings are fluid tailings mixed with sand from the extraction plant and added coagulant in a thickener, and placed into a tailings deposit. Non-segregating tailings technology is utilized by Canadian Natural, whereas composite tailings are generated by Syncrude and Canadian Natural at Muskeg River Mine. Both processes are targeting terrestrial closure with wetlands.

The fluid tailings centrifugation process involves removing the tailings from the pond, mixing them with flocculants and spinning them in a centrifuge to remove the water from the mixture. Dewatered tailings are then placed in a deposit. Similar to previous processes, this technology aims for terrestrial closure with wetlands that are currently applied by Syncrude and CNUL.

Permanent aquatic storage structure (PASS) is a new treatment technology implemented by Suncor. Initially, the tailings are treated using coagulants or flocculants and placed in a deposit. For a terrestrial closure with this technology, a unique capping

technique is required. Currently, only the initial phase of the project is approved by the Alberta Energy Board, and Suncor is required to submit research and implementation plans (for terrestrial or aquatic closure options) for PASS-treated tailings by 2023.

Water-capped technology involves placing water on top of untreated or treated (refer to PASS technology) tailings to create a water-capped deposit. It is currently an unapproved technology (as it requires further assessment, research and future policy), and it is in the demonstration and experimental phase.

2.7 Dewatering Behavior of Soft Soils and Oil Sands Tailings

The long-term dewatering behaviour of fine-grained soils can be complicated as the material experiences several phenomena upon deposition. The settling process of soft soils and tailings can be very complex as it combines several processes, i.e. sedimentation, flocculation, segregation, consolidation, which may be interconnected or occur simultaneously. Sedimentation, segregation and consolidation have been considered the main processes in tailings deposition, and these phenomena have been extensively studied by various researchers. However, even the modified theories and models may not be capable of predicting the long-term performance of these soft, fine-grained slurries. Time-dependent effects such as creep and thixotropy (or structuration) may also play an important role in the consolidation behaviour: this has been acknowledged for many years for raw FFT (Jeeravipoolvarn, 2005; M. Salam, 2020). These phenomena will be explained in more detail in this section.

2.7.1 Sedimentation and Consolidation of Soft Soils and Slurries

The two main behaviours observed in settling in concentrated slurries are sedimentation and consolidation. However, the transition from sedimentation to consolidation is complex, and in fact, both sedimentation and consolidation can occur simultaneously at different depths. Goro Imai (1981) described the process of initial dewatering as comprising three stages: flocculation, settling and consolidation. In the first stage, the initial uniformity of water content is maintained while the flocculation of soil particles occurs. Two separate zones exist in the settling stages: in the upper zone, soil flocs settle through the water while the consolidation starts to occur at the lower consolidation zone, increasing the water content in the upper region. Once the settling stage is completed, the settling zone vanishes, and the sediment thereafter undergoes consolidation. Figure 2-3 presents all three stages of the process of fine-grained soils.

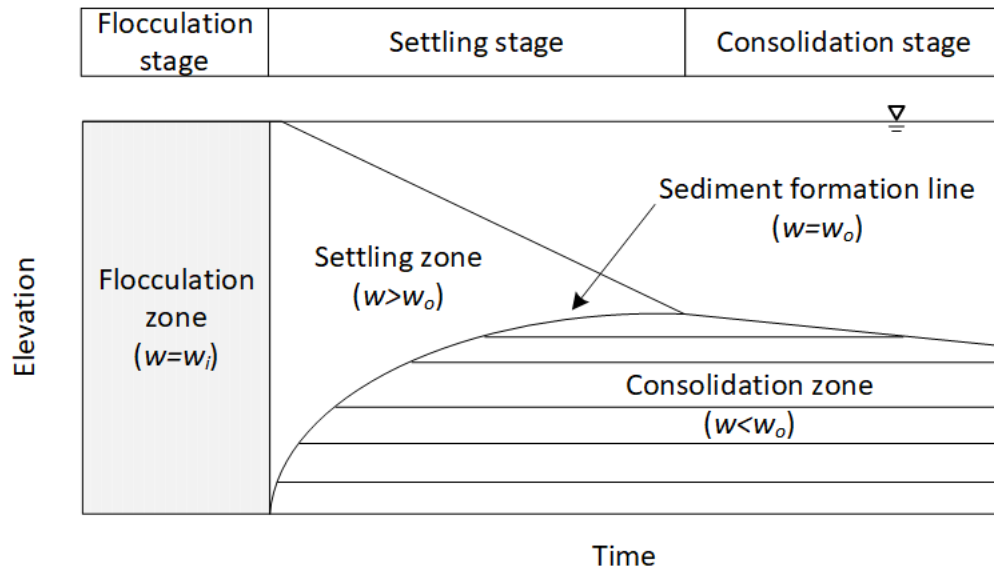


Figure 2-3: the characteristics of the sedimentation process for clay-water mixtures (modified from Jeeravipoolvarn (2010) and Goro Imai (1981))

2.7.1.1 Particulate Settling

This phenomenon usually occurs when the solids content of the slurry is very low. The soil particles are initially very far away from each other, and during this condition, they settle freely and do not hinder each other. It is also known as the clarification region. Particle segregation or sorting commences in this stage, where heavier particles settle to the bottom quickly, and smaller/lighter particles are left suspended in the water. Stokes equation can calculate the particulate settling velocity, which is presented in Equation 2.1.

$$V_s = \frac{2r^2 g (\rho_p - \rho_f)}{9\eta} \quad (2.1)$$

where V_s is particle settling velocity, ρ_p and ρ_f is particle and water densities respectively, r is a Stokes radius of the particle, g is the gravitational acceleration, and η is fluid viscosity.

2.7.1.2 Sedimentation

The process of solid particles in a suspension settling altogether is known as sedimentation or hindered settling. At this mode, there's a clear interface between the supernatant water and the settling volume, and this interface usually decreases linearly with time. The rate of sedimentation is a unique function of solids concentration, and no effective stresses are developed during this process (K Been & Sills, 1981; Holdich & Butt, 1997). As the settlement continues, the solids content increases. The mixture transforms from a suspension to soil, and it's difficult to clearly define this transition zone; it can be either sedimentation or consolidation. During this transition zone, effective stress started to develop in the soil, and at the end of hindered sedimentation, grain-to-grain interaction is

obtained with the significant development of effective stresses (Kenneth Been, 1980; K Been & Sills, 1981; Tan, Yong, Leong, & Lee, 1990).

One of the earliest theories on settling in concentrated suspensions has been presented by Kynch (1952), and aside from the modification of Stokes' law, there hasn't been any significant progress that was made on this topic up until then. Kynch's theory (Equations 2.2 and 2.3) determines the settling process from a continuity equation assuming the concentration is constant in the horizontal layer. The theory assumes that the speed of falling particles (in a dispersed state) is calculated by the local particle density. One of the setbacks of this theory is that it doesn't consider the details of the forces on the particles.

$$\frac{\partial \rho}{\partial t} = \frac{\partial S}{\partial x} \quad (2.2)$$

where $S = \rho v$

$$\frac{\partial \rho}{\partial t} + V(\rho) \frac{\partial \rho}{\partial x} = 0 \quad (2.3)$$

where $V(\rho) = -\frac{dS}{d\rho}$

where S is the particle flux (number of particles crossing a horizontal section per unit area per unit of time), ρ is density, v is fall velocity, t is time, and x is the height.

Whereas Kynch (1952)'s theory relates the settlement speed to only concentration; whereas (Kenneth Been, 1980) and Pane and Schiffman (1997)'s equation related the settling velocity to other parameters as well. The following model to determine the hydraulic conductivity values of clay suspensions calculated using the falling interface velocity at the sedimentation stage.

$$v_s = -\left(\frac{\gamma_s}{\gamma_w} - 1\right) \frac{k}{1+e} \quad (2.4)$$

where v_s is the initial settling velocity, k is hydraulic conductivity, e is the void ratio, γ_s is the unit weight of solid particles and γ_w is the unit weight of water. However, this equation is only valid as long as the settling velocity is constant or if there's a suspension at the initial void ratio at the sediment-water interface.

2.7.1.3 Segregation

Segregation or soil particles sorting may occur due to low shear strength of the soil matrix caused by low initial solids content and low attractive forces between soil particles (Mihiretu, Chalaturnyk, & Scott, 2008). As a result of this sorting, heavier/coarser particles fall to the bottom of a settling volume leaving finer/lighter particles suspended in the ponds at higher elevations. The occurrence of this phenomenon is dependent on the grain size distribution, rheological properties and the void ratio of the fines-water matrix.

Sridharan and Prakash (2001) investigated the consolidation and permeability of segregated and homogenous sediments and reported that this phenomenon creates a discrepancy in the pond in terms of the material's compression behaviour. For segregated clay slurries, the overall compressibility decreases compared to the homogenous soils as the bottom part with larger particles is subjected to higher pressures, but the top part is subjected to smaller self-weight stresses. Whereas for segregated clay soils, the compressibility decreases with the effective stress development in the segregated section, which is due to the development of shear strength at the top section. The segregated montmorillonite still has a lower compression as it behaves like an overconsolidated soil

in low effective stress ranges, whereas segregated kaolinite does not exhibit the same behaviour. Their research demonstrated that for homogeneous kaolinite clays, the compressibility of soil increases due to the increased effective stresses in layers, and once the soil develops higher effective stresses, the compressibility of this soil reduces.

The segregation process is also influenced by chemical properties such as pore fluid. The role of cation exchange on clay mineral surfaces affects the segregation of clay-sand slurries. Even without a change in the solids and fines contents, the segregation behaviour of the slurry can be manipulated (Islam, 2008). A detailed geochemical investigation is examined by Donahue et al. (2008) on chemically treated kaolinite sand slurries using NaOH. This study showed that the segregation behaviour of this material is a function of the divalent to monovalent cation ratio or $\text{Ca}^{+2}/\text{Na}^{+}$ ratio on clay surfaces.

This phenomenon also has a significant impact on tailings disposal and time-dependent behaviour. It leaves a large amount of finer particles suspended in tailings ponds, and the hydraulic conductivity of these finer/lighter particles is very low. As a result, the retention time on the tailings can be extremely long.

Segregation boundary, the boundary between non-segregating and segregated mixes, is introduced for tailings mix design to surmount the segregation problem. This boundary is also used in the oil sands industry, and the general criteria aim to capture 95% of the fines. The segregation may be preventable by different processes such as producing higher solids content or by increasing the fines content.

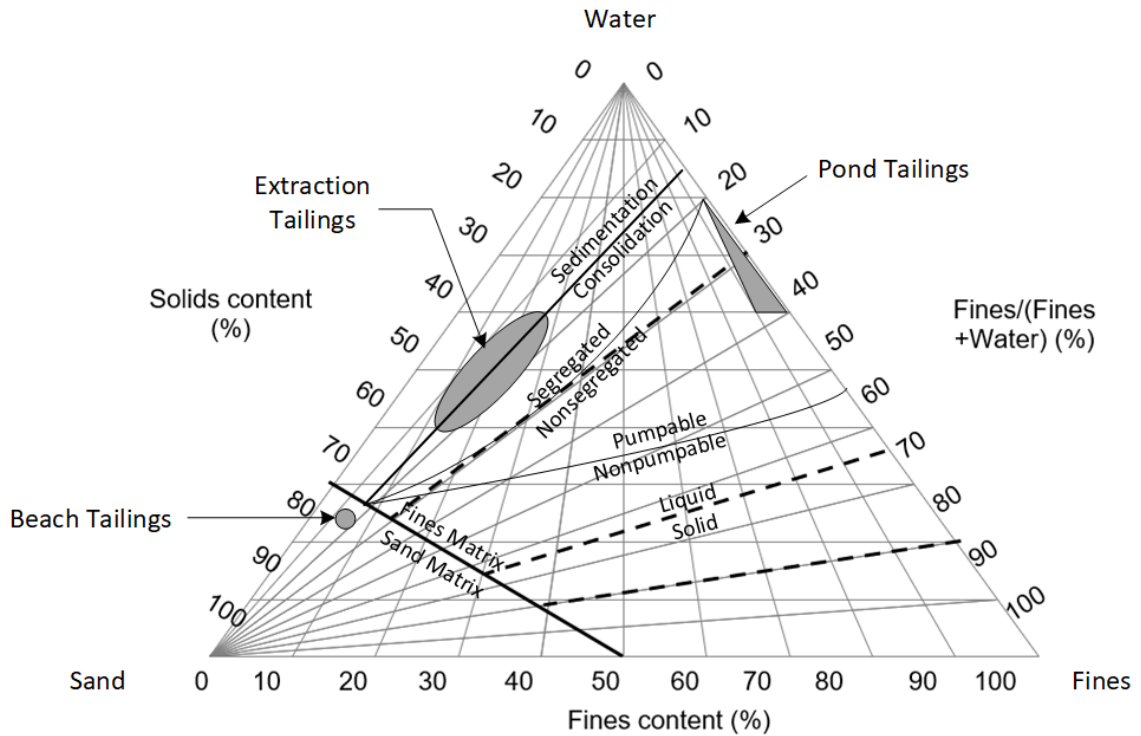


Figure 2-4: Tailings properties diagram of oil sands tailings (modified from Azam and Scott (2005))

The fluid fine tailings tested in this research fall into the “segregating tailings” category based on Figure 2-4, with having 30% solids content and 71% fines contents.

2.7.1.4 Consolidation

The process of consolidation is defined by K. Terzaghi (1943) as “a decrease of the water content of a saturated soil without the replacement of water by air.” During this process, the soil gains effective stress, and excess pore water pressures dissipate, inducing a decrease in the volume. The dissipation rate is influenced by the hydraulic conductivity of the soil and by the excess pore water pressure gradient (Chandra Paul & Azam, 2013). Different material behaviour may be observed in soft deposits comprised of particles that have undergone flocculation, sedimentation and self-weight consolidation prior to long-

term consolidation after deposition. However, two main behaviours during this process are; sedimentation and self-weight consolidation. Initially, the solids are in a suspension state, and the first step of the consolidation process is sedimentation, where the interface height decreases rapidly without measurable, effective stress (McRoberts & Nixon, 1976).

Simultaneously, self-weight consolidation starts to occur where soil particles begin to form a skeleton and transfer their weight to the bottom. Along with the continuation of dissipating pore water pressures, the soil particles are in contact and transmit their effective stresses (K. Terzaghi, Peck, & Mesri, 1996). As the soil builds up effective stresses, the slurry starts to behave as soil and eventually leads to equilibrium under its own weight (Bonin, Nuth, Dagenais, & Cabral, 2014).

The sedimentation process has been investigated as a part of consolidation theory by several researchers (K Been & Sills, 1981; McRoberts & Nixon, 1976). Large strain consolidation is associated with sedimentation for underwater depositions. However, for sub-aerial deposits, the sedimentation is very fast; therefore, it is not considered to be a part of the consolidation process (S. Koppula & Morgenstern, 1982; Seneviratne, Fahey, Newson, & Fujiyasu, 1996). The boundary between sedimentation and consolidation is difficult to distinguish. Determination of the void ratio where effective stresses start to develop is not particularly well-defined, and Goro Imai (1981) reported that it is dependant on the initial void ratio. Therefore, at the low void ratios, a number of compressibility equations may exist (Gert Bartholomeeusen, 2003; Kenneth Been, 1980; Sills, 1998). In large ponds, predicting this initial void ratio may not significantly affect the storage capacity. For higher void ratios, the permeability of the soil is high as well. Therefore, the rate of consolidation is initially high in the ponds but decreases quickly. If the assumed

initial void ratio is slightly above or below the actual value, the predicted time for the consolidation may be altered by few weeks, but it is insignificant in the sense that the consolidation of low solids content materials can take several years to complete (Carrier III et al., 1983). Generally, the boundary between sedimentation and consolidation is difficult to distinguish. The primary consolidation ends when all the excess pore water pressures are dissipated (when they reach to hydrostatic equilibrium condition), and the consolidation bed is formed (Goro Imai, 1981). Due to the highly dispersed state of clay particles, tailings display poor dewaterability and consolidation behaviour, which is often attributed to the low permeability of the material. The dissipation of excess pore water pressures is also governed by the hydraulic conductivity- void ratio relationship. As a result, it dictates the amount of settling and consolidation for these clay-rich materials with higher initial void ratios and low solids contents (N. Suthaker & Scott, 1994). The range of hydraulic conductivity for fine oil sands tailings is between 10^{-6} to 10^{-9} m/s, even with initial void ratios higher than 5. As a result, the rate of dissipation of excess pore water pressure is very slow (R. Chalaturnyk, Scott, & Özüm, 2004).

2.7.2 Theories of Consolidation

2.7.2.1 One-dimensional Consolidation Theory

The classical infinitesimal strain theory of Terzaghi is based on a few assumptions such as homogeneous soil, negligible compression and self-weight, and small strains (coefficient of compression and hydraulic conductivity of the material is constant). Incorporating these assumptions, Terzaghi's one-dimensional consolidation theory combined continuity

equation, Darcy's law and the principle of effective stress (K. Terzaghi, 1943) and presented as;

$$c_v \frac{\partial^2 u}{\partial x^2} = \frac{\partial u}{\partial t} \quad (2.5)$$

where c_v is the coefficient of consolidation, u is the pore water pressure, and x is the one-dimensional vertical coordinate.

The assumptions used in the infinitesimal strain theory are not applicable to mine tailings since the grained slurries experience considerable changes in void ratio during consolidation; therefore, the hydraulic conductivity and the compressibility are highly divergent. It was also found that incompressible soil properties are not applicable to tailings, and the hydraulic conductivity is an important parameter affecting the changes in the void ratio (Davis & Raymond, 1965; J.-C. Liu & Znidarčić, 1991).

The finite strain consolidation theory is one of the earliest and most applied hypotheses in the context of large strain consolidation theory (R. Gibson, England, & Hussey, 1967). Not only does it eliminate the limitations of infinitesimal theory, but it also considers the changes in incompressibility and hydraulic conductivity functions. The second-order partial differential equation in terms of void ratio and permeability is defined in Equation 2.6.

$$\pm \left(\frac{\rho_s}{\rho_f} - 1 \right) \frac{d}{de} \left[\frac{k(e)}{1+e} \right] \frac{\partial e}{\partial z} + \frac{\partial}{\partial z} \left[\frac{k(e)}{\rho_f (1+e)} \frac{d\sigma'}{de} \frac{\partial e}{\partial z} \right] + \frac{\partial e}{\partial t} = 0 \quad (2.6)$$

$$u = \frac{\partial}{\partial z} \left\{ - \frac{k(e)}{\gamma_w (1+e)} \frac{\partial u}{\partial z} \right\} + \frac{\partial e}{\partial \sigma'} \left\{ \frac{d}{dt} (\Delta\sigma) - \frac{\partial u}{\partial t} + \gamma_w \int_0^z \frac{\partial e}{\partial t} dz + \gamma_w \frac{\partial z}{\partial t} \int_0^z (1+e) dz \right\} \quad (2.7)$$

$$\begin{aligned}
& -\frac{d}{dx} \left[\frac{k(1+e)}{\gamma_w} \frac{d\sigma'}{de} \frac{\partial n}{\partial x} \right] - \left\{ (G_s - 1) \frac{d[k(1-n)^2]}{dn} - \frac{\partial q}{\partial n} \frac{d}{dn} \left[\frac{k(1-n)}{\gamma_w} \right] \right\} \frac{\partial n}{\partial x} \\
& + \frac{k}{\gamma_w} \frac{\partial^2 q}{(\partial x^2)(1-n)} = \frac{\partial n}{\partial t}
\end{aligned} \tag{2.8}$$

where z is the reduced materials coordinate, t is the time, k is the hydraulic conductivity, e is the void ratio, σ' is the vertical effective stress, n is the porosity, ρ_s solid density, ρ_f density of the fluid, x is the convective coordinate and q is the applied stress.

Gibson's finite strain theory has been revised by various researchers. Berry and Poshitt (1972), Gh Mesri and Rokhsar (1974) and Raymond (1969) proposed to use the theory for weightless material. Monte and Krizek (1976) introduced a "fluid limit" for the void ratio; above this limit, the soil behaves as a heavy fluid, and the application of effective stresses is not in use. S. D. Koppula (1970) and S. Koppula and Morgenstern (1982) implemented Gibson's finite strain theory utilizing excess pore water pressure, u , as a dependent variable to evaluate the progress of consolidation in a sedimenting layer (Equation 2.7). Another variation is presented by Lee and Sills (1979) following finite strain consolidation theory based on porosity while utilizing the convective coordinate (Equation 2.8).

Among the various numerical solutions to calculate the finite strain consolidation equation, finite element and finite difference schemes are the most popular (G Bartholomeeusen et al., 2002; Cargill, 1984; Fox & Berles, 1997; McVay, Townsend, & Bloomquist, 1986). Fox and Berles (1997)'s piecewise-linear solution and R. E. Gibson, Schiffman, and Cargill (1981) both use the Lagrangian approach. Shunchao Qi, Simms, Vanapalli, and Soleimani (2017) implemented this piecewise-linear algorithm using a finite-difference scheme into a novel algorithm called UNSATCON. All the numerical

large strain consolidation analysis performed in this research is carried out using this novel algorithm. Qi et al. (2019) showed that the piecewise linear approach is actually theoretically equivalent to Gibson's equation, and the continuity and force equations used in the piecewise linear approach are analytically equivalent to Gibson's combined equation.

The incorporation of sedimentation into finite-strain theory has been suggested and used by several researchers approaching the consolidation problem. Kenneth Been (1980) discussed that the only difference between these two processes (in terms of formulation) is the principal effective stress and the coordinate system, which can be deduced by setting the effective stress to zero during hindered sedimentation. Pane and Schiffman (1985) proposed that void ratios above the threshold, the material behaves as a suspension (in which the effective stress is at zero), and the finite-strain theory can be deduced to Kynch's equation. Instead of setting effective stress to zero in the dispersion region, Shodja and Feldkamp (1993) suggested introducing a constitutive model (describing the material's behaviour) to provide a distinction between the two processes. Coupled sedimentation-consolidation model proposed by Masala (1998) used hydraulic conductivity equation as a hydrodynamic interaction as this property extends to both regions to determine the solid-fluid interaction in suspensions.

2.7.2.2 Two-dimensional Consolidation Theory

One-dimensional finite strain theory has been widely used for the consolidation analysis for soft slurries and mine tailings; however, it fails to include the influence of lateral strains. The drainage through lateral boundaries is also not included in the theory. Therefore, multi-

dimensional large strain consolidation analysis might be more realistic (Fredlund, Donaldson, & Gitirana, 2009). Krizek and Somogyi (1984) derived a quasi-two-dimensional large strain consolidation model to predict full-scale behaviour. Huerta and Rodriguez (1992) considers the influence of vertical drainage and presented a pseudo-two-dimensional extension of the one-dimensional large strain consolidation theory. Bürger, Damasceno, and Karlsen (2004) proposed a consecutive two-dimensional analysis of sedimentation and consolidation. The theory assumes constant volumetric solids concentration in the horizontal direction but does not consider the horizontal pore water flow. The two-dimensional effects become significant when the width to height ratio of the impoundments are higher than five or less if associated with side drainages; however, this ratio is much greater for most of the tailings impoundments (Ahmed & Siddiqua, 2014; Bromwell, 1984).

2.7.2.3 Three-dimensional Consolidation Theory

Three-dimensional analyses are rarely employed due to various difficulties, lack of appropriate constitutive relationships, numerical difficulties related to non-linearity of the theories, and the requirements for computational time are excessive. By employing the one-dimensional derivation by R. L. Schiffman (2001), Jeeravipoolvarn, Chalaturnyk, and Scott (2008) presented a quasi multi-dimensional finite strain consolidation theory.

2.7.3 Thixotropy and Creep in Soft Soils and Slurries

Hydraulic conductivity and effective stress are considered to be the main contributors to the long-term performance of fine-grained soil slurries from a geotechnical point of view.

Conventional models usually only incorporate sedimentation and consolidation to determine the final settlement and strength of these deposits. However, there are several factors affecting the settling process of these materials, such as creep, structuration and thixotropy.

Consolidation behaviour of fine fluid tailings is also exposed to these phenomena, and FFT can be described as a composite material with unique features. A wide array of physical and chemical properties (such as creep, structuration and thixotropy) plays a role in the time-dependent behaviour of these tailings. It is necessary to adopt a more extensive approach than simply analyzing the behaviour from a single perspective to analyze and understand the long-term performance of FFTs in the field (Jeeravipoolvarn, 2010). In fact, poor dewaterability and slow rate of consolidation of oil sands tailings can be attributed to a buildup of overconsolidated structure through various time-dependent processes along with low hydraulic conductivity due to the dispersed state of clay particles (J.D. Scott, Jeeravipoolvarn, Kabwe, & Wilson, 2013). This section covers the theory behind each phenomenon and its impact on the long-term performance of fine-grained soils and tailings.

2.7.3.1 Creep Compression

Another time-dependent deformation in soils is known as creep or secondary compression. It usually occurs after the completion of consolidation and the dissipation of excess pore water pressures. Creep compression generally occurs at practically constant effective stresses (R. Robinson, 1999). Hydraulic conductivity- void ratio relationship dictates the rate and magnitude of settlement during primary consolidation for soils with high initial void ratios (Gholami, 2014; Nagula Naguleswary Suthaker, 1995). At the end of this

process, soil goes through deformation while the excess pore water pressures dissipate and effective stresses in the soil increase. During creep compression, similar to primary consolidation, hydraulic conductivity still dictates the rate of flow out of the soil. However, the rate of change in the effective stress is also affected by the viscous deformation of the soil structure (James Kenneth Mitchell & Soga, 2005). The resulting change in the volume of settlement is known as secondary compression or creep compression. Usually, creep compression is considered to have a small effect on primary consolidation. However, Fatahi, Le, Le, and Khabbaz (2013) reported that for soft soils demonstrating considerable primary consolidation, viscous creep should be considered as an important deformation mechanism since it has a large impact on the long-term settlement behaviour of these materials.

This phenomenon on fine-grained soils has been studied by several researchers. C. Crawford and Bozozuk (1990) examined the settlement behaviour of Champlain clay in the Ottawa region and found evidence of secondary compression. R. Robinson (1999) reported that the consolidation of clays continues even after the dissipation of excess pore water pressures, confirming that creep behaviour has an influence on the long-term settlement performance. Jeeravipoolvarn (2005) and Jeeravipoolvarn, Chalaturnyk, and Scott (2009) simulated large strain consolidation behaviour of oil sands tailings incorporating secondary compression based on experimental studies conducted at the University of Alberta. The experimental data were obtained from large-scale (three 10 m high and 0.9 m diameter standpipes) self-weight consolidation tests, which were studied and monitored for more than 25 years for unamended and amended FFT.

2.7.3.2 Structuration/ Ageing Effect

James K. Mitchell and Soga (1976) define the “*structure*” of soil as a combination of “*fabric*” (meaning the arrangement of soil particles) and “*bonding*” (interparticle forces). C. B. Crawford (1968) elucidated the term “*fabric*” in clays as “*the size, shape and geometric arrangement of particles, ranging from a parallel to a random or card house orientation*” and “*structuration*” term as “*a complex space frame of solid particles held together by plastic and rigid bonds.*” Many natural clay deposits demonstrate different characteristics and behaviour compared to the remoulded or reconstituted samples from the same clay. The change in this behaviour can be attributed to a bonded structure developed over a long period of time in a clay deposit. The formation of such structure is a result of a combination of extremely complex and time-dependent processes involving chemical, environmental, mechanical and thermal factors of clayey soil. The origin and evolution of the clay deposit are difficult to determine; however, experimental data concerning the structuration or ageing effects of natural clays exist in the literature (Burland, 1990; Leroueil & Vaughan, 2009; M. Liu & Carter, 1999).

Structuration manifests when the microscopic elements (soil particles) in a soil rearrange, and interparticle bonding occurs, inducing an apparent increase in the preconsolidation pressure in soft soils. Locat and Lefebvre (1986) stated that this phenomenon occurs as a combination of time-dependent processes in soils such as cementation or thixotropy in marine sediments. Whereas Leonards and Deschamps (1995) associated the effect of structuration or ageing to a number of factors such as cementation, change in pore water chemistry, mineral leaching/internal erosion, alteration of clay minerals and a combination of volumetric creep strains and the effect of time at constant effective stress in clays. Bjerrum (1967) researched the delayed compression behaviour at

constant effective stress in natural clays. This “*destruction*” can also be seen in reconstituted clay samples, as the soil is disturbed to the extent that the natural internal structure alters, shear strength decreases and soil gains compressibility. Burland (1990) tried to interpret the ageing effect of natural clays by looking at compressibility and strength characteristics of remoulded clay samples, and similar research was conducted by others as well (Delage, 2010; Leroueil & Vaughan, 2009; M. Liu & Carter, 1999; Locat & Lefebvre, 1986). Zeng, Hong, and Cui (2016) studied the yield-stress development due to ageing in high-water content dredged clays and proposed an empirical equation to estimate the ratio of vertical yield stress to effective vertical stress.

Shunchao Qi, Salam, and Simms (2017), S Qi, Salam, and Simms (2018) and M. Salam, Simms, and Ormeci (2018) conducted laboratory experiments to determine the effect of structuration in the long term dewatering and consolidation behaviour of amended FFT samples. They observed a change in the compressibility behaviour of the flocculated samples (with a high molecular weight anionic polymer), which can be associated with this time-dependent phenomenon. A pilot study of the deposition of in-line flocculated (with an anionic polymer) FFT samples also demonstrated evidence of time-dependent structuration and compressibility (Gheisari, Salam, Qi, & Simms, 2019). Also proposed an empirical equation, in combination with Zeng et al. (2016), to simulate thixotropic strength at small time scales in clay suspensions.

2.7.3.3 Thixotropy

Thixotropy can be described as a continuous decrease in apparent viscosity under shear with time and subsequent recovery when the flow stops. It is considered a rheological

process, but it can be explained from the geotechnical process as well. This phenomenon is common for clay-water mixtures, and James K Mitchell (1961) defines this behaviour as *“a continuous decrease of shear strength or softening caused by remoulding, followed by a time-dependent return to the original harder state at a constant water content and constant porosity.”* Thixotropy is believed to be developed in structured systems and is associated with the loss of thixotropic strength and the regain related to microstructural changes (Markgraf, Horn, & Peth, 2006; Osipov, Nikolaeva, & Sokolov, 1984).

The thixotropic strength ratio (for compacted clays) or sensitivity (for saturated clays) is utilized to measure the thixotropic strength gain in clays. It can be determined by the ratio of the measured undrained shear strength after an elapsed time to measured undrained shear strength after remoulding at the same water content. This ratio is preferred over the actual value of strength increase to quantify the thixotropic effect in clays (James K Mitchell, 1961; Nagula N Suthaker & Scott, 1997).

In natural clays, undrained shear strength is typically a function of in-situ effective stress, soil fabric and bonding, whereas, for normally consolidated clays, this parameter is in an approximately linear relationship with the vertical effective stress (Burland, 1990). For overconsolidated soils (i.e. sedimentary clays), an empirical correlation has been proposed between undrained shear strength and preconsolidation pressure (K. Terzaghi et al., 1996). Both structuration and thixotropy manifest from the same processes (strong particle-particle interaction, rearrangement and bonding) and this empirical relationship can demonstrate it. The critical difference between the two phenomena is that thixotropy manifests in an increase in undrained shear strength, whereas structuration manifests as a rise in preconsolidation pressure (and eventually stiffness). Both aspects are the result of

the same processes and might occur at the same time. Thixotropy leads to recovery of strength over time, whereas the structuration effect leads to a gradual improvement of stiffness in a reconstituted clay sample.

Banas (1991) identified several factors affecting the thixotropic behaviour in clays: clay mineralogy, time, rate of loading, axial strain and water content and the gain of thixotropic strength varies based on these factors. Thixotropic strength gain in clays has been studied by several researchers from various points of view. For example, Banas (1991) and Zhang, Kong, Yang, and Sayem (2017) investigated from macroscopic and/or microscopic angles. Skempton and Northey (1952) focused more on the sensitivity of clays, Seed and Chan (1959) investigated the time-dependent strength gain in compacted clays.

W. Miller, Scott, and Segoo (2010) studied the thixotropic behaviour of clay-rich FFT and the physiochemical effect produced by repulsive-attractive forces in oil sands tailings. Their study concluded that the pore water chemistry has a minor influence on the geotechnical properties of FFT but governs the development of thixotropic strength. Jeeravipoolvarn (2010) stated that the undrained shear strength is most apparent at lower effective stresses (as a result of chemical effects in FFT where the electrochemical interactions between particles govern), and the physical forces dominate the behaviour of oil sands tailings above 10 kPa. Mizani, Simms, and Wilson (2017) studied the effect of this phenomenon on the consolidation behaviour of FFT and reported on the detrimental effect on the long-term performance of this material. While the thixotropic behaviour of clay particles in FFT leads to building up bond or gel strength and developing a fines matrix with an overconsolidated structure, it can also prevent them from further compression and

releasing water by holding the fine clay particles together (W. G. Miller, 2010; James K Mitchell, 1961; J.D. Scott et al., 2013).

2.8 Consolidation and Permeability Testing on Soft Clays and Slurries

Performing consolidation tests on FFTs can be very challenging for various reasons such as low solids content, high compressibility, presence of fine clay particles, etc. To alleviate the problems that might arise from the unique properties, mineralogy and chemical composition of tailings, laboratory devices capable of accommodating large strains and applying low loads (equivalent to low range of effective stresses) at the early stages of the tests are needed as at this stage tailings would have high void ratios.

Consolidation and permeability of soft soils can be measured in the laboratory, either directly or indirectly. The following sections explain different methods used to measure hydraulic conductivity and compressibility of soft clays and tailings.

2.8.1 Direct Methods to Determine the Consolidation Properties

Slurry materials have high initial water contents and void ratios; hence during consolidation, these materials experience a significant volume change. Most consolidation testing procedures are based on Terzaghi's small-strain, or infinitesimal strain, theory with few limitations, i.e. negligible compression and self-weight, which makes the theory inapplicable for tailings. Therefore, the consolidation testing of these materials becomes a challenge.

The consolidation behaviour of FFT in the field can be very different from the laboratory experiments. Dobroslav Znidarčić, Miller, Van Zyl, Fredlund, and Wells (2011)

elucidated this discrepancy, even though their hypothesis is not proven, as, at low hydraulic gradients, the water might not be governed by Darcy's law or the relationship between the discharge velocity and the hydraulic gradient is nonlinear. In 1960, a "threshold-gradient" concept was introduced by Hansbo (1960), suggesting that when the hydraulic gradient is very low, the hydraulic conductivity of soil will significantly be reduced (even equal to zero). Non-linear finite strain theory acknowledges the validation of Darcy's law, and maybe exploring the "threshold-gradient" concept might be helpful to understand this discrepancy in the consolidation behaviour. The authors also suggested that instead of the macro-scale behaviour of FFT, the reason for the discrepancy might also be micro-scale; the balance of attractive and repulsive forces at the particle level and their interaction with the surrounding fluid might explain why FFT exhibits threshold-gradient phenomena.

2.8.1.1 Step-loading Test

Step-loading, or standard oedometer test, was initially proposed by K. Terzaghi (1927) to determine the effective stress-void ratio relationship for one-dimensional consolidation problems. The specimen is subjected to incremental loads while the vertical deformation is monitored. The procedure adapts the small-strain theory, and both the compressibility and the coefficient of consolidation are assumed to stay constant during the test; therefore, the standard oedometer test is not applicable to fine tailings (material is highly compressible with low permeability (S. A. Proskin, 1998; Nagula Naguleswary Suthaker, 1995)).

Four different methods are applied to determine the coefficient of consolidation; Terzaghi's method, the square root of time fitting method, the logarithm of time fitting

method, and the linearized finite strain procedure. All these methods assume constant compressibility and coefficient of compression values during testing, which would lead to major restrictions on the applicability of the analytical procedures (Dobroslav Znidarcic et al., 1984a). The hydraulic conductivity is not measured directly but back-calculated (from deformation vs time input) utilizing Terzaghi's consolidation theory.

Preferred due to its simplicity; however, the duration of the procedure is an apparent disadvantage. Another two main concerns about this procedure for fine-grained material is that large strains take place during testing, and the determination of hydraulic conductivity may cause seepage-induced consolidation. Also, self-weight consolidation is associated with FFT consolidation, which cannot be explained by Terzaghi's consolidation theory (S. Proskin, Segó, & Albstaz, 2010).

2.8.1.2 Slurry Consolidometer

The slurry consolidometer was developed as an alternative to the standard oedometer, which follows the conventional large strain consolidation theory (Monte & Krizek, 1976). The test is adjusted for the soils experiencing large strains, i.e. low solids content MFT specimens, which are under effective stresses up to 100 kPa from self-weight consolidation (S. A. Proskin, 1998). Instead of applying large strains, smaller strains can be applied to the specimen (Bromwell & Carrier III, 1979; Salem & Krizek, 1973; J Don Scott, Dusseault, & Carrier, 1986) to determine the effective stress-void ratio and hydraulic conductivity-void ratio relationships. The procedure is similar to the standard oedometer test – step loading procedure is applied – direct determination of stress and permeability versus void ratio is allowed. Pollock (1988) stated that the applied stress range is extensive;

0.2 kPa to 400 kPa, which requires two different loading systems; for low stresses, a rod and a plate device are used, and for high stresses, a compressed air system is used to transfer the compressed air pressure to a loading ramp. Jeeravipoolvarn (2005) reported that the applied stress range could go up to 1000 kPa.

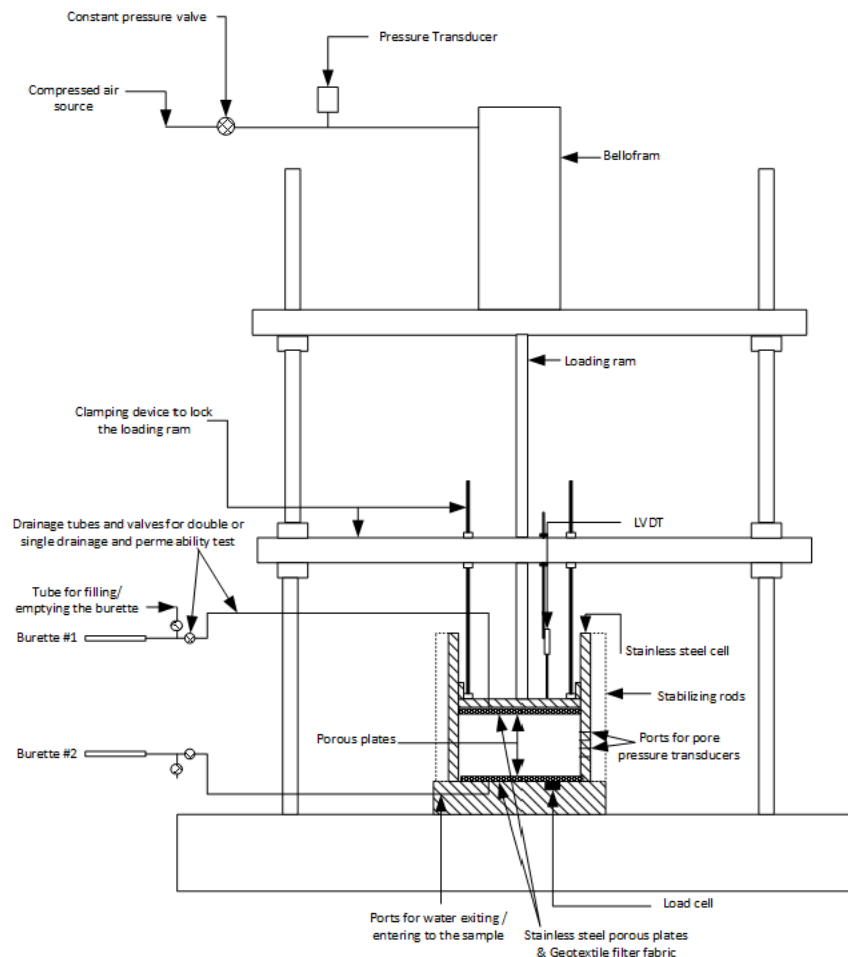


Figure 2-5: The schematic diagram of slurry consolidometer – modified Pollock (1988)

The schematic diagram of the slurry consolidometer (after Pollock (1988)) is presented in Figure 2-5. The specimen initially goes through self-weight consolidation while the bottom drainage port is open along with the top drainage port allowing double

drainage. Once the self-weight consolidation is complete, the top cap was lowered until it reaches the sludge-water interface (the top cap is required to obtain a seal for the hydraulic conductivity testing). The clamping system is utilized (described in the following paragraph) to secure the top cap. For the self-weight consolidation stage, the flow for constant head permeability is upwards in order to prevent seepage-induced consolidation. Once the desired head difference is achieved in the inflow and outflow burettes, the valves are opened, and the flow is monitored. Once the permeability testing is complete, a test for top cap friction is performed (to determine the required load necessary to achieve the desired stress plus friction). The top cap is then released from the clamping system, and load is applied to the sample. The load and the pore pressures are measured from the pressure cell in the base of the cell as well as through the pressure transducers attached to the pore pressure ports. At the same time, LVDT (linear variable differential transformer) monitors the displacement of the sludge surface. By knowing the solids content in the cell, the void ratio of the specimen can be determined. Once the consolidation of the increment is complete, the top cap is clamped back, and the permeability testing for the determined void ratio can be established. The process is then repeated with increasing loads.

The main difference from the standard oedometer test is the ability to measure hydraulic conductivity directly through the use of constant head tests after each increment (constant head test allows for extremely small head drops, less than 1 cm). One of the disadvantages of the step loading test is the possibility of seepage-induced consolidation during conducting permeability tests, which can be prevented using the load fixing device presented by Scott, Dusseault et al. (1986). Pollock (1988) utilized a clamping system to overcome this problem, which prevents movements from occurring during testing. This

clamping system is used to fix the loading cap prior to the permeability test, and a gradient is applied to the sample. The system then allows the hydraulic gradient to be applied to the sample (up until the applied consolidation pressures are equal to the induced seepage stress since, beyond that, the prevention of gradient seepage induced consolidation is not possible). The constant head test must be repeated until it reaches a constant permeability value for MFT samples since the soil behaves such that the permeability is a function of time (Estepho, 2014). Repeating the constant head tests for each data point can be very time-consuming.

The major disadvantage of this test is the extended duration of the procedure; applying smaller strains extends this duration even further. The consolidation behaviour of MFT is known to be very slow, and in order to avoid disturbing the samples, the step loading was increased slowly. For example, the experiments conducted by Pollock (1988), Nagula Naguleswary Suthaker (1995) and Jeeravipoolvarn (2005) demonstrated that the duration of the test is between one to two years for MFT samples. Several researchers tried to improve the duration of the test; one of the procedures is presented by Umehara and Zen (1980) and Zen and Umehara (1986), combining slurry consolidometer with CRD test procedure based on the finite strain consolidation theory of M Mikasa (1963). Unfortunately, their analysis requires a constant compression index and coefficient of consolidation during testing.

2.8.1.3 Constant rate of deformation (CRD)/ Constant rate of strain test

Also known as the constant rate of strain test, the CRD test is first introduced by C. B. Crawford (1964) based on the assumptions of constant hydraulic conductivity, linear

compressibility and infinitesimal strain consolidation theory. Hamilton and Crawford (1960) established significant differences between void ratio and effective stresses, which are dependent on the rate of deformation in the test. To prevent the development of excess water pressures, which existed in their specimen, the test should be performed at a slow rate. They also did not measure the pore water pressures; hence the effective stresses were unknown. Infinitesimal strain theory and constant coefficient of consolidation are not the only assumptions of the original CRD test; void ratio distribution of the soil sample or void ratio with time must be assumed (which cannot be validated), making the original CRD test procedure too restricting for slurry-like materials (Dobroslav Znidarcic et al., 1984b). Several processes are suggested to analyze CRD tests; Smith and Wahls procedure (Smith & Wahls, 1969), Wissa procedure (Wissa, 1971), Umehara and Zen procedure (Umehara & Zen, 1980) and Lee Procedure (Lee, 1981).

Scully, Schiffman, Olsen, and Ko (1984) confirm the previous results of Goro Imai (1981) and K Been and Sills (1981) regarding the dependency of compressibility on the initial void ratio and the effect of pre-consolidation to the compressibility curves. However, the authors accepted that more work is needed for soils with high void ratios to examine the hydraulic conductivity measurements obtained by the CRD test (too high or not).

Znidarčić, Schiffman et al. (1986) modified the CRD testing for very soft, remoulded clays and used non-linear finite strain consolidation theory. Since the presence of air bubbles can affect the porewater pressure reading, the specimen and the device should be free of air, which is accomplished by flushing the lines with water and by applying backpressure. After an overnight interval, a constant deformation rate is applied to the specimen triggering the consolidation process. During this process, the bottom

boundary is undrained, but drainage is allowed at the top, where continuously increasing load is applied to generate a constant rate of compressive strain. The measurements of excess pore water pressures and stresses are taken at the top boundary, and through an inversion, the consolidation properties are determined using the measured data.

Carrier III et al. (1983) utilized a constant rate of strain consolidometer to determine the consolidation properties of tailings; however, measured conductivity from this testing device is not accurate. Based on Carrier III, Bromwell et al. (1983)'s concepts, Cargill (1986) developed a new apparatus, large strain, controlled rate of strain (LSCRS) for fine-grained soils. LSCRS can monitor the excess pore water pressures during the procedure by using multiple ports (placed in positions where they spiral around the chamber to reduce the tendency for short drainage circuits) along with the sample chamber. It also has the ability to measure the self-weight consolidation and a small range of stress for the surcharge application. The author tried to directly solve the governing equations using a computer program called the controlled rate of strain test (CRST) to determine the relationship of void ratio-permeability and void ratio-effective stress by using the pore water pressures of the sample throughout the procedure. Self-weight consolidation of fine-grained materials is a time-consuming process. Therefore, the main disadvantage of this apparatus is the duration of testing. In addition, at each loading step, excess pore water pressures must be dissipated when the surcharge is applied, resulting in an increase in the duration of the procedure (Janbaz, 2016).

Caughill, Morgenstern, and Scott (1993) applied the CRD test to oil sands tailings but abandoned the procedure due to the water leaking occurring at the top piston (a combination of low friction with an effective seal is required for the loading piston; hereby,

the piston friction and the applied stress are not required to be evaluated). The authors recommended not to follow ASTM D-4186 and the procedure by Smith and Wahls (1969). Also, the excess pore pressures should remain between 3-20% and less than 50%, respectively, of the applied stress. The authors tested material with larger pore water pressures than the recommendations and concluded that the effect of pore water pressures on the test is vague, and the analysis of the text is complex.

The major advantage of the method is the shortened duration of the test compared to the step-loading test (i.e. for clays, the conventional method can take days to finish, whereas the CRD test is done in a matter of hours). Also, it is simpler to instrument compared to the constant hydraulic gradient test. However, there are also few points to be considered for soft slurries; the effect of self-weight consolidation should be accounted, a total stress cell with better piston seal should be implemented (requiring more elaborated instrumentation compared to the multi-step loading test), and finally, the test is originally designed for normally consolidated clays. Hence more appropriate extensions should be enforced for over-consolidated clays.

2.8.1.4 Controlled gradient test/ Constant hydraulic gradient test (CHG)

Originally developed by Lowe, Jonas, and Obrican (1969), the procedure is similar to the CRD test; the drainage is allowed on top, and the pore water pressure values are measured at the bottom boundary. In this test, a complex feedback mechanism is needed in order to continually adjust the loading rate (so that the pore water pressures and hydraulic gradient remains constant through the sample). The controlled gradient test adopts infinitesimal strain theory while the permeability and the void ratio are assumed to be constant and the

compressibility of the sample is linear (Ahmed & Siddiqua, 2014; Khan & Azam, 2016; Nagula Naguleswary Suthaker, 1995; D Znidarčić et al., 1986).

Initially, a load P is applied to the sample, increasing the pore water pressures by an amount of Δu . Since drainage is allowed at the top, eventually, the pore water pressures at this boundary will drop to zero, whereas they remain constant at the bottom boundary. From this point on, the load is slowly increased in a way that the pore water pressure distribution remains constant through the sample. After reaching the desired P -value, loading is stopped, and pore water pressures are allowed to dissipate. The change in the height of the sample is recorded during compression. Also, the elapsed time is recorded when the pore water pressures at the bottom boundary reach $0.1\Delta u$ (Das, 2013).

The duration of CHG is less compared to the standard oedometer test; however, the required feedback mechanism complicates the necessary laboratory equipment. Another complication may be the unknown loading rate at the beginning of the test. Theoretical limitations are similar to the standard oedometer test. Therefore, CHG is not appropriate to determine the consolidation process of tailings (Znidarcic, Croce et al. 1984, Khan and Azam 2016).

2.8.1.5 Constant rate of loading test

Based on the theoretical work of R. Schiffman (1958), this technique is first introduced in Aboshi, Yoshikuni, and Maruyama (1970) to determine the consolidation properties of low-density slurries. Initially, a total pressure on the specimen is assumed to be applied steadily at a rate of λ per unit time (over a period of time of t_f), which would be equal to the initial pore water pressure at the beginning of the test. This type of constant loading is

also known as the ramp loading. Then, in an infinitesimal time period, applied pressure on the specimen becomes λdt , resulting in an increase in pore water pressures. The pore water pressures as assumed to be distributed uniformly and some of this excess pore water pressures will be dissipated until it reaches to t_f (Sivakugan, Lovisa, Ameratunga, & Das, 2014). Olson (1977) extended Terzaghi's one-dimensional consolidation theory for ramp loading to develop a different expression to determine the average degree of consolidation during the loading and after the final time period, t_f . Olson's theory was extended by Hsu and Lu (2006), which allowed the coefficient of consolidation to vary with regards to applied pressure.

The most important advantage of this test is the shortened duration of the procedure, the consolidation-void relationship acquired from the constant rate of loading test is faster compared to the CRD test. The theoretical restrictions of the method are similar to CRD and CHG tests (constant hydraulic conductivity and coefficient of consolidation); therefore, not applicable for materials experiencing large strains. Also, the analysis is only reliable if the void ratio remains constant through the test, which may limit the rate of loading (Dobroslav Znidarcic et al., 1984a).

2.8.1.6 Continuous Loading Tests

Developed as a variation to CRD, CHG, and constant rate of loading test, in this procedure, the ratio of applied load to excess pore water pressure is kept constant (Janbu, Tokheim, & Senneset, 1981). In order to satisfy that condition, a feedback mechanism is required, which complicates the laboratory equipment. Khan and Azam (2016) established that the

hydraulic conductivity (assumed to be constant) and the compressibility could not be validated, and the procedure is not applicable to tailings due to theoretical restraints.

2.8.1.7 Seepage-Induced Consolidation Test (SICT)

Originally proposed by Goro Imai (1979), a new technique is introduced to determine consolidation parameters by applying a seepage force; applying a constant head difference to the sample results in the consolidation of the soil in a consolidometer for fine-grained sediments. He stated that the compression curve could be determined if the velocity of flow, the water content profile and the distribution of pore water pressures are established. The original apparatus is capable of employing very low stress ranges from 0.01 kPa to 50 kPa. Imai's setup demonstrated that the permeability affects the duration to reach the steady-state conditions. Hence the final height of the specimen is dependent on the void ratio along with permeability. Originally, the void ratio profiles are determined by slicing the sample or by monitoring pore water pressures during the consolidation process.

In 1988, Huerta, Kriegsmann, and Krizek (1988) proposed a one-dimensional mathematical model based on finite strain theory to determine the permeability and compressibility relationship for soft sediments. This inverse solution utilizes only the final settlement of the sample and the steady-state conditions, eliminating the need for slicing the sample to obtain consolidation properties. Huerta's approach to solving the governing equation was a breakthrough for the consolidation of soft sediments because the usage of the seepage force to induce consolidation and the measurement of permeability during the test eliminated the permeability-related problems observed in other consolidation apparatus during testing.

D Znidarcic and Liu (1989) implemented Imai's approach (for the testing apparatus) with Huerta's model (to obtain the constitutive relationships) to determine the consolidation of soft soils, and their analysis was in complete agreement with the non-linear theory of consolidation.

A. N. Abu-Hejleh, Znidarcic, and Barnes (1996) employed complete testing and the analysis of consolidation for very soft Phosphatic clays by measuring the zero-effective stress void ratio (based on the sedimentation test), the final height and the bottom effective stresses as the sample reaches a steady-state condition. These three measurements represent the experimental data in the low effective stress range, and the constitutive relations of these data are highly nonlinear. To determine the soil consolidation parameters, they applied a parameter estimation scheme for steady-state conditions.

Fox and Baxter (1997) proposed closed-form equations for the distribution of pore pressure, effective stress at steady-state flow conditions and for discharge velocity. Their approach is based on three assumptions; compression and flow are one-dimensional, one-to-one linear relationship between the logarithm of effective stress and logarithm of permeability exists, and the effect of side friction and self-weight to the distribution of total vertical stress is minimal compared to the applied pressure difference. This approach eliminates the need for specialized numerical solutions to calculate the desired constitutive relationships. However, this approach cannot be used for tests where the top effective stress is zero. Fox and Baxter (1997) also presented a piecewise-linear model, called CS4, for one-dimensional consolidation of an accreting soil layer, considering the effects of vertical strain, self-weight, variable compressibility and hydraulic conductivity during the consolidation process. However, the main disadvantage of the model is its inability to

accurately model the behaviour of high void ratio materials at the early stages of consolidation.

Sridharan and Prakash (1999) developed a simple test setup to determine the consolidation of soft sediments at low effective stress levels, based on Imai's method. The main difference between these two apparatuses' is the determination of average void ratios. Imai's method considers varying void ratios along with the specimen, whereas the proposed method uses an average void ratio at a certain applied pressure. The average void ratio is determined once the settlement becomes negligible after steady-state conditions are maintained and associated with that applied pressure. The authors also conducted a permeability test after each hydraulic gradient.

Numerical models to determine the consolidation behaviour based on the seepage-induced consolidation technique have been actively researched since the 2000s. D. T. Yao, de Oliveira-Filho, Cai, and Znidarcic (2002) proposed a software after the work by A. N. Abu-Hejleh and Znidarčić (1995). Barbetti (2009) proposed an automated version of a consolidation device, initially introduced by N. A. Abu-Hejleh and Znidarcic (1994), using the program called SICTA developed by A. Abu-Hejleh and Znidarcic (1992). This method is capable of seepage-induced consolidation for low effective stress ranges. Compared to the previous methods, this proposed method, time-wise and procedure, is the best method to determine the consolidation of fine-grained soils.

Dobroslav Znidarčić et al. (2011) expanded their work on consolidation analysis using seepage-induced consolidation test for oil sands tailings. The authors mentioned that the presence of residual oil on the sample could create some difficulties during preparation and testing. However, FFT behaves similarly to regular soil slurry, which can be described

by the finite strain theory. The results demonstrated that SICT is capable of determining the consolidation of mature fine tailings, which is useful to understand the behaviour of high void ratio materials. Estepho (2014) combined the SICT apparatus (Znidarcic' setup) with the CONDES0 program to analyze the consolidation behaviour of oil sands slurry tailings, and the results are repeatable and comparable to the other published data.

This testing technique imposes a downward seepage force through the specimen, which results in a pressure difference across the sample, and the consolidation occurs as a result (A. N. Abu-Hejleh et al., 1996; Berilgen, Berilgen, & Ozaydin, 2006). Flow can be initiated using either a controlled head system or a flow pump (which might be more advantageous due to precise control of low flow rates, rapid response time and better suitability for automatic operation and data procurement (Aiban & Znidarčić, 1989; Olsen, Nichols, & Rice, 1985). In order to increase the degree of saturation of the slurry, back pressure is applied to the specimen, allowing the measurement of material properties over a more extensive effective stress range. However, the application of backpressure might increase the possibility of sidewall leakage problems in the consolidation cell. This might be avoided by replacing the cell inside a pressure chamber (A. N. Abu-Hejleh et al., 1996; Fox & Baxter, 1997). It is also recommended to apply a surcharge load prior to flow since it eliminates the zero-effective stress condition at the top to reduce the change for sidewall leakage (A. N. Abu-Hejleh et al., 1996; Baxter, 1994). The initial surcharge load (approximately 1 kPa is recommended by Fox and Baxter (1997) can be applied in one increment, if a more significant surcharge is required, it must be applied in several daily increments) applied on top of the specimen.

The two-stage flow procedure of the seepage-induced consolidation test is described in Fox and Baxter (1997) as follows. Prior to pouring the specimen into the consolidation cell, the entrapped air must be removed using a vacuum during the preparation of the specimen. The initial height and the void ratio of the specimen are measured before applying the surcharge load. The apparatus should be designed to prevent tipping of the surcharge load, which can be achieved by fixing the load plate to a laterally supported piston. For MFT, there is an additional step at the beginning (Dobroslav Znidarčić et al., 2011), the sample is allowed to consolidate under its own weight, and the void ratio at the effective stress of zero is determined (the void ratio of the settled slurry is considered the void ratio at effective stress of zero). For the first stage of the test, a downward hydraulic gradient is applied across the sample, resulting in a significant variation in effective stress. Once it reaches the steady state, the final height, discharge velocity and effective boundary conditions are recorded. Then for the second stage, the applied hydraulic gradient is increased (doubling the hydraulic gradient is recommended). The flow is discontinued, and the apparatus is disassembled immediately as soon as the specimen reaches a steady-state condition to reduce the possibility of swelling. The specimen is then sliced to determine the local water content distribution; local void ratios are calculated based on the assumption that the specimen is fully saturated. The schematic of this testing method is presented in Figure 2-6.

The pressure differences are continued to be measured until a steady-state condition is reached. In order to determine the void ratio distribution throughout the sample, the specimen is sliced (Dobroslav Znidarcic et al., 1984a). The proposed theory is a direct measurement technique since it is not based on a consolidation theory.

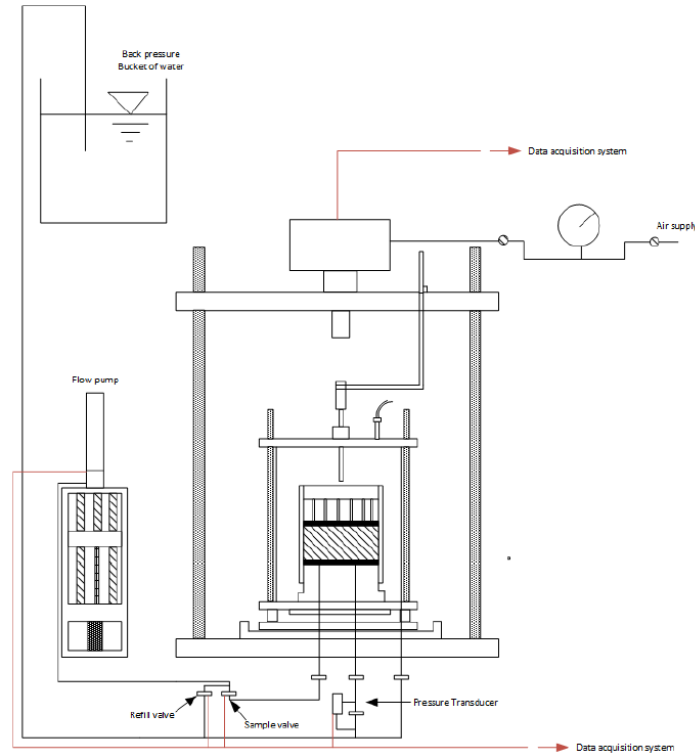


Figure 2-6: Seepage Induced Consolidation testing apparatus (modified from Estepho (2014))

There are few disadvantages of the procedure, i.e. some rebound might occur during the slicing of the sample; therefore, the measured void ratios might be slightly higher. Considering the duration of other apparatus, according to D Znidarcic and Liu (1989), the seepage-induced consolidation test reduced the duration significantly while providing better quality data for soft sediments. Fox and Baxter (1997) established that the duration of the SICT procedure is 75% shorter than the step-loading consolidation test. There are few more setbacks of this procedure for MFT, and the obtained results demonstrated that the hydraulic conductivity values are very small, increasing the duration of the procedure. Another problem is the presence and release of oil blobs during testing, the test must be analyzed with great detail to make sure it doesn't affect the obtained results.

2.8.1.8 Centrifuge Tests

Centrifuge tests are essentially self-weight consolidation tests performed in a centrifuge to simulate the behaviour of slurries in the field, most suitable for geotechnical structures where gravity is the main driving force (Masato Mikasa & Takada, 1984; YOU & Znidarcic, 1994). They are mainly conducted to examine self-weight consolidation, deriving consolidation parameters, generating data for numerical models and derive time-scaling relations between models and prototypes. Small scale models are subjected to an acceleration in a centrifuge where the acceleration speed is much higher than the gravity itself (Sorta, 2015). The schematic of the geotechnical beam centrifuge is presented in Figure 2-7.

Historically, geotechnical centrifuge testing has been studied for the large strain consolidation behaviour of clays by Bloomquist and Townsend (1984) and Masato Mikasa and Takada (1984) in the early '80s and by You and Znidarcic (1994) in the '90s. The theoretical investigation of the consolidation process in a centrifuge has also been studied by comparing the results with the experimental data during that time (Croce et al., 1985; Masato Mikasa & Takada, 1984).

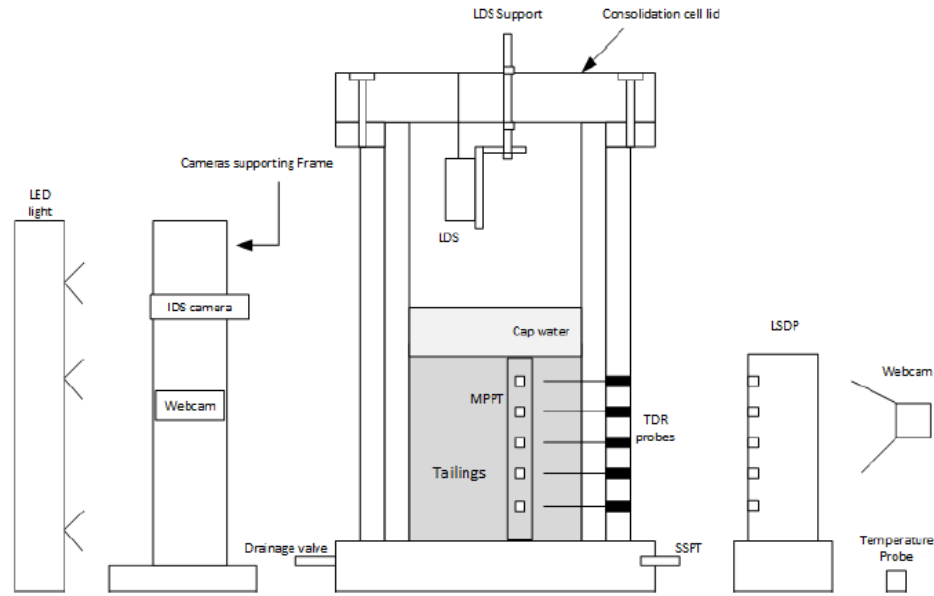


Figure 2-7: Schematic of centrifuge test setup(after Sorta, Segó, and Wilson (2012))

The same stress levels are to be maintained between the prototype and the model, and to achieve the same level stress values, due to self-weight consolidation, the thickness of the model can be decreased, or the unit weight of the sample can be increased. The objective of the test is to represent the field behaviour; therefore, the same material is used in the model (hence the density of the soil is the same). To be able to achieve the same unit weight, the gravitational acceleration is artificially increased by rotating the sample on a nearly horizontal plane in the centrifuge. Small-sized models in centrifuge modelling can be used to represent prototypes. A height scale factor of $1/N$ represents the ratio of model height to prototype height. The recommended maximum height to radius ratio for centrifuge modelling is less than 20%. Deformation is expected to be in the height scale factor between the model and the prototype, whereas the strain and pore water pressures remain the same. The height of the model is chosen based on these considerations; centrifuge capacity and payload volume, the height of the prototype while reducing the

sidewall friction and related modelling errors. To increase the centrifugal acceleration, in order to maintain the same stress, the acceleration is increased by the factor N (Sorta, 2015).

A number of different centrifuge tests are conducted at different initial solids content, and consolidation parameters are mainly determined from the water content profiles at the end of each test. The determination of density profile in the geotechnical centrifuges is not well documented in the literature. As a result, this testing method is limited to measuring settlement and pore pressures (Hurley, 1999). Bench-top centrifuges are used to model self-weight consolidation and determining consolidation of soft soils, whereas beam-type centrifuge tests are conducted to model sedimentation and self-weight consolidation of slurries/soils. Both types of centrifuges are mostly used on kaolinite (rather than natural soils), but only a few experiments were conducted on MFT using both types of centrifuges. During testing, interface settlement (utilizing laser displacement sensors), pore pressures and solids contents (using time-domain reflectometry, if in-flight measurements of solids content are utilized, there's no need to running a number of centrifuge test at different initial solids content) were recorded. Based on the measurements, the consolidation parameters can be calculated. Solids content can also be determined after slicing the samples at the end of the test by oven drying (Sorta 2015).

The main advantage of this technique is the short duration of testing. Self-weight consolidation of tailings ponds can take years to complete, whereas the same consolidation is achieved in hours during centrifuge testing. Another advantage of this test is the flexibility with the boundary conditions (different drainage conditions – one-way, two-way or seepage-drainage – can be easily used in the model. It is also relatively easier to extend from one-dimensional to two or three-dimensional modelling. It is easily instrumented,

controlled better, and the soil conditions are more uniform compared to prototype testing. It's useful to validate numerical modelling results if a prototype is not available by using the scale effect (to relate the model and prototype, centrifuge testing has theoretically derived and experimentally proven scaling laws). It is flexible with the conditions of the soil; inhomogeneity, layering and sequence of deposition can be modelled; also, the effects of various stress histories, stress paths and geometry conditions can be easily determined.

This testing method also has a few limitations or restrictions, such as the vertical stress distribution is not linear (R. Taylor, 2018). The radial acceleration field also creates a horizontal stress component during testing (Beriswill, Bloomquist, & Townsend, 1989). The nonlinear properties of the soil are dependent on the effective stresses and the stress history; therefore, maintaining the same stress in the model is crucial for these tests. Selecting a proper time scale can be tricky for centrifuge tests; time scales for weight force are not the same for the inertial force or the viscous force. Therefore, the user needs to identify which force governs the problem, and it is important to select the right timescale factor (Croce et al., 1985; R. Taylor, 2018). Centrifuge testing may also enhance the segregation of the particles; therefore, prior to run the flight tests, the segregation behaviour of the slurry might need to be evaluated at high gravity. The test has limitations in terms of modelling the influence of chemical effects, creep and thixotropy, which are highly time-dependent phenomena. The effects of side friction can be problematic in some cases, but it can also be minimized by increasing the ratio of width to height of the model or by applying proper lubrication to the internal size of the container. Instrumentation of measuring soil properties is not well developed for centrifuge modelling. It requires lightweight, small-sized instruments that have high sensitivity and range of measurements. Obtaining accurate

measurements of physical properties is essential compared to the other tests due to the scaling of the model. The rate of strain is expected to be higher than the conventional tests, which can influence the properties of the material dependent on the strain rate. The permeability calculation depends on a self-weight induced hydraulic gradient, which is not constant along with the height of the model and during the process. It can be obtained from slicing the sample to determine the water contents or indirectly calculating it through the iterative numerical model to match measured pore water pressures (Reid & Fourie, 2012). Compared to other conventional testing methods, centrifuge modelling is only available in individual research facilities or universities. Installation, operation and the instruments of this experimental method are expensive.

Similar to other consolidation tests, the MFT samples require more complex instrumentation, monitoring, data interpretation along with longer flight hours. A contact-type displacement transducer cannot be used since the material doesn't have enough strength to carry its' weight. There's also another argument on scaling the coefficient of permeability; some others indicate to scale it up to the acceleration level, whereas others argue that it's a soil parameter independent of the gravitational acceleration. It also has been reported to conduct the centrifuge tests after waiting for a day to enhance the segregation behaviour of MFT without changing their initial solids content (Sorta et al., 2012).

2.8.1.9 Hindered Settling and Self-weight Consolidation Tests

Hindered sedimentation tests were completed to measure the settling velocity of the interface between supernatant water and the slurry. These tests also have been used to

determine the hydraulic conductivity -void ratio relationship at large void ratios by correlating the settling velocity with hydraulic conductivity and void ratios. Kenneth Been (1980) and Pane and Schiffman (1997) provided the following model to determine the hydraulic conductivity values of clay suspensions calculated using the falling interface velocity.

$$v_s = -\left(\frac{\gamma_s}{\gamma_w} - 1\right) \frac{k}{1+e} \quad (2.9)$$

where v_s is the initial settling velocity, k is hydraulic conductivity, e is the void ratio, γ_s is the unit weight of soil and γ_w is the unit weight of water. The authors stated that this equation is only valid as long as the settling velocity is constant or if there is a suspension at the initial void ratio at the sediment-water interface.

A similar equation is proposed by Tan et al. (1990) based on Kynch (1952)'s theory, where a non-linear part of the settlement curve is utilized to determine the hydraulic conductivity. This analysis requires surface solids concentration, which might be challenging to determine.

$$\left(x + t \frac{dx}{dt}\right)_p = \frac{M}{\eta_c} \quad (2.10)$$

where x is the height, M is the total mass of solids, t is time, η_c is the concentration, and subscript p indicates a point in the settlement curve.

Renko (1998) derived the equation proposed by Tan et al. (1990), and the reformulated version of the model, using void ratio and height rather than solids concentration, is presented below.

$$e = \frac{(1 + e_0)(h_{int} + v_{sp}t)}{H_0} - 1 \quad (2.11)$$

where H_0 is the initial height, h_{int} is the height at interest point, e is the void ratio, e_0 is the initial void ratio and v_{sp} is the tangential velocity.

Hindered sedimentation tests and models are well accepted if the slurry is going through hindered sedimentation. However, they are usually not believed to be valid during the consolidation of soft soils. Toorman (1999) reported that if the diffusive effects are negligible, the hydraulic conductivity of soil can be determined from the initial settling rate. One-dimensional finite strain consolidation theory also provides a constant initial settling velocity for high initial void ratios. Therefore, the equation proposed by Pane and Schiffman (1997) may provide acceptable k values at a high initial void ratio during the consolidation phase. However, this is only acceptable up to a certain void ratio (until compressibility becomes large); past this limit, determination of hydraulic conductivity can be achieved during a large consolidation test.

Self-weight consolidation column tests or standpipe tests were usually conducted for two reasons: theoretical validation and compressibility determination. Similar to hindered settlement tests, these tests are usually performed in cylindrical cells and assume to be under one-dimensional consolidation. For theoretical validation, measurement and evaluation of water-slurry interface, pore water pressures, void ratios (or solids contents), and total stresses are imperative during sedimentation and consolidation phases. For compressibility analysis, the soil is usually sampled in layers at the end of the consolidation process; the measured void ratio is correlated with the effective stress (J. Scott, Jeeravipoolvarn, & Chalaturnyk, 2008; Scully et al., 1984). Another method to determine

compressibility is the direct measurement of pore water pressures and density and continuously evaluate the effective stress and void ratio (G Bartholomeeusen et al., 2002; K Been & Sills, 1981).

The side-wall effect and the accuracy of density/ solids content measurements may create complications for self-weight consolidation columns (Jeeravipoolvarn, 2010). The effect of side-wall friction has been investigated by various researchers. K Been and Sills (1981) observed this effect for mud at high void ratios (varying from 4 to 10) and reported that the effect is negligible. Caughill et al. (1993) and D. M. Elder (1985) studied the ratio of column diameter to height to minimize the effect of side-wall friction. D. M. Elder (1985) stated that the effect would be negligible for column diameters 100 mm and above. However, he only studied column heights that vary from 50 mm to 200 mm. Therefore, the effect of side-wall friction may not be negligible for taller columns with a diameter of 100 mm. At the same time, Caughill et al. (1993) found that this ratio should be higher than 2:1 for small void ratios. Since the effect of side-wall friction is a result of self-weight vertical stresses, deeper the column height higher the effective stresses (hence higher the effect of side-wall friction) would be during consolidation. Therefore, the results presented by Caughill et al. (1993) are more generic and may be more acceptable. For cohesive material such as FFT, the effect of side-wall friction may be influenced even at low effective stresses due to the adhesion of the material to the wall (Jeeravipoolvarn, 2010).

Jeeravipoolvarn (2005) and Jeeravipoolvarn (2010) reported on the compression behaviour of both amended and non-amended oil sands tailings for the long-term behaviour of three large-scale standpipe tests; the experiments were commenced in 1982. One standpipe is only filled with non-amended FFT, whereas the other two consist of a mixture

of oil sands tailings and tailings sand. These tests have been one of the longest-running tests (observed for 25 years) and the largest ones in scale, as the standpipes are 10 m high with a 0.9 m in diameter. The outcome of these self-weight consolidation tests provided a good insight into the long-term performance of FFTs and the effects of entrained tailing sands on the consolidation behaviour.

2.8.1.10 Relaxation Indentation Tests

Relaxation tests were first proposed by K. v. Terzaghi (1923) to be performed on a sample at a non-steady state condition. In order to reach this initial condition, the specimen can be deformed at an imposed rate, or a load can be applied to it. Once the specimen is in a non-steady state, further deformations on the soil are prevented, and the test begins. During the test, the parts of the specimen will consolidate, while some parts will swell. Therefore, the assumptions of monotonic loading are violated, which creates a significant objection to the theory (governing equations are based on monotonic loading). This condition requires appropriate mathematical theory for it to be treated appropriately, and until this restriction is resolved, the relaxation tests are not appropriate for determining consolidation parameters.

2.8.1.11 Inter-connected Consolidometer Tests

G. Imai and Tang (1992) developed an inter-connected consolidometer to determine the consolidation parameters of remoulded marine clays.

The consolidometer aimed to interpret the effect of layer thickness on the compression behaviour. Several thin sub-specimens are prepared in separate

consolidometers (up to 10) and loaded to different loads while their drainage channels are connected. The pore water pressures between adjacent sub-specimens in the consolidometers and settlement in each consolidometer are measured during the test. The compressibility and permeability of the soil are calculated from pore pressures, settlement and water flow velocities. The setup is even more sophisticated than seepage-induced consolidation tests, and inter-connected consolidation test is not capable of providing consolidation data at low effective stresses (less than 10 kPa) (Estepho 2014). The hydraulic conductivity is evaluated by using direct measurements of the hydraulic gradient, and the velocity of water at different locations in the specimen is determined.

2.8.2 Indirect Methods to Determine the Consolidation Properties

The indirect determination of consolidation properties has been a point of interest for various researchers. There has been extensive work on using simple correlations from easily measured properties (i.e. Atterberg limits) to estimate these parameters. The application and the performance of these models are presented in Chapters 3 and 4 in more detail.

Merckelbach and Kranenburg (2004) tried to estimate these constitutive relationships of clay-silt-sand mixtures. The authors derived the equations on the basis of the scale-invariant structure of the tested soil. The equations were verified with experimental setups, and they used physical interpretation to improve the empirical coefficients in their models. The model provided accurate results for effective stresses, but the performance for permeability was only adequate.

Wong, Mills, and Liu (2008) proposed a logical mechanistic explanation for the consolidation behaviour of nonsegregating tailings. They divide the consolidation process into three stages: suspension of sand particles in a fines matrix, the formation of local contact between the sand particles, and coarse grain skeleton formation. They have also investigated the effect of sand and fines compressibility on the compressibility of nonsegregating tailings. Similar to Pollock (1988), they have also investigated the use of fines void ratio to general permeability of the soil.

Determining hydraulic conductivity from standard oedometer tests (soil under constant stress) using a logarithm-time plot (Casagrande, 1938) or square-root time plot (D. W. Taylor, 1948) is also possible. However, back calculating hydraulic conductivity values can cause discrepancies in the permeability of field and lab experiments. (Olson & Daniel, 1981; Tavenas, Jean, Leblond, & Leroueil, 1983).

Shunchao Qi, Chen, Simms, Zhou, and Yang (2020) developed a new method to determine the constant parameters in a power form of $k-e$ function using the measured settlement curve and the predicted curves (both in the form of log time vs. height) by a LSC model. The authors discovered two important features of the predicted settlement curve; (i) the shape of the settlement curve is independent of the multiplier but controlled by the power parameter, and (ii) if the power parameter is fixed, changing the multiplier only shifts the curve in the log time-height curve. The method only requires numerical simulations and settlement data obtained from column-like tests; it can robustly determine the $k-e$ curve but only applicable to the consolidation phase.

2.8.2.1 Soil Water Flow Theory

Soil-water flow theory is studied on a macroscopic scale; with reference to a porous medium, it is considered to be continuous, and the physical properties and quantities are functions of time and space. The reference is generally made to a Newtonian fluid phase (isothermal conditions) and an interconnected gaseous phase where the pressure is equal to the atmospheric pressure. Resistance to airflow is assumed negligible; therefore, the movement of water is the only phase to be referred to. Darcy's law represents all the conditions applying to isotropic porous media, and the velocity is a function of the hydraulic conductivity of the medium, presented in the following equation.

$$v = -k\nabla H \quad (2.12)$$

where v is the velocity, k is the hydraulic conductivity and ∇ is the Laplacian operator.

The hydraulic potential of the flow domain is represented as $H = z + h$ (where z and h are gravitational and pressure heads, respectively), and hydraulic conductivity is a function of void ratio or water content in volume θ . Pressure heads in the unsaturated zones are referred to as suction or tension and have negative values. The link between pressure head and water content is not unique but is characterized by a multi-value hysteretic function (Mualem & Dagan, 1975). When the continuity equation (Equation 2.13), coupled with Darcy's law, Equation 2.14 is obtained.

$$\frac{\partial(\rho_w \theta)}{\partial t} = -\nabla(\rho_w v) \quad (2.13)$$

$$\frac{\partial(\rho_w \theta)}{\partial t} = \nabla(\rho_w k \nabla H) \quad (2.14)$$

$$\frac{\partial \theta}{\partial t} = \nabla [k \nabla (h + z)] = \frac{\partial}{\partial z} \left[k \left(\frac{\partial h}{\partial z} + 1 \right) \right] \quad (2.15)$$

where ρ_w is water density, and t indicates the time. As the variation in water density can be neglected, the equation becomes Richard's equation (Eq. 2.15).

The soil-water flow theory can represent the water movement in unsaturated soils, and the Instantaneous Profiling Method is based on this theory. This methodology is selected to analyze the column tests presented in this study and will be covered in Chapter 5 in more detail. Analytical solutions of the equations may not provide reliable results due to the non-linearity of parameters $k(e)$ and $\theta(h)$. Therefore, an adaptation of numerical integration techniques would be necessary.

2.8.2.2 Non-destructive Measurement Techniques

State-of-art soil moisture measurement techniques can be divided into two sections: classical methods and modern techniques. Classical methods include thermo-gravimetric measurements and calcium carbide techniques (gas pressure is developed due to the chemical reaction of calcium carbide reagent, and the soil moisture is determined accordingly).

Modern techniques, on the other hand, comprised of soil resistivity sensors, dielectric techniques, tensiometers etc., and presented in the following section. Non-destructive soil moisture determination is desirable for the application of soil-water flow theory; hence modern techniques will be the focus of this research.

2.8.2.2.1 Volumetric Water/Solids Content Measurement Techniques

The neutron scattering technique (NMM) is a highly accomplished method for estimating volumetric soil moisture content in the field. It employs a source of fast neutrons and a detector of slow neutrons. Even though the strength of the source is small and sealed, due to the nature of the method, it requires safety training, monitoring, regulation of shipping and handling. The fast neutrons (emitted from a nuclear source) are dispatched and eventually thermalized or slowed down by collisions with hydrogen molecules present in the moisture of the soil. The proportion of thermalized neutrons is related to the moisture content (Amoozegar, Martin, & Hoover, 1989; A. Elder & Rasmussen, 1994). It provides fast (response time is 1-2 minutes) and reliable measurements of moisture content. It's a non-destructive method and has the capability of scanning at several depths to obtain a profile of moisture distribution. The significant disadvantages include health hazards associated with exposure to radiation, high initial costs, low degree of spatial resolution, and moving the instrument to various sites is challenging (Jarvis & Leeds-Harrison, 1987; Su, Singh, & Baghini, 2014; Zazueta & Xin, 1994).

Similar to NMM, the gamma-attenuation technique is also a radioactive method to determine soil moisture content. It assumes the scattering and absorption of gamma-rays are related to the density of the soil along their path and detects the changes in moisture, assuming specific gravity remains constant (density will increase/decrease with moisture content). It is restricted to a soil depth of 25 mm, unlike NMM, which is more accurate at deeper locations. The advantages and disadvantages of this technique are almost the same as NMM, but gamma-rays are more dangerous to work with (Zazueta & Xin, 1994).

Measuring the dielectric potential of the soil is one of the methods to determine soil moisture content. Time-domain reflectometry (TDR), capacitance technique and

frequency-domain reflectometry are primary techniques used to determine this parameter. This technique is exceptionally accurate for shallow soils (Hilhorst, 2000; G. Topp, Davis, & Annan, 1982).

The time-domain reflectometry technique is one of the most commonly used methods to determine the dielectric properties of the soil. It measures the dielectric constant k_a and empirically relates this parameter to volumetric water content using the following equations (G. C. Topp, Davis, & Annan, 1980).

$$k_a = \left[\frac{ct}{2L} \right]^2 \quad (2.16)$$

$$\theta = 4.3 \times 10^{-6} (k_a)^3 - 5.5 \times 10^{-4} (k_a)^2 + 2.92 \times 10^{-2} (k_a) - 5.3 \times 10^{-2} \quad (2.17)$$

where c is the velocity of light and equal to 3×10^8 m/s, t is the transit time for an electromagnetic pulse to travel the length of a transmission line, and L is the length of the probe.

A schematic design of the probe is presented in Figure 2-8. Probes or conductors (which are embedded in soil) sent and received electromagnetic pulses, and the delay in time as these pulses propagate along a parallel waveguide is measured. These waveguides are a pair of stainless steel rods, and the length of these rods vary depending on the manufacturer. The readings from water and other soil constituents such as soil particles, air and water have an extensive range. Therefore, travel time of the pulse is dependent on the volumetric water content (Arulanandan, 1991; Campbell, 1990; Jacobsen & Schjønning, 1993; Kupfer, Trinks, Wagner, & Hübner, 2007; Selig & Mansukhani, 1975; G. Topp et al., 1982; G. Topp, Zegelin, & White, 2000; G. C. Topp et al., 1980).

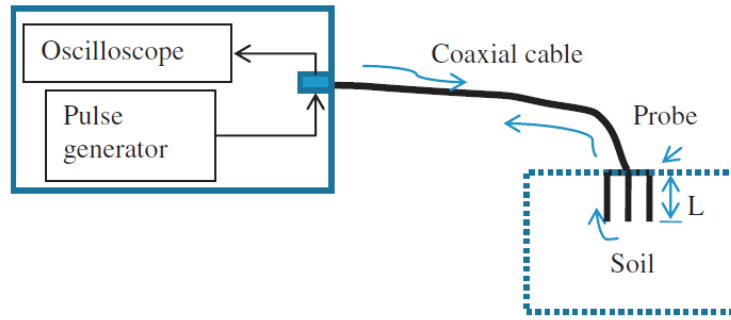


Figure 2-8: Schematics of TDR technique (from (Su et al., 2014))

There are several advantages associated with this technique, such as; (i) high temporal resolution, (ii) the fast response time (~ 28 s.), (iii) capacity to operate at a higher frequency, (iv) the repeatability of the readings, and (v) the readings' independence of soil texture, temperature and salt content, make these sensors a desirable alternative for long-term in-situ measurements. However, these probes may lose reflection at highly saline soils, and the initial cost of the instruments is expensive. In fact, the probes would perform better in arid saline soil than wet saline soils (Noborio, 2001).

Capacitance-based techniques comprise of an oscillating circuit and a sensing piece. Sensors are embedded in the soil, and the operating frequency depends on the soil dielectric constant. Soil is utilized as a medium, and these sensors measure the charge time of a capacitor, and dielectric permittivity/constant is determined. The schematics of the capacitance sensor are demonstrated in Figure 2-9(a). Each sensor has a pair of electrodes forming a capacitor, which will form a tuned circuit with the oscillator. The changes in the operating frequency (10-150 MHz) will determine the changes in the water content of the soil. The working principle behind Frequency domain reflectometry (FDR) is similar to the capacitance technique. It uses "swept frequency," which collects data over a wide range of

frequencies (Gardner, Dean, & Cooper, 1998; Minet et al., 2010; M. Robinson & Dean, 1993; Whalley, Dean, & Izzard, 1992). The schematic of an FDR probe is presented in Figure 2-9 (b).

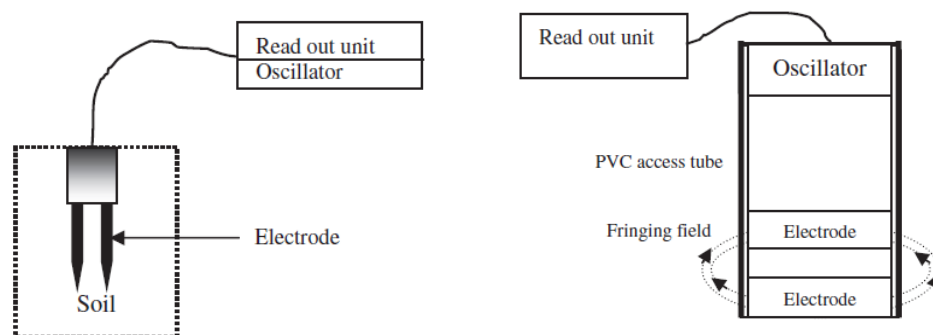


Figure 2-9: Schematics of capacitance-based sensors (a) Capacitance sensors (b) FDR probe (after Su et al., 2014).

These techniques are soil specific, and frequent calibration may be necessary. Compare to the TDR technique, the initial cost of these sensors is relatively lower, and the probes are more sensitive to detect changes at the relatively dry state of the soil (Su et al., 2014). However, they are also sensitive to air gaps between the soil, access tube and the probe.

Electrical impedance sensors measure the dielectric constant of the soil by using probes that utilize coaxial impedance dielectric reflectometry, which is a method of determining the soil moisture content using an oscillator to generate and send electromagnetic signals into the soil medium, and some of that signal is reflected back. The readings are in volts, and the sensors read both the amplitude of the reflected and incident signals. The measured volt is related to impedance and the permittivity of the soil (Gaskin & Miller, 1996; Rinaldi & Francisca, 1999).

Ground-penetrating radar (GPR) utilizes the transmission and reflection of high-frequency electromagnetic waves to determine the permittivity of subsurface material. The time for the ground wave, travelling from the source to receiver antenna, is measured and correlated to the soil property. This is a non-destructive, high-resolution method to cover larger areas of the subsurface; however, the results are not accurate for saline soils (MacDonald, 1987; Robert, 1998; D. Robinson et al., 2008).

The soil resistivity sensor technique involves quantification of soil resistivity by measuring the resistivity between probes embedded in soil or the resistivity of a material that is in equilibrium with the soil (D. Robinson et al., 2008). One of the typical applications of this method is using porous blocks to estimate matric potential. These blocks are made of gypsum, fibreglass, ceramic or nylon, and they contain two electrodes connected to a cable. When the device is embedded in the soil, water moves in and out of the block until the matric potential is in equilibrium between the block and the soil. The resistivity between two electrodes is then measured to determine soil moisture content. This technique is a cheaper alternative for field applications and provides continuous reading throughout the season. However, the response time is 2-3 hours, and the sensor fails to provide accurate reading in saline soil. (Su et al., 2014).

Thermal dissipation sensors are embedded in the soil containing a small heater inside the porous ceramic block, which is connected to a temperature sensor at the surface. A voltage is applied to the internal heater, and the dissipation of heat is measured. This is an expensive alternative to resistance blocks. The theory behind the heat flux sensor technique emerges from the application of an instantaneous pulse of heat to an infinite line source. Once the heat pulse is sent, the increase in temperature is measured and related

inversely to soil volumetric heat capacity (which is directly related to the volumetric moisture content) (Noborio, McInnes, & Heilman, 1996). Optical techniques involve measuring the incident and reflected light passing through a medium by using polarized light, fibre optic sensors and near-infrared sensors. However, practical application of this technique is yet to be established for determining soil moisture measurements (Alessi & Prunty, 1986; Kaleita, Tian, & Hirschi, 2005; D. Robinson et al., 2008; Sayde et al., 2010; Zazueta & Xin, 1994).

2.9 Summary

Fluid fine tailings demonstrate poor dewaterability and slow compressibility behaviour, which can be attributed to their poor consolidation properties of this material. The hydraulic conductivity-void ratio relationship especially dominates this behaviour for FFT, and this parameter can be highly variable (as the material is highly compressible). It is important to determine this parameter to calculate settlement rates and strength gain for tailings deposition schemes. Currently, the most commonly used conventional consolidation experimental setup in the oil sands industry is the slurry consolidometer, as it is capable of applying large strains at low solids content. This test applies an extensive range of effective stress using the step loading procedure while determining the $k-e$ relationship quite accurately. However, in order to determine the full curve, this method is found to be very time-consuming for fluid fine tailings (it can take up to a year to determine the $k-e$ relationship). Another alternative experimental test would be Seepage Induced Consolidation Test (SICT), but one of the main disadvantages of this setup is its inability to accurately model the behaviour of high void ratio materials at the early stages of the

consolidation. Also, this experimental setup is only available at certain universities and research facilities. Centrifuge tests are capable of determining an accurate $k-e$ relationship very quickly compared to all the other available methods. Full consolidation of FFTs can be achieved within a few hours, but the installation, operation and instruments of this experimental method are very expensive. Similar to SICT, it is also available in certain individual research facilities or universities.

This research aims to determine a method to easily and reliably estimate the variable $k-e$ relationship for fluid fine tailings. This will allow operators to approve or eliminate new technologies for the treatment of this material. This research tackles this problem by using two different methods, both directly and indirectly. The first portion of this study focuses on the indirect determination of the consolidation parameters by filling in the gaps from the previous studies on fine-grained soils to estimate the $k-e$ relationship and establish a new method to evaluate the consolidation behaviour. Also, a new design of a consolidometer is proposed to directly measure the $k-e$ relationship using the Instantaneous Profiling Method (based on soil water flow theory). This new design utilizes pressure transducers to measure pore water pressures and capacitance-based sensors (discussed in this chapter) to determine the volumetric water content measurements in the consolidometer. It is hoped that this method will provide a quicker means to determine the $k-e$ curve compared to the more conventional consolidometer tests.

The empirical equations, the existing database, and the new models are from the first portion of the study are discussed in Chapter 4, whereas the design of the consolidometer and the development of these methods is described in Chapters 5, 6 and 7.

Chapter 3: Tested Materials In This Study and Sample Preparation

This chapter discusses the materials tested in this study and summarizes the methods developed in the following chapters. The procedure followed to produce flocculated fluid fine tailings at targeted dosages is also presented. The characterization test and selection of optimum dosages for flocculated fluid fine tailings are discussed in Appendices A and B, respectively.

3.1 Materials

The following materials are used in the trial tests and in the prototype consolidometer.

3.1.1 Leda Clay

Leda clay utilized in this study is collected from the Navan landfill located in Ottawa, ON. The same material from this site has been studied to investigate the hydraulic performance of compacted clay liners under simulated thermal cycles by Aldaeef and Rayhani (2015), and the authors have determined the geotechnical properties of the soil (the values for liquid limit, plastic limit, clay content and specific gravity are 46, 28, 70% and 2.75 respectively). The soil comprises of 83% illite, 11% kaolinite and 6% chlorite. The particle size analysis (using both sieve analysis and hydrometer test – ASTM D422-63), the clay content of the material (31%), and more information on its physical, chemical and hydraulic properties can be found in Abdulrahman (2019). Leda Clay has also been extensively studied by C. B. Crawford (1968) and Mayne, Cargill, and Miller (2019).

3.1.2 Kaolinite

EPK kaolinite utilized in the study was purchased from Edgar Minerals and shipped from Edgar, Florida. This moisture-free powder material arrived at Carleton University in 50 lb. bags. It's high-quality ceramic kaolin with white fired colour. The liquid limit and the plastic limit are measured at Carleton using ASTM D4318-10 and determined as 44 and 26, respectively. Kaolinite is the main mineral of the soil (99-99.9%), along with crystalline silica (quartz), which consists of about 0.1-1%. The pH of the clay is 5.8. The specific surface area of the material is 28.52 m²/g, and the cation exchange capacity is 4.5 meq./100 grams. The median particle size is 1.36 microns, and the specific gravity of the soil is 2.65. More information on the chemical and physical properties of the soil can be found on Edgar Mineral's website (<http://www.edgarminerals.com/EPK-Clay.html>).

3.1.3 Thickened Gold Tailings

Thickened gold tailings were obtained from the end of a spigot at Musselwhite gold mine in Northwestern Ontario. The mining operations started in 1997. The disposal was initially conventional but switched to thickened tailings in May 2010 (Kam, Girard, Hmidi, Mao, & Longo, 2011). This material has a liquid limit of 46.4% and a plastic limit of 27.7%, with a 52% fines content (smaller than 44 microns). The specific gravity of the soil is 3.2. The grain size distribution is presented in the following figure.

3.1.4 Centrifuged Cake

Centrifuged Cake tailings were collected from a pilot plant in Fort McMurray, AB and transported to Carleton University located in Ottawa, ON. Initially shipped in 3 batches,

this study used the material transported in 2014. The same tailings used in (Mizani, 2017), and the reported solids content of this material is 50%. This material is only tested for the automation testing implemented in the prototype column (discussed in Chapter 5.3.1.2) and is diluted with water to a gravimetric water content of 199% prior to testing (decreasing solids content to 33.5%). Mizani (2017) reported the liquid and plastic limit of the material as 84.5% and 38% and has a specific gravity of 2.23. The grain size distribution of the sample is provided below, and the mineralogical composition can be found in Hurtado (2018).

3.1.5 Shell Fluid Fine Tailings

The oil sands tailings are collected from a tailings pond in Northern Alberta, AB and shipped to the Civil Engineering laboratory located at Carleton University in Ottawa, ON, in large containers. Prior to collection from the container to 20-litre buckets, the material is mixed using a drum mixer (Model Number: DLM150VGD, Mixer Direct) to restore the tailings to their original composition and initial solids content. They are mixed for 24 hours at an average speed of 129 rpm, and before each transfer, three samples of the material are collected to examine the solids content. The direction of the rotation is alternated between forwarding and backward mode to optimize mixing. Different laboratory tests were performed on this material to determine its physical, chemical and mineralogical properties. The geotechnical properties of these tailings are presented in Table 3-1 and compared with other published studies. For more detailed information on this material can be found in M. A. Salam (2019).

3.1.6 Syncrude Fluid Fine Tailings

These fluid fine tailings are also collected from Northern Alberta and shipped to Carleton University in the summer of 2018 in a large tote. Prior to collection, few litres of bleed water are collected and sent to external laboratories to determine the water chemistry of this material. Similar to Shell fluid fine tailings, this material is mixed in the tote using the same drum mixer (Model Number: DLM150VGD, Mixer Direct) for several days. For optimal mixing, the direction of the rotating blades has been reversed every 2-4 hours to restore the material to its original state. Tailings are then transferred into 20 litres buckets for further testing.

Two types of unamended FFT samples from different mines were utilized in this study; Shell fluid fine tailings and Syncrude fluid fine tailings. The physical, mineralogical and chemical characteristics of unamended Shell FFT samples were presented in M. A. Salam (2019). As for Syncrude FFT, different laboratory tests and analyses are performed to determine the baseline geotechnical characteristics of this material. The following table demonstrated their geotechnical properties and compared them with other published data from the literature. Also, Figure 3-1 provides the particle size distribution of the tested soils in this study.

Table 3-1: Geotechnical Properties of tested tailings (compared with other reported FFTs)

Property	Unit	ASTM standard	Salam (2020)	Syncrude FFT	Mizani (2017)	Y. Yao (2016)	Bajwa (2015)
Solids content	%	D2216-19	31	28	33	32	42
Water content	%	D2216-19	223	248	100	213	140
Liquid Limit	%	D4318-10	60	46	62	48-61	45
Plastic Limit	%	D4318-10	28	25	27	26-29	19
Fines content	%	D7928-16	71		79	90-93	
Clay content	%	D7928-16	39	27	30	45-50	40
Bitumen content	%	D95-05	1.4	3.1	2.9	1.3	3-4
ρ_{bulk}	g/cm³	D7263-09	1.2	1.2	1.2	1.2	1.2
Specific Gravity		D854-10	2.12	2.04	2.2	2.30	2.22

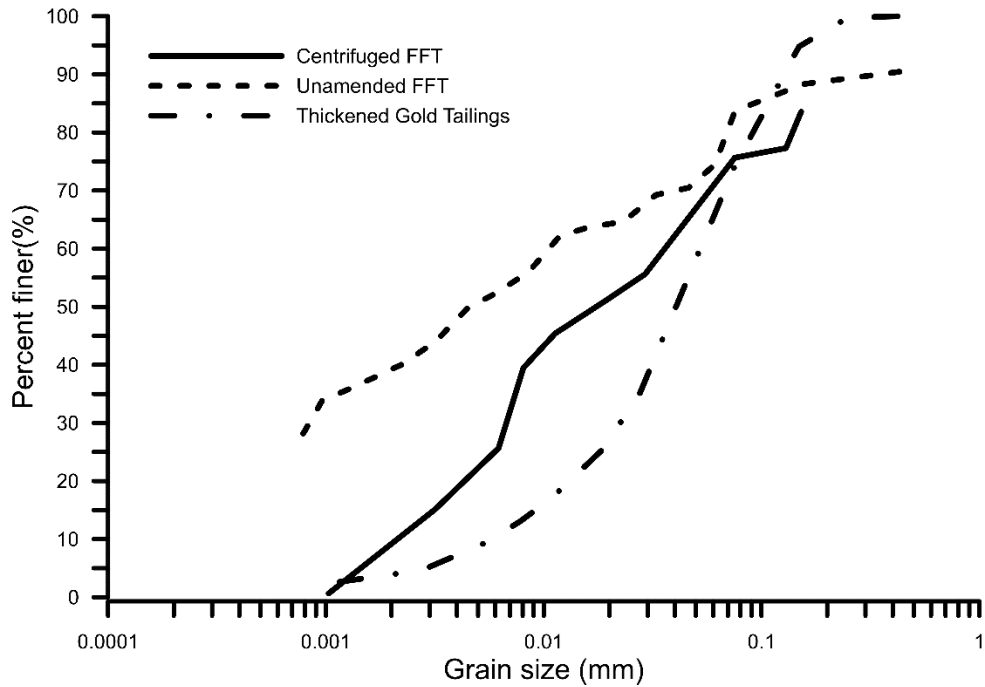


Figure 3-1: Particle size distribution size of tested materials

3.2 Sample Preparation, including Flocculation of FFT

The consolidation behaviour of both unamended and amended fluid fine tailings has been assessed in this study. Two different flocculants have been used to prepare the samples; flocculant A3338 with Shell raw FFT and Polymer B with Syncrude FFT. The preparation of amended FFT samples was described in the following sections, and dosage optimization for both raw fluid fine tailings have been performed. Based on these analyses, the samples were prepared at those dosages and tested in the self-weight consolidation column.

3.2.1 Preparation of Polymer-stock Solution

All the amended FFT samples were prepared using two different flocculants; (i) an anionic polyacrylamide (PAM) flocculant (A3338) and (ii) a cationic Poly (vinyl benzyl) trimethylammonium chloride flocculant (coded Polymer B) for the dewatering of the

samples. The PAM flocculant is a branched polymer (commercially available by SNF), and it has a molecular weight of 18×10^6 g/mol. Polymer B is developed at the University of Alberta and shipped to Carleton University in 2018. The nature of the polymer is cationic with a linear-type polymeric structure and has a hydrophobically charged backbone (Vandara, 2018). Both flocculants should be prepared at a final concentration of 0.4%. Therefore 4 grams of polymer is used in 1000 mL of deionized water for the preparation of a polymer stock solution. The solution is stirred using a jar tester (Phipps and Bird, USA) at 250 rpm for 5 minutes and 120 rpm for 55 minutes for PAM flocculant. In comparison, the duration for mixing Polymer B takes a longer time, no less than two days at 250 rpm. Once the stirring procedure is finalized, if there are any visible polymer chunks that are still present in the solution, it is mixed with a hand-mixer for another 10 minutes. Then, it is left for maturation for 1 hour.

3.2.2 Preparation of Flocculated FFT

A four-blade impeller (with a radius of 8.5 cm) is attached to an overhead mixer (IKA EUROSTAR 60 control), which is immersed in 2000 mL of raw FFT tailings in a five container. Initially, FFT tailings are mixed at a constant speed of 250 rpm for 15 minutes to affirm that they are homogenized prior to polymer addition. Then, the prepared 0.4% polymer stock solution is instantaneously added to the tailings by injected close to the rotating impeller during mixing. The required amount of polymer is determined based on the solid concentration and the amount of raw FFT tailings. The mixture is continued to be mixed for another 20 seconds after injection.

This mixing protocol was initially adapted by Shell Canada from a baseline

procedure developed in 2010 to replicate in-line flocculation and generate field representative samples in a laboratory environment. Mizani (2017) mixed the polymer stock solution and FFT at different speeds and durations to optimize this procedure and evaluated the short-term dewaterability and yield stresses of the produced samples. The results from the rheology tests demonstrated that 250 rpm is indeed the optimum mixing speed, and above this limit, the material is over-sheared, whereas mixing speeds less than this value result in inadequate mixing of the material. This mixing protocol was adopted for all tests during initial testing with sensors, i.e., SENTEK EnviroSCAN sensor testing, wall-effect testing. However, the amended FFT samples tested in the column are prepared using the optimized mixing technique discussed in the next section.

3.2.3 Optimized Mixing Technique

Aldaef and Simms (2019) proposed a quality-controlled mixing protocol for the flocculation process of FFT samples. The authors observed the relationship between the torque force developed during the flocculation process in a Couette rheometer and the quality of the flocculation. The maximum developed torque reading is achieved in 15-25 seconds after the polymer stock solution is injected. The peak torque values are thought to be associated with larger flocs in the sample as the rheometer needs to exert more considerable energy to shear them. In order to prepare the flocculated FFT samples, these torque values are monitored, and once the peak value is reached, the mixing is stopped. This protocol is adopted for all flocculated FFT samples prepared for the self-weight consolidation column test discussed in Chapters 6 and 7. Prior to self-weight consolidation testing, the dosage optimization for Shell raw FFT and Syncrude raw FFT samples were

examined utilizing flocculants A3338 and Polymer B. Based on the outcomes of this study, three dosages are selected; two using A3338 with Shell FFT and one using Polymer B with Syncrude fluid fine tailings. The optimization results are given in Appendix A for the readers' interest. For the purposes of this work, doses of 800 ppm and 1000 ppm were selected for A3338 applied to Shell FFT, and 4000 ppm dosage is selected for Polymer B applied to Syncrude FFT.

3.3 Summary of methods developed in the following chapters

3.3.1 Estimation of Consolidation Properties of Fine-grained soils using simple correlations

This study examines the application of predictive models available in the literature to predict the consolidation behaviour of various fine-grained soils. These predictive models have been studied by several researchers, and they emphasize using easily measured index properties to predict the compressibility and permeability of soft soils.

Initially, all the available correlations (11 for $\sigma'-e$ and 17 for $k-e$ relationships) are gathered in the literature applying to fine-grained soils, and an extensive data bank (including 81 data sets and 873 data points for compressibility, 79 data sets and 837 data points for hydraulic conductivity) is created to evaluate the performances of each method for three types of fine-grained soils: clays, dredged material, and oil sands tailings.

Usually, the predictive models in the literature are determined by examining a limited number of data sets. The goal of this study was to determine the best applicable predictive models for each type of soil in an extensive approach. Based on the performance evaluations, which are discussed in Appendix B (for $\sigma'-e$ relationships) and Chapter 4 (for

k - e equations), new optimized relationships are proposed for each soil type. In addition, new methods (i.e. using the compressibility curve and using a predictor at higher void ratios) have been proposed to improve the estimations of k - e relationships where the optimized models fail to predict correctly.

3.3.2 Determination of k - e function from a prototype self-weight consolidation column

This research also examined the application of the Instantaneous Profiling Method (IPM) to calculate the k - e curve for tailings. The method calculates the macroscopic flow velocity in soils from the column profiles of water content, and k values can be calculated instantaneously using these fluxes and measured interpolated gradients of the total head. The method is quite advantageous, but it requires high-resolution measurement profiles to provide accurate predictions. A preliminary assessment of the theory is tested on a case study from the literature, and it only provided a reliable k - e curve for a narrow range of void ratios, which supported the need for high-resolution measurement profiles for accurate full-range calculations. Therefore, a new self-weight consolidation test setup is designed to accommodate the application of the method. The application of the methodology, the development of the test itself, the final design of the column and the preliminary assessment are discussed in Chapters 5, 6 and 7.

Chapter 4: Improving Hydraulic Conductivity Estimation for Soft Clayey Soils, Sediments, or Tailings Using Predictors Measured at High-Void Ratio¹

4.1 Introduction

The geotechnical behaviour of soft soils or tailings is very dependent on their hydraulic conductivity-void ratio functions (henceforth $k-e$), which are highly variable, and can be time-consuming or/and expensive to obtain from experimental tests: for soft soils, these tests can range from months to years. Estimating these parameters from commonly measured geotechnical properties such as Atterberg limits or grain size curves can, therefore, be advantageous for practitioners, especially when testing candidate amendments to improve $k-e$ of dredged sediments or tailings. These correlations have been much studied, and recent review papers in the geotechnical literature include Pandian, Nagaraj, and Raju (1995); Berilgen et al. (2006); Sridharan and Nagaraj (2000); and Chandra Paul and Azam (2013). The accuracy of these correlations, however, remains insufficient for most types of design. The accuracy is typically worse where the initial water contents are substantially above the liquid limit, where the fabric of the soil will be influenced by various chemical and physical processes (for example, the influence of water chemistry on flocculation, water movement induced shear during deposition and its affect on floc size). Determining the Atterberg limits, however, requires reduction of water content, which will substantially alter the fabric, and potentially remove any signal in the

¹ A version of this chapter is published as a journal paper (Babaoglu & Simms, 2020)

Atterberg values that reflects the actual state of the soil or tailings at high water content.

Readers should be reminded that the consolidation behaviour of soft materials in this range is complex. Goro Imai (1981) described three stages during the sedimentation of dilute clay-water mixtures: flocculation, sedimentation, and consolidation. The transition between sedimentation and consolidation has been studied by various researchers (Edil & Fox, 2000; Kynch, 1952; McRoberts & Nixon, 1976; Pane & Schiffman, 1997). The rate of consolidation is also affected by electrochemical interactions between pore water and clay particles (Azam, 2010; Caughill et al., 1993; Demoz & Mikula, 2011), which alters pore size and interconnectedness through result in changes in microstructure (James Kenneth Mitchell & Soga, 2005). Time-dependent processes, such as creep and structuration, may bear on long-term consolidation analysis (Burland, 1990). However, the scope of this study deals only with the rapid prediction of the $k-e$ function.

This study proceeds by analyzing an existing data set of 79 $k-e$ functions obtained from the literature on soft soils or clayey mine tailings (listed in Table 4-2), with 17 $k-e$ correlations to Atterberg limits (presented in Table 4-1). Based on the form of the best-fitting equations, improved correlations are proposed based on two predictors providing information at a high void ratio. The two predictors are the compressibility curve itself and a single measured value of k .

4.2 Existing Hydraulic Conductivity Correlations

Most of the correlation relationships presented in the literature are demonstrated in Table 4-1.

Table 4-1: Summary of correlation relationships for k - e equation

	Correlation Relationship	Materials	Reference
(4.1)	$\log k = \frac{e}{0.01(PI) + 0.05} - 10$	Clays	Nishida and Nakagawa (1969)
(4.2)	$k = (0.00104PI^{-5.2}) \left[\frac{e^x}{1+e} \right]$	Normally consolidated remoulded clay	Samarasinghe, Huang, and Drnevich (1982)
(4.3)	$LI = 95.21(k(1+e))^{0.233} - 0.242$	Clay & Slurried mineral waste	Carrier III et al. (1983)
(4.4)	$k = \frac{0.0174 \left(\frac{e - 0.027[(PL) - 0.242(PI)]}{PI} \right)^{4.29}}{(1+e)}$	Remolded Clay	Carrier and Beckman (1984)
(4.5)	$\frac{e}{e_L} = 2.38 + 0.233 \log k$	Normally consolidated clays	Nagaraj, Pandian, and Narasimharaju (1993)
(4.6)	$\frac{e}{e_L} = 2.162 + 0.195 \log k$	Over-consolidated clay	Nagaraj, Pandian, and Raju (1994)
(4.7)	$\log k = \frac{e - 0.0535(LL) - 5.286}{0.0063(LL) + 0.2516}$	Mine Tailings	Sivapulliah, Sridharan, and Stalin (2000)
(4.8)	$\frac{e}{e_L} = 29.80(k(1+e))^{0.177} - 0.09527$	Dredged Materials	Morris, Lockington, and Apelt (2000)
(4.9)	$\frac{e}{e_L} = 2.23 + 0.204 \log k$	Normally consolidated clays	Sridharan and Prakash (2002)
(4.10)	$k (cm / s) = C_p \frac{\gamma_w}{\mu_w} \frac{e^{3+x}}{1+e} \frac{1}{\rho_s^2 (LL)^{2x}}$	Plastic soils	Mbonimpa, Aubertin, Chapuis, and Bussière (2002)
(4.10.1)	where $x = 7.7(LL)^{-0.15} - 3$		
(4.11)	$\log [k_{predicted}] = 0.5 + \log \left[\frac{e^3}{D_R^2 S_S^2 (1+e)} \right]$	Clay	Chapuis and Aubertin (2003a)
(4.11.1)	where $\frac{1}{S_S} = 1.3513 \left(\frac{1}{LL} \right) - 0.0089$		

(4.12)	$\log \left[\frac{k}{1m/s} \right] = 1.5 \left\{ 0.5 + \log \left[\frac{e^3}{D_R^2 S_s^2 (1+e)} \right] \right\} + 2$	Mine Tailings	Chapuis and Aubertin (2003a)
(4.13)	$\frac{e}{e_L} = 12.55(k(1+e))^{0.109} - 0.372$	Dredged Materials	Morris (2003)
(4.14)	$k = (2.5 \times 10^{-4} (SI)^{-3.69}) \left[\frac{e^{3.79+0.044(SI)}}{1+e} \right]$	Remoulded clays	Sridharan and Nagaraj (2005)
(4.15)	$k = \exp[-5.51 - 4 \ln(PL)] (e)^{7.52 \exp[-0.25(LI)]}$	Dredged Materials	Berilgen et al. (2006)
(4.16)	$k = \frac{6.31 \cdot 10^{-7}}{(PI - 8.74p)^{3.03}} e^{2.66(PI - 8.47p)^{0.234}}$	Clay	Dolinar (2009)
(4.16.1)	$A_s = (LL - 31.91p) / 0.81$ $A_s = (PL - 23.16p) / 0.27$ $A_s = (PI - 8.47p) / 0.54$		
(4.17)	$k = [1.06 \times 10^{-5} (PI)^{-2.24}] (e)^{16.23(PI)^{-0.4}}$	Various fine-grained soils; including clays, dredged soils and oil sands tailings	Chandra Paul and Azam (2013)

The majority of equations relate e to k through log-linear expressions or power expressions, where the characteristic parameters are liquid limit (LL), plastic limit (PL), or liquidity index (LI) (and hence the initial void ratio). Several equations are derived from the Kozeny-Carman equations (Carman (1939)), and these equations require determination of the specific surface of the soil – for these, it is often required to estimate specific surface from the Atterberg limits. All performances of the predictive methods were evaluated using a large data bank collected from the summarized references in Table 4-2.

Table 4-2: Reference list for all data used in this study

Soil Type	References
Clay	<p>Gholamreza Mesri and Olson (1971a); D Znidarčić et al. (1986); Nagaraj et al. (1993); Pane and Schiffman (1997); Tanaka, Locat, Shibuya, Soon, and Shiwakoti (2001); Sivapullaiah et al. (2000); Sridharan and Nagaraj (2000); Khan and Azam (2016)</p> <p>Compressibility: 28 individual data sets, 230 data points</p> <p>Hydraulic conductivity: 22 data sets, 175 data points</p>
Dredged Soils	<p>Cargill (1985); Shields (1988); Marian Elizabeth Poindexter (1989); Marian E Poindexter (1988); Berilgen et al. (2006)</p> <p>Compressibility: 22 individual data sets, 353 data points</p> <p>Hydraulic conductivity: 21 data sets, 409 data points</p>
Oil Sands	<p>Nagula Naguleswary Suthaker (1995); Pollock (1988);</p>
Tailings	<p>Jeeravipoolvarn (2005); Jeeravipoolvarn (2010); W. G. Miller (2010); N. A. Beier (2015); Owolagba (2013); Farkish and Fall (2013); Y. Yao (2016); Wilson, Kabwe, Beier, and Scott (2017)</p> <p>Compressibility: 31 individual data sets, 290 data points</p> <p>Hydraulic conductivity: 36 data sets, 253 data points</p>

Performance comparisons of predictive models to estimate $k-e$ of fine-grained soils are presented for all soil types separately. Each method was tested against each class of soils or tailings, and the closest comparisons are shown in Figures 4-1, 4-2 and 4-3. The results are presented in terms of the cumulative distribution function of the log of ratios

between measured and predicted hydraulic conductivity data. The ratio of measured to predicted values is demonstrated in the horizontal line in logarithmic form and the probability presented in the vertical line, which falls between 0 to 1. A perfect match would be a straight vertical line at 0 on the x-axis (indicating that the predicted values are equal to the measured data). Methods that would provide a good fit on average would be centred around the same vertical line.

4.2.1 Clays

Figure 4-1 presents the performance of the predictive models of $k-e$ for clays. Similar to the findings of Chapuis (2012), the upper and lower bounds for the predictive data are defined by Nishida and Nakagawa (1969) and Sivapullaiah et al. (2000), respectively. It was also found that the estimations from Nagaraj et al. (1993) and Sridharan and Prakash (2002) are more realistic for void ratios lower than 1.3. This conclusion has been drawn after comparing the predicted hydraulic conductivity of the data samples using both models and the measured k values. Cumulative distribution plots were also determined for lower and higher void ratios, and it concluded the same results. However, with an increase in the void ratio, the predicted values increasingly overestimate measurements.

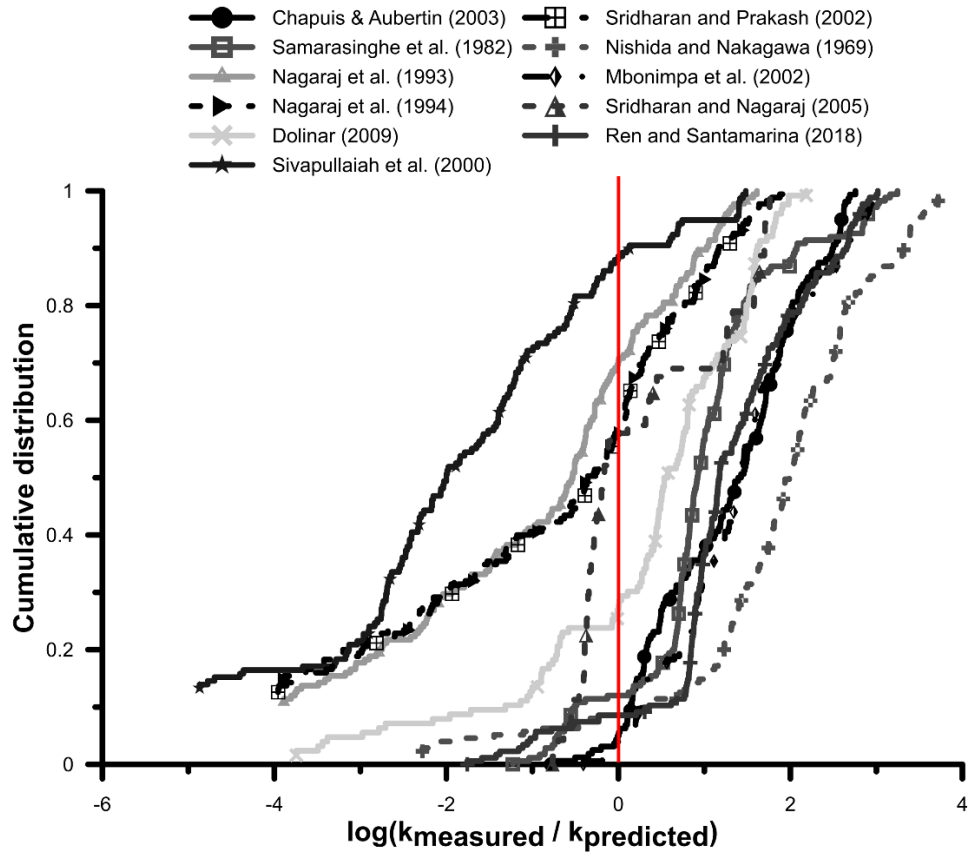
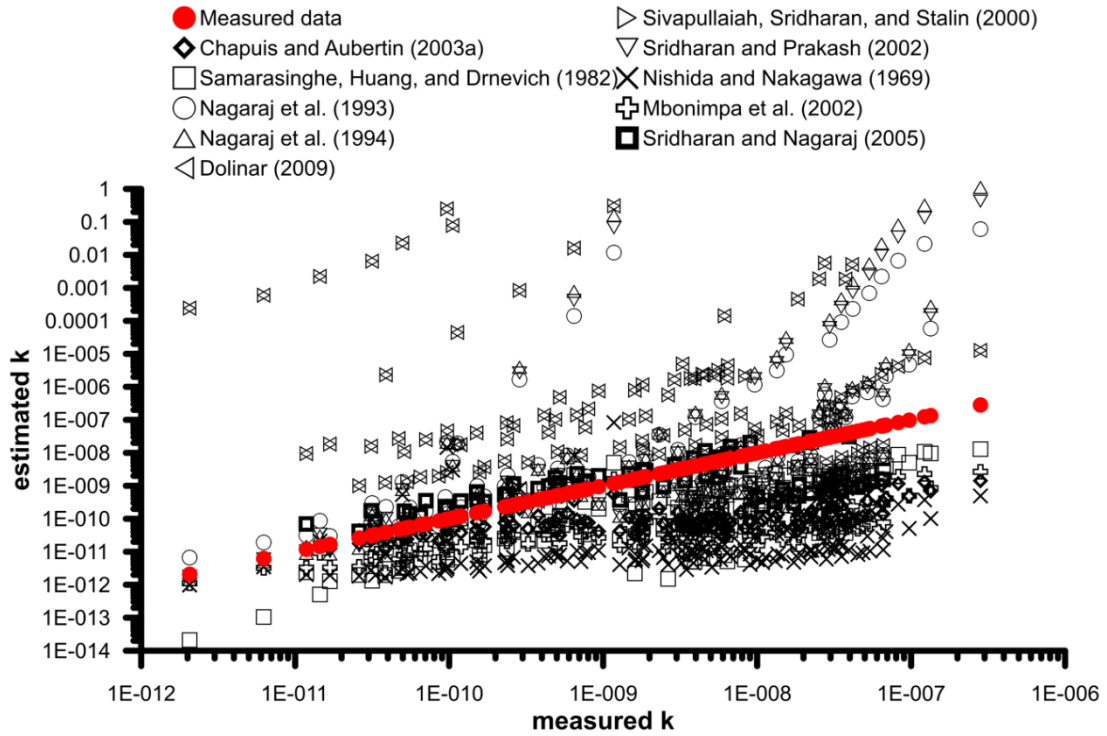
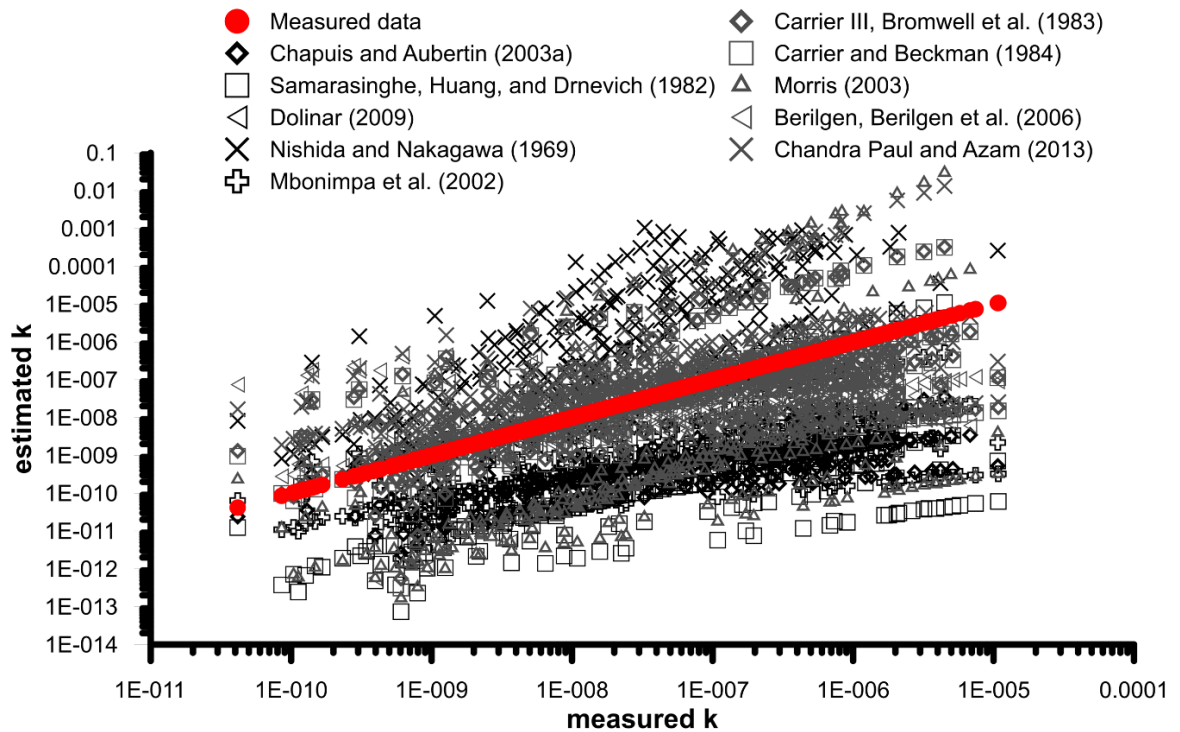


Figure 4-1: The performance of predictive models to estimate void ratio-hydraulic conductivity relationship for clays.

4.2.2 Dredged Materials

The performance of k - e predictive methods for dredged clay is presented in Figure 4-2. Nagaraj et al. (1993) and Nagaraj et al. (1994) underestimated hydraulic conductivity value by several orders of magnitude and defined the upper bound whereas Chapuis and Aubertin (2003b) and Berilgen et al. (2006) outline the lower bound.



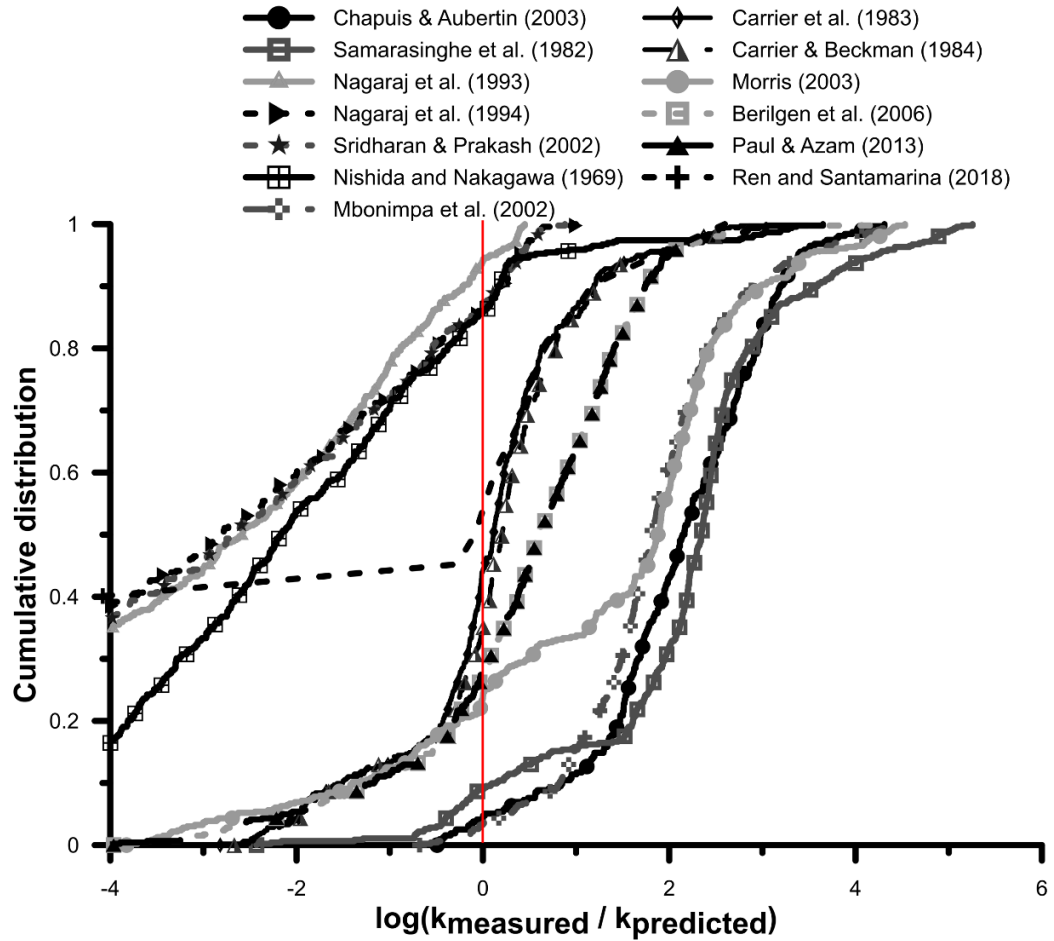
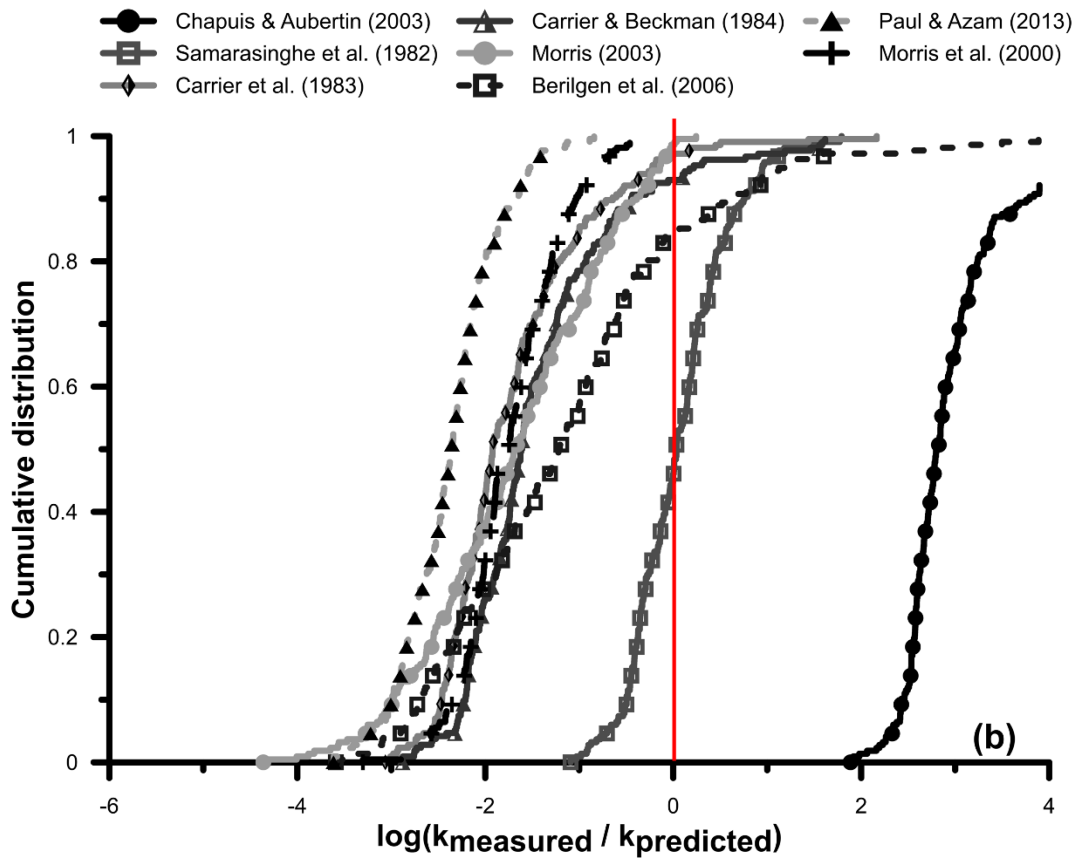
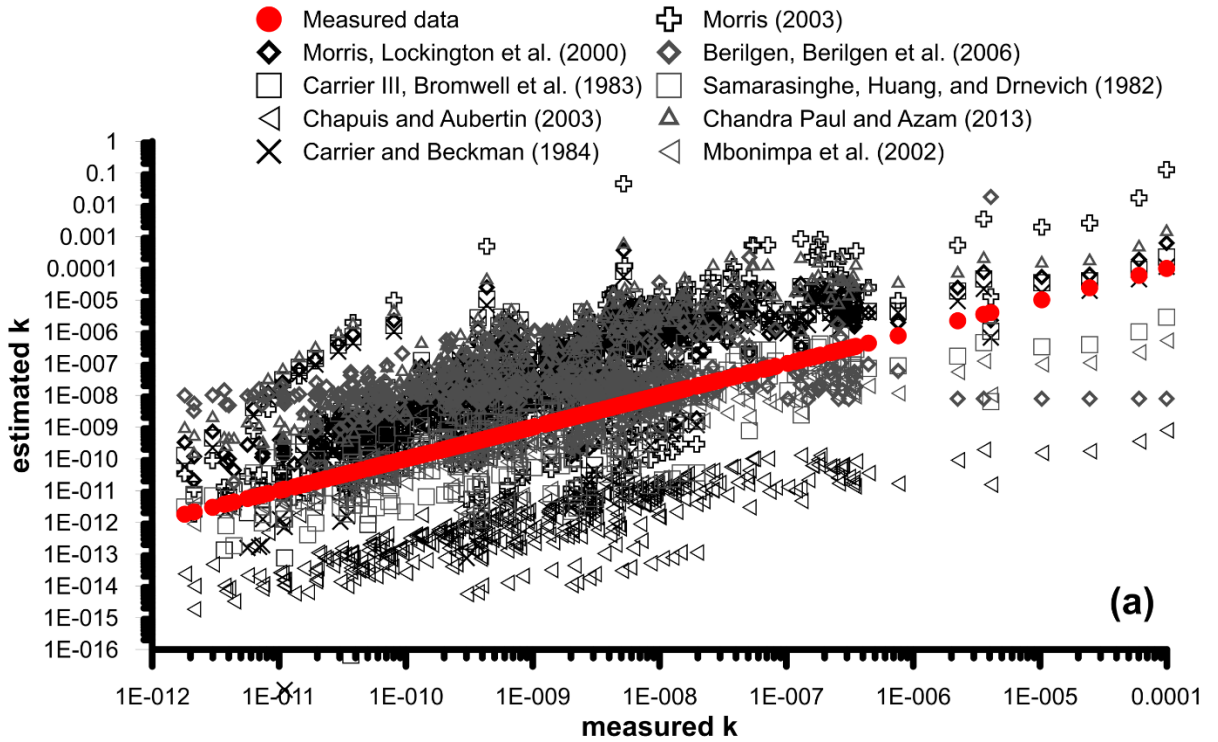


Figure 4-2: (a) Measured vs. predicted k values for dredged soils using various predictive models
 (b) Performance of k - e functions for dredged materials

4.2.3 Oil Sands Tailings

Figure 4-3 (a) shows the performance of the k - e models for the oil sands tailings data sets. For untreated tailings, Berilgen et al. (2006) overestimate the hydraulic conductivity for lower void ratios; however, as the void ratio increases, the predicted values become more realistic. On the other hand, the same method provided a better predicted capacity for treated oil sands tailings.



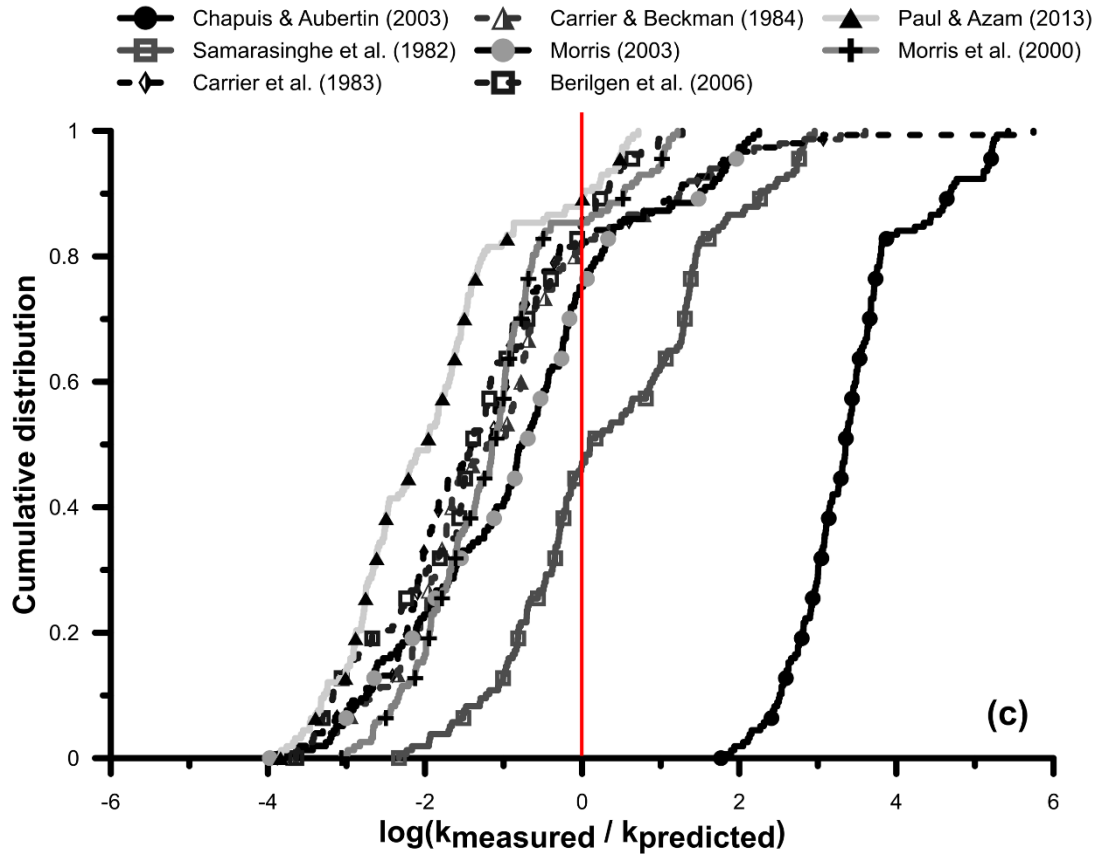


Figure 4-3: (a) Measured vs. predicted saturated hydraulic conductivity values for oil sands tailings (b-c) Performance comparison of predictive methods for estimating hydraulic conductivity for untreated and treated oil sands tailings, respectively

A number of predictive equations showed relatively good agreement with the measured data. It should be acknowledged that the specific surface methods may have apparently performed less well, only due to a lack of direct specific surface measurements for most data sets. The best agreement was shown with the Samarasinghe et al. (1982) and the Carrier and Beckman (1984) equations. The parameters of these equations (such as the power and modifier of plasticity index (PI) in the Samarasinghe equation) were optimized for each of the three data sets, using a non-linear least squares regression algorithm in MATLAB version R2018a, and are presented in Figure 4-4. The optimized equations show

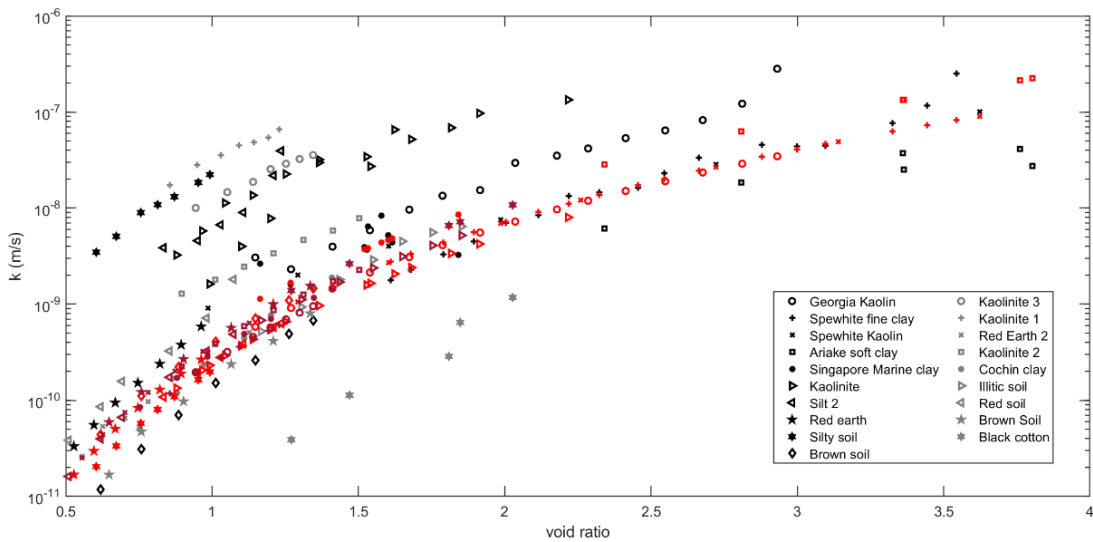
high R^2 values (>0.96). These optimized equations are:

Clays $k(m/s) = 1 \times 10^{-10} (PI)^{0.6245} \left(\frac{e^5}{1+e} \right) \quad R^2 = 0.97 \quad (4.18)$

Dredged Materials $k(m/s) = 1.756 \times 10^{-11} (PI)^{0.486} \left[\frac{e^5}{1+e} \right] \quad R^2 = 0.96 \quad (4.19)$

$LI = 18.67(k(1+e))^{0.043} - 7.353 \quad R^2 = 0.9884 \quad (4.20)$

Oil Sands Tailings $k(m/s) = 2 \times 10^{-12} (PI) \left(\frac{e^5}{1+e} \right) \quad R^2 = 0.97 \quad (4.21)$



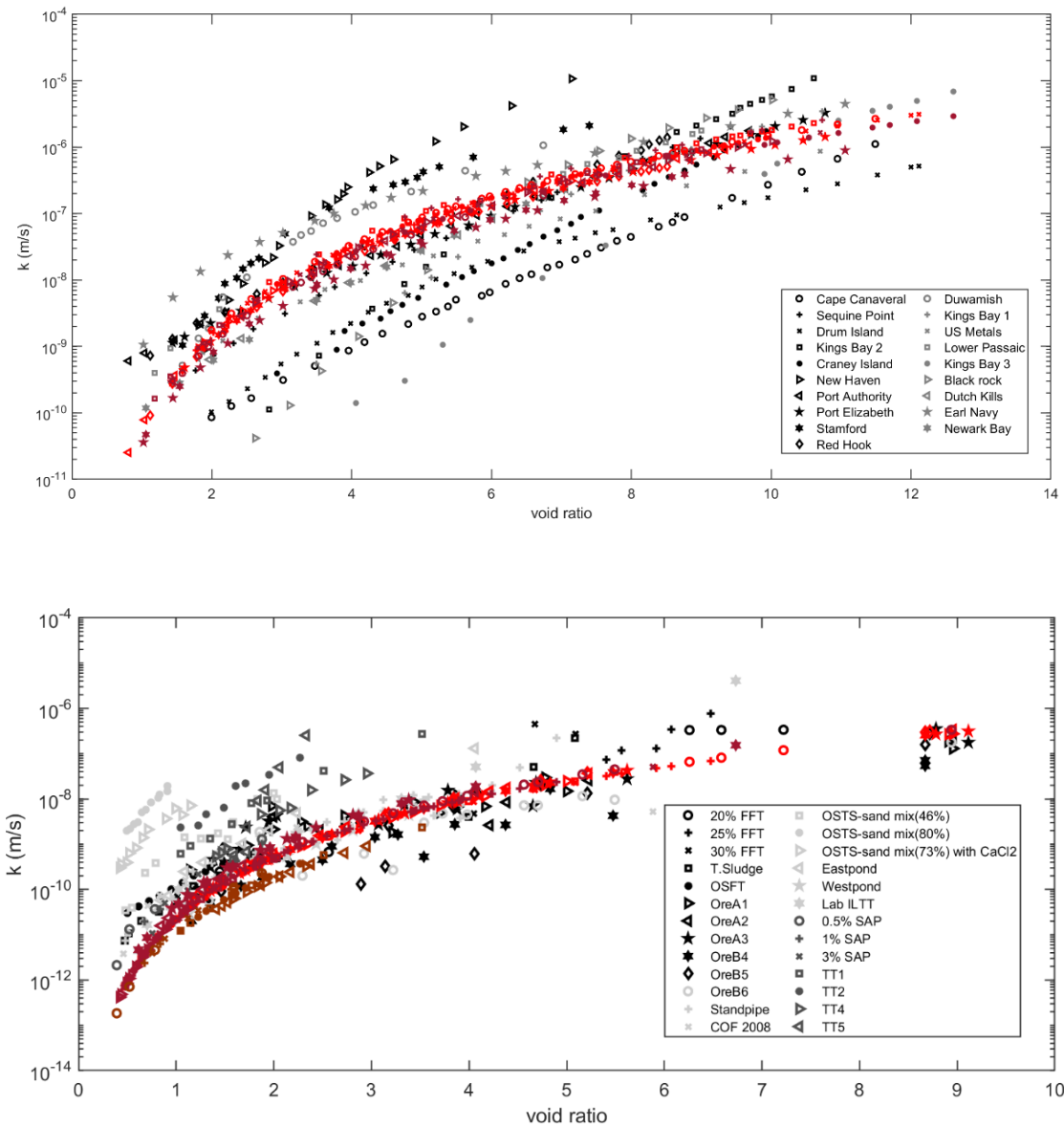
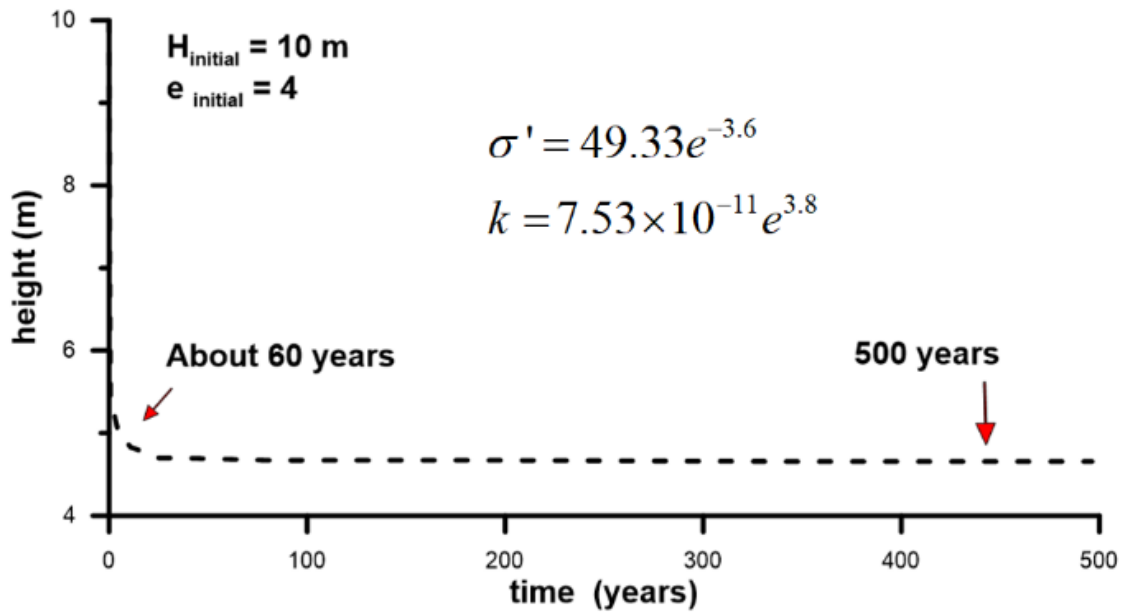


Figure 4-4: Best-fit $k-e$ models optimized to the data sets of (a) clay; (b) dredged material; and (c) oil sands tailings where coloured dots denote the predicted values.

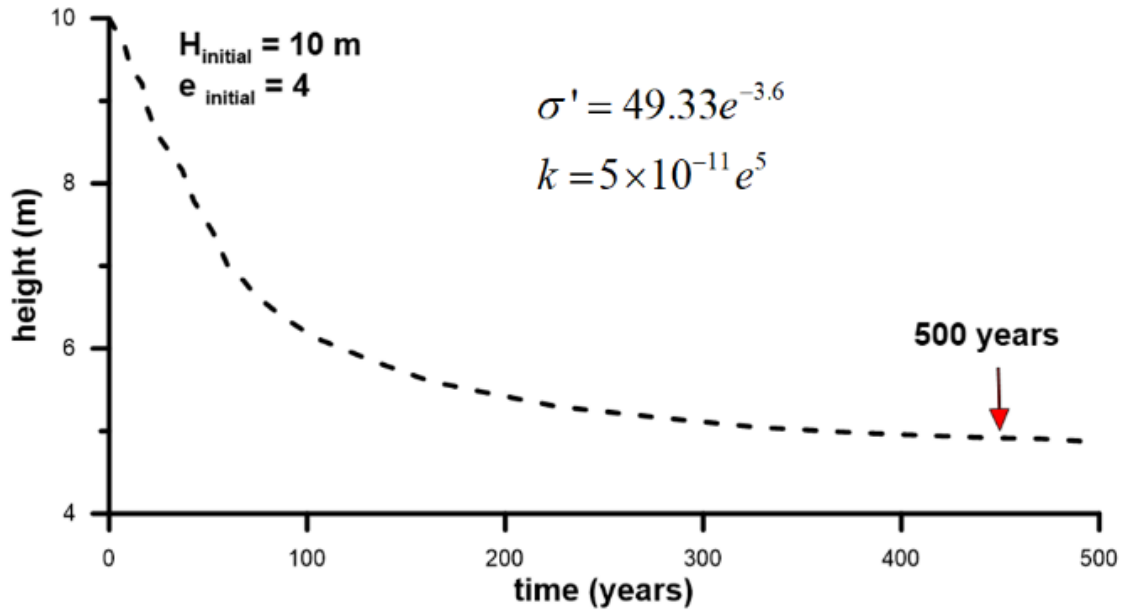
4.3 Suitability of optimized equations for design

However, the relatively high R^2 , however, is somewhat misleading in terms of the utility for the design of these $k-e$ estimates. Even the optimized methods (Eqns. 4.18 through 4.21) exhibit relatively poor predictability at water contents above the liquid limit. Above this

limit, an order of magnitude difference between predicted and measured hydraulic conductivities at a given void ratio is expected for 20 % of the dredged data and 20.6% for the oil sands data. This range will demonstrate very different results in a large strain consolidation analysis. This is illustrated in Figure 4-5, which shows the settlements predicted from a hypothetical analysis for a 10 m deposit using the large-strain consolidation model UNSATCON (Shunchao Qi, Simms, Vanapalli, et al., 2017). Predictions are made using either the measured k - e relationship, $k = 7.53 \times 10^{-11} e^{3.824}$, as provided in Jeeravipoolvarn (2010) and using the prediction of Eqn. 22, $k=5 \times 10^{-11} e^5$. The initial void ratio is 5.0, and the compressibility equation is: $\sigma' = 49.33e^{-3.6}$. The difference in the predictions is substantial.



(a) Using measured values



(b) Using predicted values

Figure 4-5: Large strain consolidation analysis of hypothetical fluid fine tailings deposited at an original thickness and void ratio of 10 m and 4, respectively

4.4 Predicting k - e using the compressibility curve

All data sets with both compressibility and k - e data were used to investigate if compressibility itself could be a useful predictor of k - e (17 for clay, 21 for dredged materials and 28 for oil sands tailings). As shown in Figure 4-6, many data sets showed an extreme similarity between k - e and e - σ'_v curves (where k - e data points are presented as dark grey dots, while e - σ'_v data is displayed are light gray colour), which could be defined by:

$$\log k = \frac{\log e}{A} - B \quad (4.22)$$

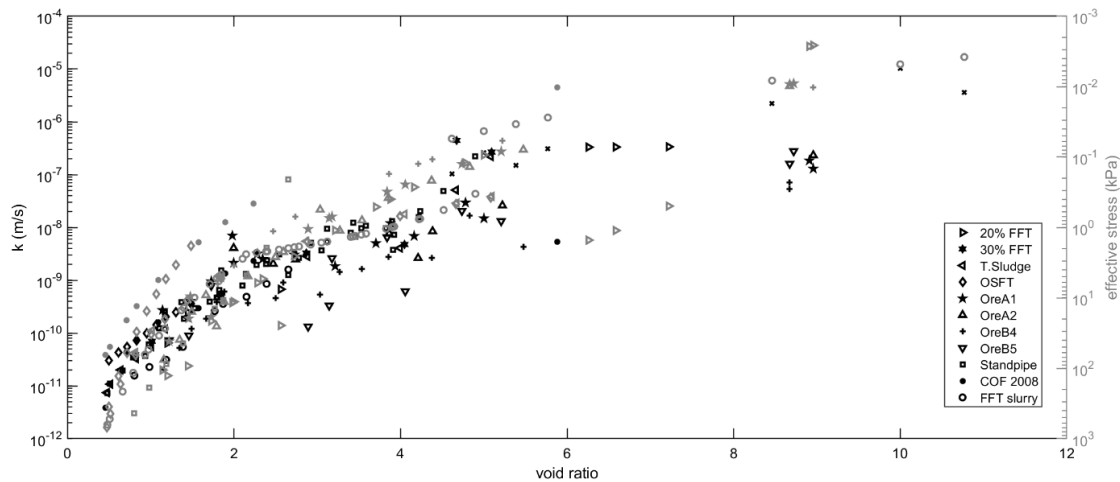


Figure 4-6: The relationship between the hydraulic conductivity-void ratio-effective stress for untreated oil sands tailings

If optimized parameters A and B are determined for each soil using a linear regression algorithm in MATLAB version R2018a and rearranged them in a power form, then the soil specific equations are:

- **Clays:** $\log k = \frac{\log e}{0.2} - 9.436 \quad \rightarrow \quad k(m/s) = 3.66 \times 10^{-10} e^5$ (4.23a)

- **Dredged soils:** $\log k = \frac{\log e}{0.2} - 10.795 \quad \rightarrow \quad k(m/s) = 1.60 \times 10^{-11} e^5$ (4.23b)

- **Oil sands tailings:** $\log k = \frac{\log e}{0.2} - 10.5 \quad \rightarrow \quad k(m/s) = 3.16 \times 10^{-11} e^5$ (4.23c)

The equations are presented in terms of the most optimized integer value of power. The common parameter in all three equations is e^5 : this is the optimal value for every half-power (that is powers of 5.5 or 4.5 give poorer results). Figure 4-7 displays different examples of fits to the linear relationship provided in Eq. 4.22 for various samples of fine-grained soils, where $A=0.2$ and parameter B varies for different types of soils. In almost

all data sets, a good fit can be obtained by changing only the B parameter (the offset). However, using Equations 4.23 only results in only marginally better agreement than using the optimized equations, as shown in Table 4-3.

Table 4-3: Sensitivity analysis for proposed optimized $k-e$ relationships

Percent error less than an order of magnitude				
Materials	Optimized $k-e$ using Atterberg limits (%)	Optimized $k-e$ using Compressibility curve (Eqn. 4.23) (%)	Eqn. 4.24 (%)	Eqn. 4.25 (%)
Clay	63	73.2	98	99
Dredged Materials	80	78.4	94	92
Oil Sands Tailings	79.4	77.3	95	92

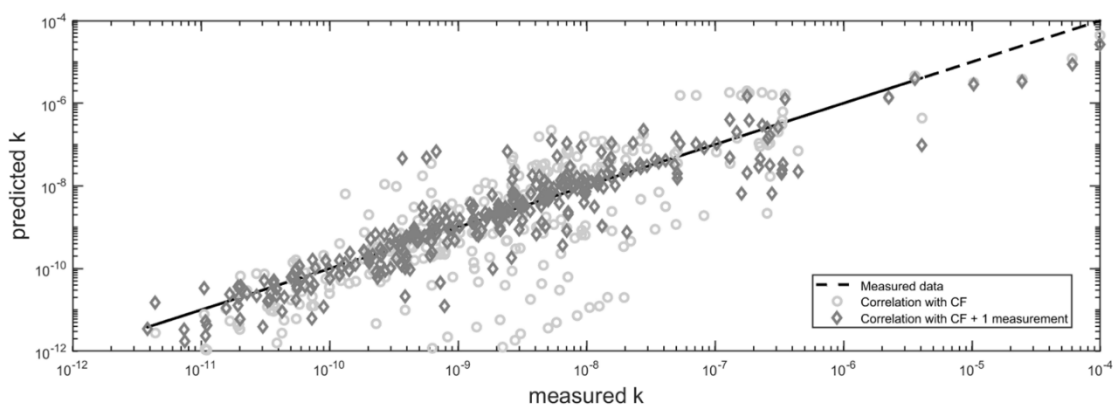
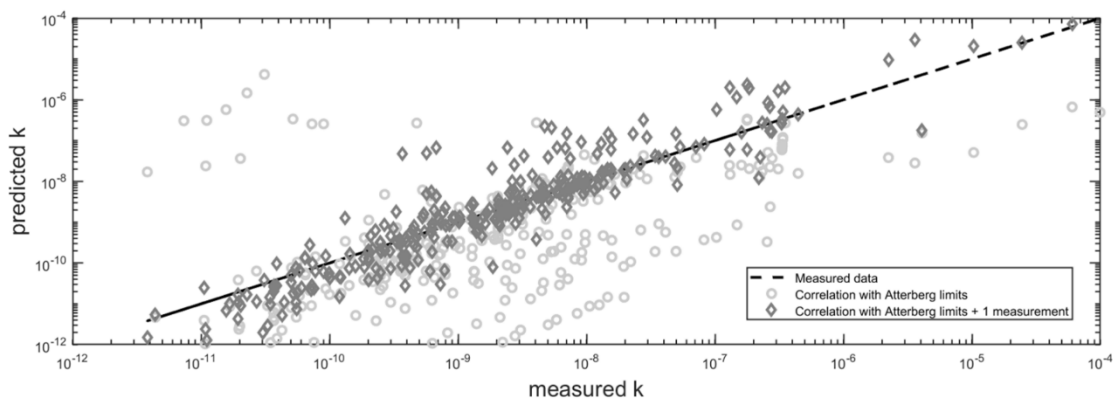
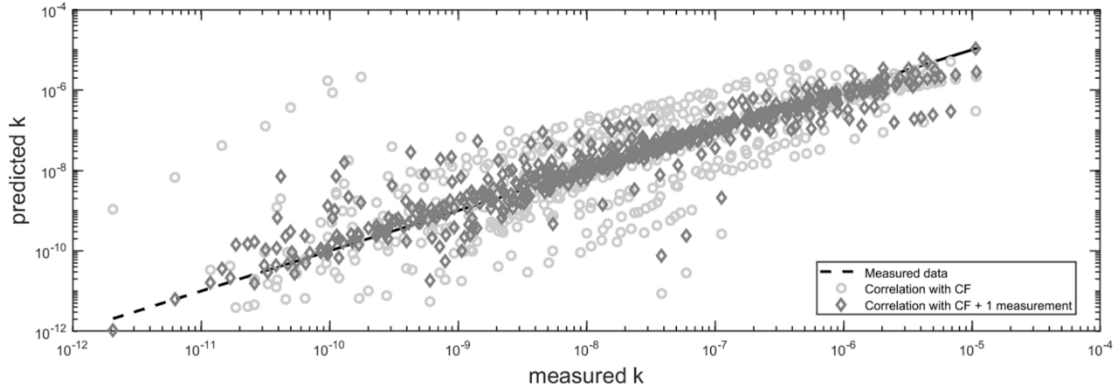
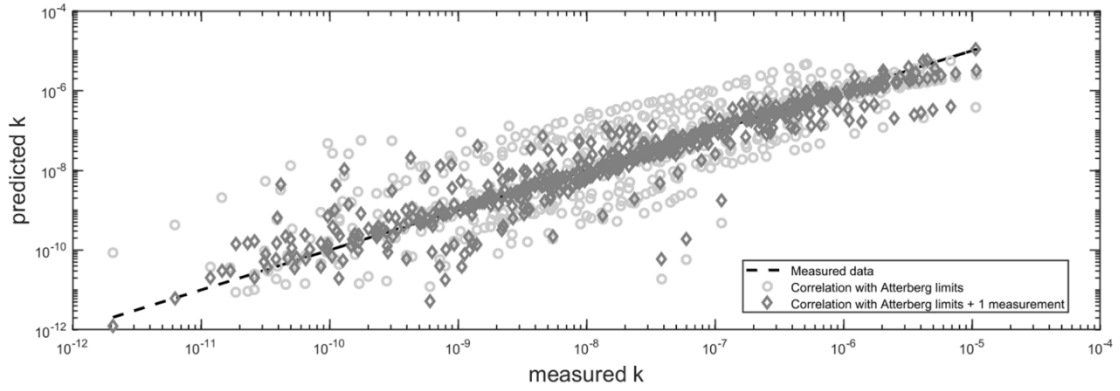


Figure 4-7: Improving the predictions of hydraulic conductivity when using a single measured data at a high-void ratio for both clays and dredged soils, also oil sands tailings (non-amended and amended), respectively.

4.5 Predicting void ratio – saturated hydraulic conductivity (e - k) relationship using a single measured data point k_{sat} at higher void ratios

As all the methods examined show the poorest performance at high void ratios, the authors have examined how the methods can be improved using only a single measurement of k at a high void ratio. When either the Atterberg limit-based equations or the compressibility equations are combined with a single measured k at a known and high void ratio, this results in the following equations:

$$k = k_{measured\ e_0} \frac{e^5}{e_0^5} \quad (4.24)$$

$$k = k_{measured\ e_0} \frac{e^5}{e_0^5} \frac{1+e_0}{1+e} \quad (4.25)$$

As shown in Figure 4-7, the agreement is much improved: For equations 4.24 and 4.25, the difference between the measured and estimated k values are less than an order of magnitude for 90% and 88% of the data for oil sands tailings, 98% and 99% of the data for clay soils, and 90% and 83% of the data for dredged soils, respectively. However, the k values at the very highest void ratios are probably most susceptible to error, and it is more practical to target given effective stress rather than a given void ratio when performing a measurement. Reanalyzing the data sets, picking the measured k value at the nearest 10, 5, 2, 1 0.5, and 0.1 kPa, it is found that the most accurate predictions are made when the $k_{measured}$ value is selected to be the measurement at effective stress between 1 or 2 kPa, and where multiple measurements exist between 1 and 2 kPa, the one closest to 2 kPa is used. This improves the agreement for dredged soil and tailings to 94% and 95 % for Eqns.

4.24, respectively, and to 92% for both data sets for Equation 4.25. An example of the agreement for a subset (9 k - e functions) of oil sands tailings is shown in Figure 4-8.

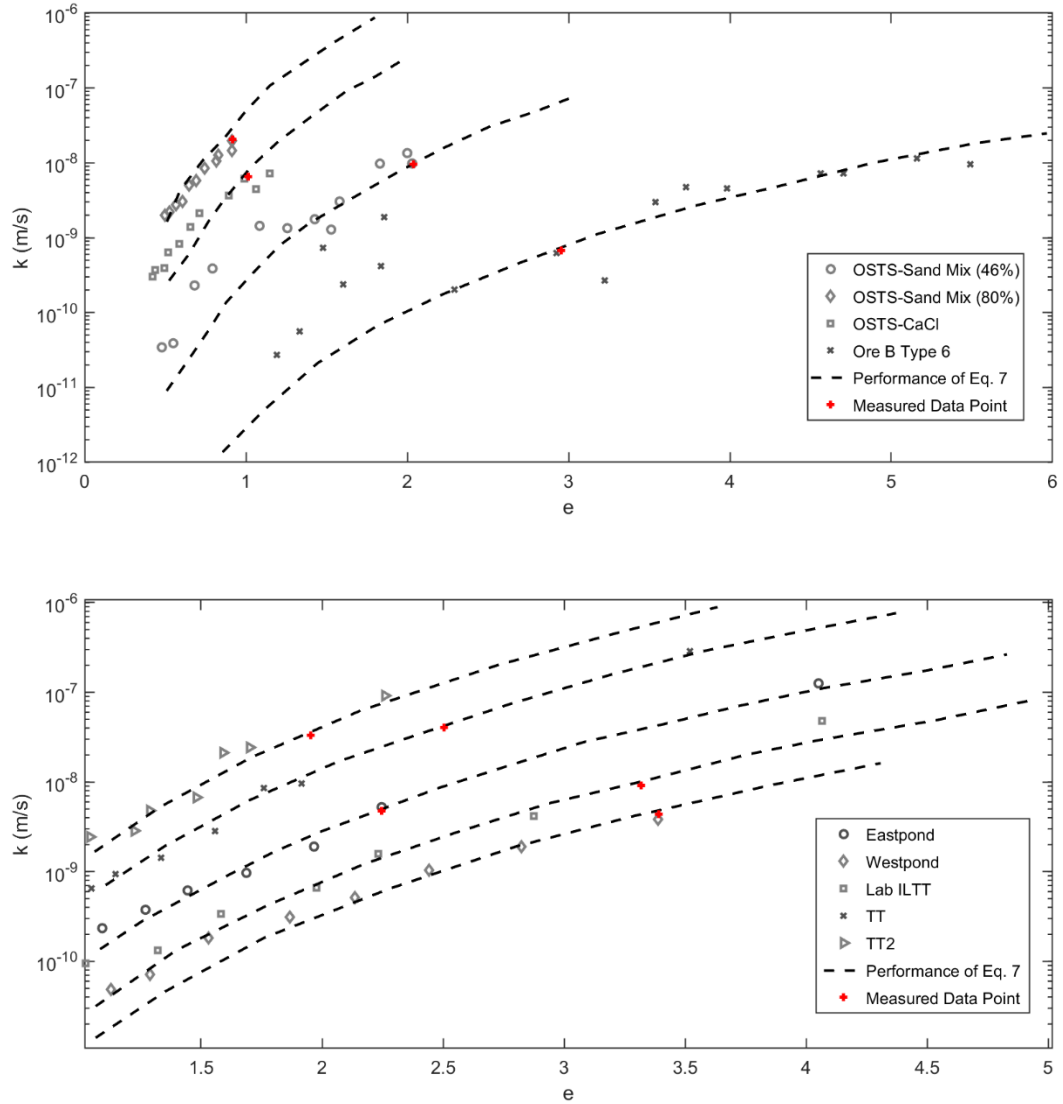


Figure 4-8: Performance of Eq. (7) using k measured for points between 1 and 2 kPa for amended oil sands tailings.

To show the utility afforded by the relatively good accuracy of Eqns. 4.24 and 4.25, predictions of a hypothetical soft soil deposit, instantaneously deposited at $e=4$ for 10 m height) is shown in Figure 4-9. Each case is simulated using the same compressibility as for Figure 4-9, and

the following three k - e functions:

Base Case: $k (m/s) = 3 \times 10^{-9} e^5$

Higher k: $k (m/s) = 3 \times 10^{-8} e^{3.34}$

Lower k: $k (m/s) = 3 \times 10^{-10} e^{6.66}$

These functions are chosen to give k values less than an order of magnitude apart at the initial void ratio, but k values two orders of magnitude apart at $e < 1$. This would be a very conservative estimate of the error due to Equations 4.24 and 4.25. Even with this very conservative estimate of the error, the spread of predictions is relatively narrow. This is because the hydraulic conductivity values at a high void ratio strongly influence the results of the consolidation modelling (k - e values at lower void ratios exert less and less influence), and these values are “anchored” to the measured value at a high void ratio.

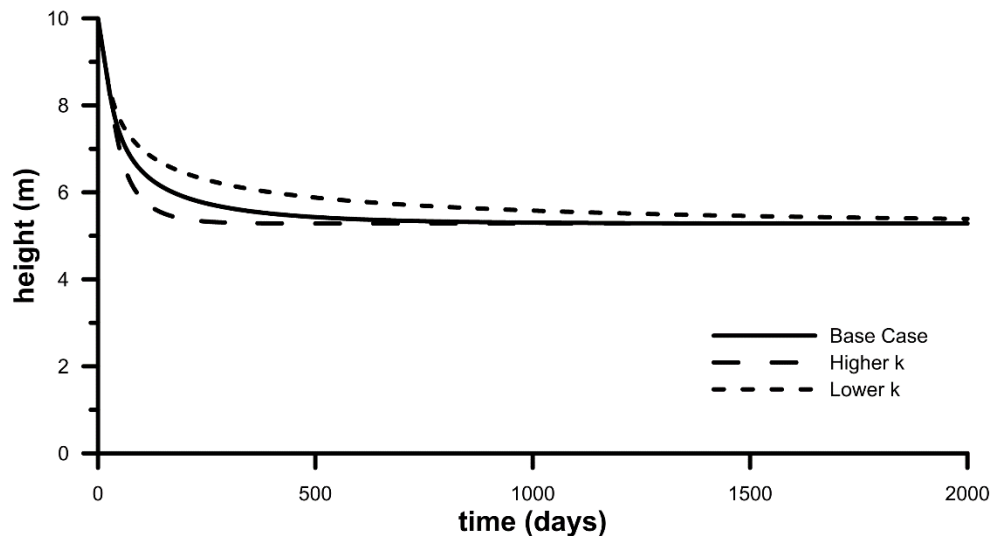


Figure 4-9: Predictions of 10 m deposit $e_0 = 4$, assuming an order of magnitude difference of k at $e=1$ between the base case and either higher or lower case

4.6 Limitations

The proposed method substantially abbreviates the time required to obtain a full k - e curve

and provides estimations that are at least accurate enough to employ the method as a screening tool, say to examine the effect of different proposed amendments (polymer or coagulant type, dose, mixing method) on the consolidation efficiency of dredged soil or tailings deposits. However, for a final design, it would still be prudent to measure the full k - e curve. The proposed method relies on accurate measurement of k at a high void ratio, which can be a challenging task for many materials.

4.7 Summary and Conclusions

This study analyzes correlations for k - e applied to soft soils – clays, clay-based tailings (oil sands), and dredged soils. The data set comprises 79 data sets of k - e . Modified versions of the best performing k - e correlations were obtained, optimized for the analyzed data on clays, oil sands tailings, and dredged soils. Despite high R^2 coefficients, these optimized correlations would still not be sufficiently accurate for even preliminary design for many applications, as demonstrated using hypothetical large strain consolidation analysis. Using the compressibility function as a predictor, somewhat improved agreement. However, the agreement between measured and predicted k - e substantially improved when hydraulic conductivity values measured at effective stresses between 1 and 2 kPa were themselves used as predictors. This approach generated functions that depended only on one value of $k_{measured}$ and assumed either power of 4 or 5 for the void ratio. Although these powers emerged from the statistical analysis of a large data set, fundamental studies have long suggested a power between 4 or 5 (Richardson and Zaki (1954), Marshall (1958)). Further discussion of fundamentals is beyond the scope of this study, although concluding with a cautionary comment that the hydraulic equation applicable to the sedimentation stage appears to be the same as for consolidation (Pane & Schiffman, 1997) for some soils, but

not (Winterwerp, 2002) for others.

A comparison of this method with other estimation methods is given in Chapter 8, which will provide additional guidance for practitioners as to the applicability of these new equations.

Chapter 5: Development of a Prototype Consolidometer and an Associated Analysis Method for Rapid Determination of the $K-e$ Curve

5.1 Introduction

Hydraulic conductivity-void ratio-effective stress relationships govern the consolidation behaviour and influence the storage and reclamation of soft soils such as dredged soils, mine tailings or sludges. Waste storage and reclamation of these highly compressible materials present a challenge in the geotechnical engineering field and finding an economically and environmentally friendly solution could be problematic. Determining the consolidation and permeability of soils with low solids contents using conventional consolidation experiments is either expensive or very time-consuming. The range of the consolidation properties of these materials is highly extensive, and they need to be determined either under minimal effective stresses or in self-weight consolidation.

The essential transport property of the soil is the hydraulic conductivity, and this property of the soil dominates the consolidation behaviour of fine-grained soils. Numerous methods relating this property to soil moisture content and capillary pressure head have been developed and studied for unsaturated soils (Richards, 1931; Watson, 1966). The methods can be determined in the field (Giesel, Lorch, Renger, & Strebel, 1970; Hillel & Gardner, 1970) and in laboratory conditions (Hillel & Gardner, 1970; A Klute, 1972; Arnold Klute & Dirksen, 1986). This study will examine the applicability of one of these methods, known as the Instantaneous Profiling Method (IPM), developed by Watson (1966), to determine the saturated $k-e$ relationship for various fine-grained soils. The model

is based on Darcy's theory and measures the one-dimensional flow at different known volumetric water contents and pressure heads to calculate hydraulic conductivity values.

The dynamic effects of unsteady flow are negligible in this method and do not affect the hydraulic conductivity. However, in the absence of this condition, the "instantaneous" hydraulic conductivity of soils can be determined from the proportionality between the velocity and the potential gradient at particular instants of time. This method is selected to determine the macroscopic flow velocity in soils from the column profiles of potential gradient and water contents during the settlement of soft soils with high initial water content.

The methodology requires two properties of the soil to be measured throughout the experiment; water contents or densities and the total potential profiles within the column. A more sophisticated experimental setup than conventional column tests is required since high-resolution profiles of water content, or density are required in space and time for accurate results. Limitations regarding deformation and validity of large strain versus small strain assumptions dictate requirements of the resolution. Higher resolution of measurement profiles is needed for this methodology to be applicable to large strain conditions, and to provide this high resolution of water content measurements, an automation system is developed for sensor movement.

The accuracy of the solids content/water content sensor, the calibration of readings from these sensors and the necessary corrections on the readings are examined in this chapter. Pore water pressures are measured at certain locations in the column, and appropriate means of interpolation are discussed. This prototype consolidometer is then

used to determine the k - e function for various fine-grained soils (discussed in Chapter 6) and amended fluid fine tailings (presented in Chapter 7) in this study.

In this chapter, the IPM method is applied to a case study as preliminary testing of the application of the methodology. The method is also illustrated and tested by analysis of synthetic data generated to ensure the model's applicability to large strain conditions. The results, along with limitations and possible improvements, are discussed.

5.2 Methodology: Instantaneous Profiling Method (IPM)

The Instantaneous profiling Method was first proposed by Watson (1966) to calculate the hydraulic conductivity for unsaturated soil. The “instantaneous profiles” are depth profiles of pore water pressure and water contents at different times. Hydraulic conductivity at different depths and times can be calculated from the gradients in water content and hydraulic head as per the groundwater flow equation:

$$\frac{\partial \theta}{\partial t} = K \frac{\partial^2 h}{\partial z^2} \quad (5.1)$$

The above equation is based on flow through a constant volume element. However, for saturated conditions with changing density, the same expression remains valid for a constant volume of solids (Fox & Berles, 1997). The volumetric water content θ can be substituted for $e/(1+e)$. For purposes of calculating k , the derivative functions can be expressed in terms of finite-difference using a central difference scheme:

$$\frac{\left(\frac{e_{t_1}}{1+e_{t_1}} \right) - \left(\frac{e_{t_3}}{1+e_{t_3}} \right)}{t_1 - t_3} = k \frac{h_1 + h_3 - 2h_2}{\Delta z^2} \quad (5.2)$$

where k is $k(z, t_2)$, $t_2 = (t_1 + t_3)/2$, h_2 is the head at elevation z at time t_2 , h_1 and h_3 are the head values measured Δz above and below z at time t_2 . In the designed consolidometer, the hydraulic heads and void ratios are utilized to calculate hydraulic conductivity values.

For strict application to large strain conditions, z should be the “height of solids” used in formulations of large strain consolidation, which will result in a non-constant elevation or a non-constant change in elevation. The change in the height of solids can be calculated by knowing the distribution of e with depth over time. Alternatively, the height of solids can be assumed to be a constant if the change in the height of the tailings is small over the time step.

From equation 5.2, other implicit assumptions or requirements are evident:

- The head is linear over Δz
- The hydraulic conductivity does not vary appreciably over Δz

When Equation 5.2 is used, k can be evaluated at any number of depths and times, given sufficient resolution of the data. The advantage of this method is that the measured k values are independent of any assumptions with respect to the dewatering mechanism, e.g., sedimentation, consolidation, or creep. The disadvantage is that relatively high resolution in density or water content measurements may be required so that these can be interpolated with accuracy.

5.3 Demonstration for IPM method with synthetic data

5.3.1 Description of synthetic experiments

The IPM method was originally developed for unsaturated conditions, and synthetic experiments are conducted to ensure that the method is applicable to large strain conditions

as well. In these analyses, a large strain consolidation software is utilized to calculate synthetic data of volumetric water contents and pore water pressures at fixed locations (with given compressibility and k - e curves). These synthetically created data are then used to back-calculate the k - e equation using the IPM method. For these analyses, two simulations of hypothetical column tests are shown, both using an identical compressibility curve but with two very different k - e functions, targeting both high and low regions of k - e data. Both simulations have the same initial height ($h=27$ cm) and void ratio ($e=3.44$). The compressibility curve and the k - e function are shown below:

$$\mathbf{\sigma'}$$
- \mathbf{e} **relationship** $e = 2.42\sigma'^{-0.165}$ (5.3)

$$\mathbf{Higher}$$
 \mathbf{k} - \mathbf{e} **relationship** $k = 1 \times 10^{-14} e^{14.36}$ (5.4)

$$\mathbf{Lower}$$
 \mathbf{k} - \mathbf{e} **relationship** $k = 5 \times 10^{-11} e^5$ (5.5)

If the IPM method is applicable for large strain conditions, it should recover the k - e curve from the analysis of the data generated by the model runs (the synthetic data). Figures 5-1 and 5-2 show the total potential and void ratio profiles at specific days determined from the synthetic analysis, respectively.

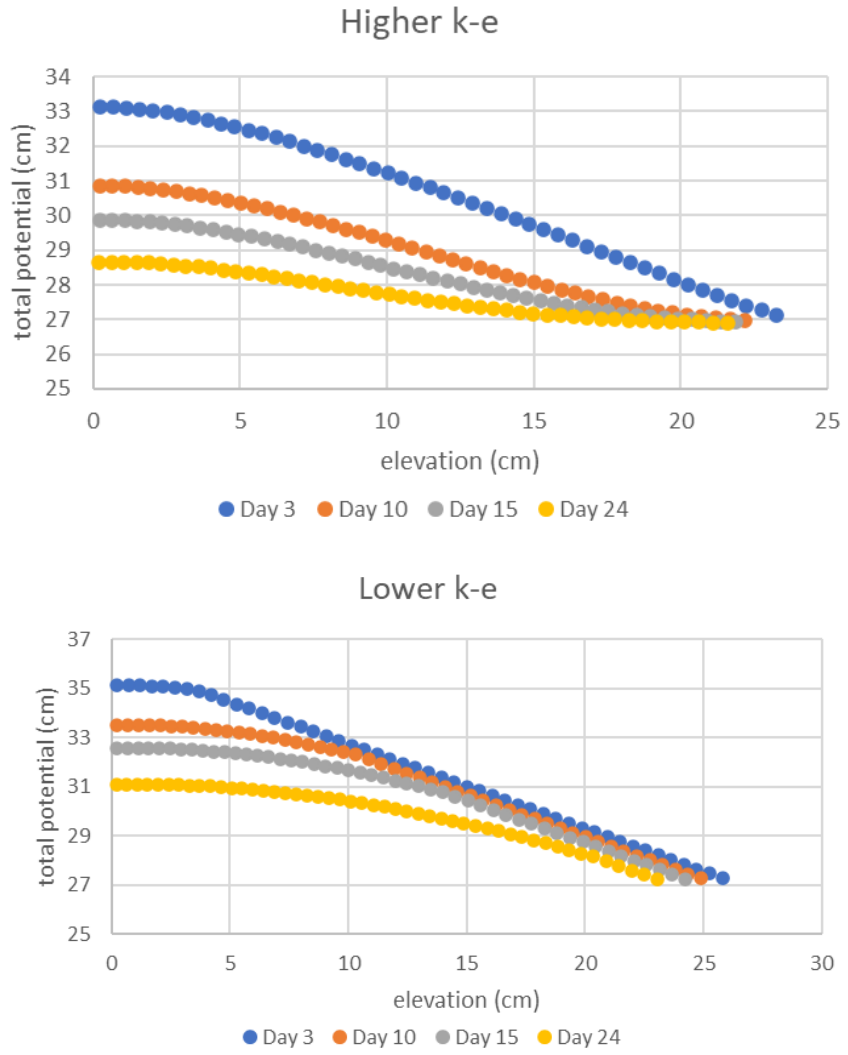


Figure 5-1: The variation of total potential profiles at different elevations at selected days

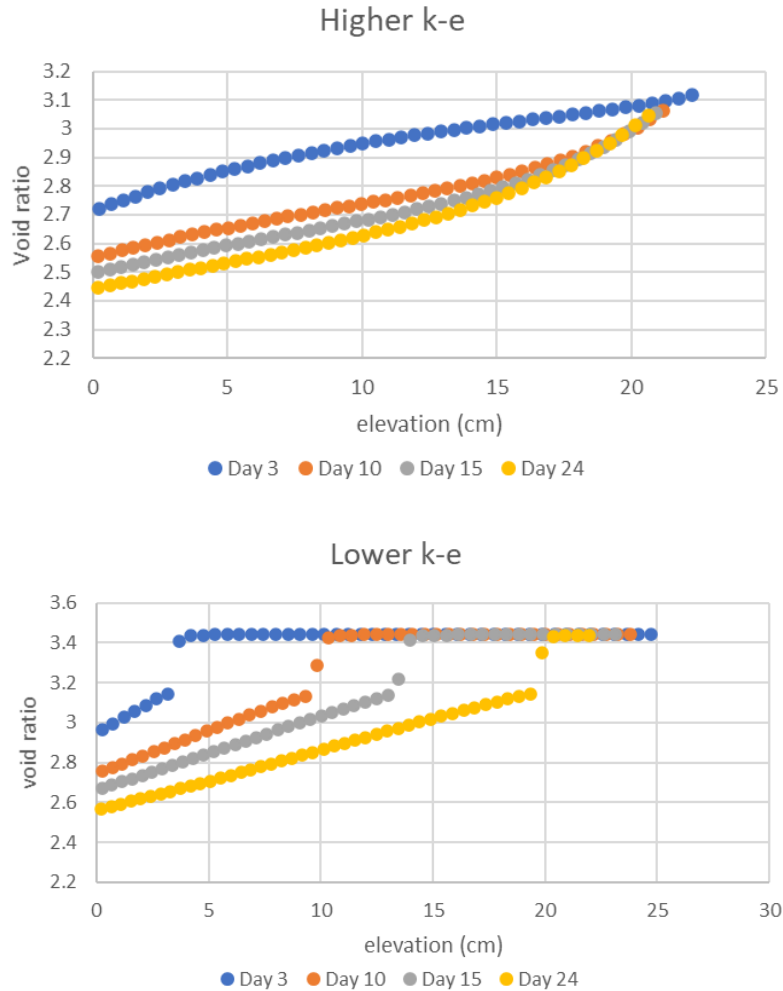


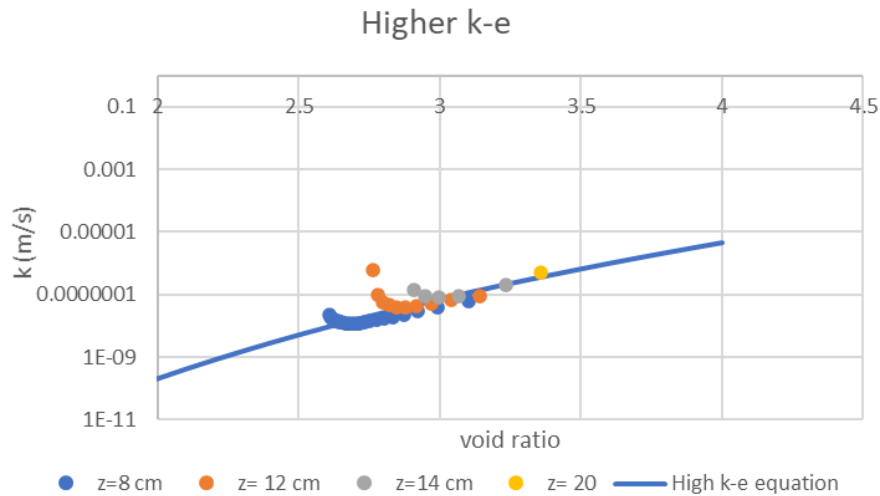
Figure 5-2: The change in void ratio profiles at different elevations at selected days

Using the IPM method with a Δt of 24 hours, the $k-e$ values for data at different heights are compared with the $k-e$ values input into the model, demonstrated in Figure 5-3.

For the high $k-e$ results, errors start to creep into the IPM method at later times. This is due to two reasons: first, the water fluxes become low, and second, regions of constant slope develop in depth-head profiles. For these regions, the second derivative of the head will be zero or approaching zero, which could lead to the overestimation of the

hydraulic conductivity. Figure 5-4 demonstrates the change in the values of the second derivative of total potentials for the higher $k-e$ test, showing the regions where the second derivatives change sign, and as a result, the $k-e$ values calculated at those regions are no longer applicable.

Similarly, for the low $k-e$ simulation, errors are prominent at the beginning, which corresponds to the early profiles of the head with depth, where again the second derivative approaches zero at high elevations. Also, it is interesting that the error for the lowest depth data seems to be the largest, though still less than half an order of magnitude. This also corresponds to the region where the second derivative becomes small, and therefore the region most susceptible to error.



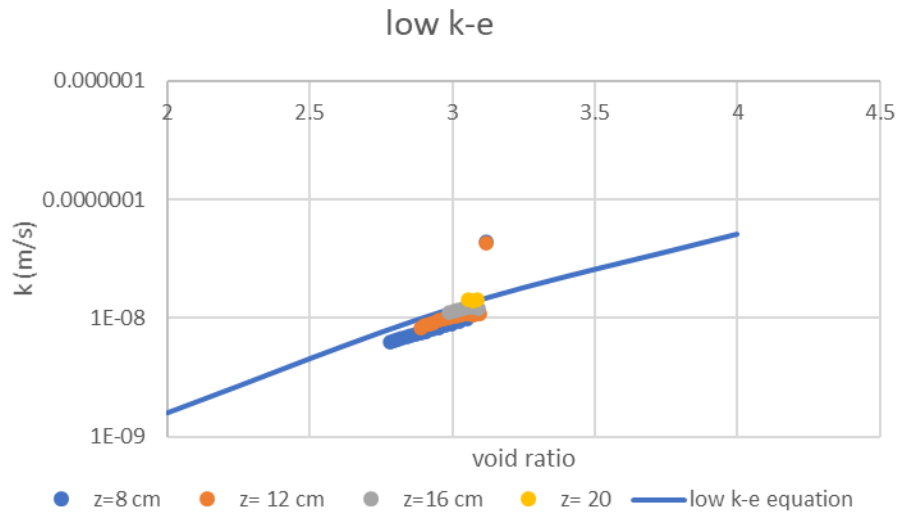


Figure 5-3: Comparison with the calculated k - e relationship with the input k - e data using the second derivative of total potential values

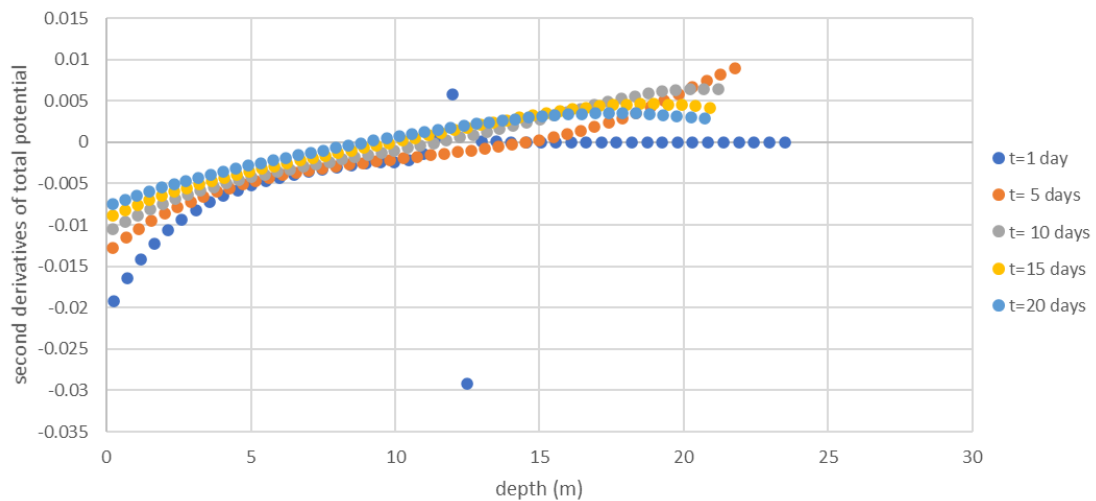


Figure 5-4: The change of sign of the second derivatives of total potential values with depth for higher k - e example

5.4 Measurement of Pore Water Pressure Profiles

5.4.1 Pore water pressure measurements

In this study, the selected pore water pressure sensors are electric transducers capable of

measuring soil pore-water pressure up to 100 kPa, with a designated accuracy of ± 0.5 kPa. The T5 pressure transducer (<https://www.metergroup.com/environment/products/t5-tensiometer-water-potential/>), along with the DL2e data logger (<https://www.deltat.co.uk/product/dl2e/>), is utilized in this study; they are presented in Figure 5-5. This sensor also has the capacity to measure negative pore-water pressure, but this is not utilized in this study.

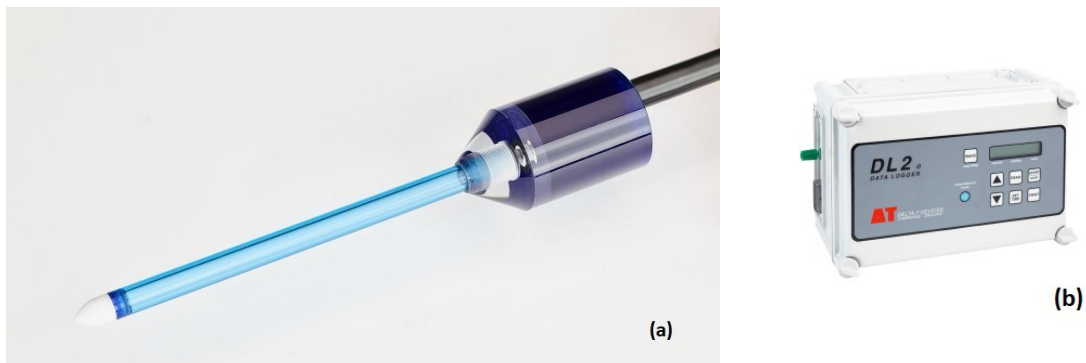


Figure 5-5: (a) The T5 Pressure Transducer by Meter Group and (b) the DL2e Data Logger by Delta-T devices utilized to measure pore water pressure measurements in this study

The pressure transducers are calibrated and checked prior to each test by changing the water levels in the designed column. Since the locations of the sensors are fixed, the readings should reflect the hydrostatic pressure within the column. Figure 5-6 represents an example of the calibration and checking procedure completed for four tensiometers utilized in the test case, comparing the hydrostatic pressure with the sensor reading from the pressure transducers. The sensor readings agreed well with the actual measurements; demonstrated that the sensors are working and calibrated for this specific test case. After the calibration process, the accuracy of the measured readings is increased to 99.1%.

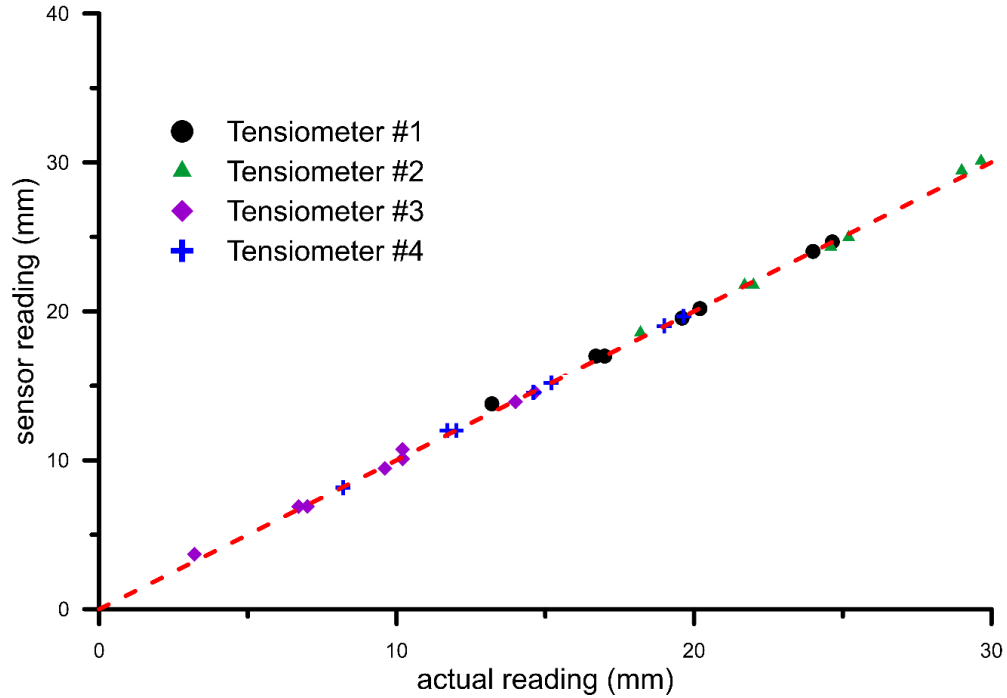


Figure 5-6: Calibration effort of pressure transducers prior to testing

5.4.2 Estimation of total potential measurements with depth within the column

During the experiments, at least three or more pressure transducers measured pore water pressures within the column, depending on the thickness of the sample. For thicker samples, the number of sensors was increased. These pressure transducers are placed on the outer wall of the designed consolidometer and provide continuous measurements of pore water pressures during the experiments.

The nature of Equation 5.1 requires measurements of pore water pressures and volumetric water contents at the same heights and depths. High-resolution measurement profiles of volumetric water contents were achieved with an automation design described in the following sections in this chapter, which allowed for measurements at every centimetre or two centimetres during most of the experiments. For every volumetric water

content data at every height, pore water pressure measurements needed to be determined as well. However, this property was measured at certain locations only (due to the availability of the number of inlets), the in-between measurements were estimated using Curve Fitting in MATLAB R2019b, using the measured data by the pressure transducers and the readings of the mudline. An example (on amended FFT sample) of predicted PWP measurements is presented in the following figure, where the colourful data points correspond to measured data at different heights, and the grey data points are the predicted values using MATLAB.

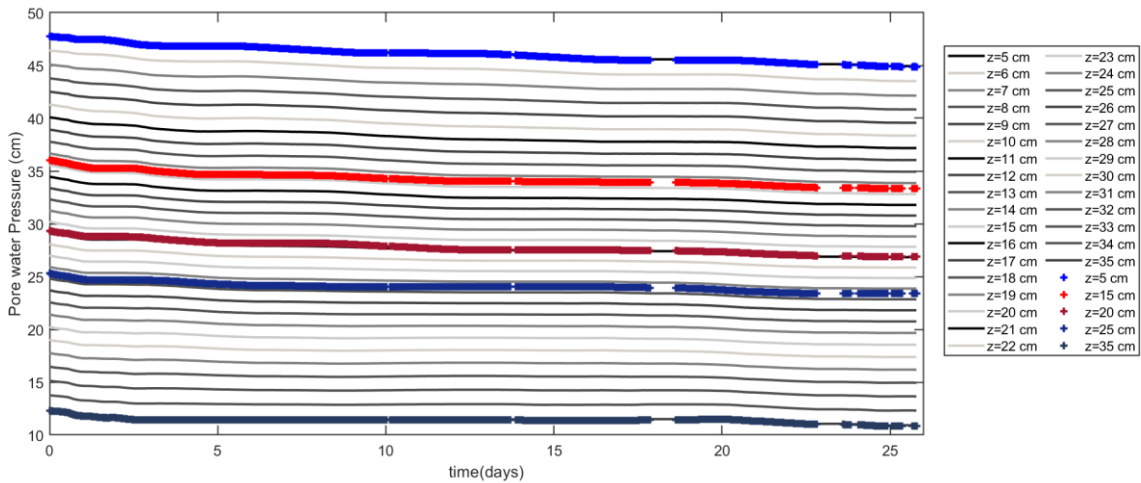
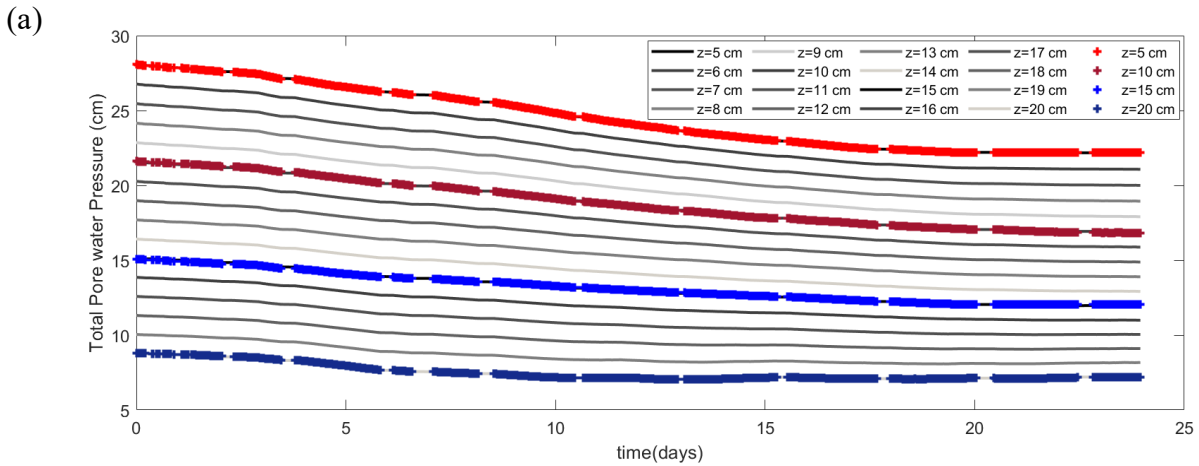


Figure 5-7: Predicted PWP measurements for the amended FFT sample.

Total potential measurements are calculated by adding the measured pore water pressure measurements and gravitational head. In real data, the pore-water pressure measurements are limited, but the estimate of the second derivative is critical to the IPM calculation. Therefore, the synthetic data is used to explore the suitability of fitting schemes for the pore-water pressure data, explained in the previous section.

5.4.3 Selecting the most appropriate method to fit pore water pressure measurement at various heights with time

Selecting the correct fitting method for pore water pressure measurements is imperative in the analysis of the IPM method. Usually, only one method provides good fitting results to the measured data; however, in some cases, different fitting methods can provide prosperous results. Therefore, selecting which method to apply might affect the calculated k - e relationship. For example, the measured pore water pressures from the Kaolinite experiment were successfully fitted to two different types the equation; power equation (with three parameters in the form of $y=ax^b+c$) and a third-degree polynomial equation (in the form of $y=ax^3+bx^2+cx+d$), as presented in Figure 5-8.



(b)

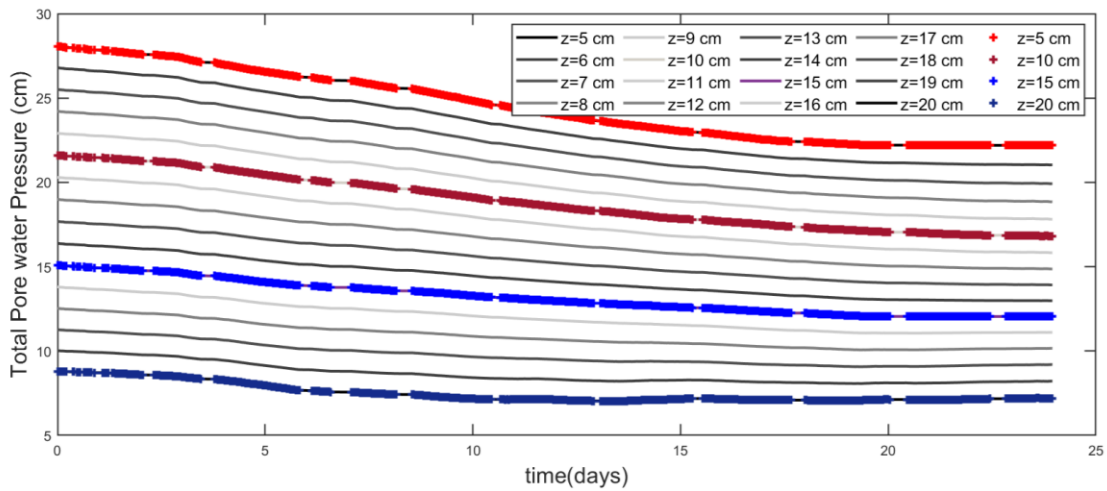


Figure 5-8: Fitting of pore water pressure measurements to (a) Polynomial (third-degree) and (b) power equations for kaolinite tests

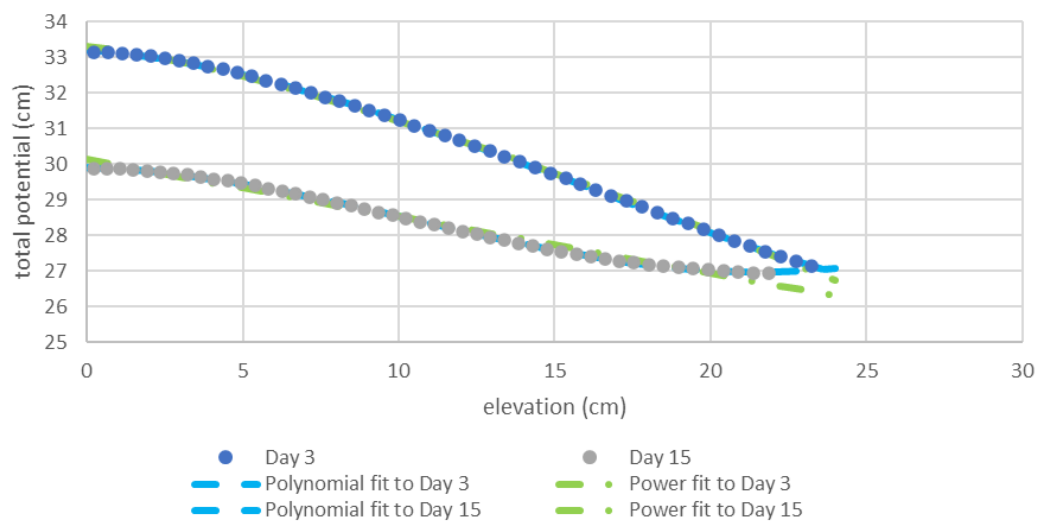
To understand the suitability of the fitting schemes and its limitation, synthetic analyses are used. When more than one fit is available for the test (i.e. Kaolinite test presented in Figure 5-8), a quick numerical analysis (UNSATCON sedimentation-consolidation model is utilized) can be conducted to determine the shape of the produced PWP measurements (hence total potentials) from the program. For this experiment, two separate $k-e$ equations are analyzed (hence synthetic data is created), and simulated measurements are compared with measured data (presented in the following figure).

From the shapes of the curves for the higher $k-e$ equation (using a higher power constant), a power equation would provide better fitting performance for the first few days, whereas polynomial fitting may be more appropriate to use later in the test. As for the curves simulated by a low $k-e$ relationship, a power fitting seemed more appropriate overall. At higher elevations, closer to the mudline, the change in the void ratio and the

second gradient of total head values are greatest, and when the shape of the second gradient fit changes at those elevations (can be identified in Figure 5-9), the polynomial fit may provide a better fit to the measured curve. However, the shape change in the second gradient curve induces sign changes in the calculated second gradient values. Considering the IPM method calculates a single k value at that range, it is not appropriate to use the model anymore. For this specific example, the polynomial fit is selected to be used for the IPM calculation.

(a)

Higher k-e



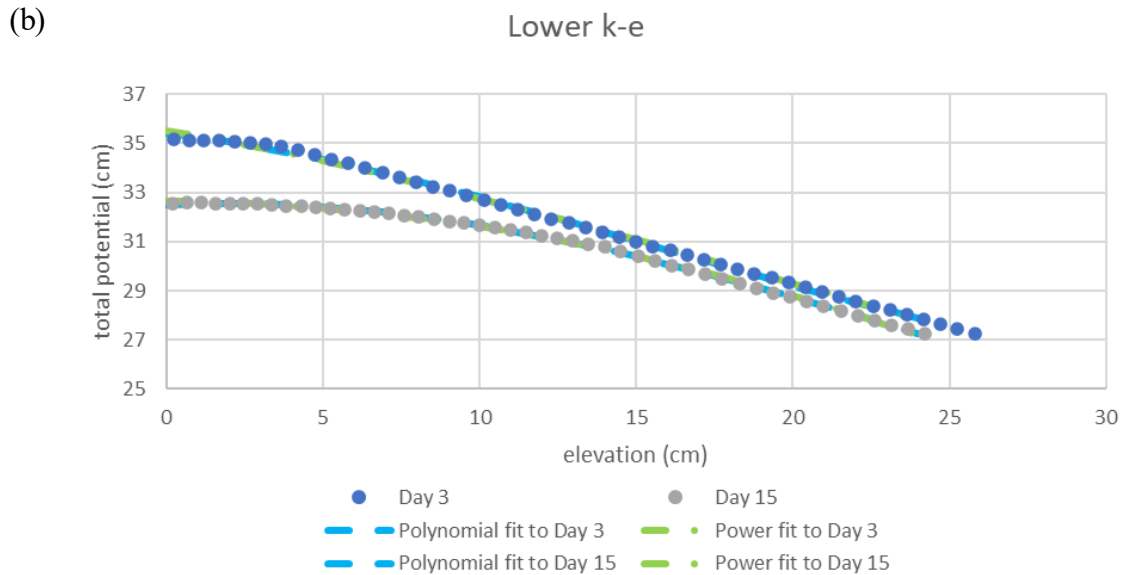


Figure 5-9: Fitted PWP measurements for Kaolinite experiment (a) Using power equation, and (b) using a polynomial fit

5.5 Measurement of Volumetric Water Content Profiles within the Column

At the preliminary stage of the experimental design, various sensors were considered to determine water content or density for the long-term self-weight consolidation column. Neutron-scattering and γ -ray attenuation techniques are the most commonly used methods to measure this property for most studies using the IPM method. They both are very effective methods, but the use of nuclear-based methods in the laboratory would have created concerns. Additionally, such methods are expensive – a modern NMR-based soil density sensor, DART manufactured by Vista Clara Inc. (<https://www.vista-clara.com>), is ~ \$100,000. CAN.

One of the most commonly used measurement techniques for moisture in the geotechnical and agriculture field is dielectric techniques (i.e. TDR or FDR). These sensors measure the soil electrical conductivity or apparent dielectric constant and empirically

calculate the volumetric water content of the material. There are many advantages associated with this technique. However, there are also several issues to consider when using these sensors, particularly for their application to tailings. For instance, such sensors are either relatively discrete points or are rods, usually inserted vertically or horizontally in a column. The rods of the sensors are long (vary from ~6-30 cm); hence densely placing sensors in a row may affect the consolidation behaviour of the material where the sensors are located. Also, the application of electrical current may create particle displacement (as the negatively charged particles will move around with the current) and eventually may lead to particle accumulation on the sensors. This will lead to faulty readings, and of course, the calculated volumetric water contents would not represent the real measurements of the sample.

For non-destructive, continuous measurements within a column, two different types of techniques were considered; electrical tomography and capacitance-based sensors. In the following sections, electrical conductivity sensors are initially examined as they are capable of calculating three-dimensional profiles of water content measurements using the electrical resistivity tomography method. Then capacitance-based sensors are considered, and they are tested for various fine-grained soils, including Leda clay, thickened gold tailings and centrifuged cake.

5.5.1 Electrical Conductivity (EC) Sensor Testing

Initially, the use of electrical sensor techniques was tested in the laboratory. A Three-electrode batch cell with a volume of 500 mL of flocculated FFT sample was tested (presented in Figure 5-10). The sample is covered with a lid, and three electrodes (i.e.

working, counter, and reference electrodes) were connected to 2 iron or aluminum rods, which penetrated the sample about 5 cm. Working and counter electrodes (anode and cathode, respectively) were 1 cm apart, and for the measurement of potential at the anode, a reference electrode was placed 0.25 cm apart from the anode. The setup is controlled by VSP Potentiostat (Bio-logic Science Instruments) (Chow & Pham, 2019). In order to slow down the movement of finer particles, the possible smallest voltage is applied from the VSP Potentiostat (0.05 A). An alternating current is applied through the sensors, the potential between the anode-reference rod and the change in the frequency are measured. Both iron and aluminum rods were tested; however, the recorded potential values did not differ from each other.

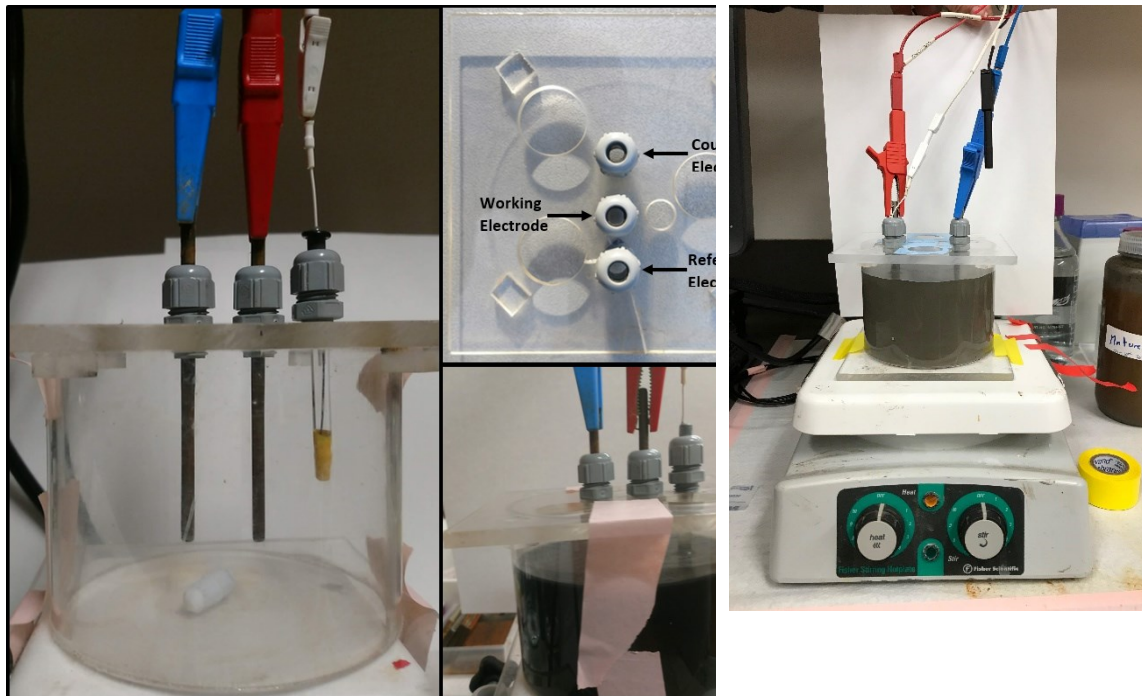


Figure 5-10: on the left: Three-electrode electrochemical cell used in EC experiments (Chow & Pham, 2019), on the right: 800 ppm FFT sample in the cell

In order to determine the effect of electrical current on fluid fine tailings samples (Shell Canada FFTs), unamended FFT and amended samples (two different dosages; 600 ppm and 800 ppm) are tested for a week, using a mixing protocol adapted after Mizani (2017) to prepare the amended samples. The potential between the anode and the reference rod was measured at 1 hour, 2 hours, 4 hours, 6 hours, 24 hours and one week. For each reading, the water accumulated on the surface is obliterated, a current is applied later (to ensure the electrical flow moves within the soil). At the end of the experiment, the rods were taken off, cleaned and set aside for the next measurement. Unfortunately, this step was necessary because even with a small current, fine-rich oil sands tailing were accumulated at the anode (Figure 5-11).



Figure 5-11: Accumulation of finer particles at the positively charged rod observed during EC sensor testing

Two duplicate samples were also set aside to be tested at the end of the week to determine the effect of the current on the same sample. Based on the results, the discrepancy between the original cell (which has been tested for the whole week), the cell that is tested once (tested once during the week and at the end of the week) and the never-tested sample (to be tested only at the end of the week) is negligible. This comparison is demonstrated in Figure 5-12, and potential readings for 800 ppm tests are presented in Figure 5-13. The readings would normally increase while the soil settles and the void ratio decreases, but for the tested amended FFT, a different behaviour was noticed. The effect of flocculation can be observed in Figure 5-13, where the potential readings decrease below the raw FFT readings for the measurements taken on the first day, only to be increased by the end of the week. The experiments need to run at least 30 seconds; stopping the test before this duration result in inaccurate potential readings. Therefore, the application of EC might have been a useful technique for other types of soils, but for fine-rich tailings, the accumulation at the sensors did create a complication for continuous measurements.

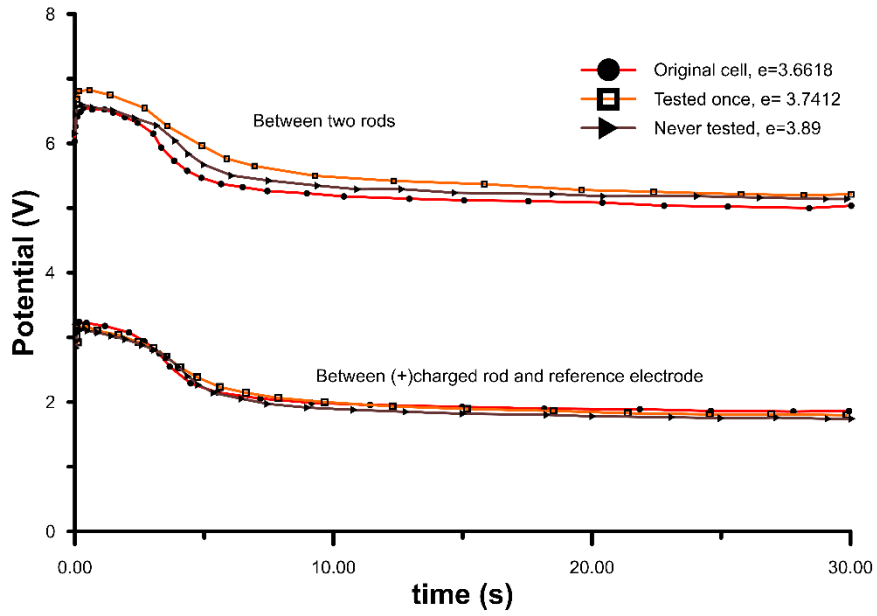


Figure 5-12: 7-day testing for 800 ppm sample on the duplicate cells

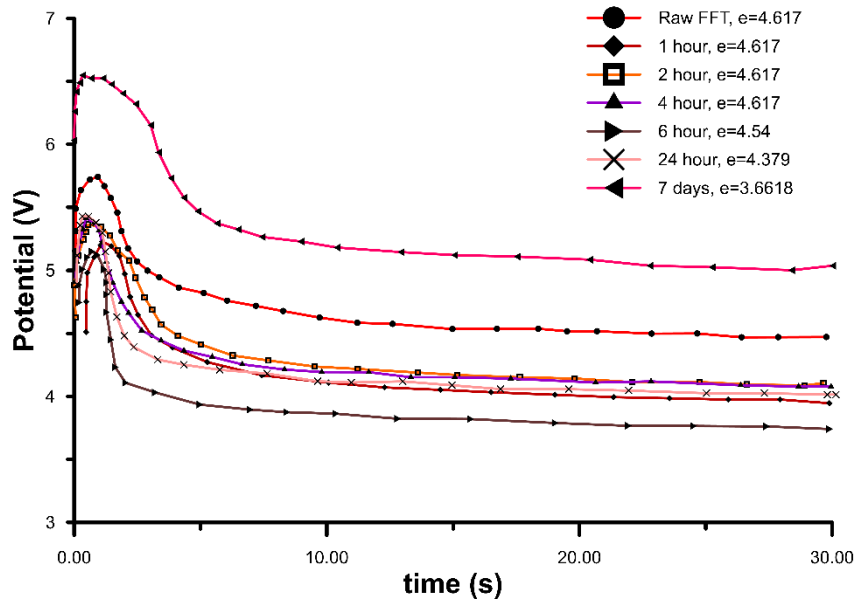


Figure 5-13: Potential readings vs. time for 800 ppm

5.5.2 Determination of Volumetric Water contents with SENTEK EnviroSCAN Sensors

For the non-intrusive measurement, we have considered most of the measurement

techniques available commercially for both laboratory and field applications; many of them are used in agricultural projects. TDR sensors are probably the most commonly used ones in this field, but for densely placed sensors on the column, walls would have probably disturbed the consolidation process due to the long rod length of the sensors, which can go up to 30 cm in length. SENTEK EnviroSCAN sensors provide a reliable alternative, as they are a non-intrusive measurement method.

SENTEK EnviroSCAN probes (available at www.campbellsci.com) provides volumetric water content profiles using the capacity-based technique covered in Chapter 2.8.2.2.1; a picture of the probe body and the sensors are presented in the following figure. The sensors allow multiple-depth soil moisture measurements and the probe is installed in a 2" PVC pipe. The probe length is one meter and ten connections on the probe (at every 10 cm) are available.



Figure 5-14: SENTEK EnviroSCAN probe

The sensors are designed for continuous long-term measurements and they are susceptible to small changes in volumetric water contents, 0.1% to be exact. These are non-intrusive measurement probes and they are not in contact with the soil directly. However,

each probe requires soil-specific calibration; their zone of influence (sphere of influence) is only 5 centimetres away from the pipe, they are sensitive to air gaps surrounding the sensor. SENTEK EnviroSCAN creates a high-frequency electrical field around each sensor and measures the electrical capacitance of the soil. The soil water content is determined accordingly. Each water content sensor outputs an SDI-12 (Serial Digital Interface at 1200 baud) signal, which is recorded by a CR300 datalogger (Campbell Scientific, Inc.). The probes themselves are not capable of logging information; therefore, it requires a device compatible with SDI-12 as a master device, which will issue SDI-12 commands to instruct the probe interface. It will retrieve data during sampling and send the measured values to the master device for storage.

5.5.2.1 Calibration of Volumetric Water Content Profiles with SENTEK EnviroSCAN sensors

Prior to testing, normalization and function test should be completed. Normalization setting provides a range of reading which the electronics are capable of. Two extreme ranges are tested, air and water, which are recorded as normalization values before sampling. The configuration of the probe and sensor is accomplished using Intelligent Probe Configuration Utility. SDI-12 probe interface uses this program to calibrate each sensor installed on the probe. SENTEK EnviroSCAN soil moisture sensors are calibrated using sensor readings or scaled frequencies with actual moisture content values over a range of soil water contents. Determination of actual water content values is necessary, which was accomplished with oven-dried samples. The calibration curve is established using scaled frequencies and independently determined volumetric water

contents. Scaled frequency (SF) readings can be determined using the following equation.

$$SF = \frac{(F_a - F_s)}{(F_a - F_w)} \quad (5.6)$$

$$\left(\frac{SF - C}{A} \right)^{\frac{1}{B}} = \theta_w \quad (5.7)$$

where F_a is the raw count in the PVC tube while suspended in air, F_s is the raw count in the PVC column in the soil at each particular depth level, F_w is the raw count in the PVC tube in a water bath, and θ_w is the volumetric water content. Before taking any measurements in soil, F_a and F_w values (hence SF values) are determined at water contents of air and water. The sensor provides θ_w as an output, and this value is converted to SF using equation 5.7.

The relationship between SF and volumetric water contents can be described by a calibration equation in a power-form, where parameters A, B and C are soil specific. The default calibration parameters for various types of soils are presented in SENTEK EnviroSCAN's Calibration Manual v2.0. At the end of each test, multiple samples are collected from the columns and oven-dried to determine the actual volumetric water contents; these determined values are then associated with SF values from the sensors, and a calibration equation is determined using Equation 5.7. An example of such a calibration equation is provided in the following figure along with various calibration parameters, A and B , determined for the column tests in this study.

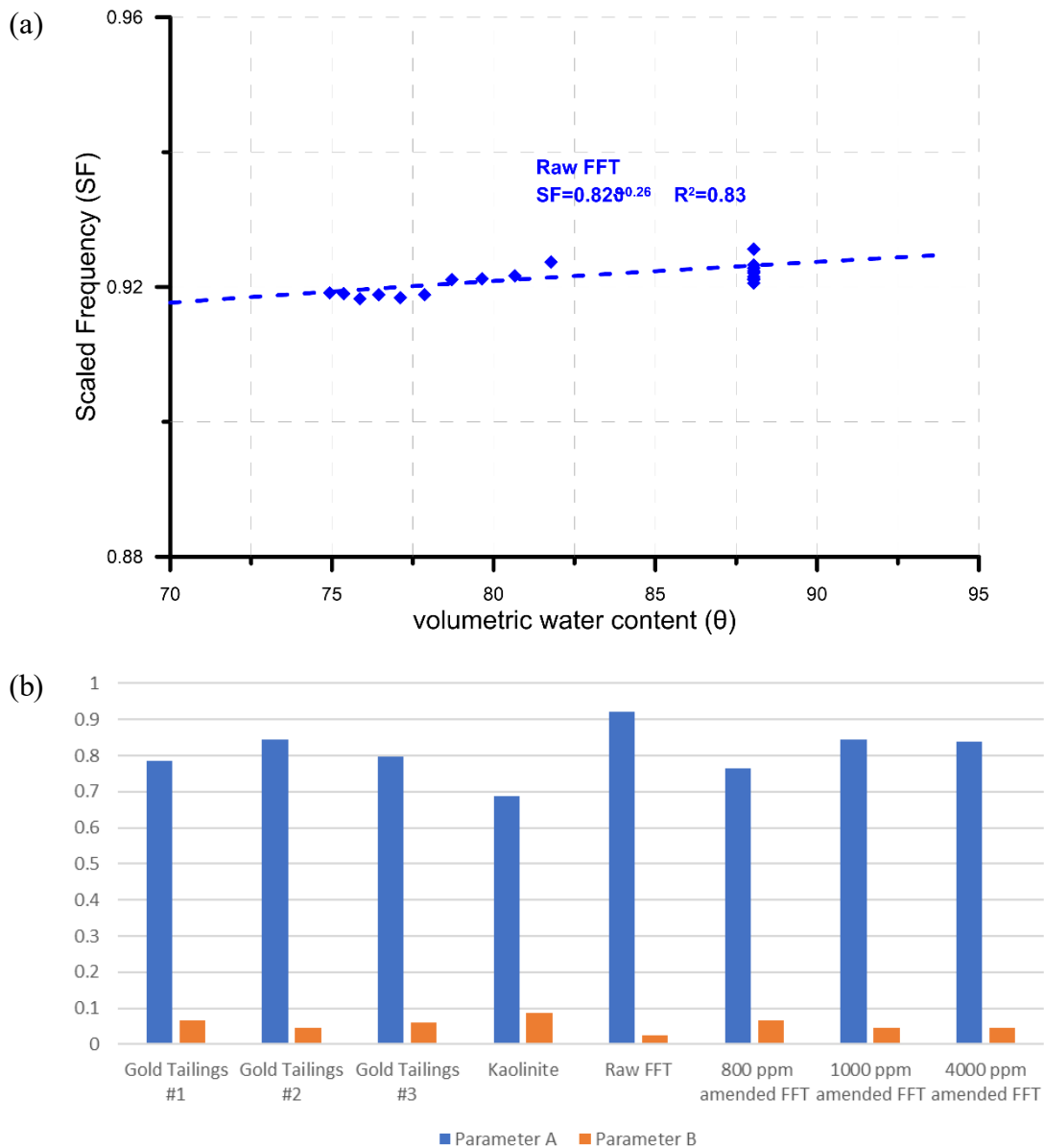


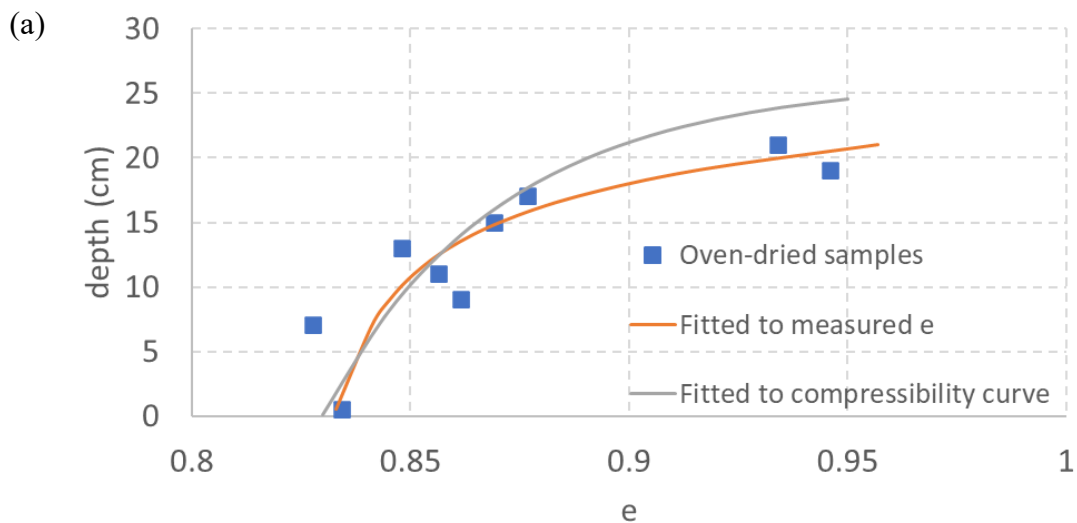
Figure 5-15: (a) Volumetric water content vs. Scaled frequency relationship for an unamended FFT sample (b) Calibrated Parameters A and B for different types of soils

For some of the experiments conducted in this study, multiple sensors have been utilized, and each sensor is calibrated for the tests. It should be noted that the sensor reads from multiple locations due to vertical movement imposed on the probe body. Default calibration parameters have been used during the experiments, and the calibration equation is determined after the completion of the tests. For each experiment, a number of samples

are collected at the beginning and at the end of the tests at different heights to calibrate each material. At least three samples are collected from the same batch of tailings (unamended or flocculated) or fine-grained soils before placing the material into the column; if multiple batches are prepared to fill the column, at least two samples are collected from all the batches and oven-dried to determine the initial water contents of the material. At the end of the test, the water-content profile within the column is determined by collecting samples at various heights (where the sensors are measuring, at least two samples are collected using a spoon at the same depth); multiple samples from the same heights are also collected. The sensors are calibrated using the oven-dried water contents at the midpoint of their range. An example of such profile is presented in Figure 5-16 (a), where the measured profiles of VWC values are fitted to a best-fitted equation or to a compressibility curve to (a power function) to provide more realistic profiles prior to associate the values with scaled frequency readings. Scaled frequency values are back-calculated from the sensor readings using the default calibration parameters and matched with the newly determined volumetric water to calculate the parameters of the calibration equation.

The preliminary tests were performed with various types of soils using a bucket, which the design is modified (a pipe is attached to the bottom of the bucket to accommodate sensors). An initial test is conducted using Leda clay, where the material is diluted to various volumetric water contents (varied from 65-198%, determined by oven-drying) to test the sensors. The scaled frequency values (determined from the sensor readings) at these volumetric water contents (measured from oven-dried samples) and to provide a comparison SF reading from water are presented in Figure 5-16 (b). These values are

utilized to determine the calibration equation presented in Equation 5.7. Another preliminary test conducted was a continuous measurement test in a sedimenting column, conducted using Musselwhite thickened gold tailings, to track the change in volumetric water content during a sedimentation process. Samples are collected for oven-drying to measure the initial water contents. At the end of the experiment, two samples are collected to determine the final VWC by oven-drying, where the sensor is reading from. Using the initial and final volumetric water contents of the material and associated SF values (measured by the sensor), the relationship is calibrated. The results demonstrated that the tailings settled to their final water content within the first two hours, and the percentage error between the determined VWC by the sensor and the measured value (calculated by evaporation method) is determined as 3.17% (Figure 5-16 (c)). Once the volumetric water content or void ratio profile is determined



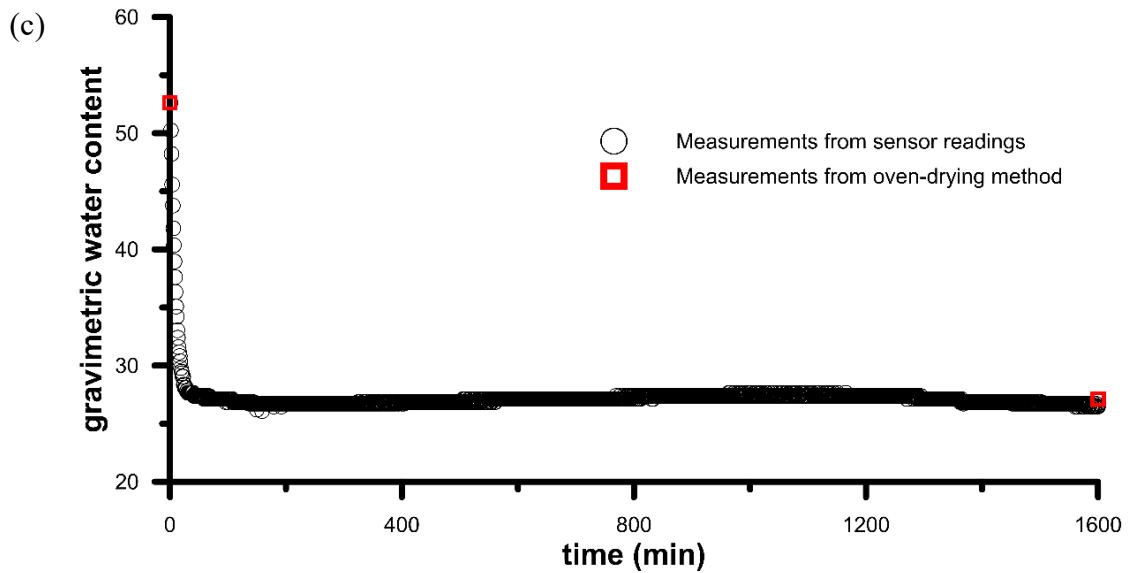
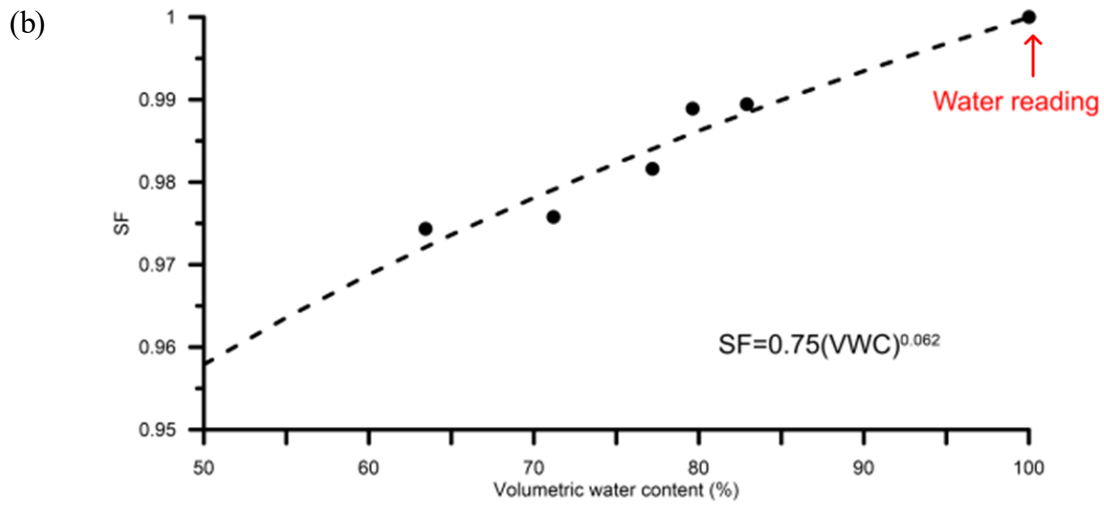


Figure 5-16: (a) A profile of VWC fitted with a best-fit polynomial curve and a compressibility curve (a power equation), (b) SF and VWC (from oven-drying) relationship from sensor testing of Leda clay, and (c) the continuous measurement test for Musselwhite gold tailings compared with final GWC from the oven-dried samples

5.5.2.2 Correction of Volumetric Water Content readings

While running the experiments, a “wave-like” behaviour of raw readings have been observed. This specific behaviour is especially more noticeable in some of the experiments where nothing is really changing in the column (i.e. the settlement height is constant), but the scaled frequency readings demonstrated a “wave-like” behaviour provided in Figure 5-17. This behaviour is probably occurring because of the sensors, as it applies to all locations, and it needs to be corrected before calculating the calibration equation. The following figure demonstrates an example for this correction procedure; an amended FFT sample is selected where the raw scaled frequency readings have been displayed. The readings from the first sensor are presented, and the settlement rate at these locations are minimal after Day 15.

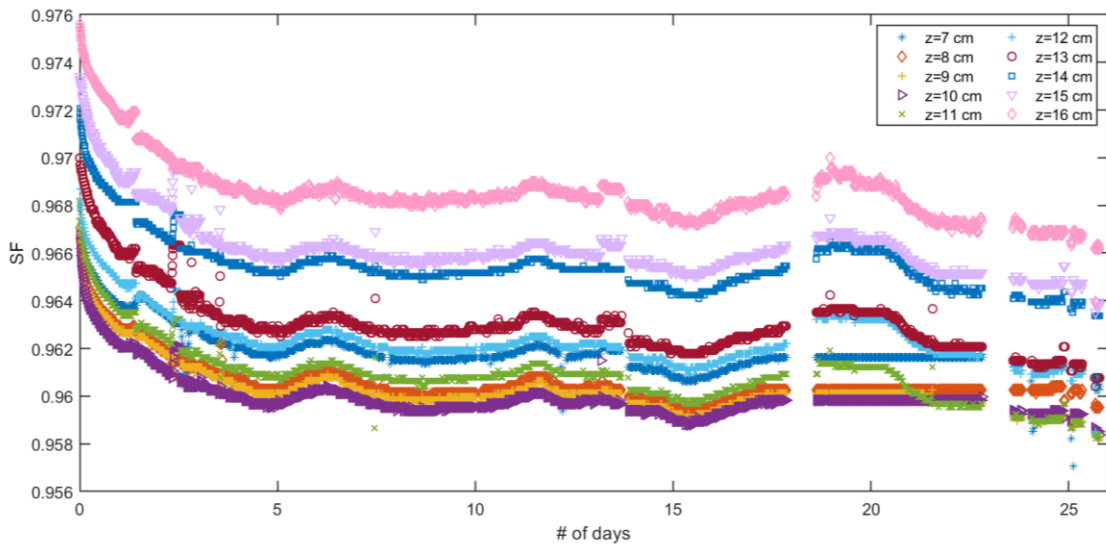


Figure 5-17: Amended FFT sample, raw VWC reading at ten different locations (at every 1 cm intervals) from sensor 1

This wave-like behaviour needs to be corrected before proceeding with the IPM method. To achieve that, a certain location is selected where the sensors are completely reading from water. For this specific example, this location is at $z=34$ cm; the sensor reads fully from the water after Day 9.7 while the settling is still occurring. The same behaviour has been observed from this sensor location as well (Figure 5-18). It is known that at this location, the scaled frequency reading should be equal to one; hence the variation in the reading have been applied to other sensor readings to correct it (Figure 5-19); and after Day 9.7, which improved the overall raw readings for all locations. The scaled frequency readings in Figure 5-19 are more realistic, as the settlement behaviour is very slow, and the change in raw readings is small.

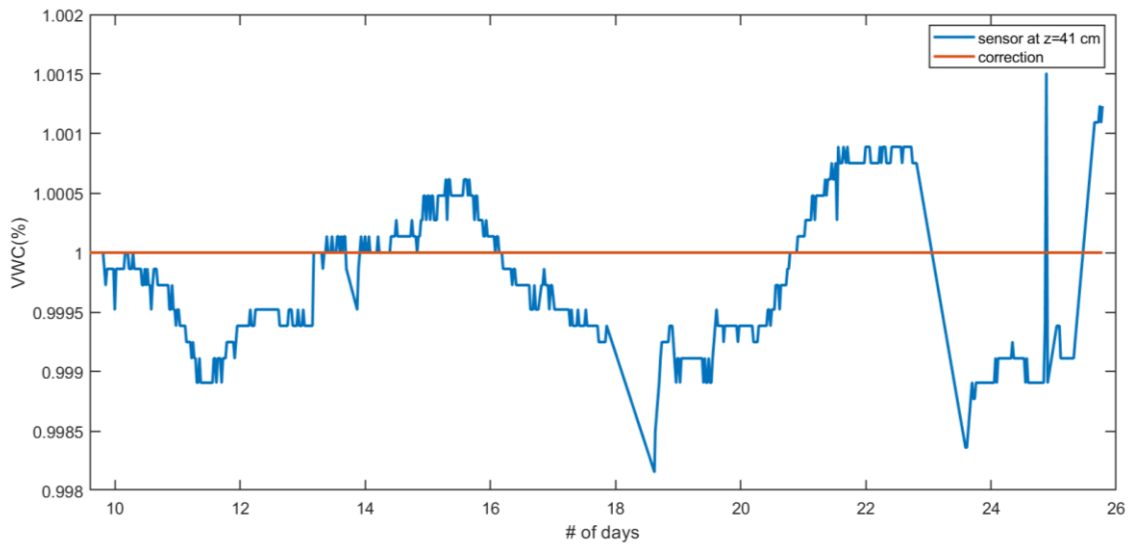


Figure 5-18: Amended FFT sample, raw scaled frequency reading from the sensor located in water ($z=34$ cm, sensor 3) and corrected reading

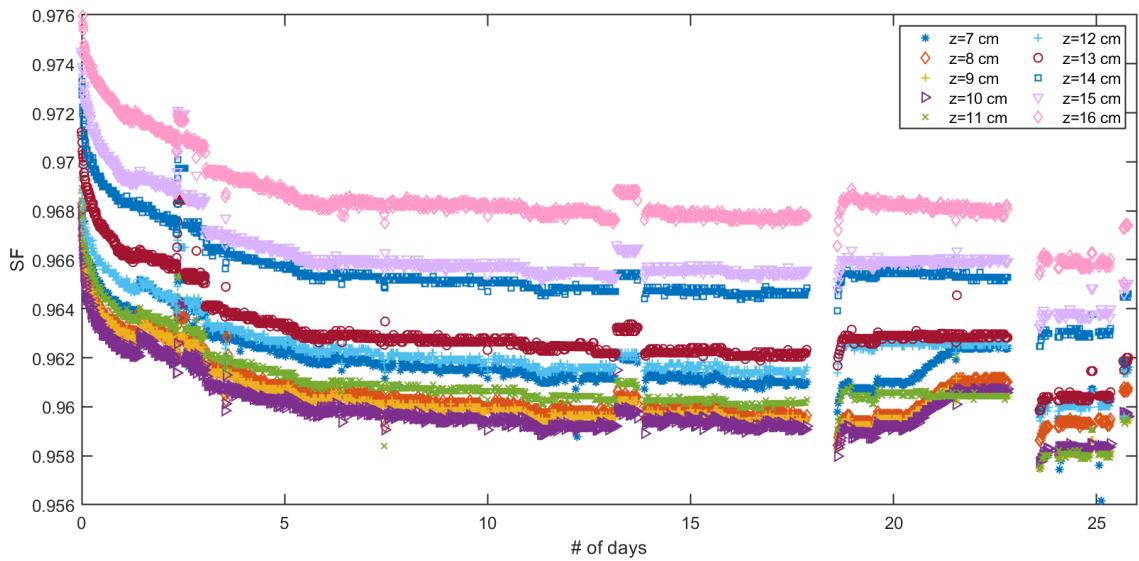


Figure 5-19: Amended FFT sample, corrected raw readings at ten different locations from sensor 1

The correction improved the readings significantly, but there is still noise present in the readings. For further correction, a data smoothing function in MATLAB is utilized to smooth the noisy data at every five cells/inputs. For this application, the “Savitzky-Golay” filter is selected as it can be more effective when the data varies rapidly. This filter smooths the data according to a quadratic polynomial that is fitted over a window of 5 cells. This applies a filter to the data to smooth the outlier readings. The smoothing range is specifically selected to be small to improve the outlier readings only rather than smoothing the whole curve. In Figure 5-20, the same example is demonstrated with the smoothed data at three different locations. It can be observed that random outlier readings are eliminated when the filter is applied. Once all correction steps are implemented on the raw scaled frequency readings, the calibration equation can then be calculated using the water content profile determined at the end of the experiment.

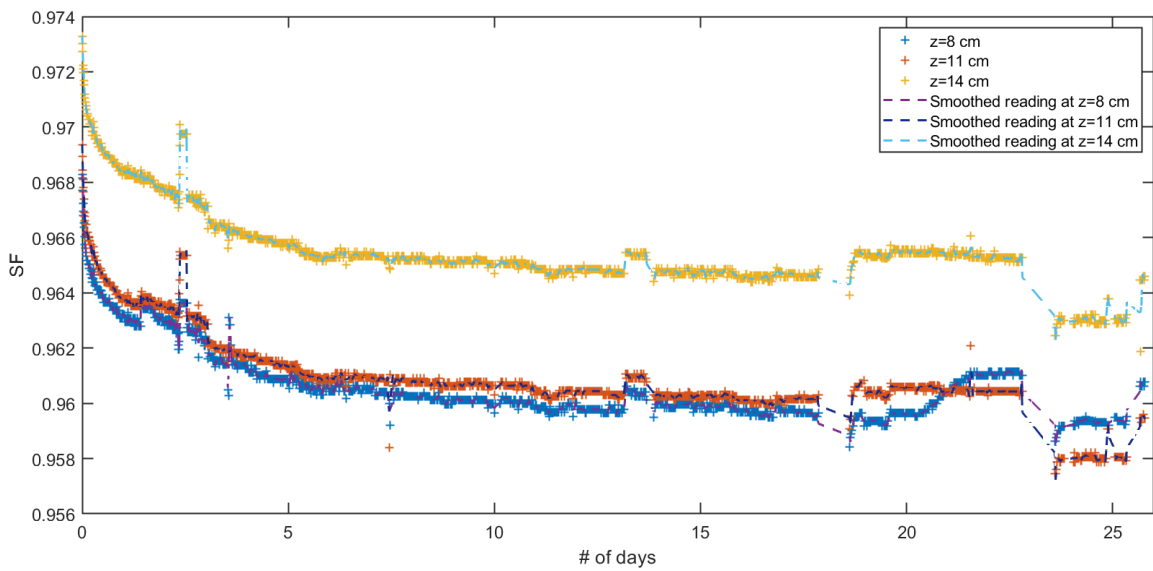


Figure 5-20: Amended FFT sample, data is smoothed at every five reading points

5.6 The Design of a New Consolidometer

The experiments conducted to determine the dimensions of the column are presented, along with the automation design and its operation in the column, which allows for high-resolution measurement profiles from the sensors.

5.6.1 Wall-effect Testing

Selecting the correct diameter for the design column was essential to confirm the wall effect or arching effect would not interfere with the consolidation process, i.e. such that FFT will not accumulate or stick to the walls of the test column. The arching effect or the horizontal arching mechanism is described by (K. Terzaghi, 1936) using a trap door test. For this test, a trap door exists on a horizontal surface (which is closed), and the soil above the surface is in a stationary position at the beginning. Then the trap-door is lowered, and the soil right above the door immediately move down with it, and sliding planes rise and intersects the

ground surface, which creates shear zones along the sliding planes, and the stress can transfer through shear stress (from the yielding soil mass, Z. Li et al. (2021)). An example of this behaviour can be observed in the soil behind retaining walls during the excavation process; i.e. the soil under the excavated surface has lower stiffness; hence the soil moves inwards towards this side and exerts a drag type of shear force upon the overlying soil. This accounts for the active arching stress distribution on the wall, and it is induced by the settlement will affect the magnitude and distribution of lateral pressures on the walls and the stress transfer from yielding mass through shear stress (M.-G. Li, Chen, & Wang, 2017; Z. Li et al., 2021). The arching or side-wall effects are typical concerns in column tests, and the diameter to height ratio needs to be large enough to eliminate these effects in the columns. Therefore, a number of tests with different fine-grained soils were conducted to determine the minimum diameter to height ratio to eliminate the wall-effect or the arching effect during the experiments. Two types of columns are tested: a polyvinyl chloride (PVC) and an acrylic column with two internal diameters (at 6 and at 12 inches). The bottom of each column is cut off and covered with a membrane and placed on a scale. The weight of the column is carried by strings, shown in Figure 5-21, which are attached to both the column and an overhanging frame. Before loading with any soil, the column is progressively lifted off the scale, until the scale reads 0 g. Therefore, during loading, only the weight of the material in the column itself would be measured from the scale. If there is any material sticking to the walls, the weight of this portion will be carried by strings/the frame that is supporting the column. This setup using both PVC and acrylic columns is presented in Figure 5-21. To simulate the presence of the interior pipe necessary for the

SENTEK EnviroSCAN sensor, a pipe was also interested in the middle of these columns and also suspended from the overhanging frame.

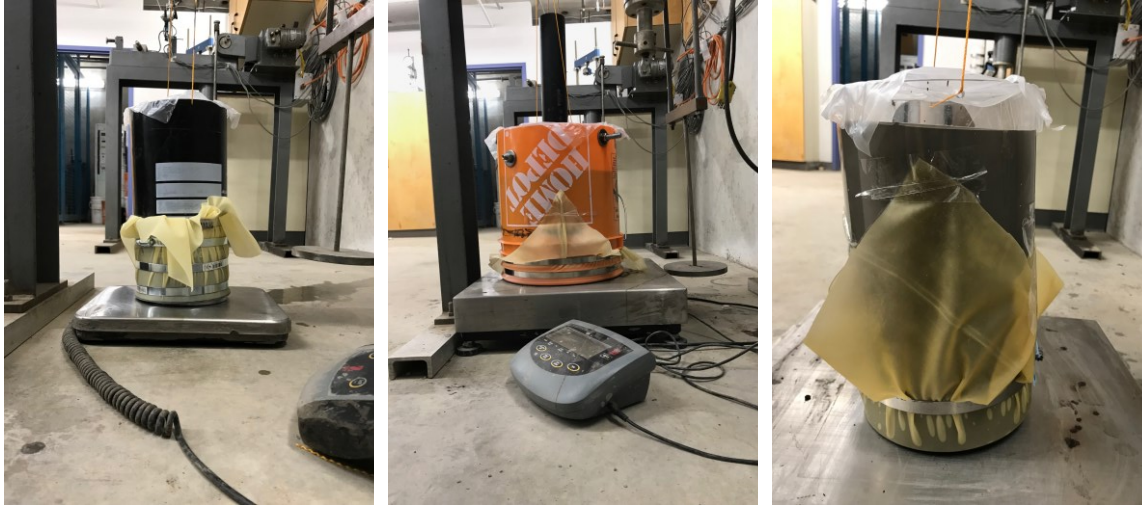


Figure 5-21: 6” PVC, 12” PVC and 6” acrylic columns setup

The total weight of the material before pouring into the column and the weight after the pour is measured. Once full, tailings were removed in smaller batches while recording the weight from the scale and weighted separately, hence back-calculation of the weight profile is determined. This allowed for the determination of the weight is carried by the strings (hence walls) and therefore could quantify the wall effect.

The properties of the tested materials are provided in Chapter 3, and specifications of wall-effect experiments were presented in Table 5-1. As expected, more accumulation was observed in centrifuged FFT and polymer-amended FFT samples. This visual accumulation on the walls for centrifuged oil sands tailings is demonstrated in Figure 5-22. The largest discrepancy in the weight profile is observed for centrifuged FFT samples, presented in Figure 5-23. It was apparent that the 6-inch radius is too small. Minimal

accumulation of material on the wall occurred for the 12” diameter PVC test (middle figure in Figure 5-21) using the same material. Therefore, for the final design of the self-weight consolidation column, a 12” diameter is selected.

Table 5-1: Specifications of six inches wall-effect experiments

	6” diameter pipe			
	Centrifuged FFT	Leda Clay	Thickened Tailings	Amended FFT (800 ppm)
Time (days)	10	2	1	7
Volume (L)	4.905	3.57	3.56	4.8
Δm (%)	7.84	2.44	2.44	7.3
w (%)	131.9	186.9	34.6	247.6
ρ_b	1.407	1.37	2.07	1.23

where ρ_b is the bulk density, w is the initial water content and Δm is the percentage of mass accumulated on the walls.

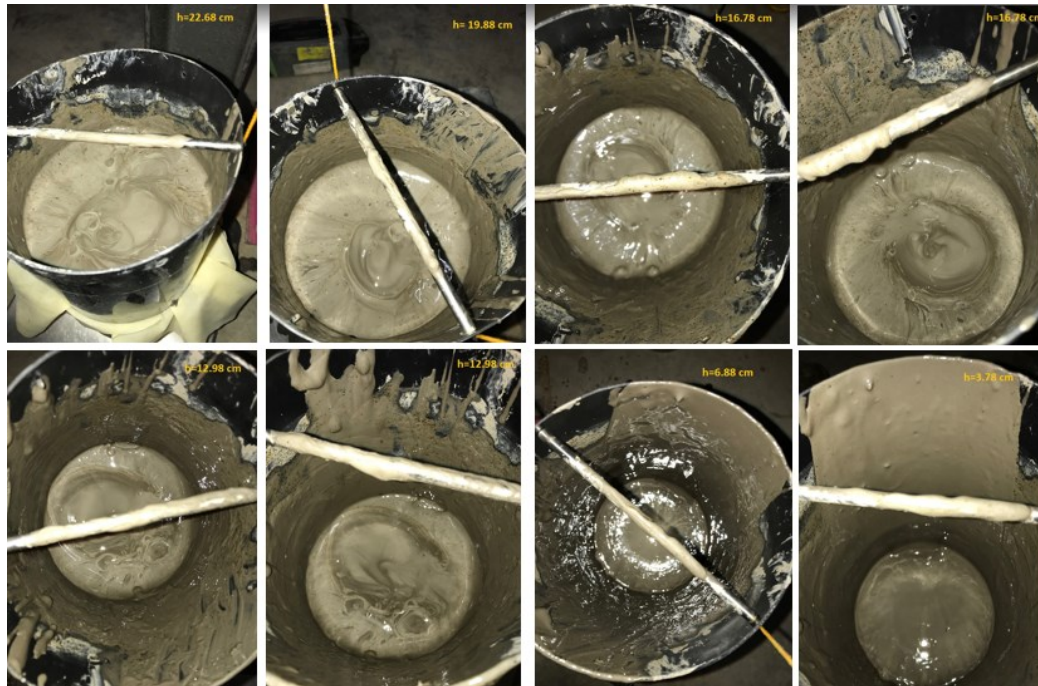


Figure 5-22: Accumulation of Centrifuged FFT on the walls

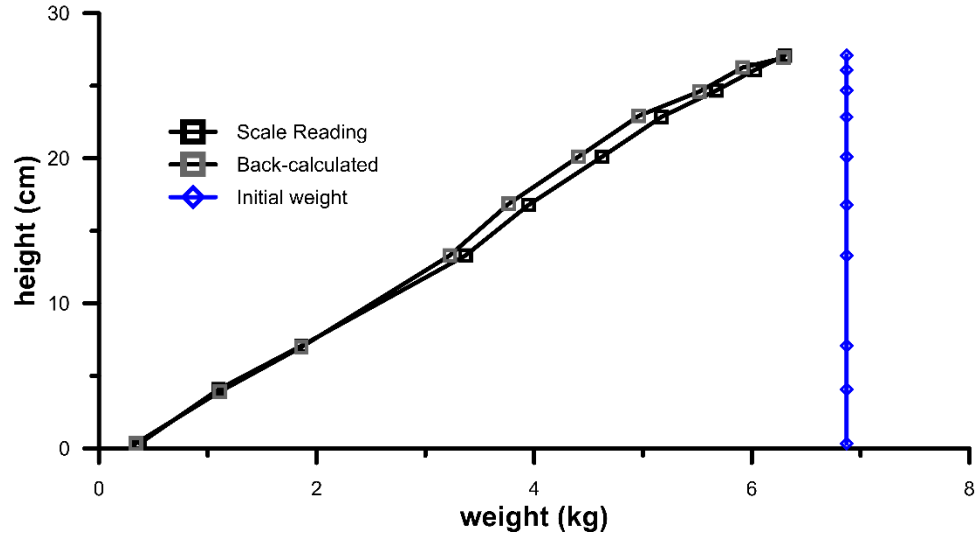


Figure 5-23: Final weight profile at the end of the experiment for centrifuged FFT on a 12'' PVC column

5.6.2 Automation Design

SENTEK EnviroSCAN sensors allow for moisture measurement at 10 cm increments, and each sensor is inserted on the probe with the same interval. However, high-resolution soil-water content profiles are required for the IPM model to be applicable in large strain conditions. Therefore the sensors would require vertical movement during testing. To provide this feature, the automation design of the probe is developed and tested prior to long-term experimental testing. The probe is connected to a motor, which is controlled by an Arduino board. Arduino is an open-source electronics platform applicable to hardware and software applications. Arduino boards are capable of reading inputs and turn them into output, activating the motor. They contain a microcontroller on the board which reads the instructions and applies the commands accordingly. Arduino has its own programming

language (based on wiring) and software (the Arduino Software (IDE)) based on processing.



Elegoo 4 relay module



TE Connectivity Relay



Arduino UNO V3



Hydroworks Linear Actuator

Figure 5-24: Different parts used in the automation of the sensors

A 12V DC linear actuator from Hydroworks is selected for the motor because the retraction of the shaft is adequately controlled. The retracted length is 6 inches, and its load capacity is 135 lb. This motor can be controlled by the Arduino board, but extra electrical components are needed. The switching on/off is achieved by using a two-channel relay module (by ELEGOO), which is compatible with the 5V Arduino controller board. However, for the voltage compatibility between the relay module and the linear actuator, two TE Connectivity relays are employed. Some of these components of the system are presented in Figure 5-25, and the electrical diagram of these parts is presented in the following figure.

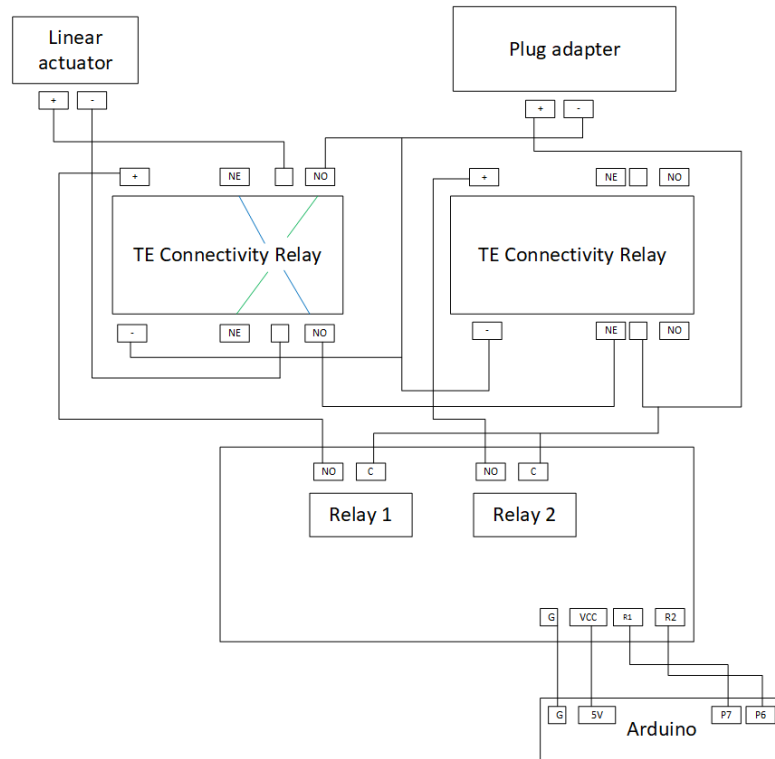


Figure 5-25: Connection diagram for parts

This linear actuator moves with a speed of 0.91 cm/s, and the probe is moved at every 1-2 cm to determine the detailed water content measurement profiles, depending on the experiment. For example, the sensors were set to read from every centimetre in the column for FFT tests. The Arduino code written for the automation of the Hydroworks linear actuator is included in Appendix D. In order to test and determine the possible complications that we might encounter, two-week testing is conducted on diluted (to 200% gravimetric water content) centrifuge cake samples. Figure 5-26 demonstrates the recorded volumetric water content profiles at every 2 cm while the automation system was activated, allowing to take readings at five different locations for each sensor.

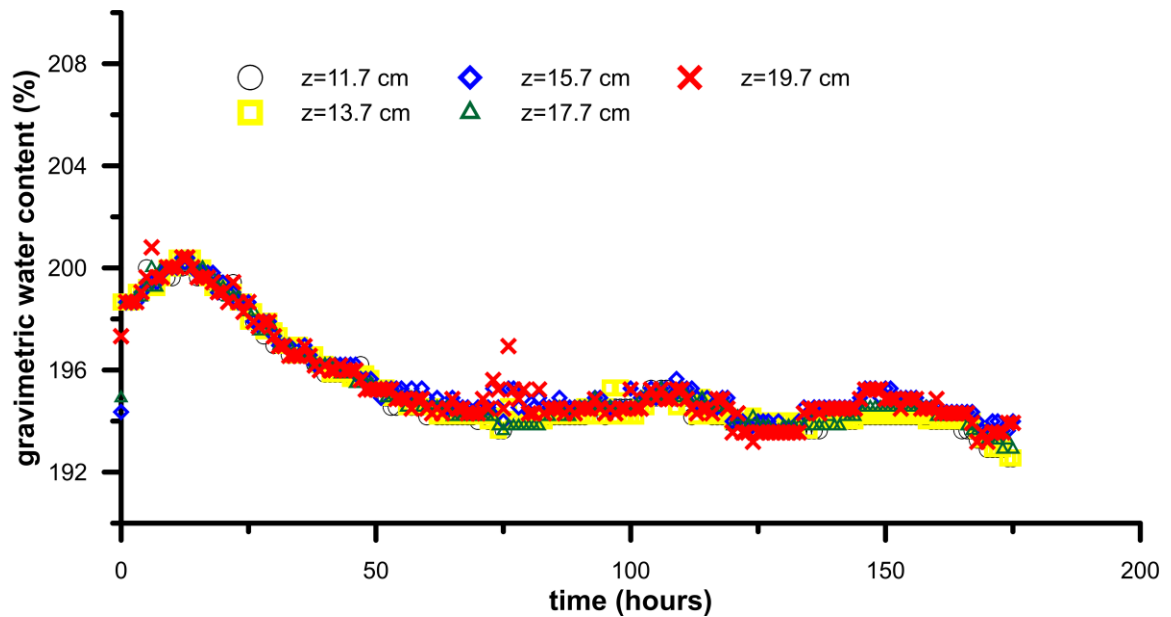


Figure 5-26: Automation Testing of SENTEK EnviroSCAN sensors.

5.6.3 Final Design of the Column

The schematics of the designed consolidometer and a picture of the column are presented in Figure 5-27. The column's outer diameter is selected as 12 inches after the wall-effect experiments; SENTEK EnviroSCAN probes are installed inside a 2 inches column located in the middle of the consolidometer. The column is 60 cm tall, and only five moisture probes can be fully in function if the column is full. The setups have ten pressure transducers inlets (one of them at the bottom), but they are placed more densely at the bottom and top portions of the column. Leakage is eliminated by inserting two small O-rings at the pressure transducers inlets, and a larger O-ring is placed inside the metal connection between the inner pipe and the column base.

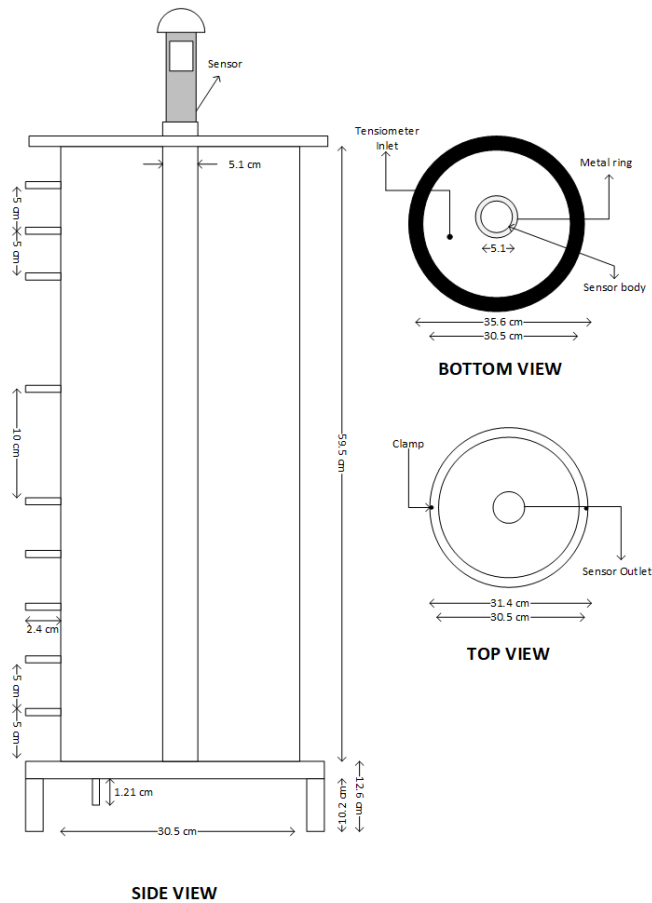


Figure 5-27: Schematics of the self-weight consolidation column.

The linear actuator is secured to the counter using metal bars for connection. Two measuring tapes are attached to the outer side of the column, and two high-resolution cameras (YI HOME Camera, streams real-time video) record the settling of the materials from two different angles.

5.7 Case study application of IPM

Prior to the setup of the design and the initial testing in the lab, a case study is selected to analyze the applicability of the methodology. The case is selected as one of the column

tests presented in the paper “Column Consolidation Testing of oil sands tailings” by Sun et al. (2014), which are conducted on thickened oil sands tailings. Density profiles are obtained through gamma-ray densitometry, and pore-water pressure measurements are made from ports connected to manometers. The authors report solids content, pore-water pressure, and effective stress profiles over time, from which can be calculated the settlement of the tailings-water interface, the total stress, and the specific gravity (which is calculated as 2.6 when back-calculated from height and density data). The case used the data from the C2 columns. The data are replotted in this study in terms of height, void ratio, and pore-water pressure in Figures 5-28 and 5-29.

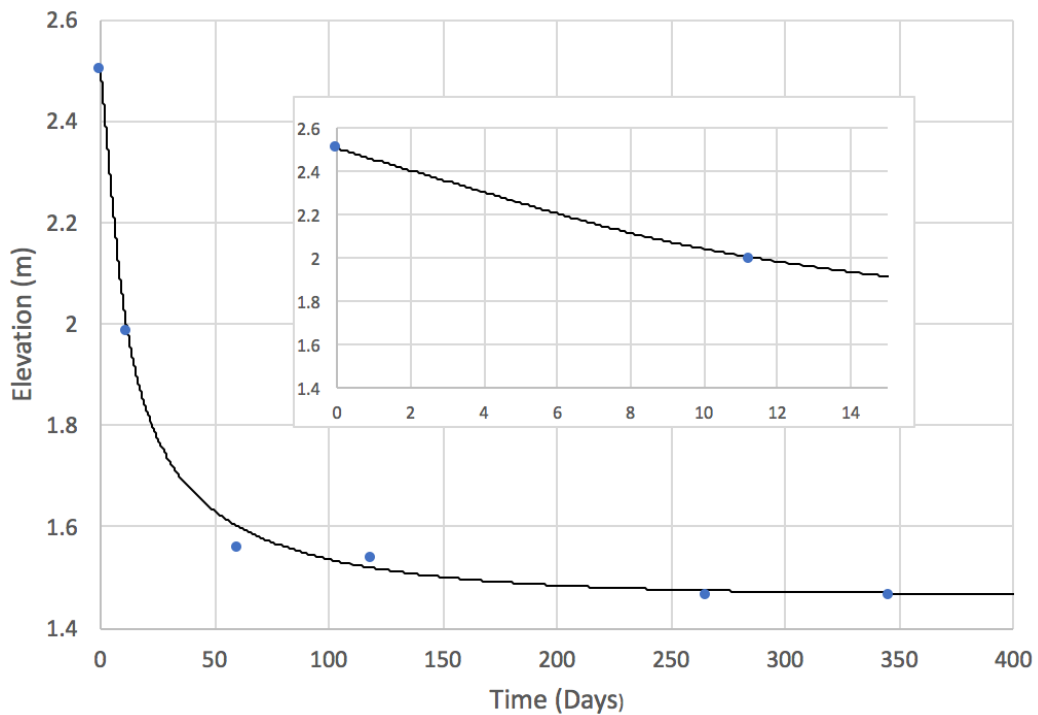


Figure 5-28: Case Study-Settlement of the tailings water interface, with insert for the first 15 days

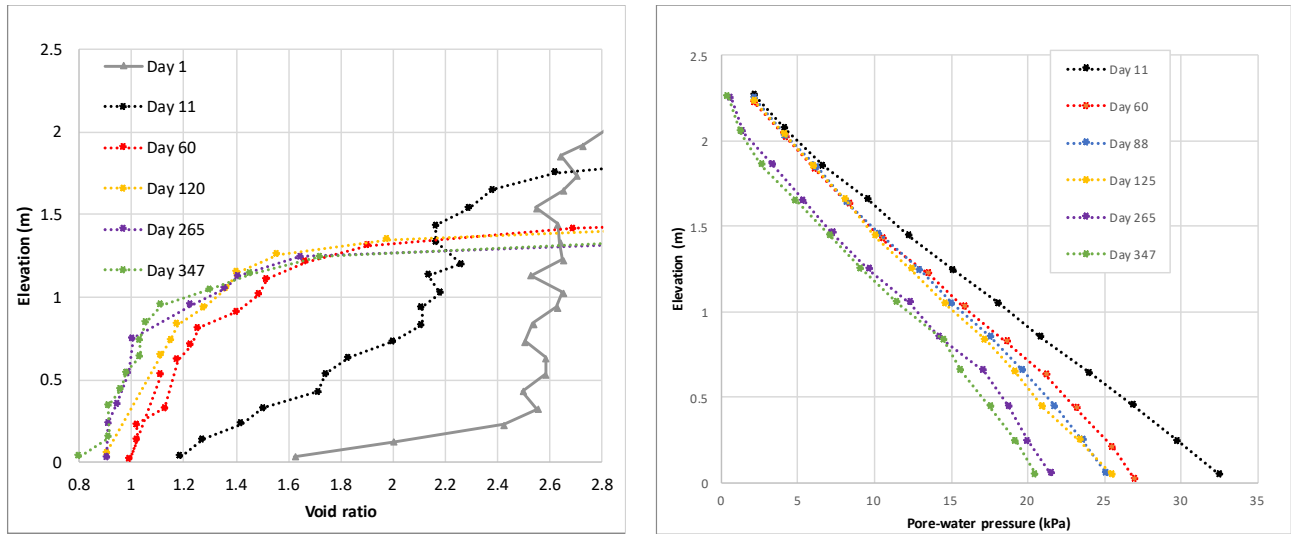


Figure 5-29: Case Study: Void ratio and pore-water pressure profiles

The hydraulic conductivities were evaluated on Day 88. The pore-water pressure profile at 88 days is used on the right-hand side of Equation 5.2. The void ratio profiles at 60 and 125 days were used to define the fluxes on the left-hand side of Equation 5.2. The data is interpolated using MATLAB to depth values every 0.1m. Given the low resolution of the density profile, Day 88 is probably the best time to apply the analyses, as there is still some deformation, but the magnitude of deformation is substantially less than at the beginning of the test, where there is a considerable change in the height of solids.

The direct application of Equation 5.2 gives the $k - e$ profile. This is then converted $k - e$ by associating z with the known profiles of e at 60 and 120 days and then averaging to estimate the $z - e$ profile at 88 days. The results are compared with the prediction equations, Equations 4.21 and 4.22 (using two different predictors), provided in Chapter 4. For the application of these two models, e_0 is selected as 2.65 as the initial void ratio. This gives a k value of 1.24×10^{-6} m/s at this void ratio. The resulting $k - e$ profiles are shown in Figure 5-30.

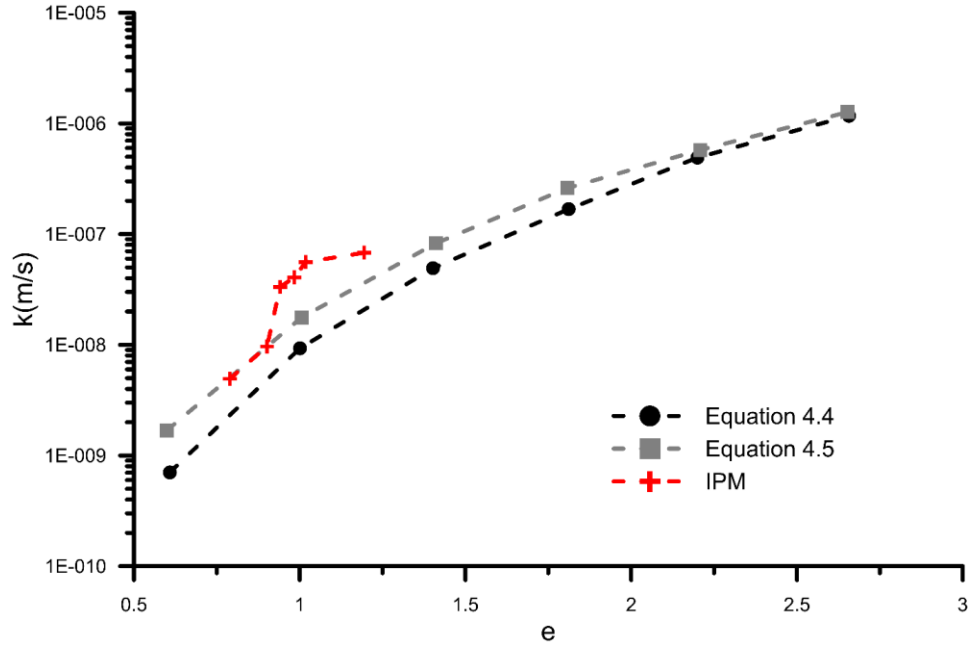


Figure 5-30: Comparison of predicted k - e from IPM method

Theoretically, the most valid results should come from the IPM based method, as it is a direct measurement, as opposed to empirical equations. However, it is a “data-hungry” method that requires high resolution in measurements for accuracy. Even so, the IPM results for the case study are still quite close to the other predictions, so it appears to be a credible approach.

The results from the case study demonstrated that the method is promising for directly calculating the k values for oil sands tailings if the high-resolution measurement can be determined throughout the experiment. The prototype consolidometer discussed in this chapter allows for detailed profiling of water content and pore water pressures of the tailings deposit. This setup is utilized for the application of the Instantaneous Profiling Method for fine-grained soils and for amended fluid fine tailings, which are discussed in Chapters 6 and 7 in more detail.

Chapter 6: Trials of New Consolidometer with Gold tailings, Kaolinite, and Raw FFT

6.1 Introduction

Large amounts of water are used for mineral processing in many types of mining operations. Water acts as a lubricant for the grinding process, facilitates extraction and separation of the ore particles, as well as assists hydraulic transportation of tailings to the deposition sites. The amount of water added to the by-product of these operations is usually 100% for hard rock mining, 200% for bauxite and oil sands tailings, resulting in the production of large volumes of mineral wastes to be deposited in tailings dams (Simms, 2017; Vick, 1990; Wills & Napier–Munn, 2006).

The initial loose state of these high-water content materials will densify as the soil drains and consolidates over time. However, prior to deposition, understanding the consolidation behaviour of these materials is essential. The large strain consolidation behaviour of these mineral slurries regulates the performance of tailings management and reclamation plans.

It is well-known that the geotechnical behaviour of soft soils is very dependent on the compressibility and hydraulic conductivity functions, which can be highly variable for fine-grained soils. The hydraulic conductivity-void ratio relationship primarily influences this behaviour, dominating the long-term performance of fine-grained slurries with higher initial water contents.

Determination of this variable parameter can be very time-consuming or expensive to obtain from conventional laboratory tests. Therefore, rapid estimation of the $k-e$ curve

is desirable, as it will accelerate innovation in the industry by allowing quick evaluation of new or improved technologies in terms of their long-term dewatering potential.

Compared to compressibility, the determination of the hydraulic conductivity of this fine material is more complex. Determining hydraulic conductivity at a range of void ratios using conventional methods, such as the large strain consolidation test, can take a considerable amount of time for tailings and other soft soils; often months or even up to a year (Pane et al., 1983; Nagula N Suthaker & Scott, 1996; D Znidarčić et al., 1986). Furthermore, the behaviour of soft soils, slurry or tailings, at a high void ratio is complex, which poses difficulties for the determination of the hydraulic conductivity-void ratio relationship of these materials.

This study focuses on calculating the k - e relationship using the Instantaneous Profiling Method (IPM) (Watson, 1966), which is derived from Darcy's equation, using profiles of pore water pressures and water contents. Similar research studies have been conducted using the IPM method such as Askarinejad, Beck, Casini, and Springman (2012), G Bartholomeeusen et al. (2002), (Dikinya, 2005), (Fisher, Williams, de Lourdes Ruivo, de Costa, & Meir, 2008) and (Leung, Co, Ng, & Chen, 2016).

A particular advantage of the method is that the computed hydraulic conductivity is independent of the compressibility curve, which may shift during consolidation at low stresses (Hawlder, Muhunthan, & Imai, 2008). A column setup is designed to allow for non-destructive measurements of volumetric water content profiles and an automation system to allow for detailed profiling using capacitance-based sensors. This setup will allow for rapid, simultaneous and non-destructive calculation of the k - e curve using the IPM method. The consolidation of gold tailings at different water contents, Kaolinite and

unamended oil sands tailings (raw fluid fine tailings (FFT)) are examined in this study. The measured settlement behaviour is then compared with the predicted behaviour using a large strain consolidation software package (UNSATCON, the method is described in Chapter 2.7.2.1), employing the measured $k-e$ values. The transitional void ratio, from sedimentation to consolidation, also needed to be assessed to correctly analyze the settling behaviour of tailings. This threshold parameter is determined by fitting the compressibility curve in the form of $e = a(\sigma' + c)^b$ to find parameters a, b and c, which are then utilized to measure the transitional void ratio using $e_t = a(c)^b$.

6.2 Summary of Conducted Experiments

The $k-e$ relationship is determined by using the Instantaneous Profiling Method (IPM) initially proposed by Watson (1966) but adopted for large strain conditions (presented in chapter 5). The instantaneous profiles in the column can be established by the profiles of the macroscopic flow velocity, the potential gradients in water content and hydraulic head, as per the groundwater flow equation. The method allows for a simultaneous, rapid and non-destructive calculation of k values.

Table 6-1: Initial and final conditions of tested materials

	Gold tailings, Test 1	Gold tailings, Test 2	Gold tailings, Test 3	Kaolinite	Raw FFT
Initial θ (%)	53	64	61	77.5	88.0
Initial w (%)	35	55	48	130	347.2
Solids content (%)	74	64.3	67.5	43.4	22.4
Initial void ratio	1.12	1.77	1.54	3.44	7.4
Initial height (cm)	26.2	33.8	28.0	27.0	33.1
Final height (cm)	23.4	25	22.3	22.1	17.7
Pressure sensor positions (in cm, from the bottom)	5-15-20	5-15-25	5-15-20	5-10-15-20	5-10-15-20
Test duration	24 hours	24 hours	24 hours	24 days	52 days
Settlement duration	11.8 hours	6.6 hours	8 hours	Continuous	Continuous

The design of the prototype self-weight consolidation column is reviewed in Chapter 5. Pore water pressures are measured using miniature pore pressure sensors (T5 from UMS), and volumetric water contents are determined using capacitance-based sensors (SENTEK EnviroSCAN) in the column. The automation system was used to take measurements at every 2 cm for thickened gold tailings tests and at every centimetre for Kaolinite and Raw FFT experiments. The settlement is observed using two high-resolution cameras throughout the experiment. At the end of each test, two samples from selected depths are collected (by scooping): one closer to the wall and another one closer to the pipe containing sensors. These collected samples, along with the initial samples, are then used to calibrate the VWC sensors. The geotechnical properties of tested soils and the initial and final heights of the experiments are presented in Table 6.1.

6.3 Thickened Gold Tailings

For the initial evaluation of the self-weight consolidation behaviour of fine-grained slurried tailings, thickened gold tailings were selected and tested at three different solids contents. The conventional gold tailings usually have solids content around 50% (GWC=100%), whereas this value can increase up to 70% or higher with the thickening technologies. Tailings below a certain density are susceptible to grain size segregation; all the densities tested in this study are above that threshold.

6.3.1 Initial Conditions

Table 6.1 summarized the initial and final conditions of all three tests of thickened gold tailings performed in the self-weight consolidation column. Only three tensiometers are utilized (only four inlets are available for the thickness of the materials in the column), and the pore water pressure readings in-between locations are estimated using non-linear regression models in MATLAB, as described in Chapter 5. The volumetric water content profiles are measured at 2 cm intervals. The tests are performed for 24 hours, but the settlement of solid particles completed prior to that. Tailings are prepared at various water contents (by adding tap water and mixed in 20 litres buckets using a hand mixer), and immediately after mixing for about 10 minutes, the columns are filled in a single batch to avoid settling in the mixing.

Total potential measurements are calculated by adding the measured pore water pressure measurements and gravitational head. They are presented in Figure 6-1 at different heights and times for all three experiments.

The volumetric water content profiles of the three tests are presented in Figure 6-2.

During testing, a limitation of SENTEK EnviroSCAN sensors is discovered. Each sensor averages the reading within a 10 cm depth, and closer to the mudline, a sudden increase in the readings is detected. This is due to the sensor reading partially from water; hence the average value increases. For an accurate implementation of IPM, the sensor should not be influenced by the water readings. Therefore, only the measurements within the soil are considered in this study (i.e., for Test #1, the final height is $z=23.4$ cm; hence only the sensor readings below $z=17$ cm are fully immersed in soil), and this application has been practiced at all of the experiments in this study.

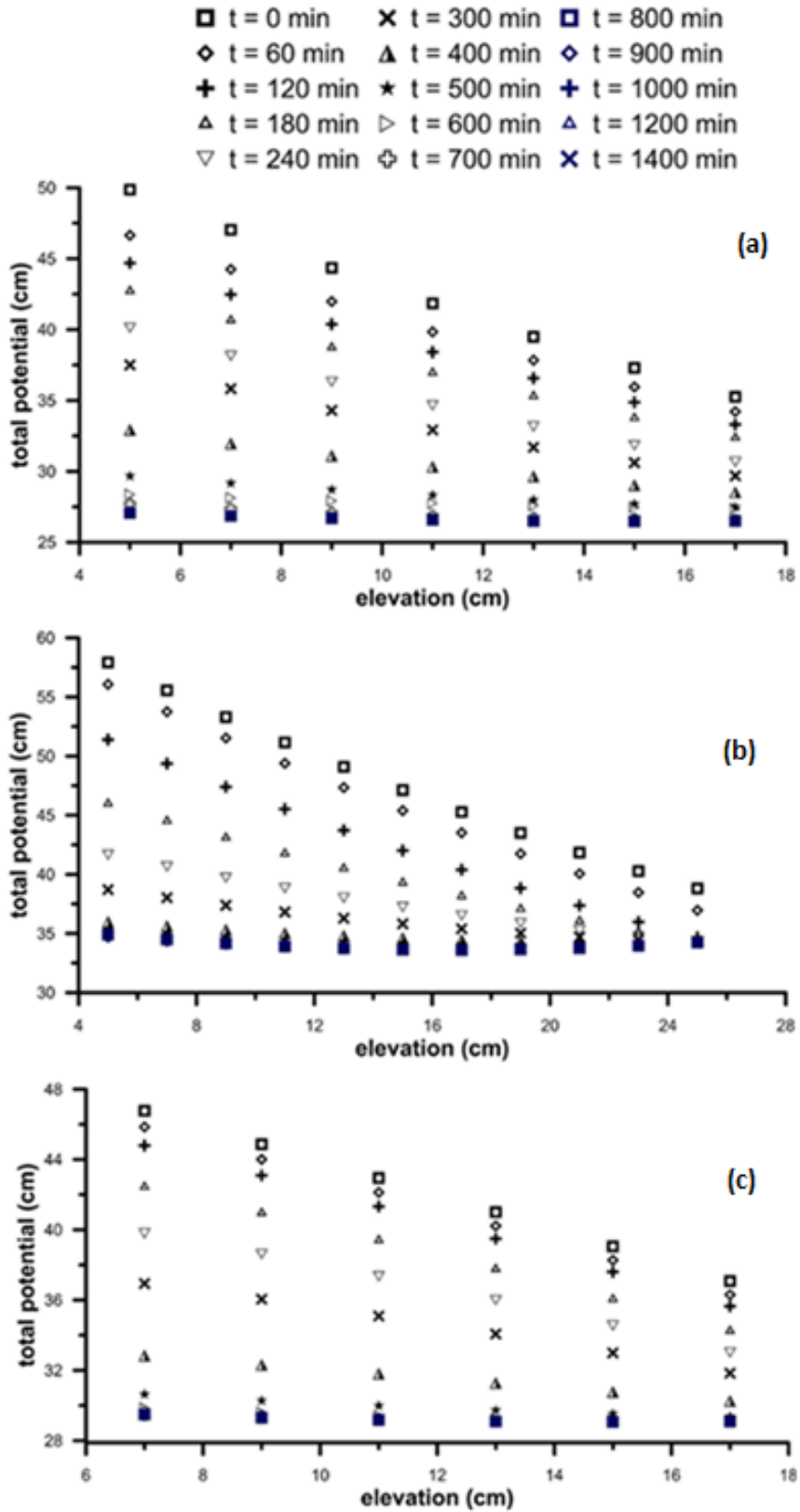


Figure 6-1: Total potential profiles for (a) Test#1, (b) Test#2 and (c) Test#3

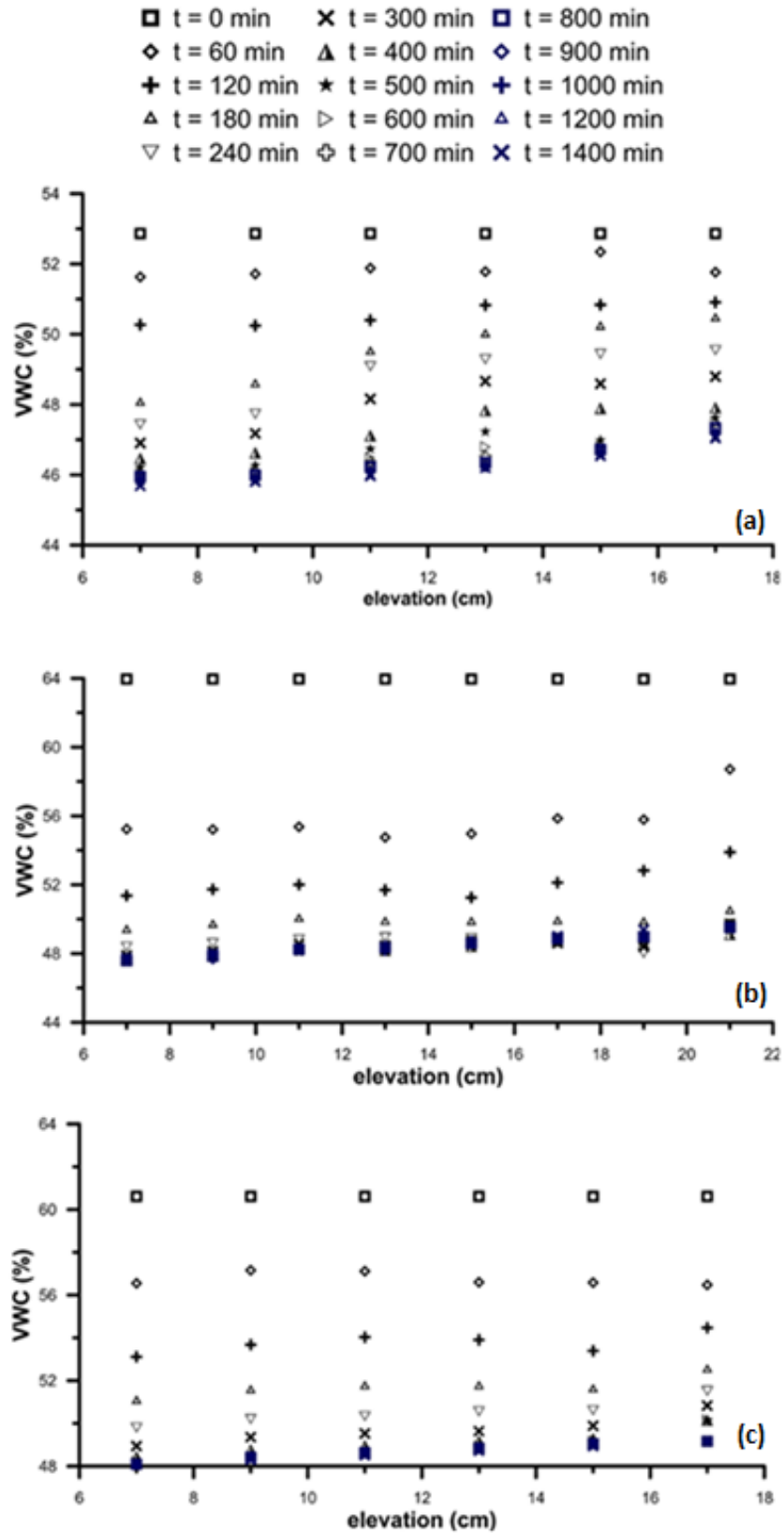


Figure 6-2: Volumetric water content profiles for (a) Test#1, (b) Test#2 and (c) Test#3.

6.3.2 Results and Discussion

The final water content profiles (average of two samples) and the settlement of the tailings for all three tests are presented in Figure 6-3(a). The first few hours of settlement behaviour in Test #1 could not be tracked due to camera malfunction, but the problem was resolved for the other experiments. SENTEK EnviroSCAN sensors require calibration prior to being utilized in the experiment, and the calibration was completed using the initial water content and the final gravimetric water contents presented in Figure 6-3(a).

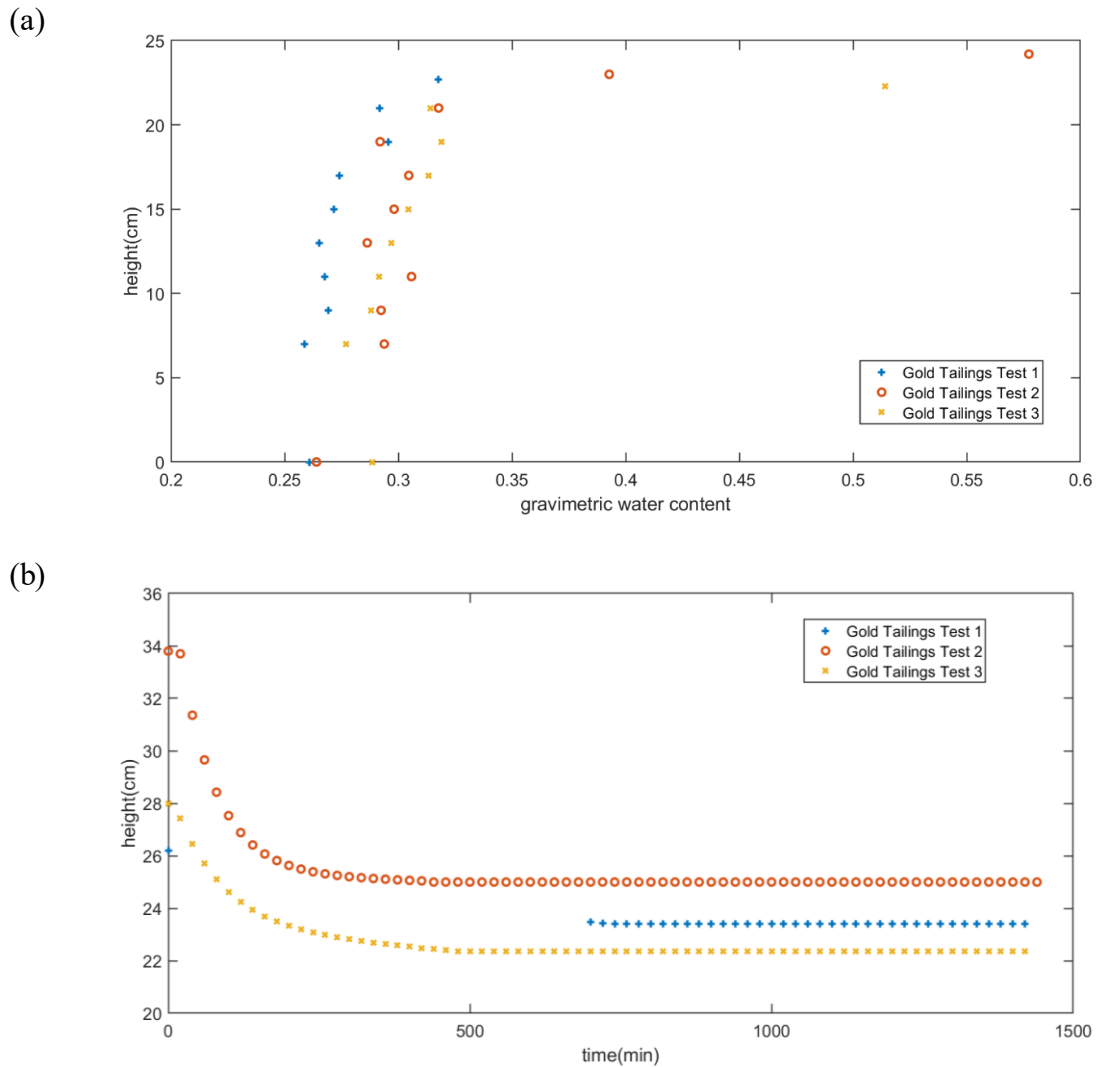


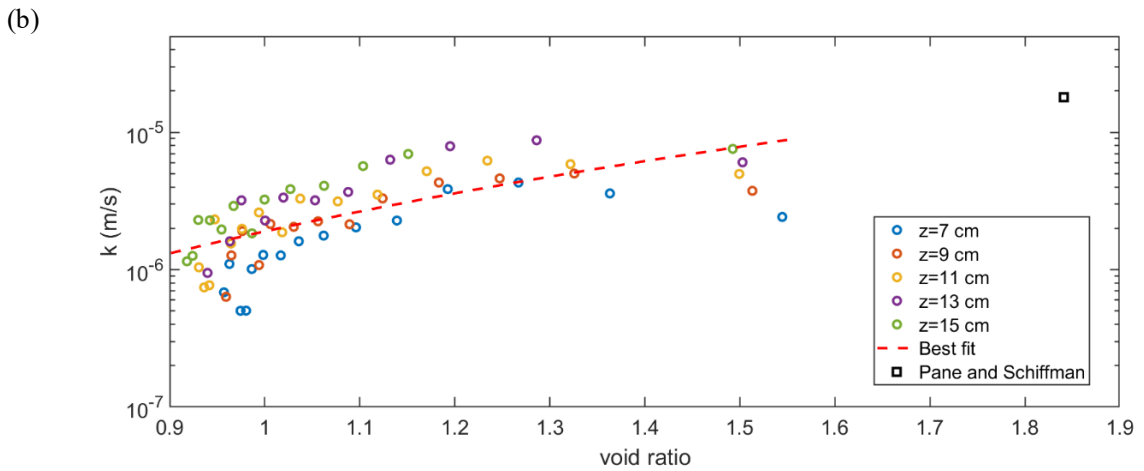
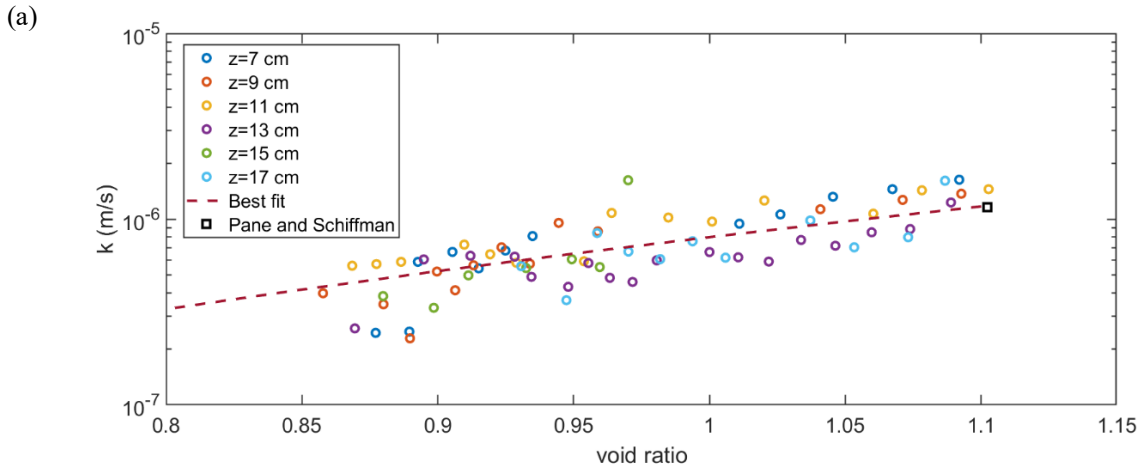
Figure 6-3: (a) Final gravimetric water contents from oven drying, (b) Water-tailings interface height versus time

The hydraulic conductivity was determined by the Instantaneous Profiling Method as described in Chapter 5, which is presented below for all three cases. Figure 6-4 demonstrates the k - e data points calculated at different heights.

Test #1 $k = 8 \times 10^{-7} e^4$ (6.1.1)

Test #2 $k = 1.6 \times 10^{-6} e^{6.9}$ (6.1.2)

Test #3 $k = 2 \times 10^{-6} e^{5.1}$ (6.1.3)



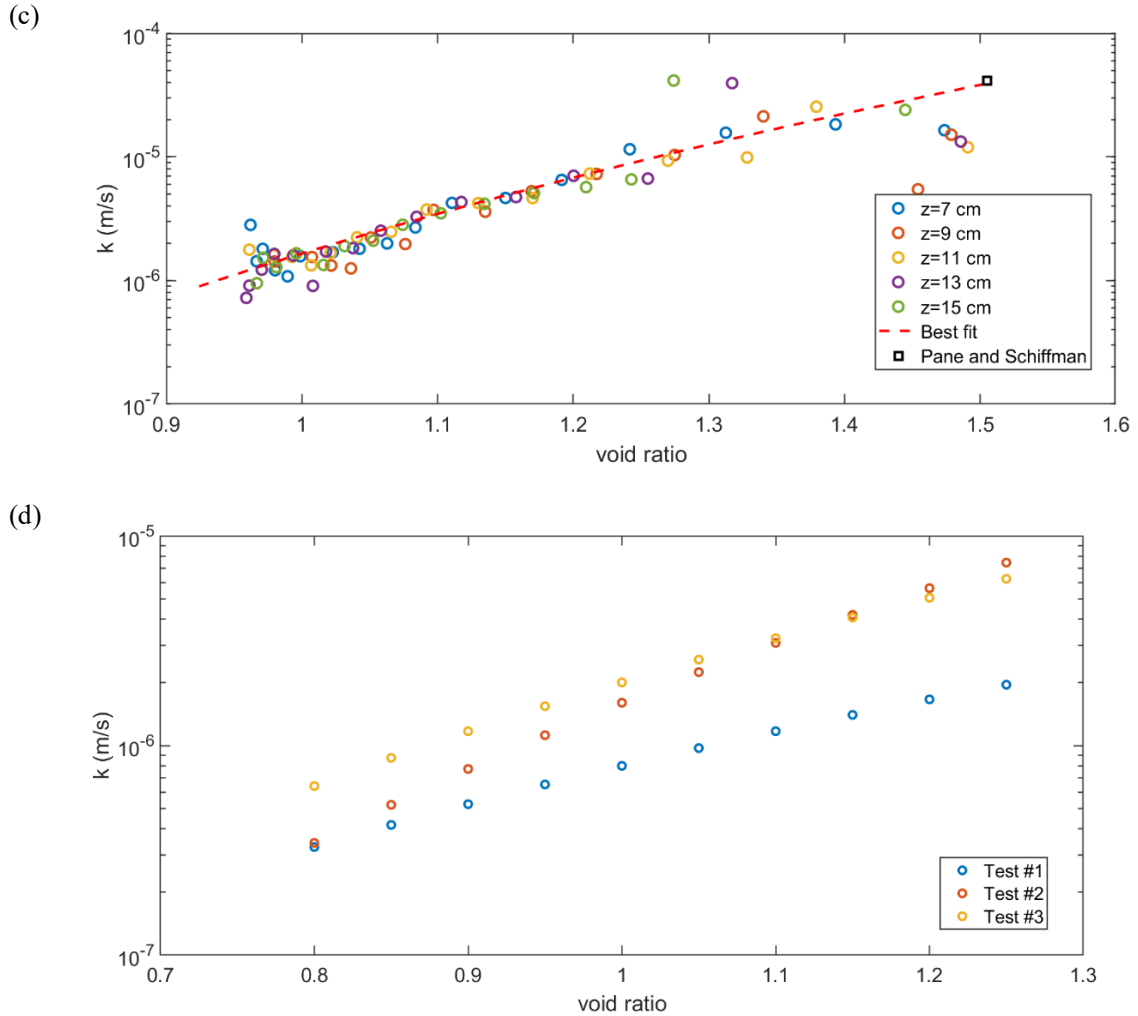


Figure 6-4: k - e relationships for (a) Test #1, (b) Test #2, (c) Test 3, and (d) Comparison of all models

The structure of the IPM method (Equation 5.2) allows for the calculation of k values at different times and locations during the experiments, which may lead to dispersed k - e data. The best-fitted power equation is selected to represent each test, as presented in Figure 6-4, using non-linear regression models in MATLAB. Each experiment is simulated using a large strain consolidation analysis software (UNSATCON) to test the k - e relationships determined by the IPM method, and the measured volumetric water content profiles are compared with the predicted data from the model at different times and

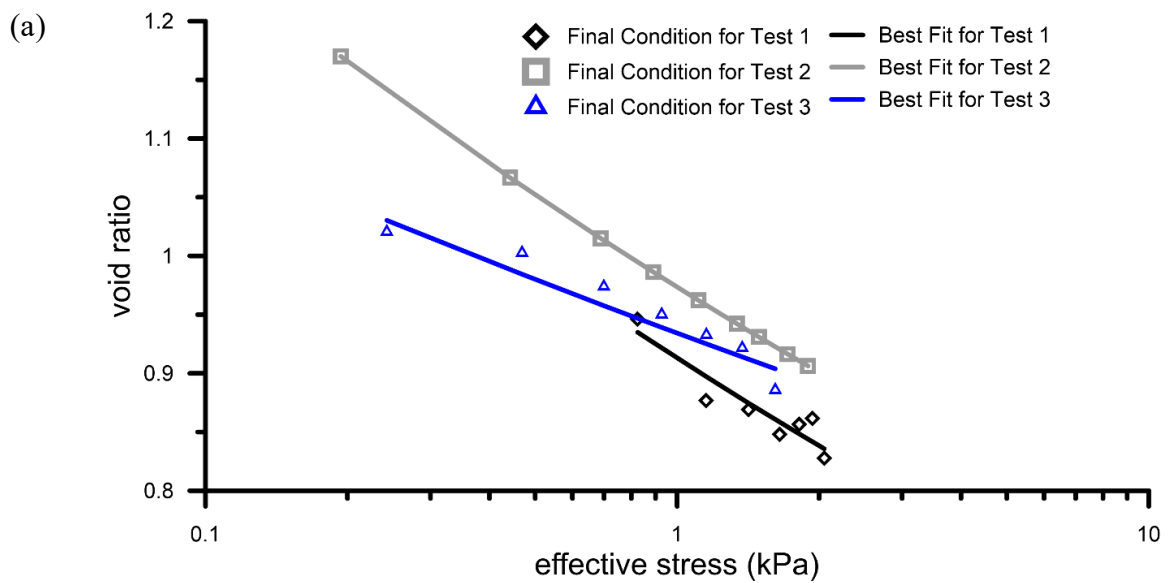
locations.

Two separate compressibility curves can be determined using the experimental setup: the first one can be calculated using the measured pore water pressures and volumetric water contents throughout the experiment, and the second one can be determined from the final condition. The final effective stress-void ratio relationship is determined from the final condition (presented in Figure 6-5), and the equations are calculated as:

Test #1: $e = 0.90\sigma^{-0.15}$ (6.2.1)

Test #2: $e = 1.02\sigma^{-0.11}$ (6.2.2)

Test #3: $e = 0.93\sigma^{-0.07}$ (6.2.3)



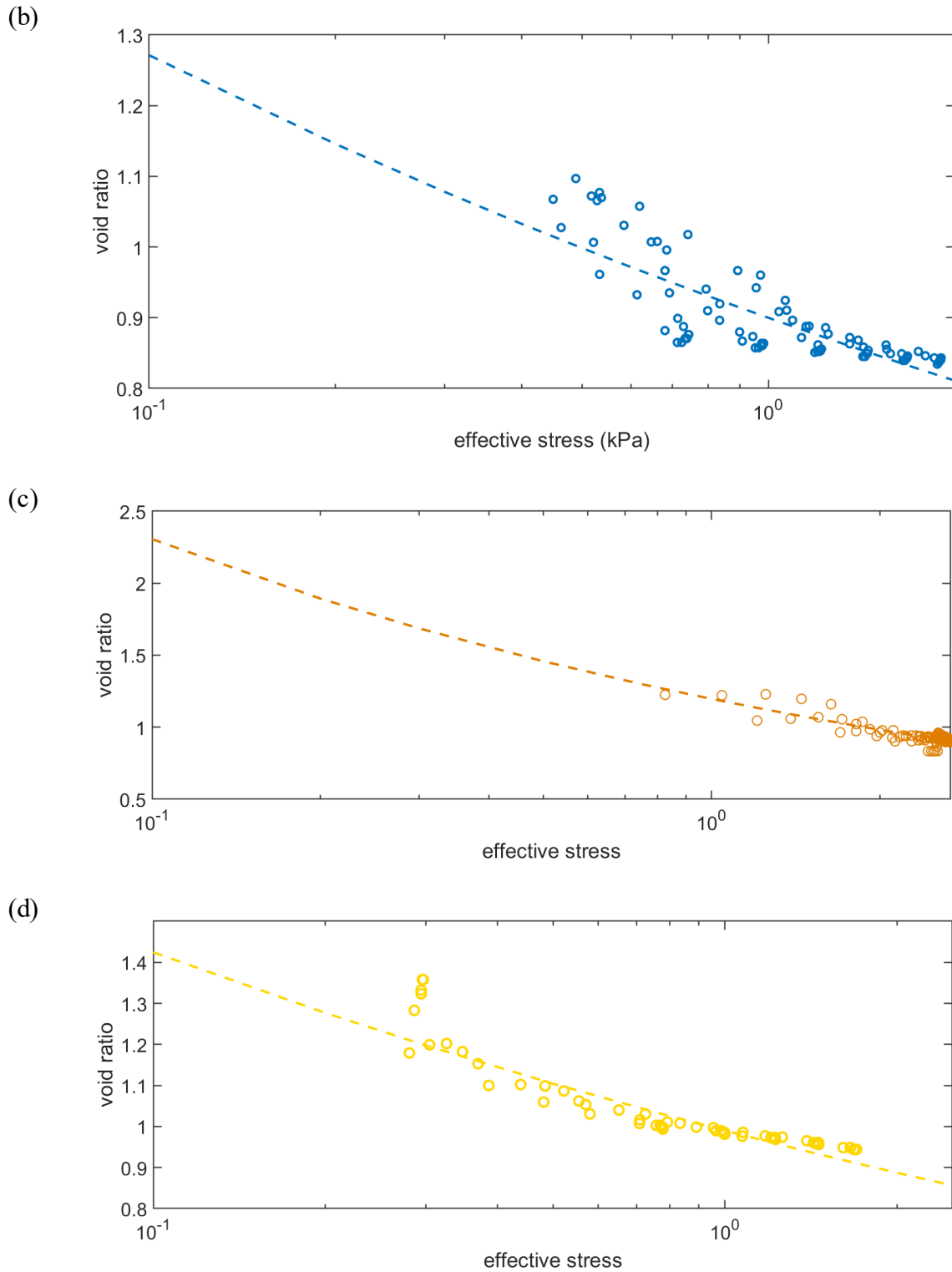


Figure 6-5: (a) The compressibility curves determined from the final condition, (b-d) The compressibility curves determined from measured PWP and VWC measurements during Tests 1, 2 and 3, respectively

It should be noted that Test #2 has the highest initial water content, and the final compressibility curve, as presented in Figure 6-5(a), differs from the other two experiments. If the compressibility equation is calculated using the measured pore water pressures and volumetric water contents during the experiment, the parameters change to:

$$\text{Test \#1:} \quad e = 0.92\sigma^{-0.11} \quad (6.3.1)$$

$$\text{Test \#2:} \quad e = 0.99\sigma^{-0.13} \quad (6.3.2)$$

$$\text{Test \#3:} \quad e = 0.99\sigma^{-0.16} \quad (6.3.3)$$

The comparisons of compressibility curves (both in-situ and final) for all three tests are presented in the following figure. The settlement is modelled and shown in Figure 6-6(b) using the effective stress-void ratio-hydraulic conductivity relationships presented in Eqs. 6.1 and Eqs. 6.3. The compressibility curves are selected for these simulations are determined using measured pore water pressure and volumetric water content from the sensors (in-situ curves); the variation of these curves can be noticed in Figure 6-6(a). The tailings settle fast; therefore, the compressibility curves determined with measured data are utilized in the large strain consolidation analysis to simulate the settling behaviour. The initial settlement behaviour for Test #1 is missing data for the first 11.3 hours due to a malfunction in the camera system at the beginning of the tests. The simulations follow the measured rate of settlement very closely, though the final modelled heights are slightly different. The final settlement height depends on the compressibility curve rather than the k-e function, which can be observed in Figure 6-6 (b).

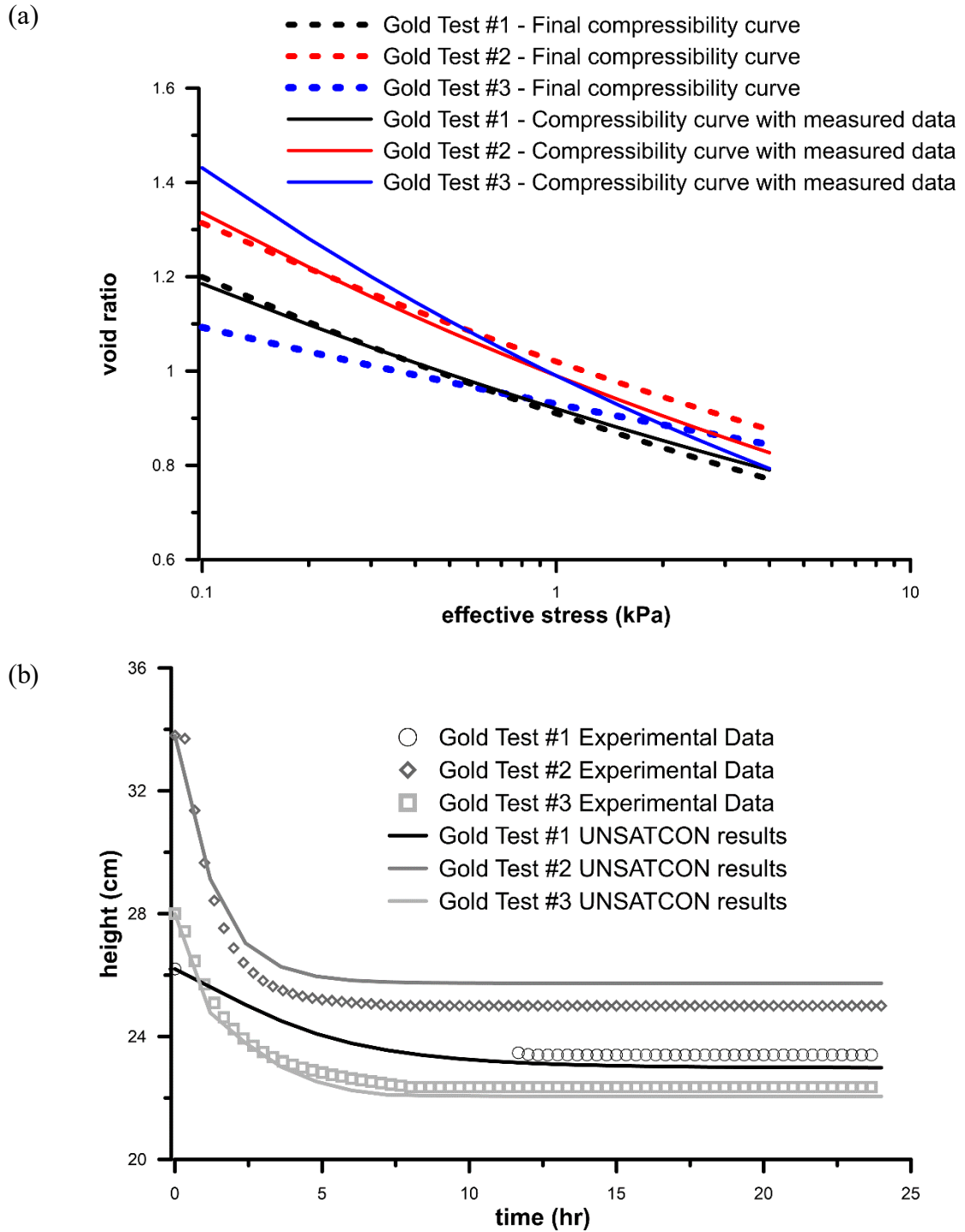


Figure 6-6: (a) Comparison of compressibility curves for all three tests (b) Settlement behaviour of thickened gold tailings at different volumetric water contents (Test #1: 53%, Test #2: 64% and Test #3: 61%) using Equation 5.

Other interesting behaviours are apparent in the settlement data. In the gold tailings, there is an apparent delay during the first 20 minutes, where the settlement is much slower. This could be due to some dynamic effect due to deposition into the column, which was done quickly (within a minute), but also could be due to a real flocculation stage, where an increase in effective particle size would increase the rate of sedimentation. Also, for the gold tailings, there is a divergence between the $k-e$ values above and below the transitional void ratio – the values at high void ratio are all calculated during the first 60 minutes, are so affected by the initial “slow settling” stage.

The predicted water content profiles are compared with the measured data (at different heights) to analyze the capability of the $k-e$ relationships provided in Equation 5.2. The measured values agreed well with the predicted data for all three tests. Figure 6-7 presents the comparison for Test #1.

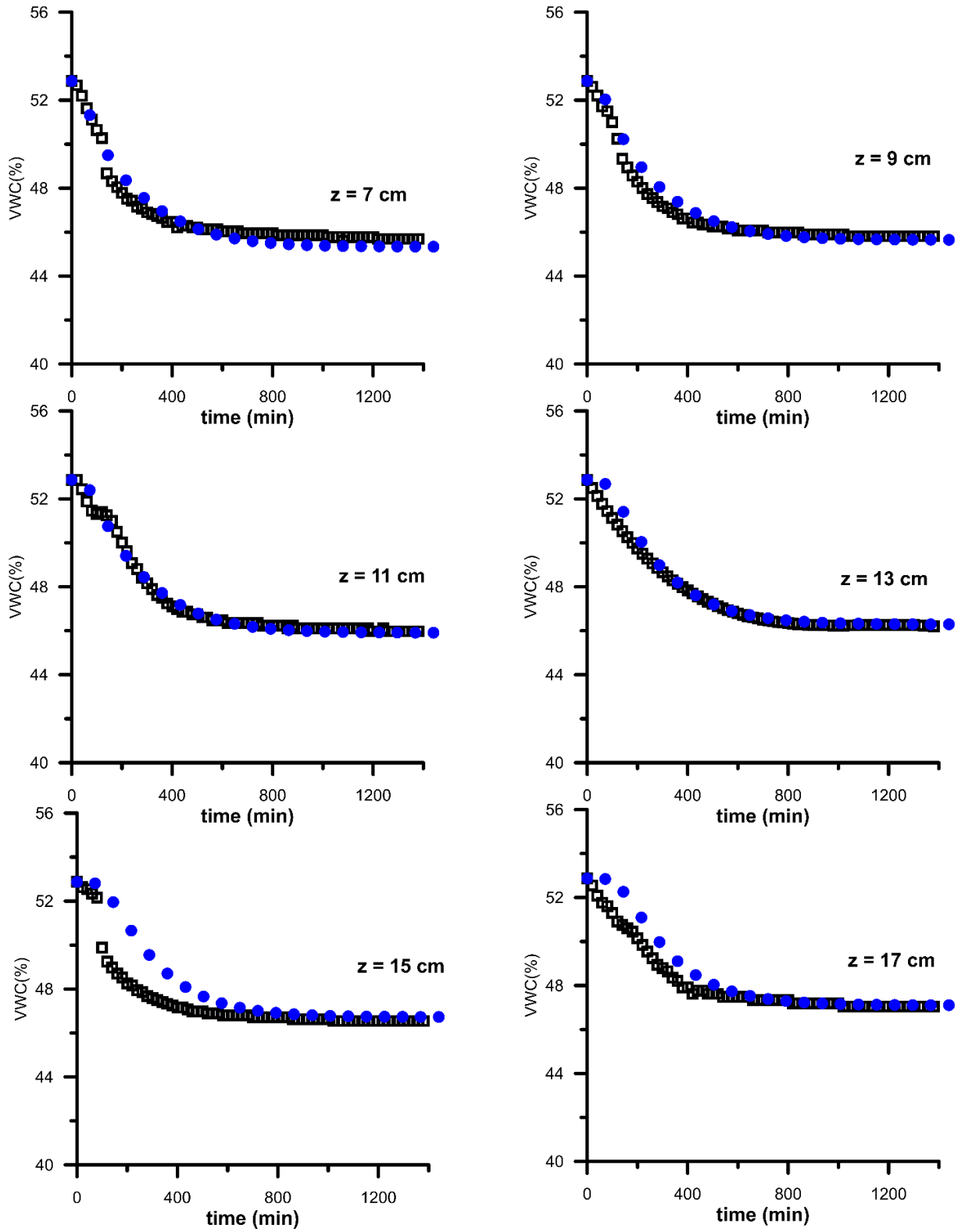


Figure 6-7: Comparison of predicted and measured volumetric water content profiles at different depths for Test#1.

6.4 Kaolinite

This sample has been prepared from Kaolinite powder by mixing with tap water to reach its slurry state (at 43.4% solids content). The material is prepared in a 20 litres bucket and mixed in smaller batches. Each batch is mixed for 20 minutes to ensure its consistency; it was then deposited into the column as a single batch. The initial and final conditions (height, void ratio, volumetric water content, positions of PWP sensors in the column etc.) of the experiment can be found in Table 6.1.

6.4.1 Initial Conditions

The pore water pressures are measured using miniature pore pressure sensors (T5 by UMS) at locations 5, 10, 15 and 20 cm from the bottom of the prototype column and in-between locations are estimated using MATLAB R2019b. The volumetric water content profile is measured at every centimetre in the column with SENTEK ENVIROScan sensors with 60-minute intervals for 23.9 days. More pore pressure sensors are utilized for this experiment compared to gold tailings tests, and considering the slow settlement behaviour, the time interval is increased to 60 minutes. Both profiles at selected times are presented in Figure 6-8.

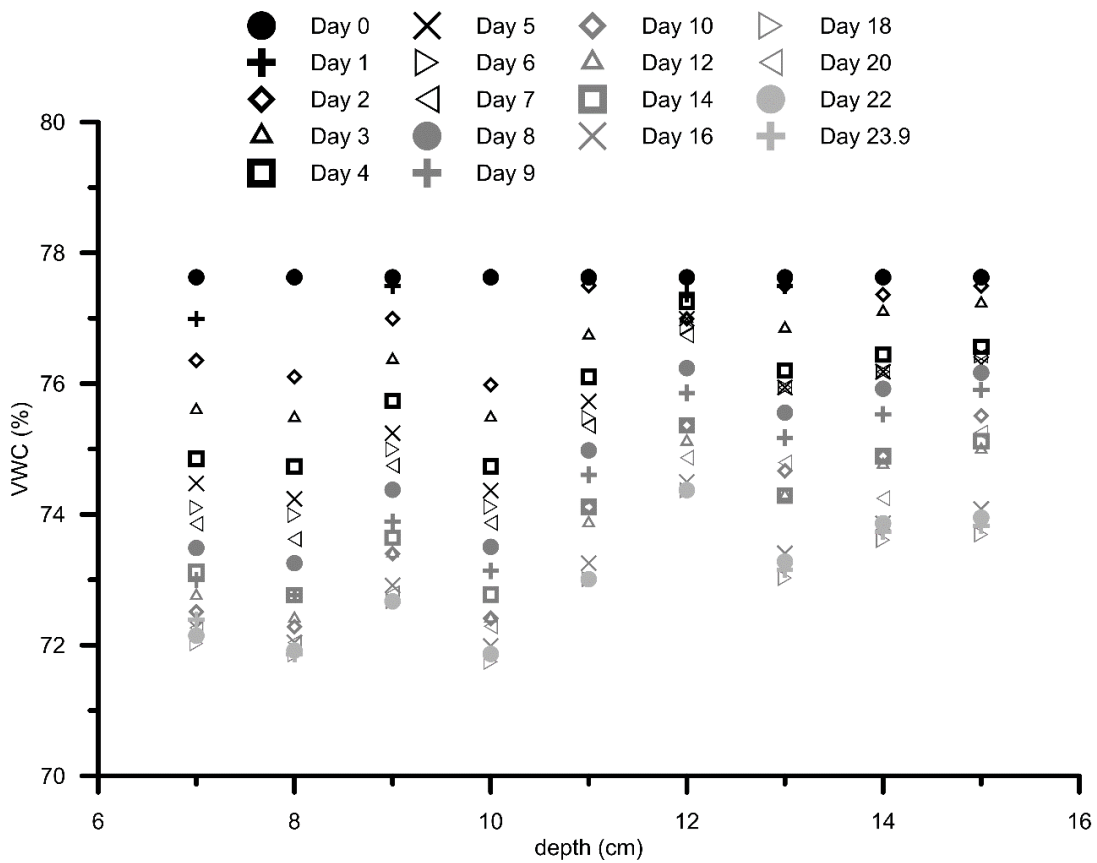
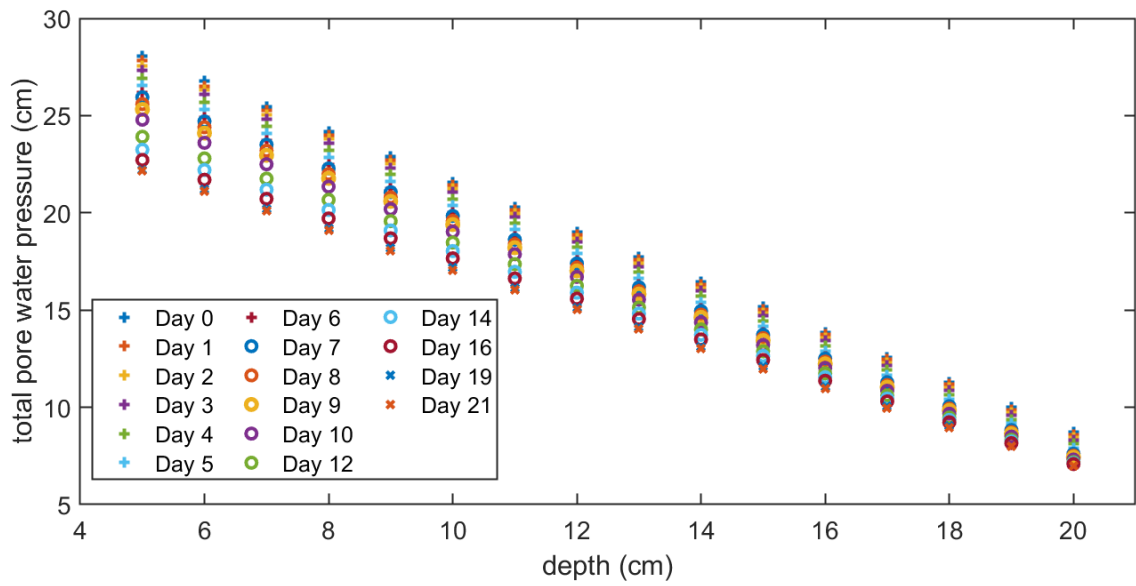


Figure 6-8: Measured total pore water pressure and volumetric water content profiles at selected times

6.4.2 Results and Discussion

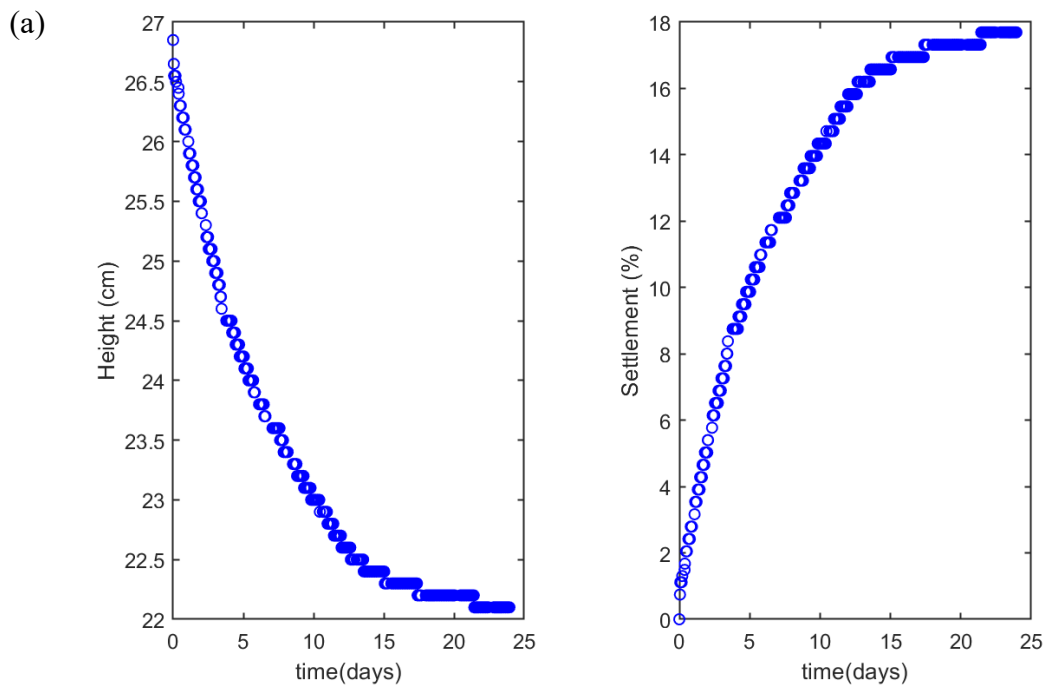
The settlement behaviour and the final VWC profile in the column for the Kaolinite sample have been presented in Figure 6-9. The change in height decreased steadily until Day 15 and eventually slowed down. The transitional void ratio is calculated as 3.34. The compressibility equations are determined (i) from the final condition and (ii) using the measured pore water pressure and water content profiles throughout the experiment.

From the final condition

$$e = 2.5\sigma^{1-0.08} \quad (6.4)$$

Using measured PWP and VWC measurements

$$e = 2.42\sigma^{1-0.165} \quad (6.5)$$



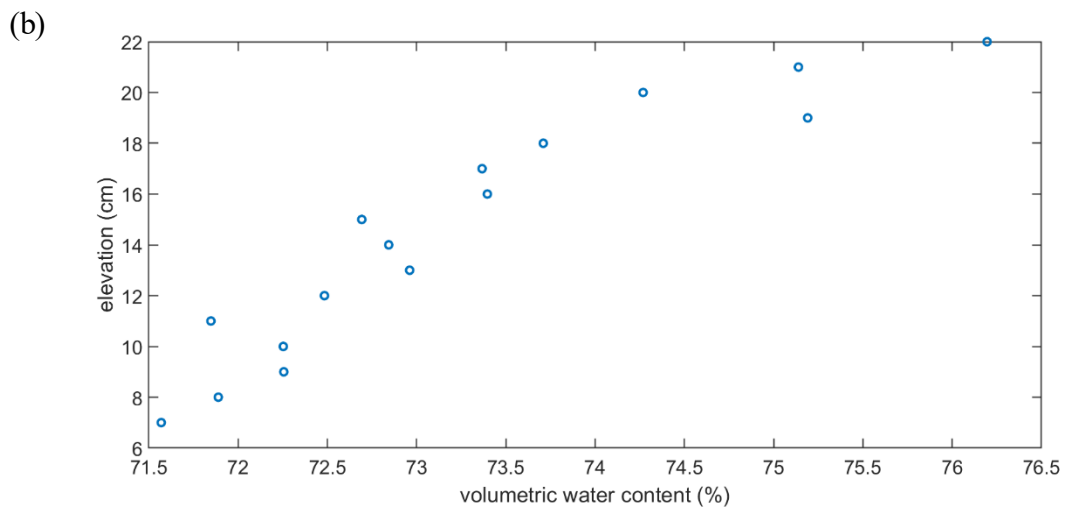
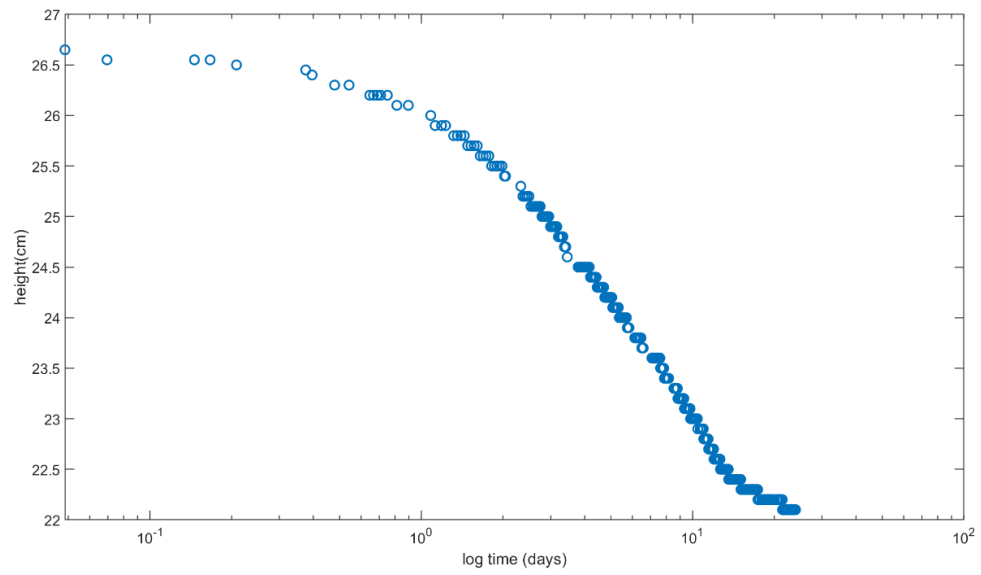


Figure 6-9: (a) The settlement behaviour of Kaolinite (b) Final measured gravimetric water content profile in the column

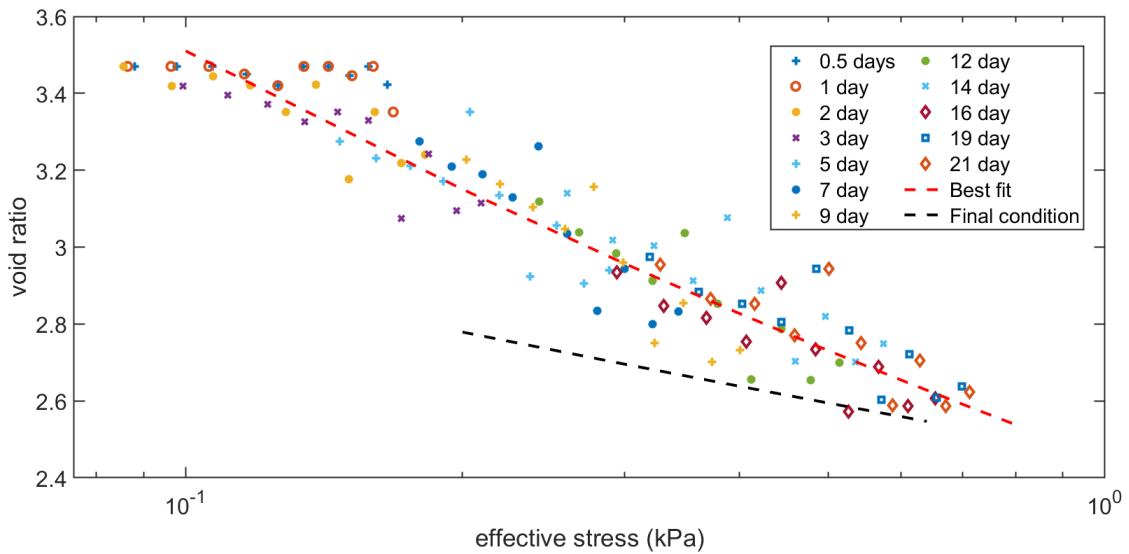


Figure 6-10: The effective stress-void ratio relationship at different days

In Figure 6-10, the change in the compressibility curve after Day 3 is noticeable, and the best fit line is fitted using the data points after Day 3. Therefore, Equation 6.5 is calculated using the data measured from Days 3 to 21. The $k-e$ relationship is determined using the IPM method (presented in Figure 6-11) and calculated as:

$$k = 4.7 \times 10^{-10} e^5 \quad (6.6)$$

The calculated hydraulic conductivity-void ratio relationship has been compared with other published studies on Kaolinite in the literature, presented in Figure 6-12 (Gholamreza Mesri & Olson, 1971b; Pane & Schiffman, 1997; Sridharan & Nagaraj, 2005; D Znidarčić et al., 1986). The $k-e$ curve from the IPM method has a steeper curve compared to other relationships, and until the void ratio of 2.8, estimated k values are within the range of published works. The hydraulic conductivity at the initial void ratio also agreed well with the data point (at $e=3.44$ and $k=1.8 \times 10^{-7}$) calculated using Pane and Schiffman's method (uses the following equation).

$$k = \frac{(1+e)v_s}{G_s - 1} \tag{6.7}$$

Where G_s is the specific gravity, e is the initial void ratio and v_s is the initial settling velocity of the solids.

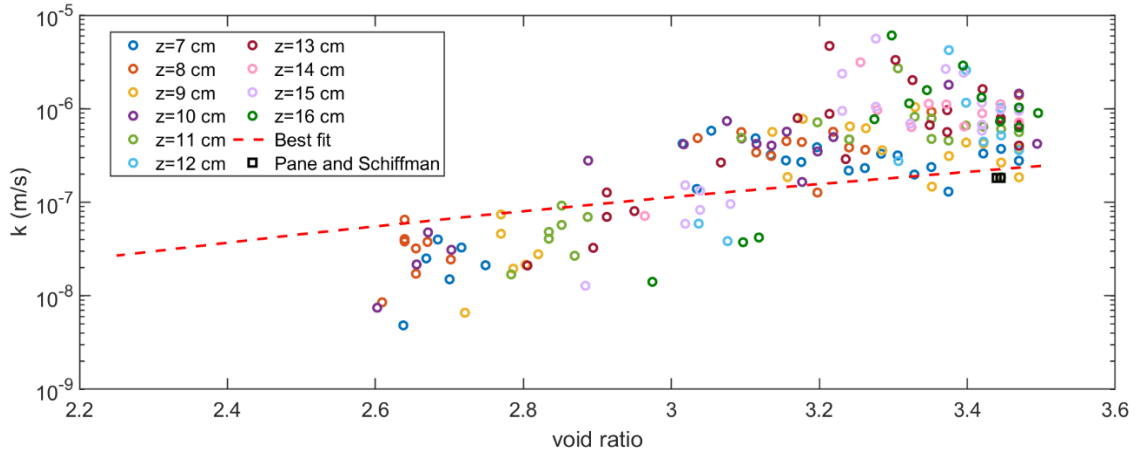


Figure 6-11: Calculated k - e relationship for Kaolinite

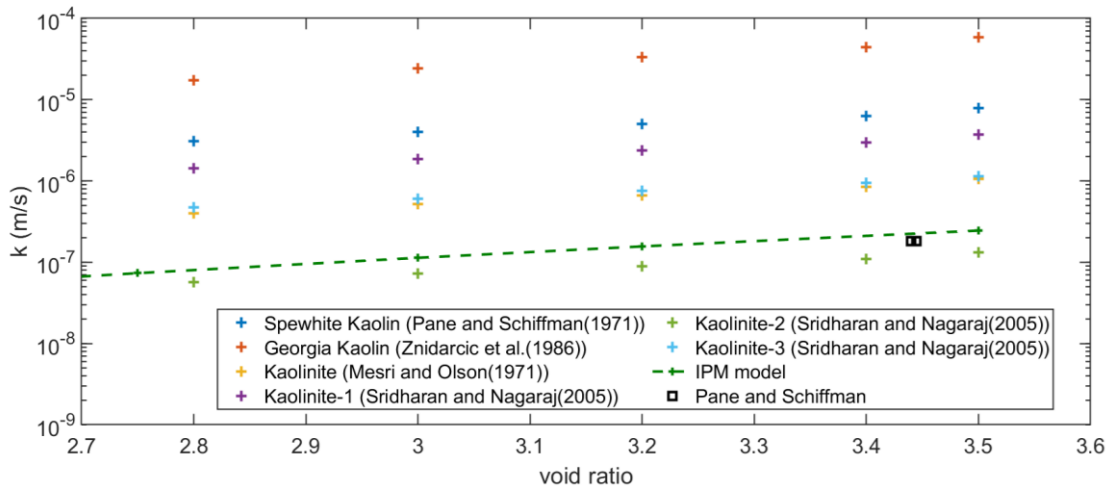


Figure 6-12: Comparison of calculated k - e to other published studies

A large-strain consolidation model is utilized to compared the predicted settling behaviour with the measured data, presented in Figure 6-13. The sedimentation-

consolidation would provide a near-identical result, as the transition void ratio (~ 3.34) was very close to the initial void ratio (3.44). The model prediction is very close to the measured settlement, though the final height was off (~ 0.5 cm); this discrepancy is due to the use of the in-situ compressibility function rather than the final compressibility function.

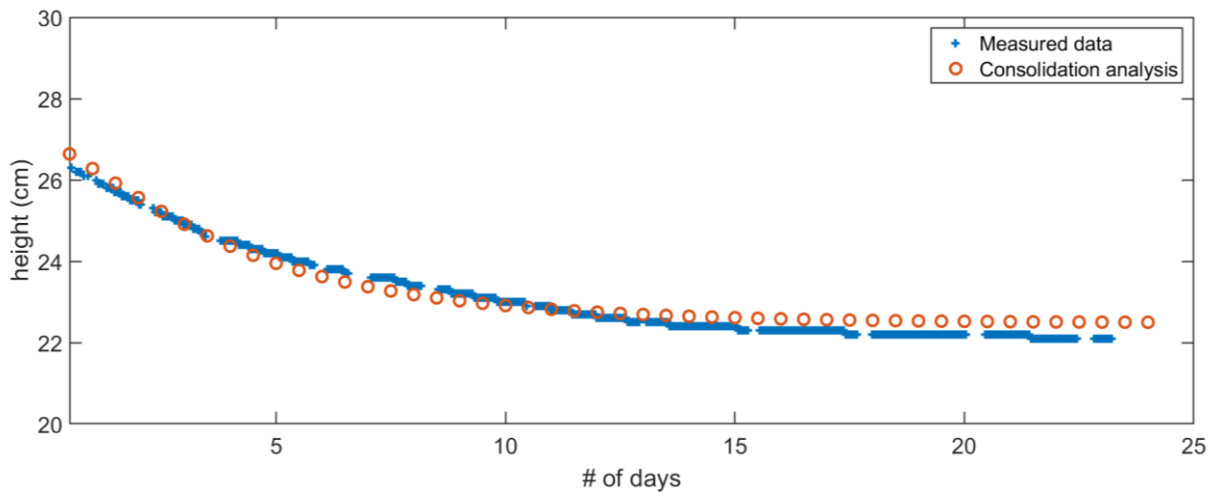


Figure 6-13: The settlement modelling comparison with measured data for Kaolinite

It must be acknowledged that this relatively good estimation of the k-e function by the IPM methods may be fortuitous. As seen in Figure 6-11, there is considerably more scatter in this data than for the gold tailings. This may be due to the longer timescale of the experiment and associated fluctuations in the SENTEK EnviroSCAN sensor readings.

6.5 Unamended Fluid Fine Tailings

A long-term self-weight consolidation test is conducted on unamended fluid fine tailings from Shell. This raw FFT is mixed with polymer A3338 to create amended soil samples for testing, which is discussed in Chapter 7. This experiment was conducted under

unexpected circumstances; the laboratory at Carleton University closed within the first days of the test. Data collection was accomplished through remote connections; however, problems have arisen during the experiment both due to sensors and the camera system. A few day's worth of data were lost during the experiment, but a fair amount of control was achieved within the first 25 days. From Day 25 to 37, the remote connection to the camera system malfunctioned. Another problem occurred on capacitance-based sensors due to power failures in the lab (which also affect the data loggers), and these issues influence the volumetric water content readings after Day 42.

6.5.1 Initial Conditions

Similar to previous experiments, the pore water pressure and volumetric water content profiles are measured throughout the test. The data is measured every 60 minutes, but only readings at selected days are presented in Figure 6-14. The final water content profile is determined at the end of Day 52, and the sensor readings are calibrated using the initial and final water contents.

The sensor readings were corrected (as suggested in Chapter 5) using a certain location ($z = 28$ cm, located and reading in water) to minimize the noise. Despite the improvement in the readings, an anomaly was spotted in VWC profiles after Day 42. The water content readings from Day 42 to Day 52 seemed to increase, which can also be observed in Figure 6-14. At that time, access to the laboratory was not an option, and only the readings until Day 42 are included in the assessment of the Instantaneous Profiling method for this experiment.

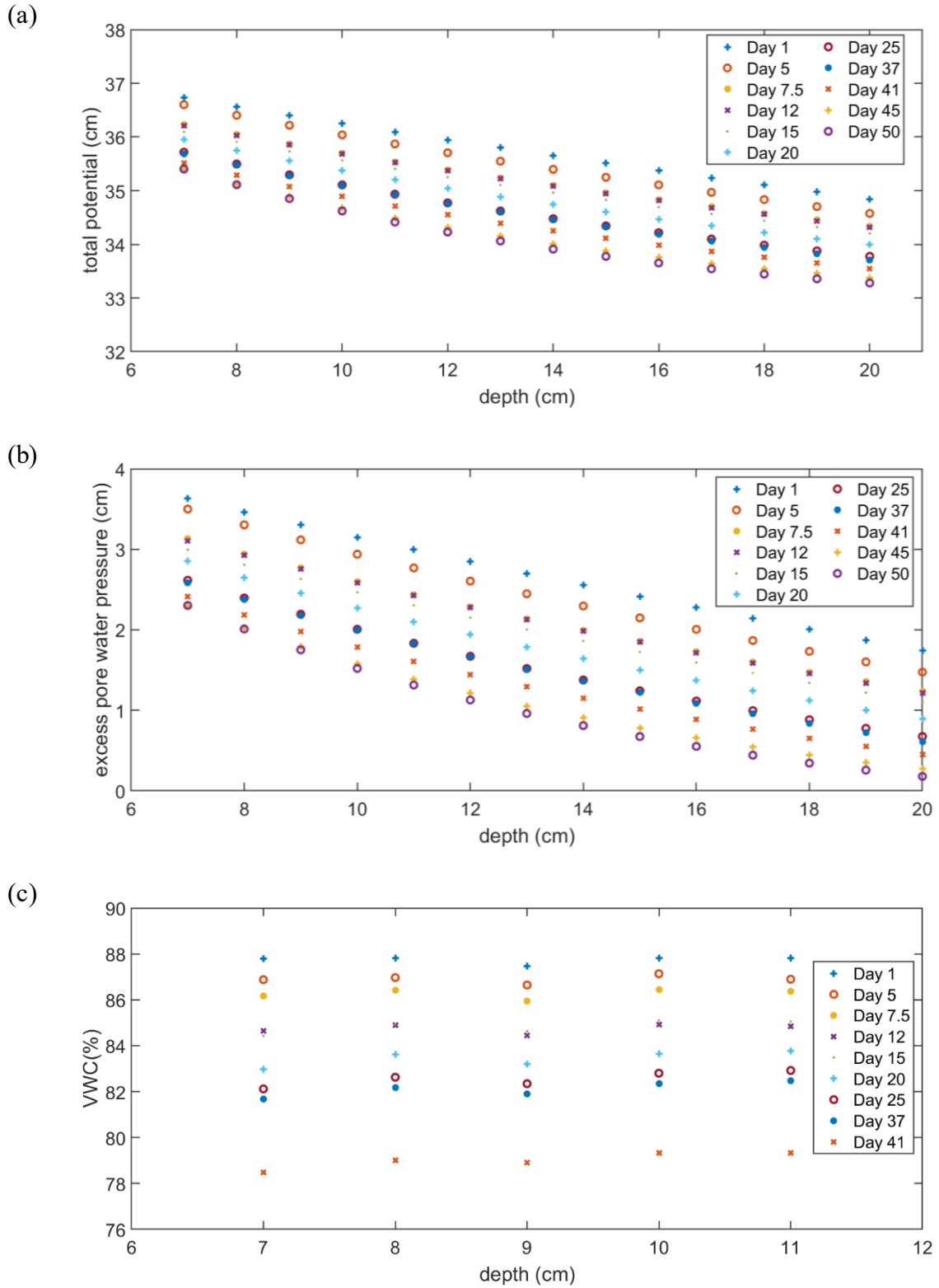
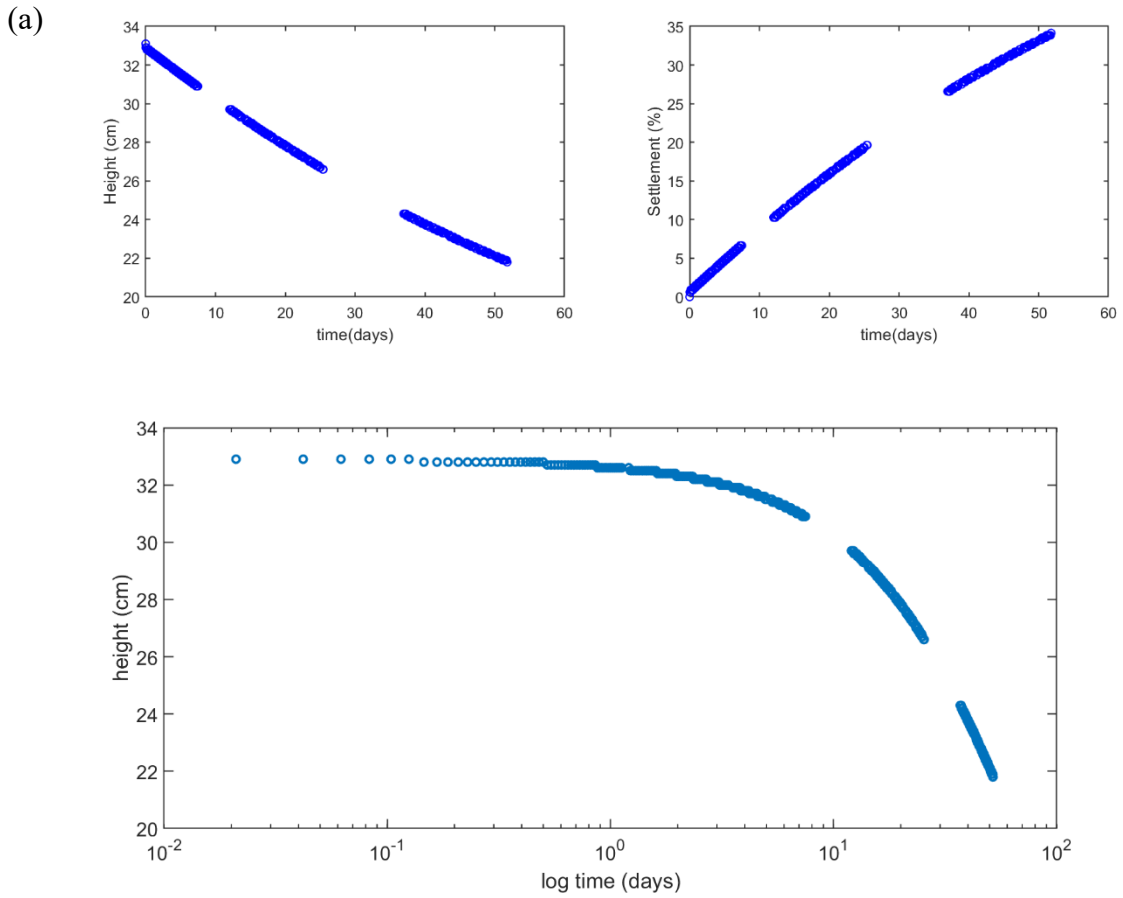


Figure 6-14: (a) Total potential measurements, (b) excess pore water pressures, and (c) Volumetric water content profiles at selected times

6.5.2 Results and Discussion

The height change, the percentage of settlement during the experiment and the final VWC profile in the column are presented in the following figure. The missing data points are attributed to the malfunction of the remote system along with the cameras during the experiment.



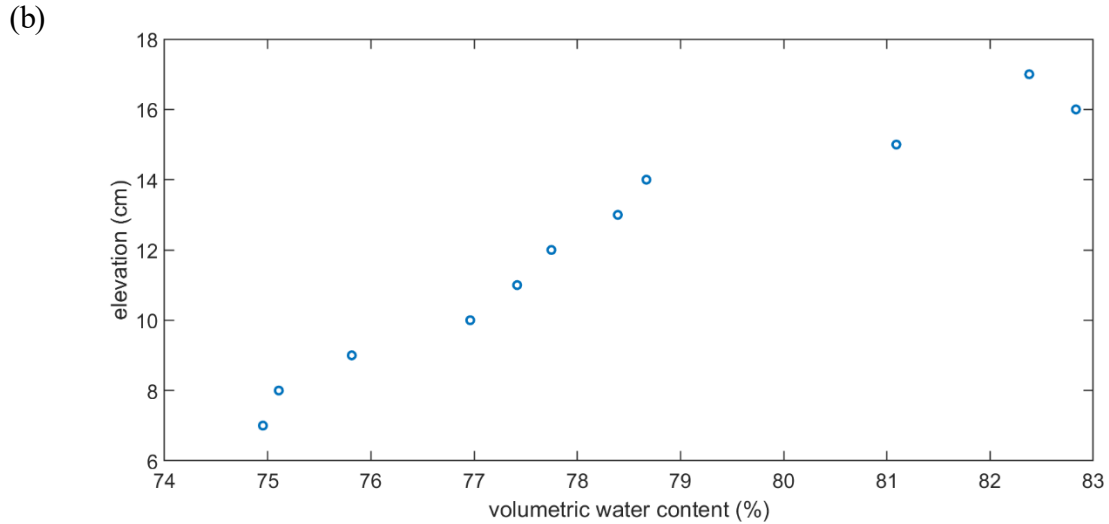


Figure 6-15: (a) The settlement behaviour of unamended FFT, and (b) Final volumetric water content profile in the column determined with oven-dried samples

The compressibility curve is determined both (i) from the final condition and (ii) using the measured data of pore water pressures and water contents throughout the experiment. Figure 6-16 demonstrates the change in the compressibility curve, and the behavioural change can be observed after Day 7; therefore, Equation 6.9 corresponds to the data measured after this time.

From the final condition $e = 2.46\sigma^{r-0.08}$ (6.8)

Using measured PWP and VWC measurements $e = 2.88\sigma^{r-0.35}$ (6.9)

Hydraulic conductivity-void ratio relationship has been determined using the IPM method (presented in Figure 6-17) and calculated as:

$$k = 4 \times 10^{-9} e^{2.1} \quad (6.10)$$

Both Equations 6.9 and 6.10 have been calculated with the data measured until Day

25. As mentioned previously, a fair amount of problems arose during the experiment after that day.

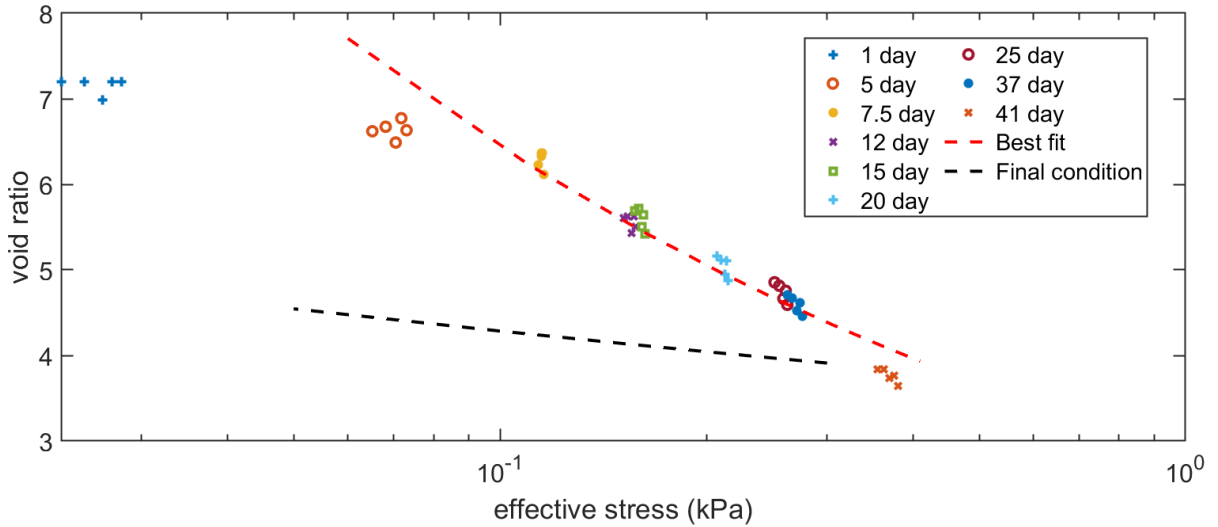


Figure 6-16: The effective stress-void ratio relationship at different days

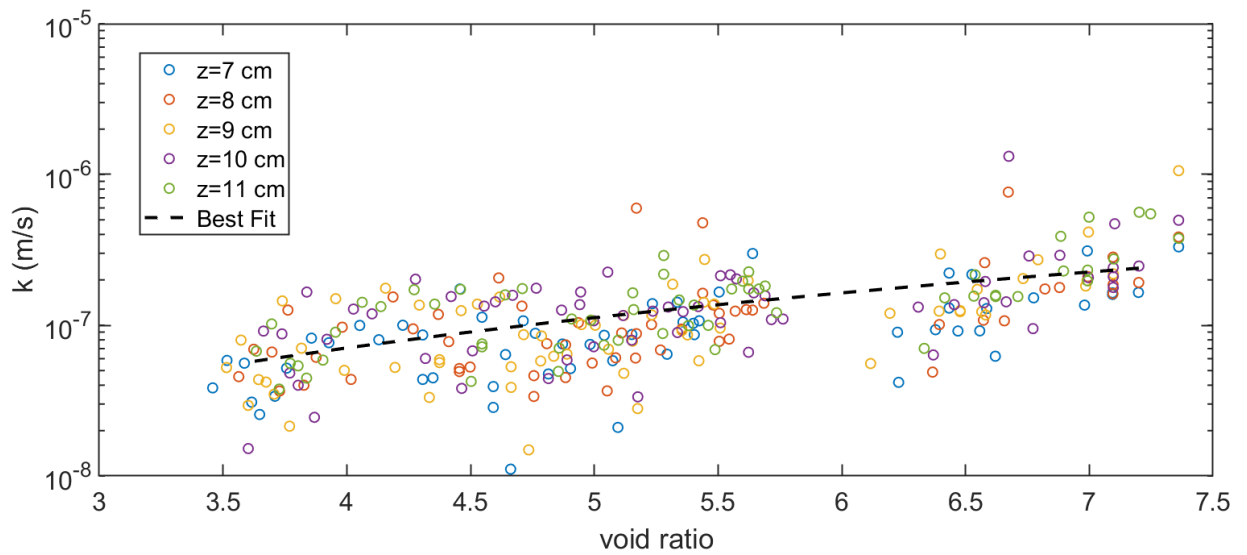


Figure 6-17: Calculated k - e relationship of unamended FFT

A large-strain consolidation (LSC) test has been conducted at the University of Alberta for this FFT sample, and the results are compared in the next figure with the k - e relationship calculated using the IPM method. Also, k values at initial void ratios are

calculated using Pane and Schiffman's equation (Equation 6.7). The k value calculated using this method agreed well with the k - e equation calculated using the IPM method, and independent measurements from LSC underestimated the predicted values. However, it should be noted that the void ratio after the first loading step in the LSC consolidation tests is ~ 5 , whereas the measured initial void ratio in this experiment is 7.36.

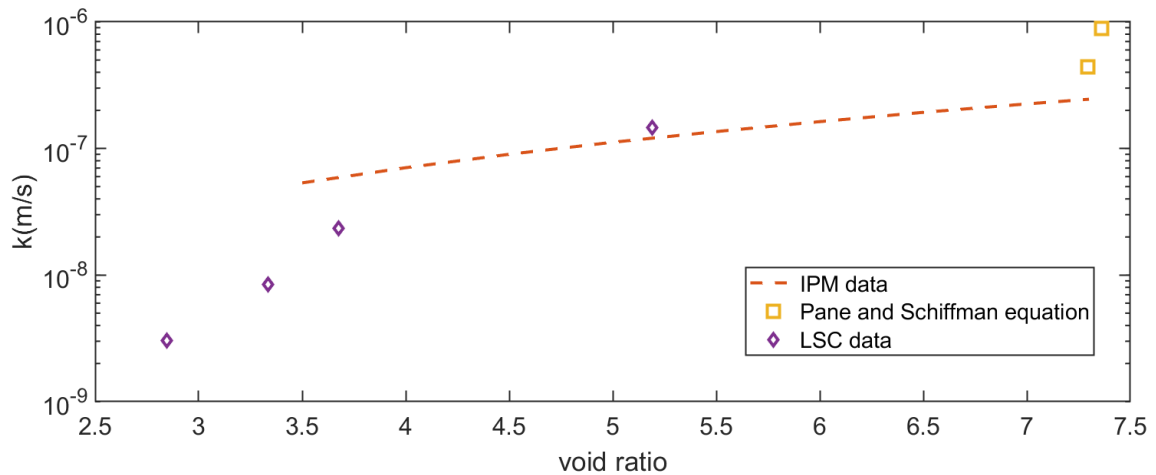


Figure 6-18: Comparison with independent measurements from LSC and Pane and Schiffman

The settlement behaviour of the sample is simulated using a large strain consolidation software; the model uses Equations 6.9 and 6.10 for its compressibility and hydraulic conductivity-void ratio relationships. The transitional void ratio is determined as 6.5, and the effect of sedimentation on the settlement behaviour has also been analyzed. It should be noted that equations 6.9 and 6.10 are determined until Day 25, which can explain why the predicted settlement data agreed well with the measured one in Figure 6-19(a). However, the use of the same equations provides slightly off predicted curves for 52 days. Both consolidation only and sedimentation-consolidation simulations overestimated the final height. However, both these predictions were superior to the model using the k - e

relationship from the LSC test. The superior performance of the IPM method is likely due to the higher resolution of measurements at void ratios above the first measurement point of the LSC test, which was conducted at effective stress of 0.58 kPa.

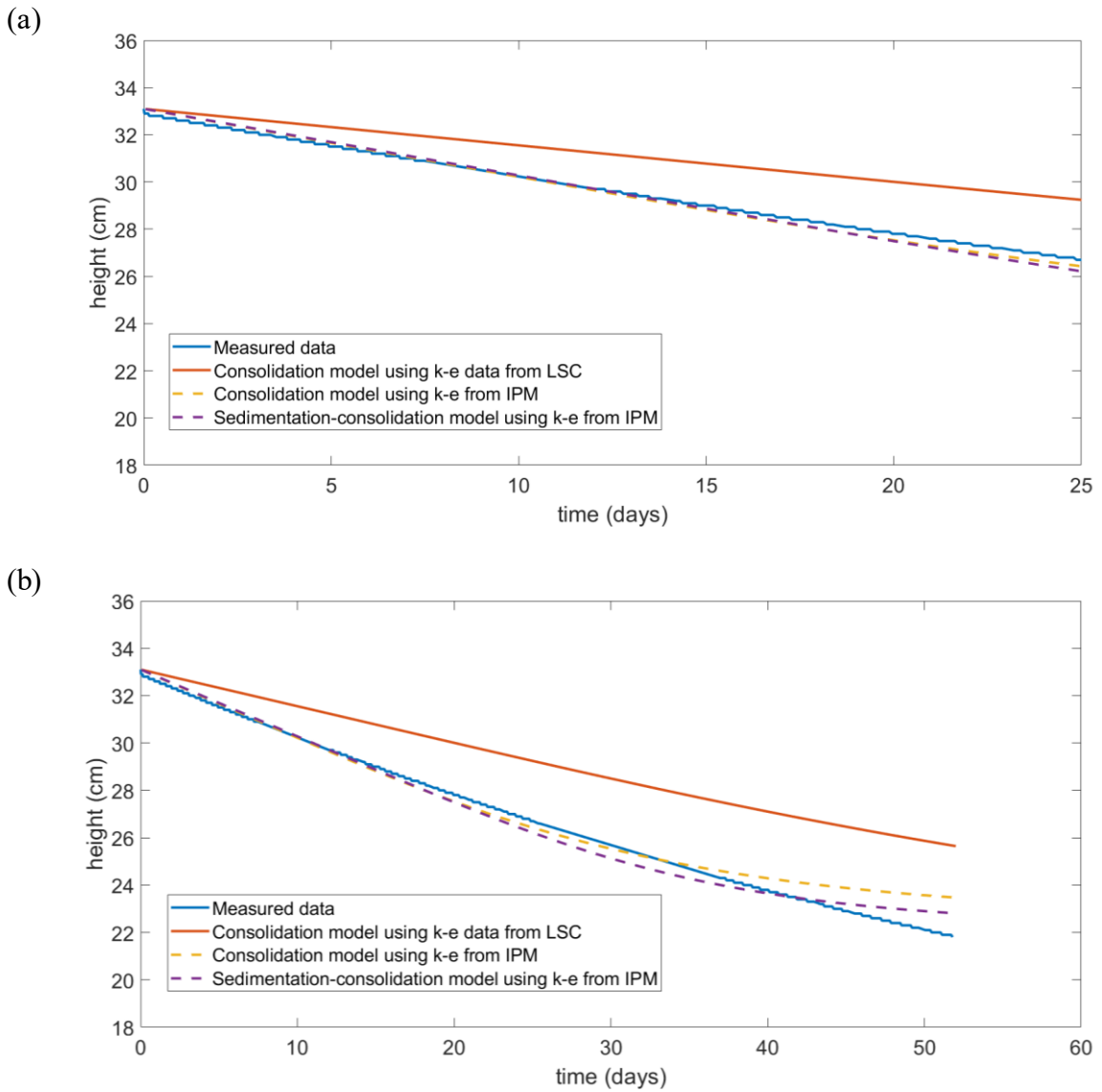


Figure 6-19: The settlement modelling comparison of unamended FFT sample for (a) First 25 days and (b) until the end of the experiment

For these simulations, the in-situ compressibility curve is utilized similar to the

previous experiments, and the predicted curves agreed well with the measured data, especially for the first 25 days. The predicted final settlement heights (at the end of Day 52), however, varied slightly from the measured data, which is due to using the selected compressibility curve as opposed to the final compressibility curve in the simulations.

6.6 Conclusion

This study examined the application of the IPM method, which derives from Darcy's law, to calculate the $k-e$ relationship for various fine-grained soils. The hydraulic conductivity curve can be determined by the variations in pore water pressure and volumetric water content profiles from a 1D column test. Capacitance-based SENTEK EnviroSCAN sensors are selected for this application to provide sufficient resolutions of water contents with depth, and an automation system is implemented to provide vertical movement to the probe, achieving high-resolution measurement profiles.

The settlement behaviours are compared with the estimated curves predicted by a large strain consolidation analysis program UNSATCON, using the calculated $k-e$ curves from the IPM method. For thickened gold tailings, the results demonstrated small discrepancies between the measured and predicted settlement behaviour for Tests 2 and 3 (which can be attributed to the selected compressibility equation as they provide a better fit if Eqs.6.3 is used in the model). However, the predicted volumetric water content profiles at different heights and durations agreed well with the measured data, which demonstrated the potency of the calculated $k-e$ curves from the IPM model. For Kaolinite and unamended FFT samples, raw readings from VWC sensors are corrected (as suggested in Chapter 5) prior to analysis. The transitional void ratio is calculated and utilized in

sedimentation-consolidation models for predicting the settlement behaviour of the tests. The final predicted settlement behaviour is compared with the measured data for all experiments.

Chapter 7: Consolidometer Trials for Flocculated Fluid Fine Tailings

7.1 Introduction

The consolidation characteristics of tailings, particularly the hydraulic conductivity – void ratio function ($k-e$), govern the rate of settlement and densification in any tailings impoundment. Well-established methods exist to determine $k-e$, such as the large strain consolidation test or the seepage induced consolidation test, which involves direct measurement of k at fixed void ratio and stresses, or column tests, which are analyzed through back-calculation methods to arrive at a $k-e$ function. The two first tests may take considerable time, months in the case of clayey tailings, while the latter are subject to various assumptions, such as the form of the $k-e$ function and assumptions as to the uniqueness of the compressibility function, for example. There are well-known procedures to back-calculate $k-e$ from column tests (A. N. Abu-Hejleh et al. (1996), Pane and Schiffman (1997)), which take advantage of special characteristics, such as the initial slope of the height versus time curve and the hydraulic conductivity at the surface (K Been & Sills, 1981). Recent proposed techniques for estimating $k-e$ use special characteristics of the full settlement curve (Shunchao Qi and Simms (2020), Shunchao Qi et al. (2020)), though they still presume certain forms for the $k-e$ and compressibility functions. The power equation describes many if not most measured data sets of $k-e$ (Babaoglu and Simms (2020)); however, some data sets do suggest or more complex behaviour at high void ratios. Therefore, there is a need for more rapid and accurate measurements of $k-e$, especially at a high void ratio.

This study describes calculating the $k-e$ relationship using the “Instantaneous

Profiling Method” or IPM (Watson, 1966) in a specially fabricated column. IPM requires a high-resolution of water content in space and time to calculate fluxes and then calculates hydraulic conductivity directly from Darcy’s law using measured head profiles. For the case of soft soils, the resolution of the measurements in time and space must be sufficient to ensure small-strain conditions. Similar researches have been conducted using the IPM method such as Leung et al. (2016), Askarinejad et al. (2012), Dikinya (2005), Fisher et al. (2008), while similar approaches have been used in slurry consolidation tests (G Bartholomeeusen et al., 2002), though at relatively low resolution. A particular advantage of this technique is that the computed hydraulic conductivity is independent of the compressibility curve, which may shift during consolidation at low stresses (Hawlder et al., 2008). This study presents a specialized column test designed to allow for non-destructive measurements of volumetric water content profiles and an automation system to allow for detailed profiling using capacitance-based sensors. Here we present data on tests on three different types of polymer flocculated oil sands fluid fine tailings (fFFT); two using the polymer A3338 at different dosages and another one using Polymer B, which is developed at the University of Alberta. k - e measurements obtained by IPM are compared with independent measurements (a large strain consolidation test is conducted at the University of Alberta for amended tailings with 800 ppm dosage), and the column data is also analyzed using a large strain consolidation software (UNSATCON, Shunchao Qi, Simms, and Vanapalli (2017) and Shunchao Qi, Simms, Vanapalli, et al. (2017)) using the measured k - e and compressibility curves.

7.2 Properties of Tailings and Initial Conditions

The methodology of the Instantaneous Profiling Method and prototype column design is introduced in Chapter 5. The pore water pressures within the column are measured using miniature pore pressure sensors (T5 from UMS), which are inserted using the inlets at the exterior wall of the column. There are ten inlets at various locations, but it might be necessary to point out that depending on the thickness of the deposit, the number of available inlets changes; maximum of five inlets were utilized for this study.

For the high-resolution measurement profiles of water contents, capacitance-based sensors were selected after consideration of a range of ultrasonic and electromagnetic-based techniques. The VWC sensors are designed to obtain measurements along a ten-centimetre length; therefore, for more detailed profiling, a vertical motion of the sensor body is required. An automation system is designed for this task, which consists of a motor (12 V DC linear actuator is selected), an Arduino board and multiple parts for the electronics design (i.e. relay modules to control the retraction of the actuator, connectivity relays for voltage compatibility). The automation system is programmed to take measurements at every centimetre for all the experiments in this study.

Each sensor requires its own calibration and is sensitive to small changes in the geometry of the inner tube. Therefore, the sensors are calibrated at each depth following the procedures explained in Chapter 5.3, and the raw readings are corrected using “water readings” (raw readings from sensor locations fully submerged underwater, discussed in Chapter 5.4) from the sensors. As the sensors cannot directly measure the soil at the mudline directly, water contents close to the mudline are found algorithmically, through knowledge of how the readings progressively change as the sensor moves from the surface

water into the tailings. The settlements during the experiments are observed using two high-resolution cameras.

The geotechnical properties of the tailings (consists of two different types of fluid fine tailings (FFTs), the initial and the final conditions of the experiments are presented in Table 7.1. It has been reported that the initial solids content of slurry fluid fine tailings varies from 30-35% (Nicholas Beier et al., 2013); however, one of the FFT that has been tested in this study has an initial solids content of 28%.

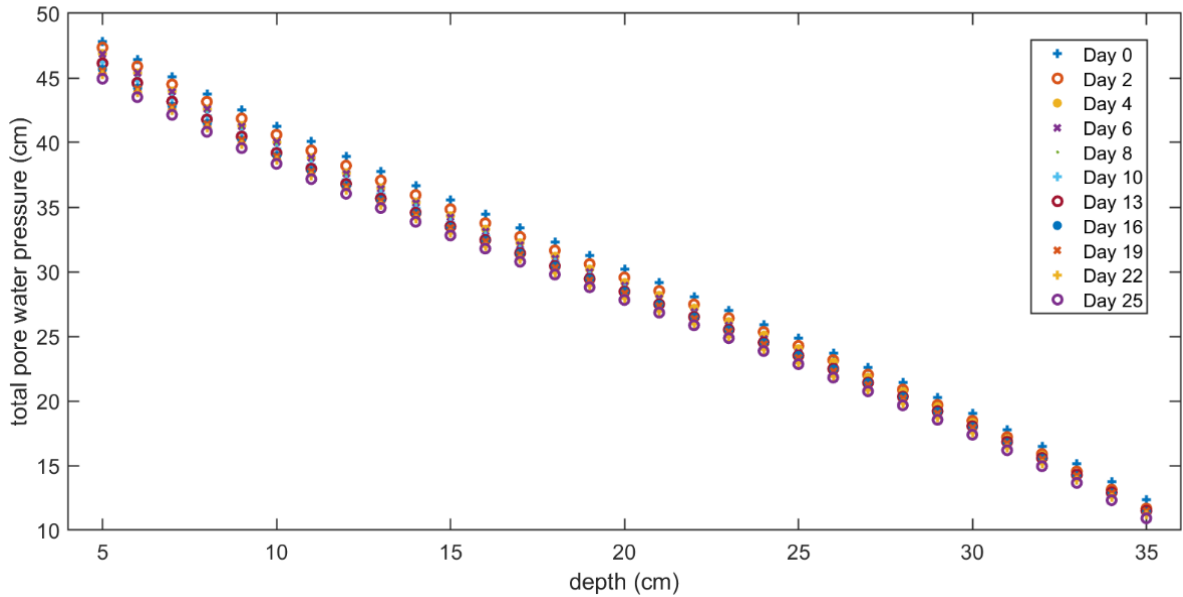
Table 7-1: Geotechnical Properties of Tailings and Initial conditions of the experiments

	800 ppm Test (A3338)	1000 ppm Test (A3338)	4000 ppm Test (Polymer B)
Initial θ (%)	84	83.9	87.5
Initial w (%)	248	246	330
Solids content (%)	28.8	29.0	22.6
Initial void ratio	5.25	5.2	7.0
Initial height (cm)	46.0	48.1	26.0
Final height (cm)	33.65	32.3	20.6
Pressure sensor positions (in cm, from the bottom)	5-15-20-25-35	5-15-20-25-35	5-10-15-20
Test duration	25 days	57 days	22.4 days
Settlement duration	Continuous	Continuous	Continuous

Two different types of raw fluid fine tailings are examined in this study; Shell FFT and Syncrude FFT. Both tailings are shipped to Carleton University at a solids content of 31% and 28%, respectively. An anionic flocculant (A3338, used for Shell FFT) and a cationic polymer (Polymer B, used for Syncrude FFT) are utilized to prepare flocculated FFT at specific doses.

7.3 Amended Tailings with 800 ppm dosage using A3338

For the first amended tailings, or flocculated fluid fine tailings (fFFT), the sample is prepared with Shell fluid fine tailings using Polymer A3338 at 800 ppm dosage. The data collected by the PWP and water content sensors are shown in Figure 7-1, while the settlement behaviour is shown in Figure 7-2. Final profiles of gravimetric water content with depth are extracted at the end of the test, which is used in the calibration exercise for the VWC sensors. The volumetric water contents are measured at every centimetre in the column, and the depth profile data is only shown for certain times in Figure 7-1.



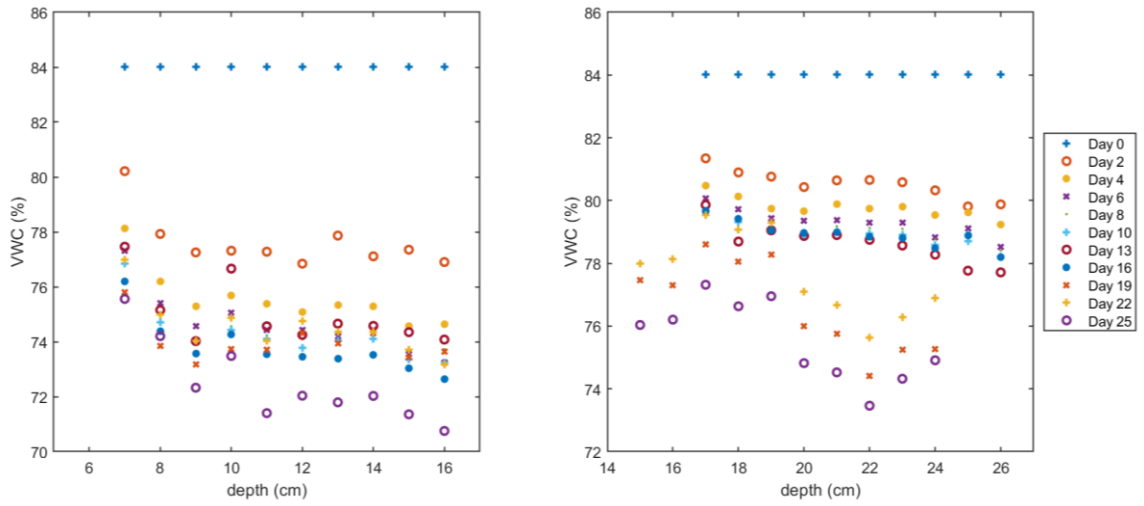
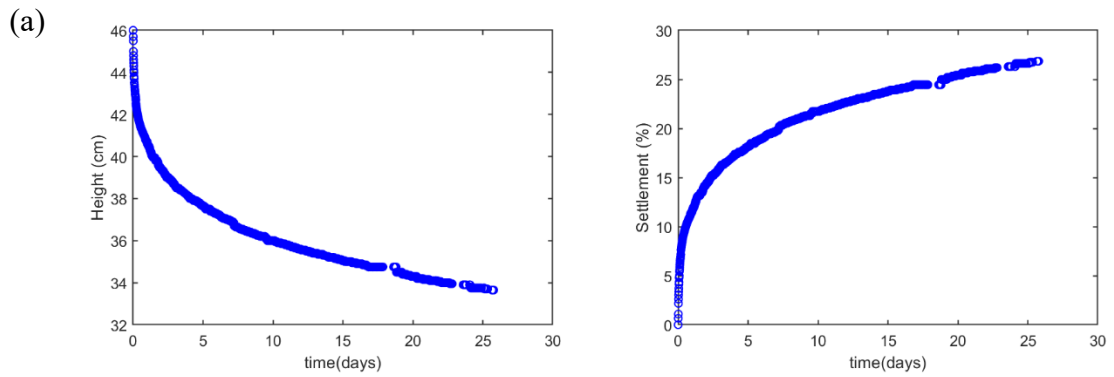


Figure 7-1: Measured pore water pressures and uncorrected volumetric water contents for fFFT tailings at 800 ppm dosage



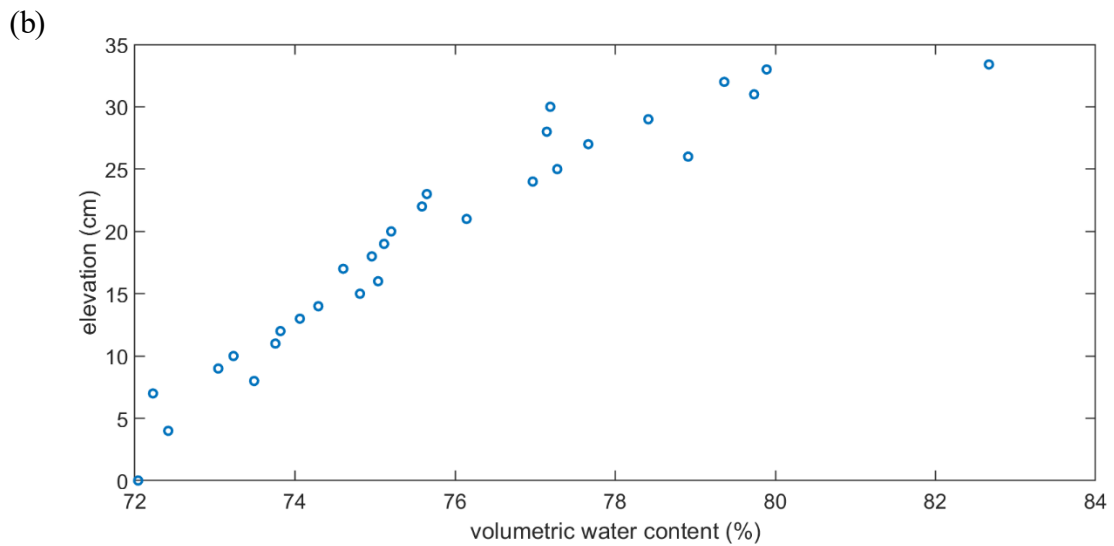
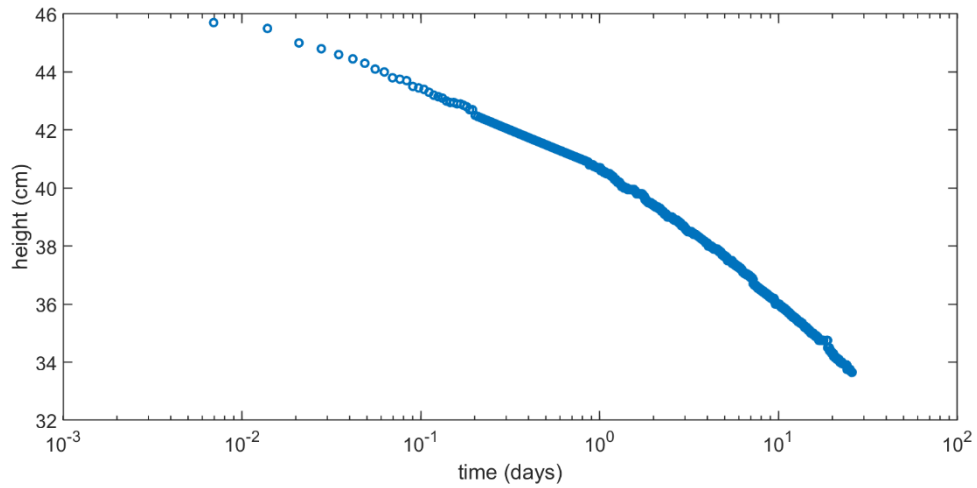


Figure 7-2: (a) Settlement behaviour of the sample for 800 ppm fFFT, and (b) The final measured VWC profile in the column

The compressibility equation of both experiments are calculated using two different methods; (i) from the final condition and (ii) by using the volumetric water content and pore water pressure measurements throughout the experiment (presented in Figure 7-3), and calculated as:

Method (i)
$$e = 2.65\sigma^{-0.07} \quad (7.1)$$

Method (ii)

$$e = 2.42\sigma^{-0.412}$$

(7.2)

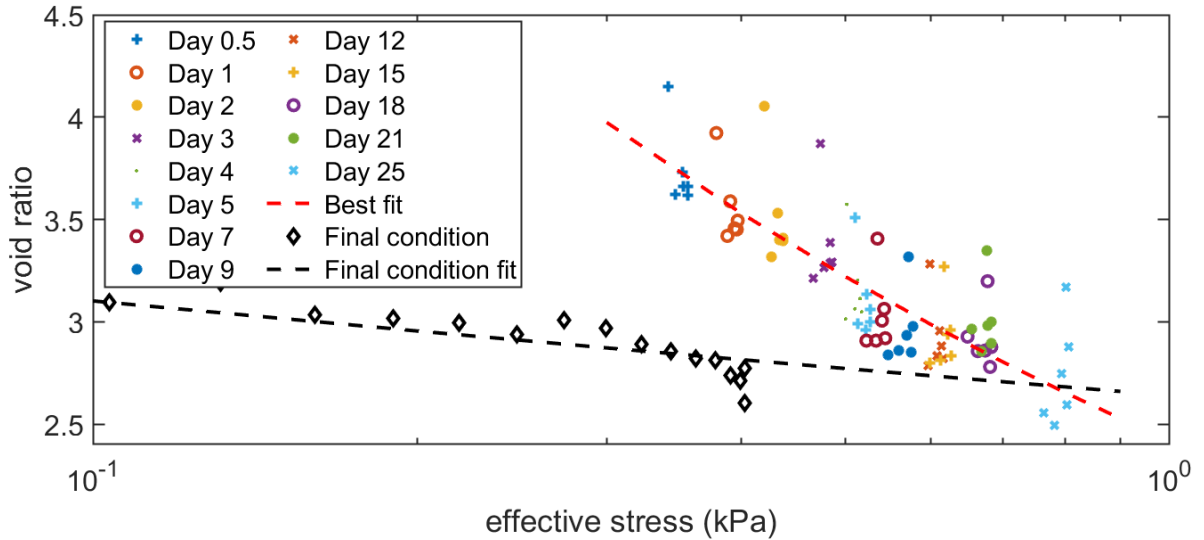


Figure 7-3: The compressibility of 800 ppm FFT

The hydraulic conductivity value calculated by the IPM method is shown in Figure 7-4. For the fFFT, independent measurements using a large strain consolidometer Amoako, Abdulnabi, Beier, Soares, and Simms (2020) are shown. Additionally, Pane and Schiffman's equation is used to estimate hydraulic conductivity at the initial void ratio, which is shown in the same figure. A sharp settling behaviour is observed within the first half a day; hence the k - e equation is calculated separately for this period of time.

General k - e relationship

$$k = 6 \times 10^{-12} e^{7.5} \quad (7.3)$$

First 0.5 day:

$$k = 4 \times 10^{-9} e^{4.2} \quad (7.4)$$

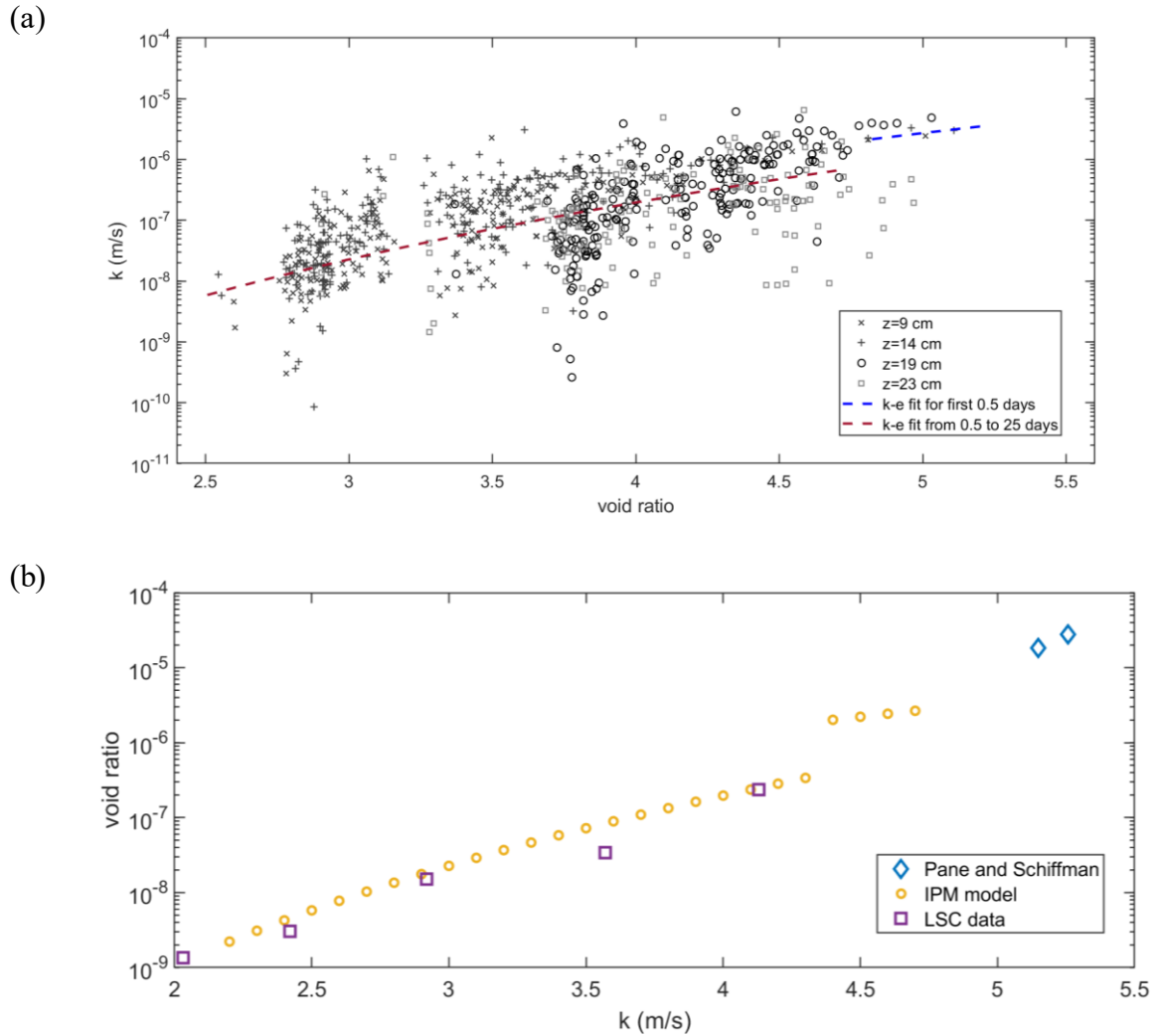


Figure 7-4: (a) The k - e relationship for 800 ppm fFFT tailings and (b) Comparison with independent measurements from LSC and Pane and Schiffman

In the fFFT, the data generally lies somewhat above the trend through the LSC values. Much data in tailings and other soft soils suggest that hydraulic conductivity in the sedimentation phase can be different than during the consolidation phase; this is shown definitively for some other polymer-FFT mixtures (Amoako et al., 2020). Finally, when modelling the height using a large strain consolidation software (UNSATCON), a good agreement could only be achieved using two distinct power functions above (Figure 7-5).

A sedimentation-consolidation simulation is also conducted, and for both consolidation and sedimentation-consolidation models, two $k-e$ equations are used in the simulations. The transitional void ratio is determined by fitting the compressibility curve to parameters a , b , and c . The methodology to determine the transitional void ratio is explained in Chapter 6.1 in detail. Predicted settlement behaviour using two $k-e$ equations agreed well with the measured data from Day 7 until the end of the experiment. However, it could not simulate the sharp decrease within the first five days, which can be observed in Figure 7-5. The same behaviour can be observed when the measured and predicted volumetric water contents are compared (Figure 7-6). For these simulations, two $k-e$ equations are used in the consolidation model to predict the change in VWC over time. At higher locations in the column, the measured VWC is lower compared to the predicted ones from UNSATCON, indicating when the sedimentation-consolidation model is implemented in the analysis, the predicted behaviour is more similar to the measured data at the beginning of the tests, but it overestimated the settlement at Day 25. The error between the measured and the predicted final settlement height is calculated at 1.5%. This modelling is done using the compressibility curve fitted to the measured data throughout the experiment (or equation 7.2).

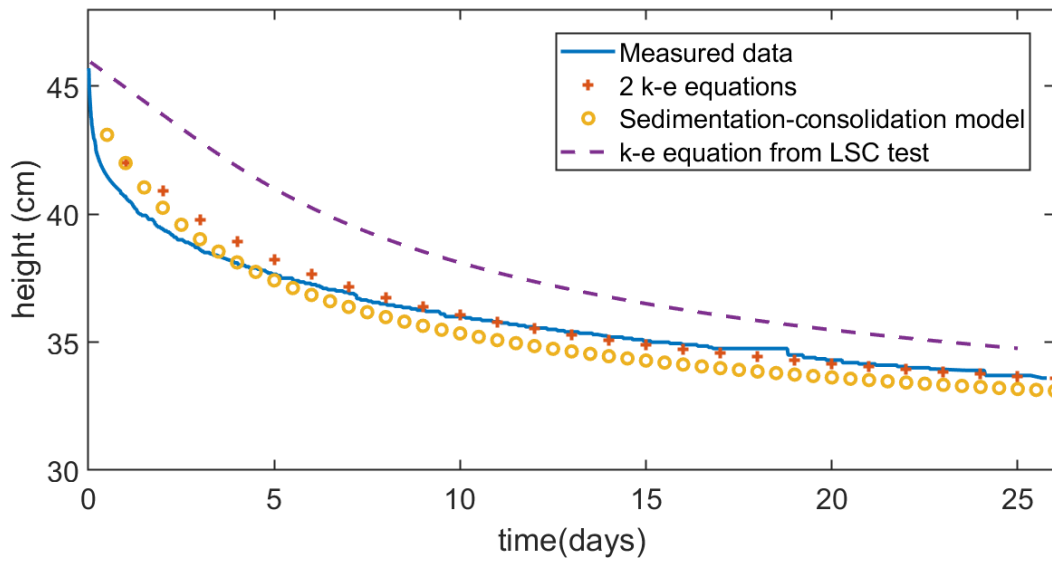


Figure 7-5: Modelling of the height data from the 800 ppm fFFT experiment

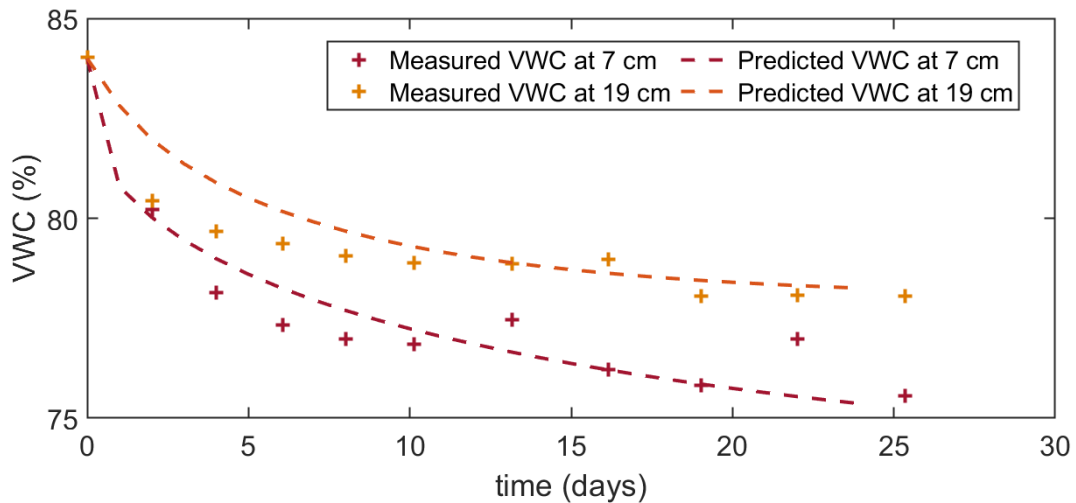


Figure 7-6: Comparison of measured volumetric water contents at two different locations (two separate sensors)

7.4 Amended Tailings with 1000 ppm dosage using A3338

Similar to the previous experiment, another amended fluid fine tailings have been prepared using the same raw tailings at a higher dosage. The optimization results for this anionic polymer demonstrated promising results in their dewatering behaviour for both 800 ppm

and 1000 ppm dosages; hence an additional experiment is conducted with the higher dosage as well. The pore water pressures are measured at five locations within the column during the experiment, at depths 5, 15, 20, 25 and 35 cm from the bottom of the column. Pore water pressures at in-between locations are estimated using MATLAB (R20189b), and volumetric water contents are determined at every centimetre (presented in Figure 7-7).

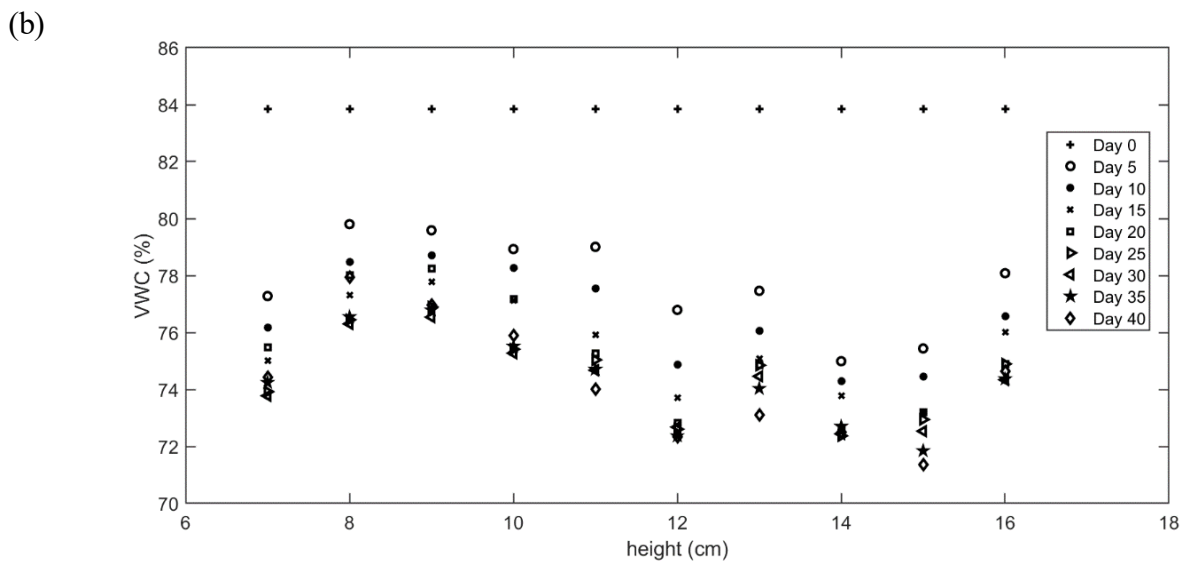
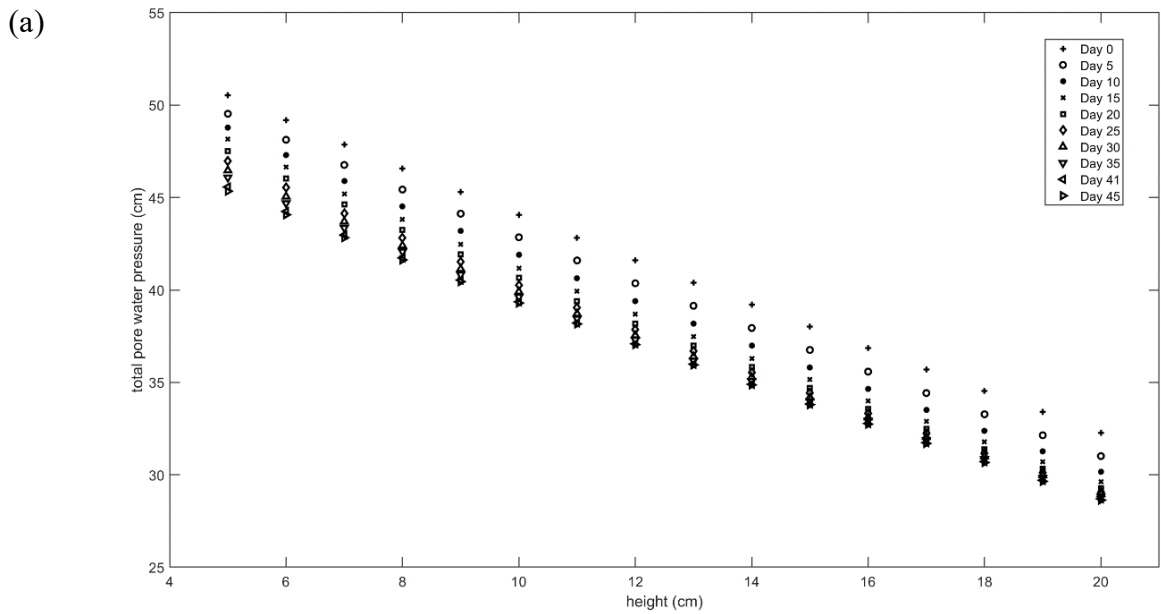


Figure 7-7: (a) The pore water pressure distribution and (b) uncorrected volumetric water contents from the first sensor for fFFT sample with 1000 ppm dosage

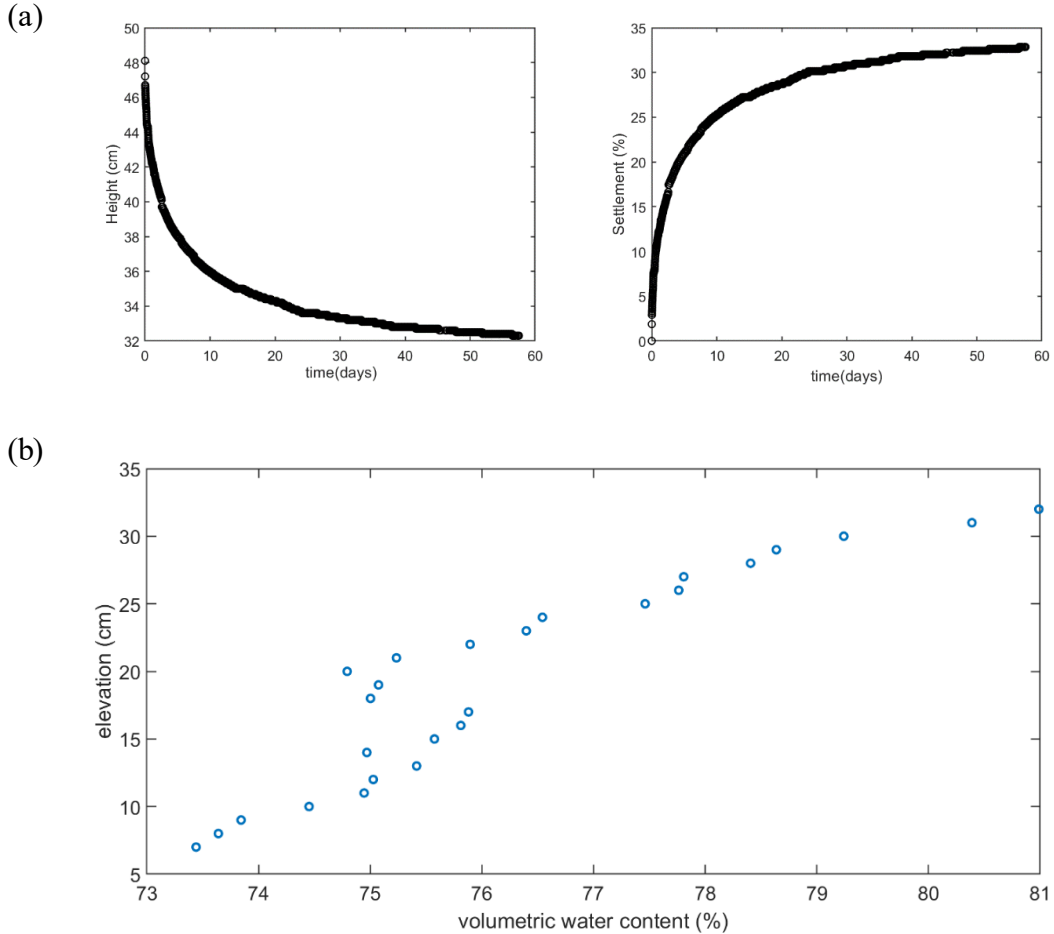


Figure 7-8: (a) The settlement behaviour for fFFT experiment at 1000 ppm dosage, and (b) The final measured VWC profile in the column

Similar settlement behaviour is observed in this experiment as well; during the sedimentation phase, tailings settle incredibly fast. This fast dewatering occurs within the first few hours, and the rate of settlement decreases over time; this behaviour can be observed in Figure 7-8(a). The compressibility curve is determined using the same two methods described in the previous sections, and the equations are calculated as;

From the final condition $e = 3.04\sigma^{-0.082}$ (7.5)

Using measured PWP and VWC measurements $e = 2.55\sigma^{-0.25}$ (7.6)

No significant effective stress development has been observed after Day 35; hence it is excluded from Figure 7-9 to declutter the figure. The hydraulic conductivity-void ratio relationship is calculated using the IPM method. The k - e relationship is determined as:

k - e relationship: $k = 4 \times 10^{-12} e^{7.92}$ (7.7)

The best-fitted data to the measured data points are demonstrated in Figure 7-9 for the compressibility curve and in Figure 7-10 (a) for the k - e relationship (using the IPM method). The estimation of k value at initial void ratios also has been calculated using Pane and Schiffman's equation, and the comparison with the 800 ppm experiment is presented in Figure 7-10 (b).

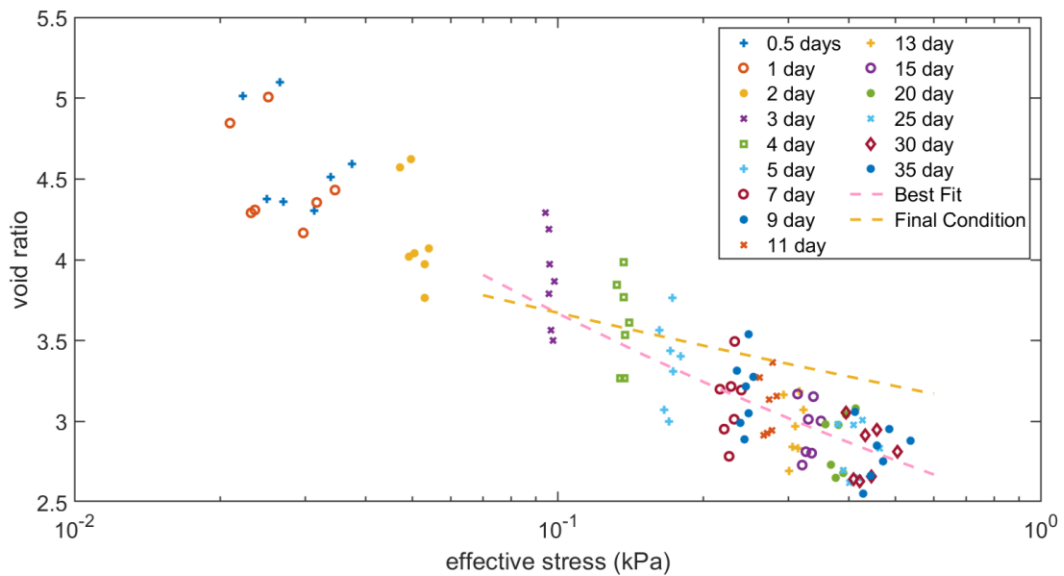


Figure 7-9: The compressibility curve using the measured data for 1000 ppm fFFT

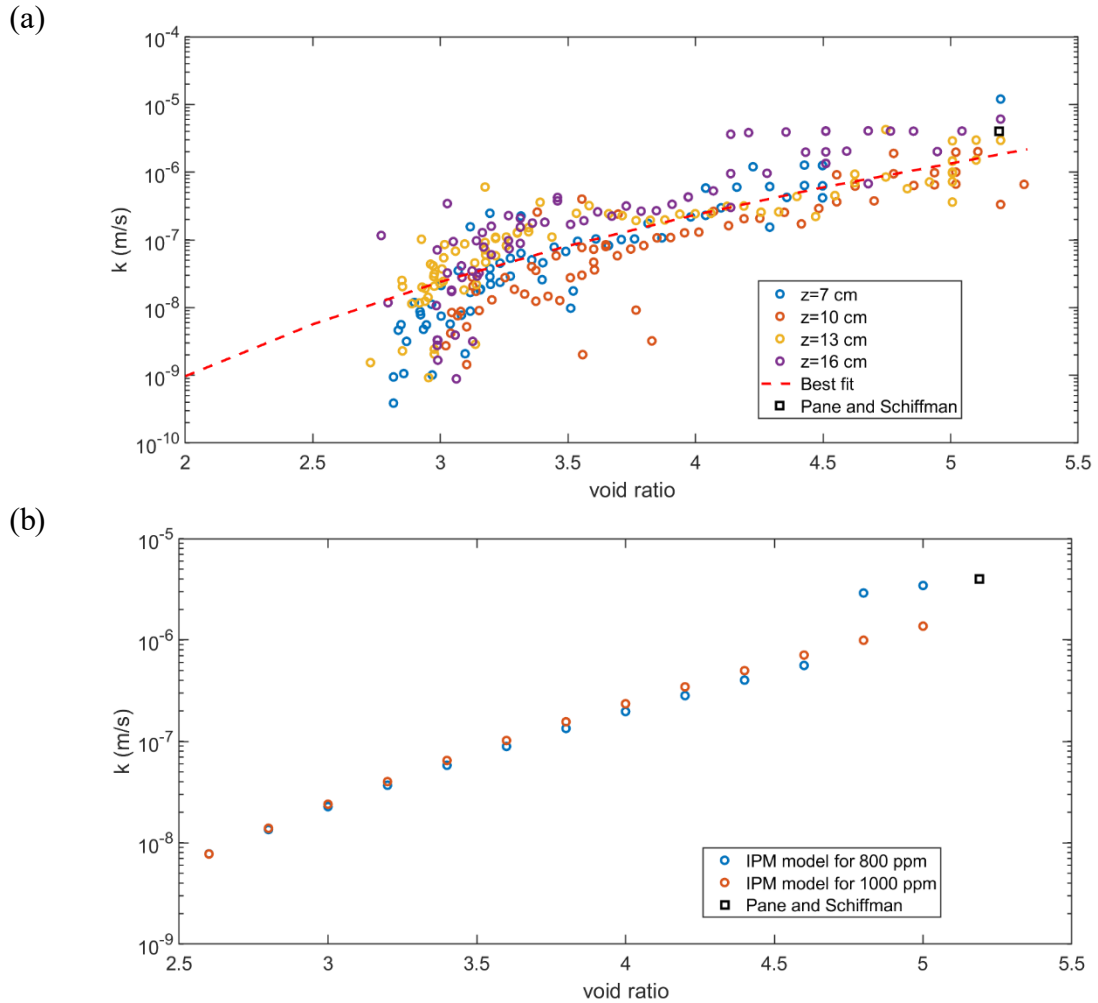


Figure 7-10: (a) The k - e relationship for 1000 ppm fFFT tailings, (b) Comparison of with 800 ppm test and Pane and Schiffman's equation

The initial k value from Pane and Schiffman's equation at the void ratio of 5.19 is determined as 3.9×10^{-6} m/s, which is slightly higher than an order of magnitude from the k value calculated using the IPM method. The settling behaviour was during this test was similar to the 800 ppm experiment; hence calculated k - e relationships have been compared as well. Unlike the 800 ppm test, there was no substantial change have been observed in the first few days. The modelling of height data is presented in the next figure. The

transitional void ratio is 4.45, and the sedimentation-consolidation model's simulation uses Equation 7.7. Similar to the sample with a lower dosage, both models agreed well with the final height, but a small discrepancy has been observed on the first day. It appears as with the 800 ppm dose; there are hydraulic conductivities at early times or the higher void ratios, which fall above the best-fit curve to the IPM data. This discrepancy is apparent from the difference between the IPM data and the estimate of k at $e=5.2$ using Pane and Schiffman's equation. With greater resolution in the water content measurements, it may be possible to more confidently use the IPM data at the highest void ratios, which would give a very close fit to the measured settlement curve when those k -values are employed in a consolidation model. The compressibility curves in both simulations use Equation 7.6.

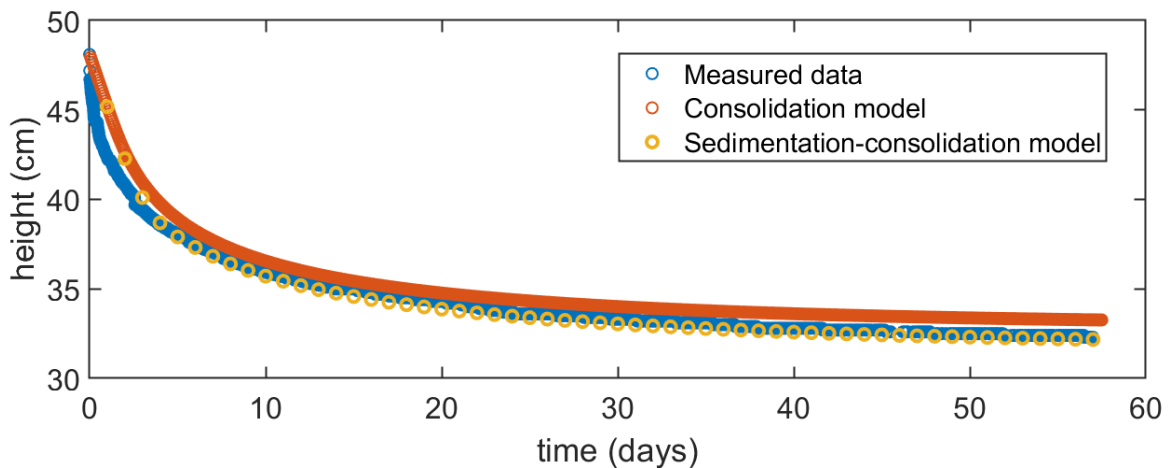


Figure 7-11: The settlement modelling comparison with measured data for 1000 ppm fFFT

7.5 Amended Tailings with 4000 ppm dosage using Polymer B

The flocculated fluid fine tailings sample is prepared using raw Syncrude fluid fine tailings with Polymer B. The dosage optimization experiments (discussed in Appendix A) demonstrated that 4000 ppm dosage provided the best results compared to other dosages; hence for testing in the prototype column, this dosage is selected. Same as the previous

experiments, pore water pressures are measured throughout the test, and the sensors are located at 5, 10, 15 and 20 cm from the bottom of the column. The in-between locations are estimated, and water content profiles are measured at every centimetre within the column; the data is presented below.

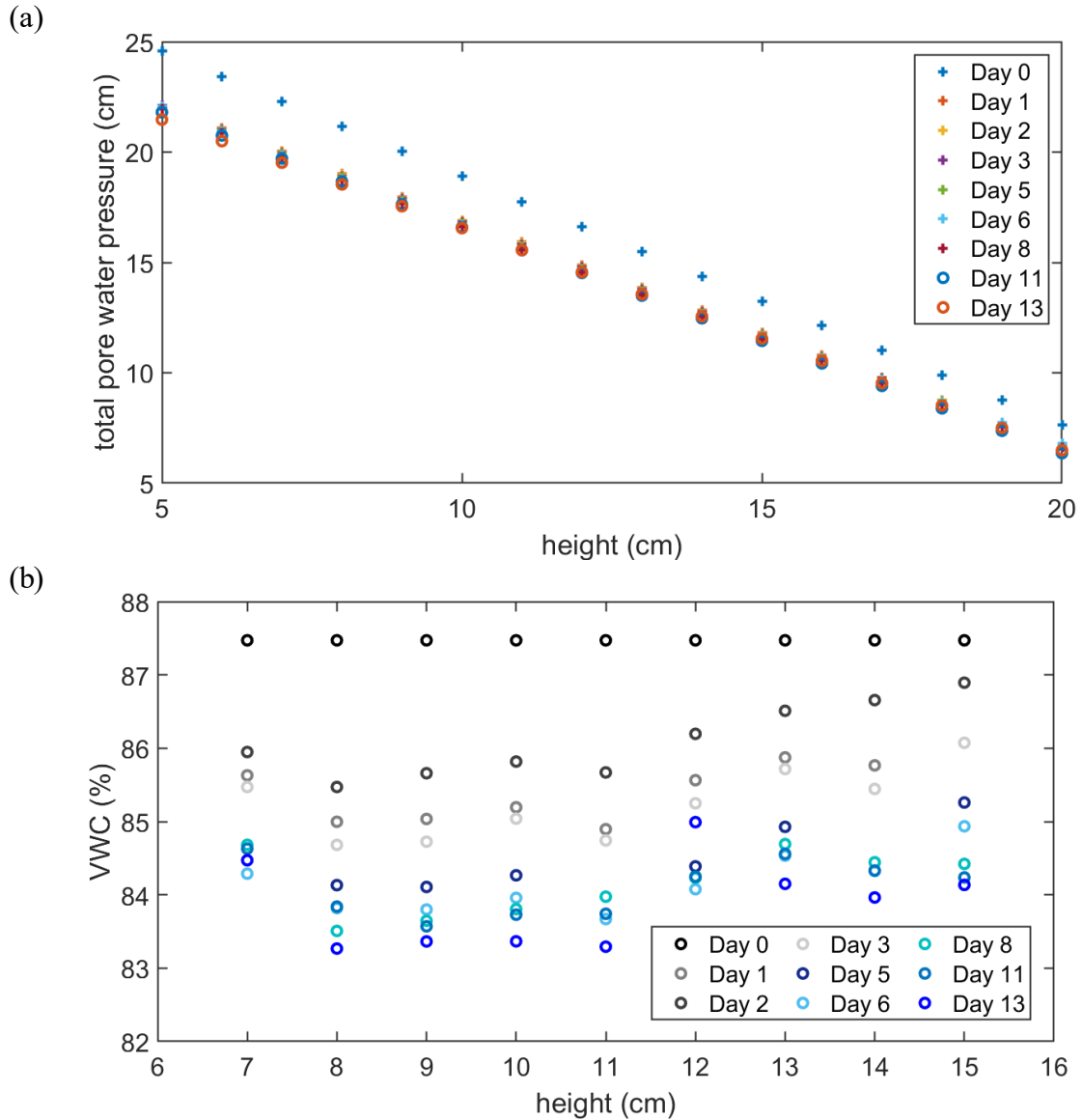


Figure 7-12: (a) The pore water pressure distribution and (b) uncorrectd volumetric water for FFT sample prepared using Polymer B

The settlement of the tailing deposit is presented in Figure 7-13. Unlike the other samples prepared with polymer A3338, most of the settlement of this fFFT is completed within the first two days, and the rate of the settlement decreased significantly after this time period.

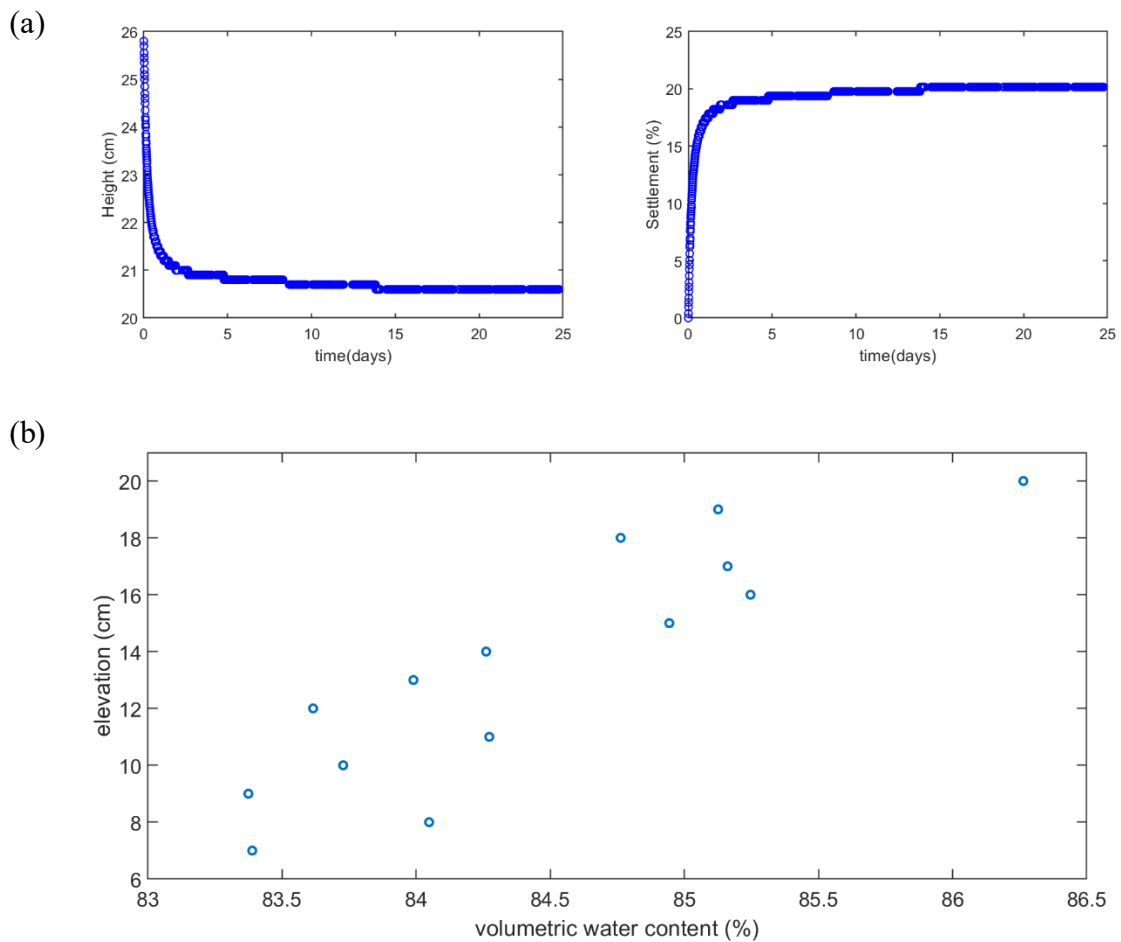


Figure 7-13: The settlement behaviour for fFFT experiment using Polymer B

The compressibility curve is presented for (a) the first two days and (b) until the end of the experiment in Figure 7-14, and the $k-e$ data determined using the IPM method is provided in Figure 7-15. The hydraulic conductivity at the initial void ratio is calculated using Pane and Schiffman's equation.

The effective stress-void ratio relationships are determined as:

From the final condition
$$e = 4.96\sigma^{-0.032} \quad (7.9)$$

Using measured PWP and VWC measurements
$$e = 4.93\sigma^{-0.051} \quad (7.10)$$

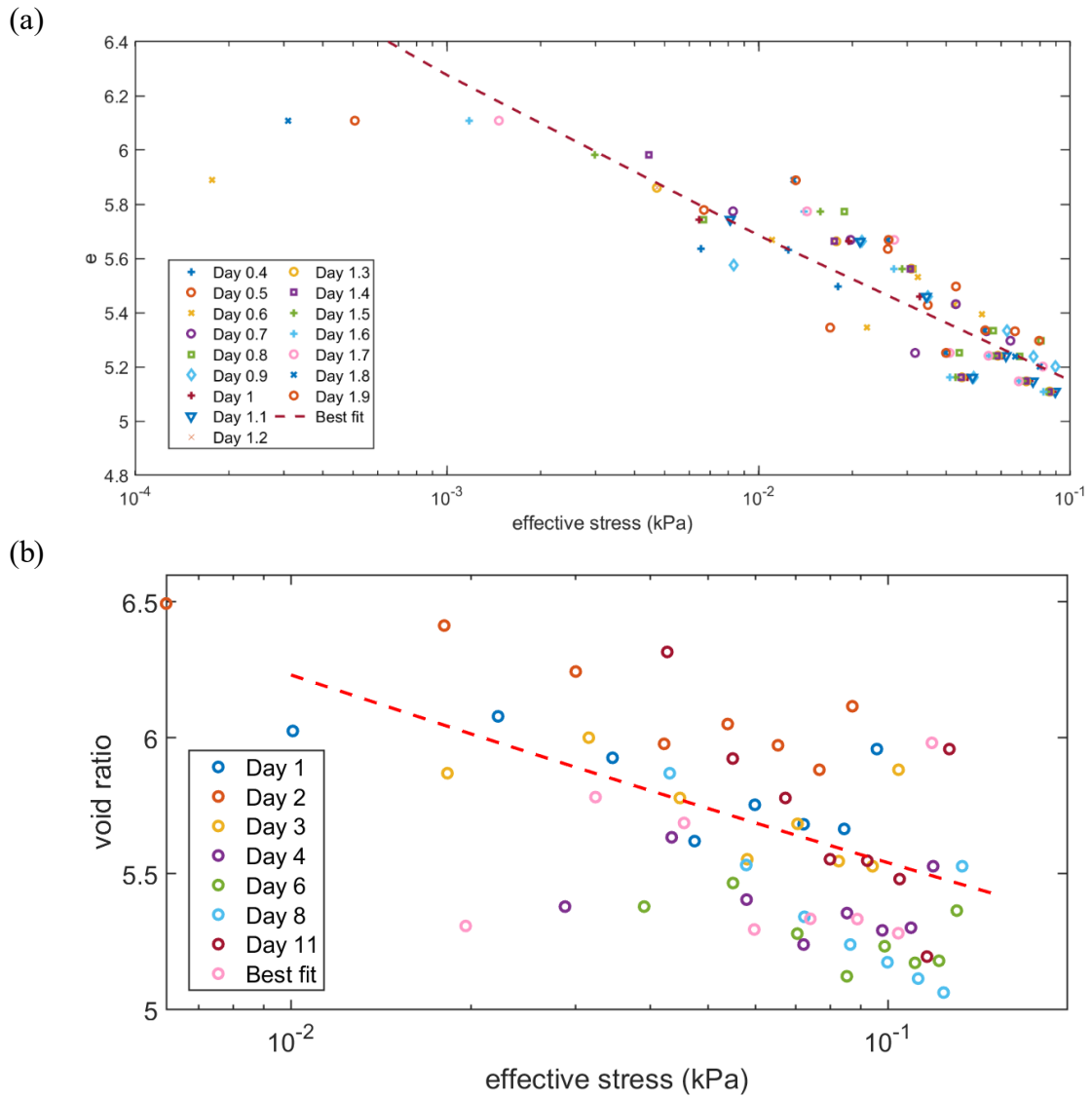


Figure 7-14: The compressibility curve for (a) First 2 days and (b) Until Day 11

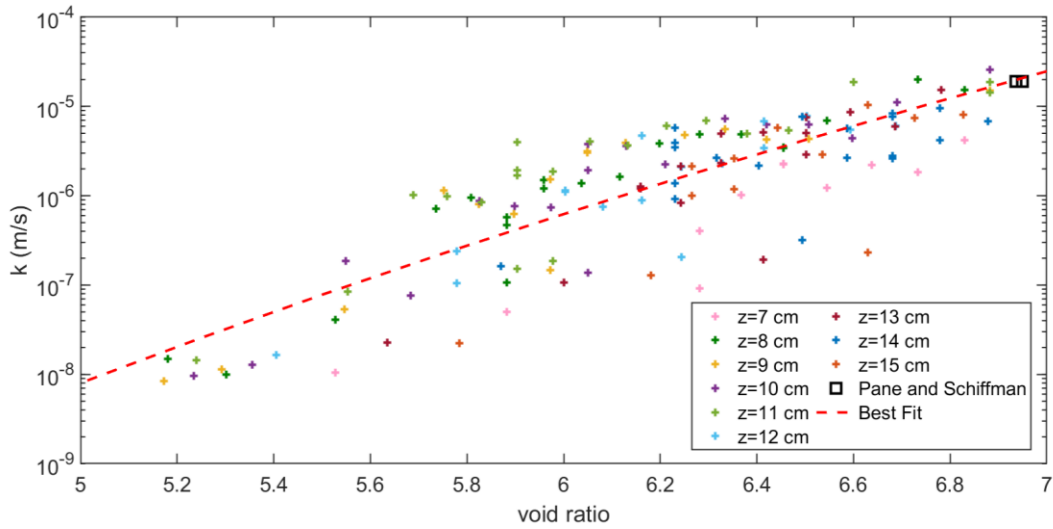


Figure 7-15: The k - e relationship for 4000 ppm fFFT tailings and comparison of with initial k - e data point (calculated using Pane and Schiffman’s equation)

The k - e equation is determined using the Instantaneous Profiling method (Equation 7.11). The transitional void ratio is defined as 5.5 (from fitting the compressibility curve), and this value is utilized in the sedimentation-consolidation model. The settlement behaviour agreed well with the measured data, which is presented in Figure 7-16. The final height from the consolidation model is overestimated, and the percentage error between the predicted and measured final height is calculated as 1.8%.

k - e relationship
$$k = 1.6 \times 10^{-25} e^{23.89} \quad (7.11)$$

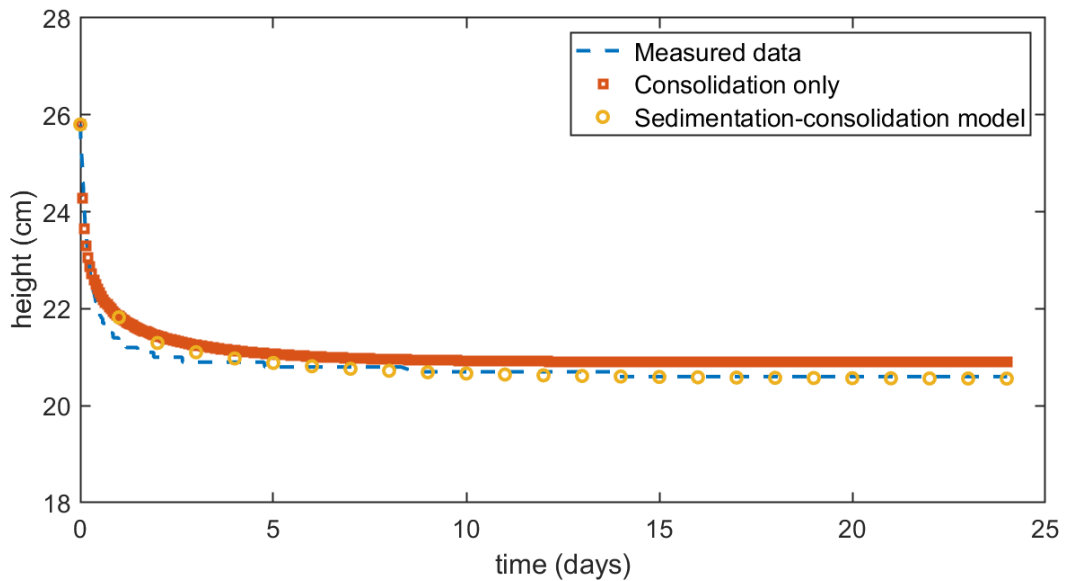


Figure 7-16: The settlement modelling comparison with measured data for 4000 ppm fFFT

7.6 Discussion

Resolution and accuracy of the IPM method

The resolution of the IPM method varies with soil type, and in terms of the soils and tailings tested, decreases with the following order:

Gold tailings (highest) – Kaolinite – B polymer FFT – 1000 ppm A3338 FFT -800 ppm A3338 FFT – raw FFT.

The decrease in resolution is primarily due to increasing scatter in the SENTEK EnviroSCAN water content measurements, which seem to increase with the timescale of the test. However, even so, the hydraulic conductivity of the test with the highest scatter (raw FFT) still compares well with independent measurements using a LSC, and furthermore, provides much richer data at higher void ratios. As shown by the comparisons of the model results using k - e functions from the LSC, or k - e function from IPM, the latter provides much closer fits to the observed settlement curves. This is important for practice,

as most dewatering in a tailings impoundment will occur where the dewatering is dominated by consolidation at relatively high void ratios. Therefore, even though the method shows considerable scatter in the $k-e$ data, the resolution and accuracy represent an important improvement in estimating the $k-e$ function for tailings and soft soils.

The observed shift in the compressibility functions

There are substantial shifts in the compressibility functions over time for the oil sands tailings tests, and perhaps also, but less remarkable, for the kaolinite samples. The shift in this function has been observed in other soft soils (G Bartholomeeusen et al., 2002; Hawlader et al., 2008). For the tests in this thesis, it was observed that a better-modelled fit to the settlement data was obtained when the best fit line through the shifting compressibility data was used, rather than when the final compressibility curve was obtained. This, however, for modelling purposes, is not precise, as there tends to be some inaccuracy in the prediction of final height. The shifting of the compressibility curve at these early times should be assessed using field size models to quantify its significance. There are also implications for methods to estimate the $k-e$ function that relies on the final compressibility curve.

Chapter 8: Discussion

This study developed methods to estimate or measure the $k-e$ relationship to rapidly assess the dewatering performance of new or potentially improved tailings technologies and create an alternative option to conventional consolidation tests. Figure 8-1 compares the developed methods with the conventional consolidation tests based on cost, availability of the setup and the duration of the experiment. The cost of the prototype design is significantly less (~\$20,000) compared to other methods, and as for duration, both methods can successfully determine the $k-e$ curve within weeks. The predictive model requires a single measured data point at a higher void ratio, which can be determined from a conventional test (hence the availability is high due to many options), but it would still take a few weeks to determine that data point.

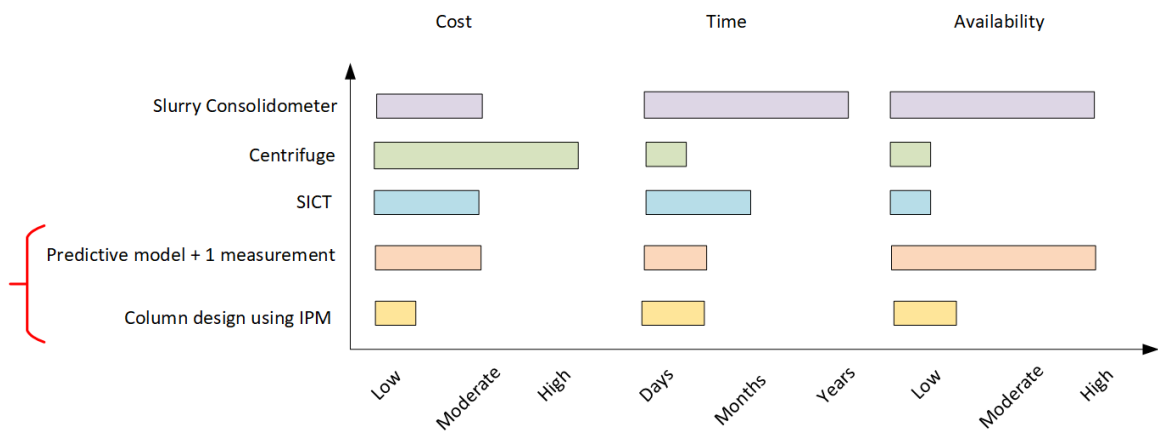


Figure 8-1: Comparison of conventional tests with developed methods in this study

8.1 When and how can practitioners use the different methods developed in this thesis?

To provide some guidance, $k-e$ functions for the flocculated fluid fine tailings (at 800 ppm dosage) measured by LSC and using the methods developed in this thesis are shown in

Figure 8-2 (a). Additionally, an estimate of $k-e$ directly from the settlement curve using the method of Qi et al. (2020) – this method, also developed in our research group, uses general characteristics of settlement data produced from consolidation simulations, which is then matched with measured settlement data to estimate a $k-e$ curve – an example calculation is provided in Appendix D for the reader’s interest.

The single measurement point methods both use the LSC data point at ~ 2 kPa, corresponding to a void ratio of 2.9. As expected, these provide a good comparison with the LSC data at lower void ratios but unpredict the $k-e$ values at higher void ratios. The IPM method provides a close agreement with the LSC data over its entire range but does not include void ratios less than 2.6 due to the limited development of effective stress in the column. For the “Qi” prediction, the agreement is good with IPM at the high range but poor at the low range. Indeed, it is probable that the “Qi” method can provide a better estimate of $k-e$ at the very highest void ratios, which the IPM method cannot resolve, as the second derivative is zero during the initial sedimentation phase in the column. However, the “Qi” method cannot accurately predict k values at lower void ratios. The drawback of the “Qi” method is the accuracy is restricted to void ratios measured at that specific column test.

Certainly, the differences between the estimated $k-e$ values matter, as shown in Figure 8-2 (b), which uses the $k-e$ data in a hypothetical analysis of a 20-m thick tailings deposit (with same initial conditions as 800 ppm test). The compressibility function used in these analyses are all the same; the in-situ compressibility curve determined from the 800 ppm test is utilized in the simulations. Since the long-term behaviour of fluid fine tailings is conventionally predicted using the $k-e$ curve determined from LSC tests, the

settlement modelled using the k - e functions from the different methods can be compared with the model result that uses the LSC data.

The settlement behaviour of the 1 point method is more conservative than the LSC test in the high void ratio range, but for this case, it is less conservative (predicts higher k values) at void ratios lower than the matching point. The discrepancy at the high void ratio range is expected and is similar to what is observed for comparisons with other tailings (such as the Eastpond ILTT comparison in Figure 4-8). The somewhat unconservative prediction of k values at the lower range is not generally seen in the other comparisons of this method with tailings LSC data (Figures 4-7 and Figures 4-8). For this case, however, predictions using the 1 point methods do show slightly faster dewatering at medium times (5 to 15 years) than predictions using the LSC data.

The IPM method delivers the closest settlement curve to the LSC derived settlement curve. However, both the IPM and Qi method predict faster settlement rates at earlier times, and given the comparisons with the real data presented in this thesis, these methods (Qi and IPM) provide better estimates to the true k - e function (due to higher measurement resolution) at higher void ratios. This may explain some informal observations reported to the author by industry, which suggests early-time dewatering is often faster than predicted by consolidation models using LSC measured k - e curves.

Therefore, complimentary use of the different methods is warranted. One such strategy might be:

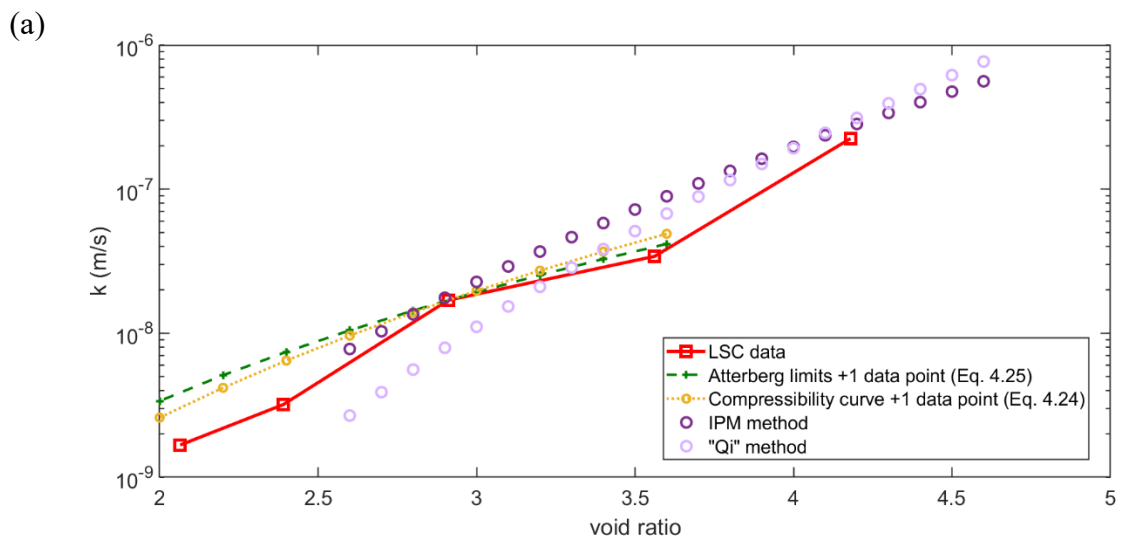
1. Perform a LSC test up to an effective stress between 1 and 2 kPa, but only measure the hydraulic conductivity at the last loading step. Up to the 1-2 kPa at stress level,

perform LSC tests as usual, i.e., avoiding excess heads gradient by loading steps as usual.

2. Use this data point to estimate the k - e curve at lower void ratios
3. Perform an instrumented column test similar to the one developed in this thesis. Ideally, the column should be similarly instrumented to allow for the IPM procedure.
4. Calculate k - e in the high void ratio ranges, using both IPM and the method of “Qi”. The method of “Qi” can be used to generate k values for those times early in the column experiment where the second derivative is zero or near zero.
5. Compile a composite data set using all the k - e data. Fit appropriately with a k - e function or multiple k - e functions or bounding k - e functions.

The performance of the composite material is compared with the LSC data, “Qi” method and other methods developed in this study which is presented in Figure 8.2

(b).



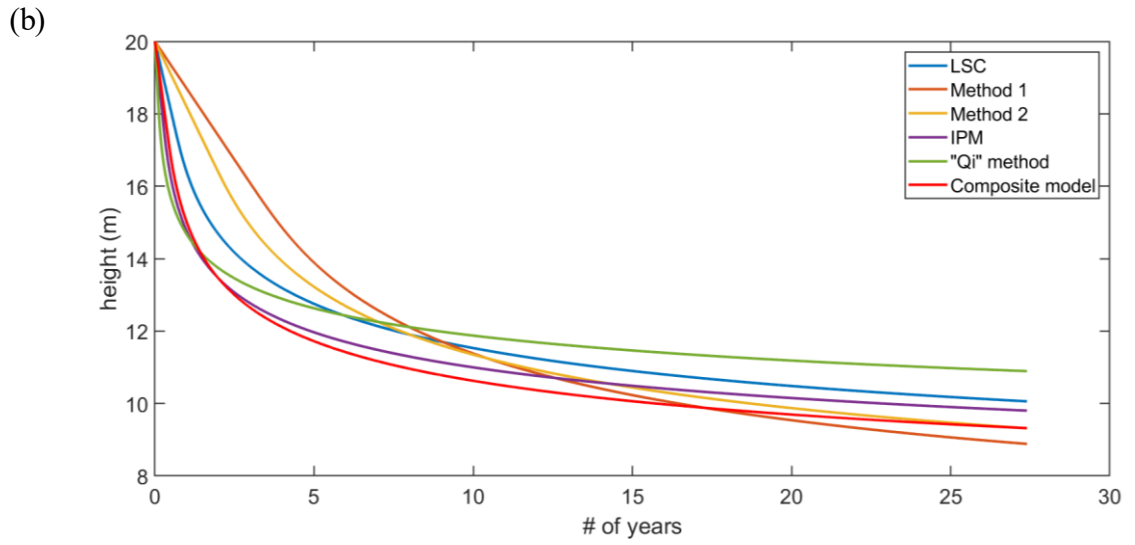


**Figure 8-2: (a) Comparison of all methods applying to flocculated FFT sample (at 800 ppm dosage),
 (b) Comparison of settlement performance of a hypothetical analysis**

Chapter 9: Summary and Conclusions

9.1 Summary

The toxic by-product of oil sands mining operations are known as the fluid fine tailings (FFT), composed of a mixture of bitumen, mineral content and water, discharged into containment areas or dedicated disposal areas. Upon deposition, the coarser fraction settles at the bottom, forming beaches and dykes, whereas the finer fraction, along with the residual bitumen, flows in the pond. This finer fraction has been observed to stabilize at high water contents (~30% solids content or 230% gravimetric water contents) and associated with poor consolidation properties such as having low hydraulic conductivity and high thixotropic strength. This finer fraction stays in its loose wet state even after decades and poses environmental risks. The disposal management of this material becomes a major challenge for the operators, and the assessment of consolidation properties becomes essential to satisfy environmental regulations.

Two major problems associated with these tailings dams are: the ponds occupy large extension of lands and the amount of water entrapped in the ponds, which cannot be reused. Therefore, the objective of using tailing treatments is to increase the settling rate to fasten the time for liquid-solid separation in the pond and to recover the maximum volume of water possible. Some of these dewatering technologies demonstrated promising results, but the innovations of these technologies are still progressing. Despite the advancements in dewatering technologies, it would still take a few decades for this material to reach that strength and to satisfy environmental regulations; hence the operators need to work towards this goal over the mine life.

Prior to the implementation of any new technology, it should be tested to discover the long-term performance of the tailings in the containment areas. Consolidation tests would determine the compressibility and hydraulic conductivity of the soils, which govern the consolidation behaviour of tailings. Consolidation properties, especially the hydraulic conductivity-void ratio relationship of FFTs, are highly variable, and the determination of this parameter can be very time-consuming or expensive as it might need a large number of field or laboratory tests. Currently, the most commonly used experimental methods include slurry consolidometers (it can take up to a year to determine the full $k-e$ curve), centrifuge tests (expensive to install and operate, also not commonly available in most of the research facilities and universities), and seepage induced tests. Each dewatering technology must be tested prior to application, and the duration of conventional tests slows down the progress in the industry.

Two separate studies were undertaken to develop methods to estimate or measure the hydraulic conductivity-void ratio curve to rapidly assess new or improved tailings treatment technologies. The first study focuses on establishing a relationship between the easily measured index properties, such as Atterberg limits or the grain size curves, etc., and the consolidation parameters of the oil sands tailings. All available compressibility and hydraulic conductivity correlations equations in the literature are collected and analyzed using a large data bank (over 100 data sets and 1700 data points). Based on the best-performed models, optimized $\sigma'-e$ and $k-e$ correlations are proposed. The conclusions from the first study can be summarized as:

- The equations provide reliable estimations for lower ranges of void ratios, but they failed at the higher ranges

- The application of these optimized models would not be sufficient for preliminary design for many applications
- Instead of relying on index properties, usage of the compressibility curves was investigated. There was a discernable improvement demonstrated with the new correlations
- The most advancement was recorded when a single measured data point is included in the assessment. The previous efforts were usually unsuccessful at estimating the long-term consolidation behaviour of the FFTs at the higher void ratios. However, the use of compressibility curves along with the single measured data (at effective stresses between 1-2 kPa) substantially improved the estimated $k-e$ curves for the fine-grained soils

The second study focused on designing an experimental setup to evaluate the $k-e$ relationship using the Instantaneous Profiling method (IPM) under self-weight consolidation of fine-grained soils. IPM is capable of determining the macroscopic flow velocity from the column profiles of potential gradients and water contents. For the reliable application of this model, high-resolution measurement profiles are required for soft soils. In order to achieve this, multiple numbers of sensors needed to be inserted into the column. However, stacking up sensors on the column walls will affect the consolidation behaviour of the materials and measured data may not be too reliable. For that reason, non-destructive volumetric water content sensors are investigated. Initially, electrical conductivity sensors are examined as they are capable of calculating 3D profiles of water content measurements using the electrical resistivity tomography method. However, the results demonstrated that this method would become problematic for long-duration experiments as the fine

negatively charged particles in the tailings accumulate on the positively charged sensor rods continuously. SENTEK EnviroSCAN sensors are then considered, and they are tested for various fine-grained soils, including Leda clay, thickened gold tailings and centrifuged cake, and these sensors proved prosperous results. The experimental setup is improved by implementing an automation system to provide vertical movement to the SANTEK sensors for more detailed profiling in the column.

The applicability of the IPM method to estimate the $k-e$ relationship for soft soils with low initial solids content is then investigated. Initially, the method is applied to a case study published in the literature, and the determined $k-e$ equation was similar to the other predictions. However, it also confirmed that high-resolution profiling in the column is necessary; hence several experimental tests with different fine-grained soils were carried out in the laboratory; such as thickened gold tailings, Kaolinite, unamended FFT sample, as well as amended FFT soils using different polymers and dosages. The results are then compared with independently measured $k-e$ curves (measured using slurry consolidometer at the University of Alberta for the Shell FFT - unamended and 800 ppm dosage samples, $k-e$ curves for the gold tailings determined in another study, and kaolinite $k-e$ curves obtained from the literature). The observations from the second study are:

- The results from the IPM method compare well with independent estimates of $k-e$, or produce reasonable predictions of consolidation in the columns when used in a large strain consolidation model
- Additionally, the higher density of data provides more information on the $k-e$ curve at higher void ratios, the region most susceptible to variability

- As predictions of consolidation are strongly sensitive to k values in the higher void ratio range, the increased accuracy of the IPM method can provide improved predictions of consolidation, even at the current resolution of the data provided by IPM
- The k values from IPM, however, are noisy, and future work should focus on reducing this noise
- Complimentary use of IPM and other “cheap” methods (the single point methods and methods of Qi and Simms (2020) and Qi et al.(2020)) can result in an estimate of $k-e$ comparable in accuracy to those of the LSC test.
- Shifting of the compressibility function occurs in all the FFT experiments. This is similar to what is observed in other soft clayey soils (Barth. et al. 2002).

9.2 Novelty and Impact

The methods developed in this thesis can help the industry by speeding the progress of trying new or improved tailings treatment technologies, and aside from applied contributions, it also has scientific contributions. This study demonstrates the application of the Instantaneous Profiling Method’s to large strain conditions, approving its capability with the use of the newly developed experimental setup. The database collected in the first study, along with the detailed profiles from the second part of this thesis, could provide data for other researchers in the future.

9.3 Limitations

Both methods have advantages and limitations associated with them. The results from the first study demonstrated that realistic predictions could be achieved with the use of a

compressibility curve along with a single measured data to estimate $k-e$. However, the compressibility curve still needed to be measured or estimated, and it would still take few weeks to determine the single k data point at higher void ratios.

The second study utilizes the designed consolidometer to apply the IPM method, which is capable of determining the $k-e$ relationship accurately at higher void ratios. However, the self-weight consolidation of FFT is very slow, and the duration of these tests can still take few weeks to determine this curve. The noise from the water content sensors is another challenge that needs to be focused on as it can affect the hydraulic conductivity values determined by the IPM method. Though the resolution is sufficient to produce data that compares well to other methods, the accuracy can still certainly be improved in future.

9.4 Future Recommendations

Two recommendations can be provided for future work regarding the consolidometer, i) further reducing the duration of testing and ii) eliminating the noise from the water content sensors.

- While the $k-e$ relationships can be determined rapidly and accurately using the prototype consolidometer (compared to some of the available LSC tests), the duration of the experiment can be further decreased with the following techniques:
 - a. By allowing two-way drainage: The current setup uses a one-way drainage boundary condition (from the top), but the design can be upgraded and tested for an open boundary condition at the bottom as well. The two-way drainage might affect the flocculation process of amended FFTs at the beginning of the experiment; hence, the bottom boundary should be closed for a certain amount of time (~6-7

days) until the material stabilizes. Once it is open, to ensure drainage at the bottom is continuous, it should be kept saturated during the experiment, and the level of water can be monitored.

- b. By applying loads on top: Another upgrade that can be implemented in the column is applying loads on top of the sample to speed up the dewatering process. To achieve this, water above the mudline will be collected once the material gains some strength, and the load will be applied accordingly.
- Another further recommendation eliminating noise from the water content sensors (w) needs more attention; the source in the noise of dw will need further evaluation (i.e., temperature fluctuations).

Bibliography

- Abdulrahman, A. A. H. (2019). *Load Transfer and Creep Behavior of Pile Foundations in Frozen Soils*. Carleton University.
- Aboshi, H., Yoshikuni, H., & Maruyama, S. (1970). Constant loading rate consolidation test. *Soils and Foundations*, 10(1), 43-56.
- Abu-Hejleh, A., & Znidarcic, D. (1992). User manual for computer program SICTA. *Rep. Prepared for FIPR, 2*.
- Abu-Hejleh, A. N., & Znidarčić, D. (1995). Desiccation theory for soft cohesive soils. *Journal of Geotechnical Engineering*, 121(6), 493-502.
- Abu-Hejleh, A. N., Znidarcic, D., & Barnes, B. L. (1996). Consolidation characteristics of phosphatic clays. *Journal of Geotechnical Engineering*, 122(4), 295-301.
- Abu-Hejleh, N. A., & Znidarcic, D. (1994). *Estimation of the consolidation constitutive relations*. Paper presented at the International conference on computer methods and advances in geomechanics.
- AER. (2017). *Directive 085 - Fluid Tailings Management for Oil Sands Mining Projects*. Retrieved from
- AER. (2019a). *Alberta Energy Outlook*. Retrieved from
- AER. (2019b). *State of Fluid Tailings Management for Mineable Oil Sands*. Retrieved from Calgary, AB:
- Ahmed, S. I., & Siddiqua, S. (2014). A review on consolidation behavior of tailings. *International Journal of Geotechnical Engineering*, 8(1), 102-111.
- Aiban, S., & Znidarčić, D. (1989). Evaluation of the flow pump and constant head techniques for permeability measurements. *Geotechnique*, 39(4), 655-666.

- Aldaef, A., & Rayhani, M. T. (2015). Hydraulic performance of compacted clay liners under simulated daily thermal cycles. *Journal of environmental management*, 162, 171-178.
- Aldaef, A., & Simms, P. (2019). *Influence of pipeline transport on sedimentation and consolidation of flocculated fluid fine tailings* Paper presented at the Geo St.John's - 72nd Canadian Geotechnical Conference, St. John, NL Canada.
- Alessi, R., & Prunty, L. (1986). Soil-water Determination Using Fiber Optics 1. *Soil Science Society of America Journal*, 50(4), 860-863.
- Amoako, K. A., Abdulnabi, A., Beier, N. A., Soares, J., & Simms, P. H. (2020). Long-term Consolidation of Two New Polymer Treatments of Oil Sands Fluid Fine Tailings.
- Amoozegar, A., Martin, K., & Hoover, M. (1989). Effect of access hole properties on soil water content determination by neutron thermalization. *Soil Science Society of America Journal*, 53(2), 330-335.
- Arulanandan, K. (1991). Dielectric method for prediction of porosity of saturated soil. *Journal of Geotechnical Engineering*, 117(2), 319-330.
- Askarinejad, A., Beck, A., Casini, F., & Springman, S. M. (2012). Unsaturated hydraulic conductivity of a silty sand with the instantaneous profile method *Unsaturated Soils: Research and Applications* (pp. 215-220): Springer.
- Azam, S. (2010). Large strain settling behavior of polymer-amended laterite slurries. *International Journal of Geomechanics*, 11(2), 105-112.
doi:10.1061/(ASCE)GM.1943-5622.0000031

- Azam, S., & Scott, J. D. (2005). Revisiting the ternary diagram for tailings characterization and management. *GEOTECHNICAL NEWS-VANCOUVER*-, 23(4), 43.
- Babaoglu, Y., & Simms, P. (2020). Improving Hydraulic Conductivity Estimation for Soft Clayey Soils, Sediments, or Tailings Using Predictors Measured at High-Void Ratio. *Journal of geotechnical and geoenvironmental engineering*, 146(10), 06020016.
- Bajwa, T. M. (2015). *Microstructure and macroscopic behaviour of polymer amended oil sands mature fine tailings*. Carleton University, Ottawa, ON.
- Banas, L. (1991). *Thixotropic Behaviour of oil sands tailings sludge*, MS. c. Thesis, University of Alberta, Edmonton, Canada.
- Barbetti, L. (2009). *Determination of consolidation parameters of a sludge using the 'Seepage Induced Consolidation Test'*. Paper presented at the 4th International Young Geotechnical Engineers' Conference (4-iYGEC'09).
- Bartholomeeusen, G. (2003). *Compound shock waves and creep behaviour in sediment beds*. Oxford University, UK.
- Bartholomeeusen, G., Sills, G., Znidarčić, D., Van Kesteren, W., Merckelbach, L., Pyke, R., . . . Winterwerp, H. (2002). Sidere: numerical prediction of large-strain consolidation. *Geotechnique*, 52(9), 639-648.
- Baxter, C. D. P. (1994). Gradient effects on measured hydraulic conductivity. *MSCE thesis, School of Civ. Engrg., Purdue Univ., West Lafayette, Ind.*
- Been, K. (1980). Stress strain behaviour of a cohesive soil deposited under water.

- Been, K., & Sills, G. (1981). Self-weight consolidation of soft soils: an experimental and theoretical study. *Geotechnique*, 31(4), 519-535.
- Beier, N., Alostaz, M., & Segó, D. (2009). *Natural dewatering strategies for oil sands fine tailings*. Paper presented at the Proceedings of the 13th Annual Conference on Tailings and Mine Waste.
- Beier, N., Wilson, W., Dunmola, A., & Segó, D. (2013). Impact of flocculation-based dewatering on the shear strength of oil sands fine tailings. *Canadian Geotechnical Journal*, 50(9), 1001-1007.
- Beier, N. A. (2015). Development of a Tailings Management Simulation and Technology Evaluation Tool. doi:10.7939/R3FT8DS9T
- Berilgen, S., Berilgen, M., & Ozaydin, I. (2006). Compression and permeability relationships in high water content clays. *Applied Clay Science*, 31(3), 249-261. doi:10.1016/j.clay.2005.08.002
- Beriswill, J., Bloomquist, D., & Townsend, F. (1989). Reclamation of Phosphatic Clay Waste Ponds by 'Capping'.
- Berry, P., & Poshitt, T. (1972). The consolidation of peat. *Geotechnique*, 22(1).
- BGC Engineering, B. E. (2010). *Oil Sands Tailings Technology Review*. Retrieved from Edmonton, AB:
- Bjerrum, L. (1967). Progressive failure in slopes of overconsolidated plastic clay and clay shales. *Journal of Soil Mechanics & Foundations Div.*
- Bloomquist, D., & Townsend, F. (1984). *Centrifugal modeling of phosphatic clay consolidation*. Paper presented at the Sedimentation Consolidation Models—Predictions and Validation.

- Bonin, M. D., Nuth, M., Dagenais, A.-M., & Cabral, A. R. (2014). Experimental study and numerical reproduction of self-weight consolidation behavior of thickened tailings. *Journal of geotechnical and geoenvironmental engineering*, 140(12), 04014068.
- Bromwell, L. G. (1984). *Consolidation of mining wastes*. Paper presented at the Sedimentation Consolidation Models—Predictions and Validation.
- Bromwell, L. G., & Carrier III, W. (1979). *Consolidation of fine-grained mining wastes*. Paper presented at the Proceedings of the Sixth Pan American Conference on Soil Mechanics and Foundation Engineering, Lima, Peru.
- Bürger, R., Damasceno, J. J., & Karlsen, K. H. (2004). A mathematical model for batch and continuous thickening of flocculated suspensions in vessels with varying cross-section. *International Journal of Mineral Processing*, 73(2), 183-208.
- Burland, J. (1990). On the compressibility and shear strength of natural clays. *Geotechnique*, 40(3), 329-378. doi:10.1680/geot.1990.40.3.329
- Campbell, J. E. (1990). Dielectric properties and influence of conductivity in soils at one to fifty megahertz. *Soil Science Society of America Journal*, 54(2), 332-341.
- Cargill, K. W. (1984). Prediction of consolidation of very soft soil. *Journal of Geotechnical Engineering*, 110(6), 775-795.
- Cargill, K. W. (1985). *Mathematical model of the consolidation/desiccation processes in dredged material*: US Army Engineer Waterways Experiment Station.
- Cargill, K. W. (1986). *The large strain, controlled rate of strain (LSCRS) device for consolidation testing of soft fine-grained soils*. Retrieved from

- Carman, P. C. (1939). Permeability of saturated sands, soils and clays. *The Journal of Agricultural Science*, 29(02), 262-273.
- Carrier III, W. D., Bromwell, L. G., & Somogyi, F. (1983). Design capacity of slurried mineral waste ponds. *Journal of Geotechnical Engineering*, 109(5), 699-716. doi:10.1061/(ASCE)0733-9410(1983)109:5(699)
- Carrier, W., & Beckman, J. (1984). Correlations between index tests and the properties of remoulded clays. *Geotechnique*, 34(2), 211-228. doi:10.1680/geot.1984.34.2.211
- Casagrande, A. (1938). *Notes on soil mechanics: First Semester*. Harvard University.
- Caughill, D. L., Morgenstern, N., & Scott, J. (1993). Geotechnics of nonsegregating oil sand tailings. *Canadian Geotechnical Journal*, 30(5), 801-811. doi:10.1139/t93-071
- Chalaturnyk, R., Scott, J., & Özüim, B. (2004). Oil sands tailings production for environmental disposal *Mining Science and Technology* (pp. 615-620): CRC Press.
- Chalaturnyk, R. J., Don Scott, J., & Özüim, B. (2002). Management of oil sands tailings. *Petroleum Science and Technology*, 20(9-10), 1025-1046.
- Chandra Paul, A., & Azam, S. (2013). Assessment of slurry consolidation using index properties. *International Journal of Geotechnical Engineering*, 7(1), 55-61. doi:10.1179/1938636212Z.0000000005
- Chapuis, R. P. (2012). Predicting the saturated hydraulic conductivity of soils: a review. *Bulletin of engineering geology and the environment*, 71(3), 401-434.

- Chapuis, R. P., & Aubertin, M. (2003a). On the use of the Kozeny Carman equation to predict the hydraulic conductivity of soils. *Canadian Geotechnical Journal*, 40(3), 616-628. doi:10.1139/T03-013
- Chapuis, R. P., & Aubertin, M. (2003b). *Predicting the coefficient of permeability of soils using the Kozeny-Carman equation*: École polytechnique de Montréal.
- Chow, H., & Pham, A. L.-T. (2019). Effective removal of silica and sulfide from oil sands thermal in-situ produced water by electrocoagulation. *Journal of hazardous materials*, 380, 120880.
- Crawford, C., & Bozozuk, M. (1990). Thirty years of secondary consolidation in sensitive marine clay. *Canadian Geotechnical Journal*, 27(3), 315-319.
- Crawford, C. B. (1964). Interpretation of the consolidation test. *Journal of Soil Mechanics & Foundations Div*, 90(Proceeding Paper Pt 1).
- Crawford, C. B. (1968). Quick clays of eastern Canada. *Engineering Geology*, 2(4), 239-265.
- Croce, P., Pane, V., Znidarcic, D., Ko, H., Olsen, H., & Schiffman, R. (1985). Evaluation of consolidation theories by centrifuge modelling. *Publication of: Balkema (AA)*.
- Cymerman, G., Kwong, T., Lord, E., Hamza, H., & Xu, Y. (1999). Thickening and disposal of fine tails from oil sand processing. *The 3rd UBC-McGill Int. Sym. Fund. of Mineral Processing (CIM), Quebec City QC*.
- Das, B. M. (2013). *Advanced soil mechanics*: Crc Press.
- Davis, E., & Raymond, G. (1965). A non-linear theory of consolidation. *Geotechnique*, 15(2), 161-173.

- Delage, P. (2010). A microstructure approach to the sensitivity and compressibility of some Eastern Canada sensitive clays. *Geotechnique*, 60(5), 353.
- Demoz, A., & Mikula, R. J. (2011). Role of mixing energy in the flocculation of mature fine tailings. *Journal of Environmental Engineering*, 138(1), 129-136. doi:10.1061/(ASCE)EE.1943-7870.0000457
- Dikinya, O. (2005). Comparison of the Instantaneous Profile Method and inverse modelling for the prediction of effective soil hydraulic properties. *Soil Research*, 43(5), 599-606.
- Dolinar, B. (2009). Predicting the hydraulic conductivity of saturated clays using plasticity-value correlations. *Applied Clay Science*, 45(1), 90-94. doi:10.1016/j.clay.2009.04.001
- Donahue, R., Segó, D., Burke, B., Krahn, A., Kung, J., & Islam, N. (2008). *Impact of ion exchange properties on the sedimentation properties of oil sands mature fine tailings and synthetic clay slurries*. Paper presented at the Proceedings of the First International Oil Sands Tailings Conference, Edmonton, AB, Canada.
- Edil, T. B., & Fox, P. J. (2000). *Geotechnics of high water content materials*: ASTM West Conshohocken, PA.
- Elder, A., & Rasmussen, T. C. (1994). Neutron probe calibration in unsaturated tuff. *Soil Science Society of America Journal*, 58(5), 1301-1307.
- Elder, D. M. (1985). Stress strain and strength behaviour of very soft soil sediment.
- Energy, A. (2017). Oil Sands - Facts and Stats.
- Estepho, M. (2014). *Seepage induced consolidation test: characterization of mature fine tailings*. University of British Columbia.

- Farkish, A., & Fall, M. (2013). Rapid dewatering of oil sand mature fine tailings using super absorbent polymer (SAP). *Minerals Engineering*, 50, 38-47.
doi:10.1016/j.mineng.2013.06.002
- Fatahi, B., Le, T. M., Le, M. Q., & Khabbaz, H. (2013). Soil creep effects on ground lateral deformation and pore water pressure under embankments. *Geomechanics and Geoengineering*, 8(2), 107-124.
- Feng, T.-W. (2000). Fall-cone penetration and water content relationship of clays. *Geotechnique*, 50(2), 181-187.
- Feng, T.-W. (2001). A linear log d log w model for the determination of consistency limits of soils. *Canadian Geotechnical Journal*, 38(6), 1335-1342.
- Fine Tailings Fundamentals Consortium, F. (1995). Advances in oil sands tailings research. *Alberta, Canada: Alberta Dept. of Energy, Oil Sands and Research Division*.
- Fisher, R. A., Williams, M., de Lourdes Ruivo, M., de Costa, A. L., & Meir, P. (2008). Evaluating climatic and soil water controls on evapotranspiration at two Amazonian rainforest sites. *agricultural and forest meteorology*, 148(6-7), 850-861.
- Fox, P. J., & Baxter, C. D. (1997). Consolidation properties of soil slurries from hydraulic consolidation test. *Journal of geotechnical and geoenvironmental engineering*, 123(8), 770-776.
- Fox, P. J., & Berles, J. D. (1997). CS2: a piecewise-linear model for large strain consolidation. *International Journal for Numerical and Analytical Methods in Geomechanics*, 21(7), 453-475.

- Fredlund, M., Donaldson, M., & Gitirana, G. (2009). *Large-Strain 1D, 2D, and 3D Consolidation Modeling of Mine Tailings*. Paper presented at the Proceedings of the Tailings and Mine Waste Conference.
- Gardner, C., Dean, T., & Cooper, J. (1998). Soil water content measurement with a high-frequency capacitance sensor. *Journal of agricultural engineering research*, 71(4), 395-403.
- Gaskin, G., & Miller, J. (1996). Measurement of soil water content using a simplified impedance measuring technique. *Journal of agricultural engineering research*, 63(2), 153-159.
- Gheisari, N., Salam, M., Qi, S., & Simms, P. (2019). *Structuration in natural clays, dredged sediments, and oil sands tailings*. Paper presented at the 72nd Canadian Geotechnical Conference, St. John, NL.
- Gholami, M. (2014). *Shear behaviour of oil sand fine tailings in simple shear and triaxial devices*. Carleton University.
- Gibson, R., England, G., & Hussey, M. (1967). The Theory of One-Dimensional Consolidation of Saturated Clays: 1. Finite Non-Linear Consolidation of Thin Homogeneous Layers. *Geotechnique*, 17(3), 261-273.
- Gibson, R. E., Schiffman, R. L., & Cargill, K. W. (1981). The theory of one-dimensional consolidation of saturated clays. II. Finite nonlinear consolidation of thick homogeneous layers. *Canadian Geotechnical Journal*, 18(2), 280-293.
- Giesel, W., Lorch, S., Renger, M., & Strebel, O. (1970). Water flow calculations by means of gamma absorption and tensiometer field measurements in the unsaturated soil profile. *Isotope Hydrology*, 663-672.

- Hamilton, J., & Crawford, C. (1960). *Improved determination of preconsolidation pressure of a sensitive clay*. Paper presented at the Papers on Soils 1959 Meetings.
- Hansbo, S. (1960). *Consolidation of clay, with special reference to influence of vertical sand drains*. Retrieved from
- Hawlder, B., Muhunthan, B., & Imai, G. (2008). State-dependent constitutive model and numerical solution of self-weight consolidation. *Geotechnique*, 58(2), 133-141.
- Hilhorst, M. (2000). A pore water conductivity sensor. *Soil Science Society of America Journal*, 64(6), 1922-1925.
- Hillel, D., & Gardner, W. (1970). Measurement of Unsaturated Conductivity and Diffusivity by Infiltration Through AN Impeding Layer. *Soil Science*, 109(3), 149-153.
- Holdich, R., & Butt, G. (1997). Solid/liquid separation by sedimentation. *Proceedings of the Institution of Mechanical Engineers, Part E: Journal of Process Mechanical Engineering*, 211(1), 43-52.
- Hsu, T.-W., & Lu, S.-C. (2006). Behavior of one-dimensional consolidation under time-dependent loading. *Journal of Engineering Mechanics*, 132(4), 457-462.
- Huerta, A., Kriegsmann, G. A., & Krizek, R. J. (1988). Permeability and compressibility of slurries from seepage-induced consolidation. *Journal of Geotechnical Engineering*, 114(5), 614-627.
- Huerta, A., & Rodriguez, A. (1992). Numerical analysis of non-linear large-strain consolidation and filling. *Computers & structures*, 44(1-2), 357-365.
- Hurley, S. J. (1999). *Development of a settling column and associated primary consolidation monitoring systems for use in the geotechnical centrifuge:*

- investigation of geotechnical-geophysical correlations*. Memorial University of Newfoundland.
- Hurtado, O. R. (2018). *Desiccation and Consolidation in Centrifuge Cake Oil Sands Tailings*. Carleton University.
- Imai, G. (1979). Development of a new consolidation test procedure using seepage force. *Soils and Foundations*, 19(3), 45-60.
- Imai, G. (1981). Experimental studies on sedimentation mechanism and sediment formation of clay materials. *Soils and Foundations*, 21(1), 7-20.
- Imai, G., & Tang, Y. (1992). A constitutive equation of one-dimensional consolidation derived from inter-connected tests. *Soils and Foundations*, 32((2)), 83-96.
- Islam, N. (2008). *The role of cation exchange on the sedimentation behavior of oil sands tailings*. Retrieved from Edmonton, AB:
- Jacobsen, O. H., & Schjønning, P. (1993). A laboratory calibration of time domain reflectometry for soil water measurement including effects of bulk density and texture. *Journal of Hydrology*, 151(2-4), 147-157.
- Janbaz, M. (2016). *Consolidation characteristics of soft sediments by seepage induced consolidation test*. Rutgers University-Graduate School-New Brunswick.
- Janbu, N., Tokheim, O., & Senneset, K. (1981). *Consolidation tests with continuous loading*. Paper presented at the Proc. 10th Int. Conf. Soil Mech. and Foundation Engineering, Stockholm.
- Jarvis, N., & Leeds-Harrison, P. (1987). Some problems associated with the use of the neutron probe in swelling/shrinkling clay soils. *Journal of Soil Science*, 38(1), 149-156.

- Jeeravipoolvarn, S. (2005). *Compression behaviour of thixotropic oil sands tailings*. University of Alberta.
- Jeeravipoolvarn, S. (2010). *Geotechnical behavior of in-line thickened oil sands tailings*. (Doctor of Philosophy), University of Alberta.
- Jeeravipoolvarn, S., Chalaturnyk, R., & Scott, J. (2008). *Consolidation modeling of oil sands fine tailings: History matching*. Paper presented at the Proceedings of 61st Canadian Geotechnical Conference, Edmonton, AB, September.
- Jeeravipoolvarn, S., Chalaturnyk, R., & Scott, J. (2009). Sedimentation–consolidation modeling with an interaction coefficient. *Computers and Geotechnics*, 36(5), 751-761.
- Kaleita, A. L., Tian, L. F., & Hirschi, M. C. (2005). Relationship between soil moisture content and soil surface reflectance. *Transactions of the ASAE*, 48(5), 1979-1986.
- Kam, S., Girard, J., Hmidi, N., Mao, Y., & Longo, S. (2011). *Thickened tailings disposal at Musselwhite Mine*. Paper presented at the Proceedings of the 14th International Seminar on Paste and Thickened Tailings.
- Kaminsky, H. (2014). *Demystifying the methylene blue index*. Paper presented at the 4th International Oil Sands Tailings Conference.
- Khan, F. S., & Azam, S. (2016). Determination of consolidation behaviour of clay slurries. *International Journal of Mining Science and Technology*, 26(2), 277-283. doi:10.1016/j.ijmst.2015.12.014
- Klute, A. (1972). The determination of the hydraulic conductivity and diffusivity of unsaturated soils¹. *Soil Science*, 113(4), 264-276.

- Klute, A., & Dirksen, C. (1986). Hydraulic conductivity and diffusivity: Laboratory methods. *Methods of Soil Analysis: Part 1 Physical and Mineralogical Methods*, 5, 687-734.
- Koppula, S., & Morgenstern, N. (1982). On the consolidation of sedimenting clays. *Canadian Geotechnical Journal*, 19(3), 260-268.
- Koppula, S. D. (1970). *Consolidation of Soil in Two Dimensions and Moving Boundaries*. Univ Alberta.
- Krizek, R. J., & Somogyi, F. (1984). *Perspectives on modelling consolidation of dredged materials*. Paper presented at the Sedimentation Consolidation Models—Predictions and Validation.
- Kupfer, K., Trinks, E., Wagner, N., & Hübner, C. (2007). TDR measurements and simulations in high lossy bentonite materials. *Measurement Science and Technology*, 18(4), 1118.
- Kynch, G. J. (1952). A theory of sedimentation. *Transactions of the Faraday society*, 48, 166-176.
- Langseth, J., Luger, D., Jacobs, W., Sisson, R., Sittoni, L., Hedblom, E., & Greenleaf, T. (2015). *Placement of caps on soft and fluid tailings*. Paper presented at the Tailings and Mine Waste, Vancouver.
- Lee, K. (1981). Consolidation with constant rate of deformation. *Geotechnique*, 31(2), 215-229.
- Lee, K., & Sills, G. (1979). *A moving boundary approach to large strain consolidation of a thin soil layer*. Paper presented at the Proc., 3rd Int. Conf. on Numerical Methods in Geomechanics.

- Leonards, G. A., & Deschamps, R. J. (1995). *Origin and significance of the quasi-preconsolidation pressure in clay soils*. Paper presented at the Proceedings of International Symposium on Compression and Consolidation of Clayey Soils-IS-Hiroshima., Rotterdam.
- Leroueil, S., & Vaughan, P. (2009). The general and congruent effects of structure in natural soils and weak rocks *Selected papers on geotechnical engineering by PR Vaughan* (pp. 235-256): Thomas Telford Publishing.
- Leung, A. K., Coo, J. L., Ng, C. W. W., & Chen, R. (2016). New transient method for determining soil hydraulic conductivity function. *Canadian Geotechnical Journal*, 53(8), 1332-1345.
- Li, M.-G., Chen, J.-J., & Wang, J.-H. (2017). Arching effect on lateral pressure of confined granular material: numerical and theoretical analysis. *Granular Matter*, 19(2), 20.
- Li, Z., Lin, W., Ye, J., Chen, Y., Bian, X., & Gao, F. (2021). Soil movement mechanism associated with arching effect in a multi-strutted excavation in soft clay. *Tunnelling and Underground Space Technology*, 110, 103816.
- Liu, J.-C., & Znidarčić, D. (1991). Modeling one-dimensional compression characteristics of soils. *Journal of Geotechnical Engineering*, 117(1), 162-169.
- Liu, M., & Carter, J. (1999). Virgin compression of structured soils. *Geotechnique*, 49(1), 43-57.
- Locat, J., & Lefebvre, G. (1986). The origin of structuration of the Grande-Baleine marine sediments, Québec, Canada. *Quarterly Journal of Engineering Geology and Hydrogeology*, 19(4), 365-374.

- Lothian, N. (2017). Fifty years of oilsands equals only 0.1% of land reclaimed.
- Lowe, J., Jonas, E., & Obrican, V. (1969). Controlled gradient consolidation test. *Journal of Soil Mechanics & Foundations Div*, 92(SM5, Proc Paper 490).
- MacDonald, J. R. (1987). Impedence Spectroscopy--Emphasizing Solid Materials and Systems. *Wiley-Interscience, John Wiley and Sons*, 1-346.
- Marcus, O. P., Tijseen, M., & Winkelman, M. O. (2017). *APPLYING PROVEN DREDGE DESIGNS IN A NON-STANDARD SITUATION; THE OIL SANDS*. Paper presented at the Dredging Summit & Expo, Vancouver, B.C.
- Markgraf, W. (2006). *Microstructural changes in soils: rheological investigations in soil mechanics*.
- Markgraf, W., Horn, R., & Peth, S. (2006). An approach to rheometry in soil mechanics—structural changes in bentonite, clayey and silty soils. *Soil and Tillage Research*, 91(1-2), 1-14.
- Marshall, T. (1958). A relation between permeability and size distribution of pores. *Journal of Soil Science*, 9(1), 1-8. doi:10.1111/j.1365-2389.1958.tb01892.x
- Masala, S. (1998). *Numerical Solution of sedimentation and consolidation of fine tailings*. MSc Thesis, University of Alberta, Edmonton, AB.
- Mayne, P. W., Cargill, E., & Miller, B. (2019). Geotechnical characteristics of sensitive Leda clay at Canada test site in Gloucester, Ontario. *AIMS Geosci*, 5, 390-411.
- Mbonimpa, M., Aubertin, M., Chapuis, R., & Bussière, B. (2002). Practical pedotransfer functions for estimating the saturated hydraulic conductivity. *Geotechnical & Geological Engineering*, 20(3), 235-259.
- McEachern, P. (2009). Environmental management of Alberta's oil sands.

- McRoberts, E., & Nixon, J. (1976). A theory of soil sedimentation. *Canadian Geotechnical Journal*, 13(3), 294-310. doi:10.1139/t76-031
- McVay, M., Townsend, F., & Bloomquist, D. (1986). Quiescent consolidation of phosphatic waste clays. *Journal of Geotechnical Engineering*, 112(11), 1033-1049.
- Merckelbach, L., & Kranenburg, C. (2004). Determining effective stress and permeability equations for soft mud from simple laboratory experiments. *Geotechnique*, 54(9), 581-591.
- Mesri, G., & Olson, R. E. (1971a). MECHANISMS CONTROLLING THE PERMEABILITY OF CLAYS.
- Mesri, G., & Olson, R. E. (1971b). Mechanisms controlling the permeability of clays. *Clays and clay minerals*, 19(3), 151-158. doi:10.1346/CCMN.1971.0190303
- Mesri, G., & Rokhsar, A. (1974). Theory of consolidation for clays. *Journal of geotechnical and geoenvironmental engineering*, 100(10740 Proc Paper).
- Mihiretu, Y., Chalaturnyk, R., & Scott, J. (2008). *Tailings segregation fundamentals from flow behaviour perspective*. Paper presented at the First international Oil Sands Tailings Conference. Edmonton, AB, December.
- Mikasa, M. (1963). The consolidation of soft clay—a new consolidation theory and its application.
- Mikasa, M., & Takada, N. (1984). *Selfweight consolidation of very soft clay by centrifuge*. Paper presented at the Sedimentation Consolidation Models—Predictions and Validation.

- Miller, W., Scott, J., & Segoo, D. (2010). Influence of extraction process and coagulant addition on thixotropic strength of oil sands fine tailings. *CIM journal*, 1(3), 197-205.
- Miller, W. G. (2010). *Comparison of geoenvironmental properties of caustic and noncaustic oil sand fine tailings*. University of Alberta.
- Minet, J., Lambot, S., Delaide, G., Huisman, J. A., Vereecken, H., & Vanclooster, M. (2010). A generalized frequency domain reflectometry modeling technique for soil electrical properties determination. *Vadose zone journal*, 9(4), 1063-1072.
- Mitchell, J. K. (1961). Fundamental aspects of thixotropy in soils. *Transactions of the American Society of Civil Engineers*, 126(1), 1586-1620.
- Mitchell, J. K., & Soga, K. (1976). *Fundamentals of soil behavior* (Vol. 422): Wiley New York.
- Mitchell, J. K., & Soga, K. (2005). *Fundamentals of soil behavior*.
- Mizani, S. (2017). *Experimental Study and Surface Deposition Modelling of Amended Oil Sands Tailings Products*. Carleton University.
- Mizani, S., Simms, P., & Wilson, W. (2017). Rheology for deposition control of polymer-amended oil sands tailings. *Rheologica Acta*, 56(7-8), 623-634.
- Monte, J. L., & Krizek, R. (1976). One-dimensional mathematical model for large-strain consolidation. *Geotechnique*, 26(3), 495-510.
- Morris, P. (2003). Compressibility and permeability correlations for fine-grained dredged materials. *Journal of waterway, port, coastal, and ocean engineering*, 129(4), 188-191. doi:10.1061/(ASCE)0733-950X(2003)129:4(188)

- Morris, P., Lockington, D., & Apelt, C. (2000). Correlations for mine tailings consolidation parameters. *International Journal of Surface Mining, Reclamation and Environment*, 14(3), 171-182. doi:10.1080/13895260008953321
- Mualem, Y., & Dagan, G. (1975). A dependent domain model of capillary hysteresis. *Water resources research*, 11(3), 452-460.
- Nagaraj, T., & Murthy, B. S. (1983). Rationalization of Skempton's compressibility equation. *Geotechnique*, 33(4), 433-443.
- Nagaraj, T., Pandian, N., & Narasimha-Raju, P. (1993). Stress state-permeability relationships for fine-grained soils. *Geotechnique*, 43(2).
- Nagaraj, T., Pandian, N., & Raju, P. N. (1994). Stress-state—permeability relations for overconsolidated clays. *Geotechnique*, 44(2), 349-352.
- Nagaraj, T., & Srinivasa Murthy, B. (1986). A critical reappraisal of compression index equations. *Geotechnique*, 36(1), 27-32.
- Nasser, M., & James, A. (2008). Degree of flocculation and viscoelastic behaviour of kaolinite-sodium chloride dispersions. *Colloids and Surfaces A: Physicochemical and Engineering Aspects*, 315(1-3), 165-175.
- Nishida, Y., & Nakagawa, S. (1969). *Water permeability and plastic index of soils*. Paper presented at the Proceedings of IASH-UNESCO Symposium Tokyo, Pub.
- Noborio, K. (2001). Measurement of soil water content and electrical conductivity by time domain reflectometry: a review. *Computers and electronics in agriculture*, 31(3), 213-237.

- Noborio, K., McInnes, K., & Heilman, J. (1996). Measurements of Soil Water Content, Heat Capacity, and Thermal Conductivity With A Single Tdr Probe1. *Soil Science*, 161(1), 22-28.
- Olsen, H., Nichols, R., & Rice, T. L. (1985). Low gradient permeability measurements in a triaxial system. *Geotechnique*, 35(2), 145-157.
- Olson, R. E. (1977). Consolidation under time-dependent loading. *Journal of the Geotechnical Engineering Division*, 103(1), 55-60.
- Olson, R. E., & Daniel, D. E. (1981). Measurement of the Hydraulic conductivity of fine-grained soils. *Permeability and groundwater contaminant transport. ASTM International*.
- Osipov, V., Nikolaeva, S., & Sokolov, V. (1984). Microstructural changes associated with thixotropic phenomena in clay soils. *Geotechnique*, 34(3), 293-303.
- Owolagba, J. O. (2013). *Dewatering Behavior of Centrifuged Oil Sand Fine Tailings for Surface Deposition*. Faculty of Graduate Studies and Research, University of Regina. Retrieved from <http://hdl.handle.net/10294/5470>
- Pandian, N., Nagaraj, T., & Raju, P. N. (1995). Permeability and compressibility behavior of bentonite-sand/soil mixes. *Geotechnical Testing Journal*, 18(no. 1), 86-93. doi:10.1520/GTJ10124J
- Pane, V., Croce, P., Znidarcic, D., Ko, H.-Y., Olsen, H., & Schiffman, R. L. (1983). Effects of consolidation on permeability measurements for soft clay. *Geotechnique*, 33(1), 67-72.
- Pane, V., & Schiffman, R. (1985). A note on sedimentation and consolidation. *Geotechnique*, 35(1).

- Pane, V., & Schiffman, R. (1997). The permeability of clay suspensions. *Geotechnique*, 47(2), 273-288. doi:10.1680/geot.1997.47.2.273
- Poindexter, M. E. (1988). *Evaluation of dredged material for use as Sanitary Landfill Cover*. Retrieved from
- Poindexter, M. E. (1989). Behavior of subaqueous sediment mounds: Effect on dredged material disposal site capacity.
- Pollock, G. W. (1988). *Large strain consolidation of oil sand tailings sludge*. (M.Sc. degree), University of Alberta.
- Proskin, S., Sego, D., & Alostaz, M. (2010). Freeze–thaw and consolidation tests on Suncor mature fine tailings (MFT). *Cold Regions Science and Technology*, 63(3), 110-120.
- Proskin, S. A. (1998). A geotechnical investigation of freeze-thaw dewatering of oil sands fine tailings.
- Qi, S., Chen, X., Simms, P., Zhou, J., & Yang, X. (2020). New method for determining the permeability function parameters of soft soils considering synchronous sedimentation and consolidation. *Computers and Geotechnics*, 127, 103781.
- Qi, S., Salam, M., & Simms, P. (2017). *Modelling thixotropy at short and long time scales in dewatering analyses for soft soil or tailings*. Paper presented at the Proceedings the 70th Canadian Geotechnical Conference.
- Qi, S., Salam, M., & Simms, P. (2018). *Creep and Structuration in Tailings and Natural Clays*. Paper presented at the Proceedings of IOSTC Edmonton, Alberta.

- Qi, S., & Simms, P. (2020). Robust methods to estimate large-strain consolidation parameters from column experiments. *Canadian Geotechnical Journal*, 57(5), 683-705.
- Qi, S., Simms, P., & Vanapalli, S. (2017). Piecewise-linear formulation of coupled large-strain consolidation and unsaturated flow. I: Model development and implementation. *Journal of geotechnical and geoenvironmental engineering*, 143(7), 04017018.
- Qi, S., Simms, P., Vanapalli, S., & Soleimani, S. (2017). Piecewise-Linear Formulation of Coupled Large-Strain Consolidation and Unsaturated Flow. II: Testing and Performance. *Journal of geotechnical and geoenvironmental engineering*, 143(7), 04017019. doi:10.1061/(ASCE)GT.1943-5606.0001658
- Raymond, G. (1969). Consolidation of deep deposits of homogeneous clay. *Geotechnique*, 19(4), 478-494.
- Reid, D., & Fourie, A. (2012). *Accelerated consolidation testing of slurries using a desktop centrifuge*. Paper presented at the Accelerated Consolidation Testing of Slurries using a Desktop Centrifuge.
- Renko, E. K. (1998). Modelling hindered batch settling Part II: A model for computing solids profile of calcium carbonate slurry. *WATER SA-PRETORIA-*, 24, 331-336.
- Richards, L. A. (1931). Capillary conduction of liquids through porous mediums. *Physics*, 1(5), 318-333.
- Richardson, J., & Zaki, W. (1954). Fluidization and sedimentation—Part I. *Trans. Inst. Chem. Eng*, 32, 38-58.

- Rinaldi, V., & Francisca, F. (1999). Impedance analysis of soil dielectric dispersion (1 MHz–1 GHz). *Journal of geotechnical and geoenvironmental engineering*, 125(2), 111-121.
- Robert, A. (1998). Dielectric permittivity of concrete between 50 MHz and 1 GHz and GPR measurements for building materials evaluation. *Journal of applied geophysics*, 40(1-3), 89-94.
- Robinson, D., Campbell, C., Hopmans, J., Hornbuckle, B. K., Jones, S. B., Knight, R., . . . Wendroth, O. (2008). Soil moisture measurement for ecological and hydrological watershed-scale observatories: A review. *Vadose zone journal*, 7(1), 358-389.
- Robinson, M., & Dean, T. (1993). Measurement of near surface soil water content using a capacitance probe. *Hydrological processes*, 7(1), 77-86.
- Robinson, R. (1999). Consolidation analysis with pore water pressure measurements. *Geotechnique*, 49(1), 127-132.
- Salam, M. (2020). *Effects of Polymer on Short- and Long-term dewatering of oil sands tailings*. (Ph.D. Dissertation), Carleton University, Ottawa, ON.
- Salam, M., Simms, P., & Ormeci, B. (2018). *Structuration in Polymer Amended Oil Sands Fine Tailings*. Paper presented at the 71st Canadian Geotechnical Conference, Edmonton, AB.
- Salam, M. A. (2019). *Effects of polymers on short- and long-term dewatering behaviour of oil sands tailings*. (Doctor of Philosophy), Carleton University, Ottawa, ON.
- Salem, A. M., & Krizek, R. J. (1973). CONSOLIDATION CHARACTERISTICS OF DREDGING SLURRIES. *ASCE J Waterw Harbors Coastal Eng Div*, 99(WW4), 439-457.

- Samarasinghe, A. M., Huang, Y. H., & Drnevich, V. P. (1982). Permeability and consolidation of normally consolidated soils. *Journal of the Geotechnical Engineering Division*, 108(6), 835-850.
- Sayde, C., Gregory, C., Gil-Rodriguez, M., Tuffillaro, N., Tyler, S., van de Giesen, N., . . . Selker, J. S. (2010). Feasibility of soil moisture monitoring with heated fiber optics. *Water resources research*, 46(6).
- Schiffman, R. (1958). *Consolidation of soil under time-dependant loading and varying permeability*. Paper presented at the Highway Research Board Proceedings.
- Schiffman, R. L. (2001). *Theories of consolidation*: University of Colorado.
- Scott, J., Jeeravipoolvarn, S., & Chalaturnyk, R. (2008). *Tests for wide range of compressibility and hydraulic conductivity of flocculated tailings*. Paper presented at the The 61st Canadian Geotechnical Conference, Edmonton, Alberta.
- Scott, J. D., Dusseault, M. B., & Carrier, W. D. (1986). Large-scale self-weight consolidation testing *Consolidation of Soils: Testing and Evaluation*: ASTM International.
- Scott, J. D., Jeeravipoolvarn, S., Kabwe, L., & Wilson, G. W. (2013). *Properties which affect the consolidation behaviour of mature fine tailings*. Paper presented at the Tailings and Mine Waste '13: Proceedings of the 17th international conference on tailings and mine waste, Banff, Alberta.
- Scully, R. W., Schiffman, R. L., Olsen, H. W., & Ko, H.-Y. (1984). *Validation of consolidation properties of phosphatic clay at very high void ratios*. Paper presented at the Sedimentation Consolidation Models—Predictions and Validation.

- Seed, H. B., & Chan, C. K. (1959). Thixotropic characteristics of compacted clays. *Transactions of the American Society of Civil Engineers*, 124(1), 894-916.
- Selig, E. T., & Mansukhani, S. (1975). Relationship of soil moisture to the dielectric property. *Journal of geotechnical and geoenvironmental engineering*, 101(ASCE# 11517 Proceeding).
- Seneviratne, N., Fahey, M., Newson, T., & Fujiyasu, Y. (1996). Numerical modelling of consolidation and evaporation of slurried mine tailings. *International Journal for Numerical and Analytical Methods in Geomechanics*, 20(9), 647-671.
- Sethi, A. (1995). Methylene Blue Test for Clay Activity Determination in Fine Tails. *MRRT Procedures*.
- Sharma, B., & Bora, P. K. (2015). A study on correlation between liquid limit, plastic limit and consolidation properties of soils. *Indian Geotechnical Journal*, 45(2), 225-230.
- Shields, F. (1988). Consolidation and settling of shoal material, Kings Bay, Georgia. *Internal Working Document EL-88*, 3.
- Shodja, H. M., & Feldkamp, J. R. (1993). Numerical analysis of sedimentation and consolidation by the moving finite element method. *International Journal for Numerical and Analytical Methods in Geomechanics*, 17(11), 753-769.
- Sills, G. (1998). Development of structure in sedimenting soils. *Philosophical Transactions of the Royal Society of London. Series A: Mathematical, Physical and Engineering Sciences*, 356(1747), 2515-2534.

- Simms, P. (2017). 2013 Colloquium of the Canadian Geotechnical Society: Geotechnical and geoenvironmental behaviour of high-density tailings. *Canadian Geotechnical Journal*, 54(4), 455-468.
- Sivakugan, N., Lovisa, J., Ameratunga, J., & Das, B. M. (2014). Consolidation settlement due to ramp loading. *International Journal of Geotechnical Engineering*, 8(2), 191-196.
- Sivapullaiah, P., Sridharan, A., & Stalin, V. (2000). Hydraulic conductivity of bentonite-sand mixtures. *Canadian Geotechnical Journal*, 37(2), 406-413. doi:10.1139/t99-120
- Skempton, A., & Northey, R. (1952). The sensitivity of clays. *Geotechnique*, 3(1), 30-53.
- Smith, R. E., & Wahls, H. E. (1969). Consolidation under constant rates of strain. *Journal of Soil Mechanics & Foundations Div.*
- Sobkowicz, J. (2013). *Developments in treating and dewatering oil sand tailings*. Paper presented at the Proceedings of the 16th International Seminar on Paste and Thickened Tailings. Edited by RJ Jewell, AB Fourie, and J. Pimenta. Belo Horizonte.
- Sobkowicz, J., & Morgenstern, N. (2009). *A geotechnical perspective on oil sands tailings*. Paper presented at the Proceedings of the 13th International Conference on Tailings and Mine Waste, Banff, Alta.
- Sorta, A. R. (2015). Centrifugal modelling of oil sands tailings consolidation.

- Sorta, A. R., Segoo, D. C., & Wilson, W. (2012). Effect of thixotropy and segregation on centrifuge modelling. *International Journal of Physical Modelling in Geotechnics*, 12(4), 143-161.
- Sridharan, A., & Nagaraj, H. (2000). Compressibility behaviour of remoulded, fine-grained soils and correlation with index properties. *Canadian Geotechnical Journal*, 37(3), 712-722. doi:10.1139/t99-128
- Sridharan, A., & Nagaraj, H. (2005). Hydraulic conductivity of remolded fine-grained soils versus index properties. *Geotechnical & Geological Engineering*, 23(1), 43-60.
- Sridharan, A., & Prakash, K. (1999). Simplified seepage consolidation test for soft sediments. *Geotechnical Testing Journal*, 22(3), 235-244.
- Sridharan, A., & Prakash, K. (2001). Consolidation and permeability behavior of segregated and homogeneous sediments. *Geotechnical Testing Journal*, 24(1), 109-120.
- Sridharan, A., & Prakash, K. (2002). Determination of liquid limit from equilibrium sediment volume. *Geotechnique*, 52(9), 693-696. doi:10.1680/geot.54.9.611.56941
- Su, S. L., Singh, D. N., & Baghini, M. S. (2014). A critical review of soil moisture measurement. *Measurement*, 54, 92-105.
- Suthaker, N., & Scott, J. (1994). *Large strain consolidation testing of oil sand fine tails in a wet landscape*. Paper presented at the Proceedings, 47th Canadian Geotechnical Conference.
- Suthaker, N. N. (1995). *Geotechnics of oil sand fine tailings*. (Doctor of Philosophy), University of Alberta.

- Suthaker, N. N., & Scott, J. D. (1996). Measurement of hydraulic conductivity in oil sand tailings slurries. *Canadian Geotechnical Journal*, 33(4), 642-653.
- Suthaker, N. N., & Scott, J. D. (1997). Thixotropic strength measurement of oil sand fine tailings. *Canadian Geotechnical Journal*, 34(6), 974-984.
- Tan, T., Yong, K., Leong, E., & Lee, S. (1990). Sedimentation of clayey slurry. *Journal of Geotechnical Engineering*, 116(6), 885-898.
- Tanaka, H., Locat, J., Shibuya, S., Soon, T. T., & Shiwakoti, D. R. (2001). Characterization of Singapore, Bangkok, and Ariake clays. *Canadian Geotechnical Journal*, 38(2), 378-400. doi:10.1139/t00-106
- Tavenas, F., Jean, P., Leblond, P., & Leroueil, S. (1983). The permeability of natural soft clays. Part II: Permeability characteristics. *Canadian Geotechnical Journal*, 20(4), 645-660.
- Taylor, D. W. (1948). Fundamentals of soil mechanics. *Soil Science*, 66(2), 161.
- Taylor, R. (2018). Centrifuges in modelling: principles and scale effects *Geotechnical centrifuge technology* (pp. 19-33): CRC Press.
- Terzaghi, K. (1927). *Principles of final soil classification*.
- Terzaghi, K. (1936). Stress distribution in dry and in saturated sand above a yielding trap-door.
- Terzaghi, K. (1943). *Theory of Consolidation*: Wiley Online Library.
- Terzaghi, K., Peck, R. B., & Mesri, G. (1996). *Soil mechanics in engineering practice*: John Wiley & Sons.
- Terzaghi, K. v. (1923). Die berechnung der durchlässigkeitsziffer des tones aus dem verlauf der hydrodynamischen spannungserscheinungen. *Sitzungsberichte der*

Akademie der Wissenschaften in Wien, Mathematisch-Naturwissenschaftliche Klasse, Abteilung IIa, 132, 125-138.

- Toorman, E. (1999). Sedimentation and self-weight consolidation: constitutive equations and numerical modelling. *Geotechnique*, 49(6), 709-726.
- Topp, G., Davis, J., & Annan, A. (1982). Electromagnetic Determination of Soil Water Content Using TDR: I. Applications to Wetting Fronts and Steep Gradients 1. *Soil Science Society of America Journal*, 46(4), 672-678.
- Topp, G., Zegelin, S., & White, I. (2000). Impacts of the real and imaginary components of relative permittivity on time domain reflectometry measurements in soils. *Soil Science Society of America Journal*, 64(4), 1244-1252.
- Topp, G. C., Davis, J., & Annan, A. P. (1980). Electromagnetic determination of soil water content: Measurements in coaxial transmission lines. *Water resources research*, 16(3), 574-582.
- Umehara, Y., & Zen, K. (1980). Constant rate of strain consolidation for very soft clayey soils. *Soils and Foundations*, 20(2), 79-95.
- Vandara, K. (2018). *Polymer Assessment on Dewatering of Oil Sands Tailings*. Retrieved from Ottawa, ON:
- Vedoy, D. R., & Soares, J. B. (2015). Water-soluble polymers for oil sands tailing treatment: A Review. *The Canadian Journal of Chemical Engineering*, 93(5), 888-904.
- Vick, S. G. (1990). *Planning, design, and analysis of tailings dams*: BiTech.

- Watson, K. (1966). An instantaneous profile method for determining the hydraulic conductivity of unsaturated porous materials. *Water resources research*, 2(4), 709-715.
- Wells, P., Revington, A., & Omotoso, O. (2011). *Mature fine tailings drying B—■ technology update*. Paper presented at the Proceedings of the 14th International Seminar on Paste and Thickened tailings.
- Wells, P. S. (2011). Long term in-situ behaviour of oil sands fine tailings in Suncor's pond 1A. *Proceedings Tailings and Mine Waste 2011*.
- Whalley, W., Dean, T., & Izzard, P. (1992). Evaluation of the capacitance technique as a method for dynamically measuring soil water content. *Journal of agricultural engineering research*, 52, 147-155.
- Wills, B., & Napier–Munn, T. (2006). *Mineral Processing Technology*, Elsevier Science & Technology Books. *PP108-117*, 267-352.
- Wilson, G. W., Kabwe, L. K., Beier, N. A., & Scott, J. D. (2017). Effect of various treatments on consolidation of oil sands fluid fine tailings. *Canadian Geotechnical Journal(ja)*. doi:10.1139/cgj-2017-0268
- Winterwerp, J. C. (2002). On the flocculation and settling velocity of estuarine mud. *Continental shelf research*, 22(9), 1339-1360. doi:10.1016/S0278-4343(02)00010-9
- Wissa, A. (1971). Consolidation at constant rate of strain. *Journal of Soil Mechanics & Foundations Div.*

- Wong, R., Mills, B., & Liu, Y. (2008). Mechanistic model for one-dimensional consolidation behavior of nonsegregating oil sands tailings. *Journal of geotechnical and environmental engineering*, 134(2), 195-202.
- Yao, D. T., de Oliveira-Filho, W. L., Cai, X. C., & Znidarcic, D. (2002). Numerical solution for consolidation and desiccation of soft soils. *International Journal for Numerical and Analytical Methods in Geomechanics*, 26(2), 139-161.
- Yao, Y. (2016). *Dewatering Behaviour of Fine Oil Sands Tailings: An Experimental Study*. (Doctor of Philosophy), Delft University of Technology.
- YOU, Z., & Znidarcic, D. (1994). *Initial stage of soft soil consolidation*. Paper presented at the International conference centrifuge 94.
- Zazueta, F. S., & Xin, J. (1994). Soil moisture sensors. *Soil Sci*, 73, 391-401.
- Zen, K., & Umehara, Y. (1986). A new consolidation testing procedure and technique for very soft soils *Consolidation of Soils: Testing and Evaluation*: ASTM International.
- Zeng, L.-L., Hong, Z.-S., & Cui, Y.-J. (2016). Time-dependent compression behaviour of dredged clays at high water contents in China. *Applied Clay Science*, 123, 320-328.
- Zhang, X., Kong, L., Yang, A., & Sayem, H. (2017). Thixotropic mechanism of clay: A microstructural investigation. *Soils and Foundations*, 57(1), 23-35.
- Zhu, Q. (2013). Understanding the role of caustic addition in oil sands processing.
- Znidarcic, D., Croce, P., Pane, V., Ko, H.-Y., Olsen, H. W., & Schiffman, R. (1984a). The theory of one-dimensional consolidation of saturated clays: III. existing testing procedures and analyses.

- Znidarcic, D., Croce, P., Pane, V., Ko, H.-Y., Olsen, H. W., & Schiffman, R. (1984b). The theory of one-dimensional consolidation of saturated clays: III. existing testing procedures and analyses. *Geotechnical Testing Journal*, 7(3), 123-134.
- Znidarcic, D., & Liu, J. (1989). *Consolidation characteristics determination for dredged materials*. Paper presented at the Proc.
- Znidarčić, D., Miller, R., Van Zyl, D., Fredlund, M., & Wells, S. (2011). *Consolidation testing of oil sand fine tailings*. Paper presented at the Proceedings of Tailings and Mine Waste.
- Znidarčić, D., Schiffman, R., Pane, V., Croce, P., Ko, H., & Olsen, H. (1986). The theory of one-dimensional consolidation of saturated clays: part V, constant rate of deformation testing and analysis. *Geotechnique*, 36(2), 227-237.

Appendix A Geotechnical Characterization Tests

The results from the following characterization tests are discussed in Chapter 3. The methodology for the each test are presented below.

A.1 Solid Content (C_s)

ASTM standard test method (D2216-19) was conducted to determine the solids content of the tested materials. It can be calculated as:

$$C_s = \frac{M_s}{M_t} \times 100 \quad (\text{A.1})$$

where M_s is the mass of solids in tailings (including bitumen), measured after oven-drying, and M_t is the initial mass of the tailings prior to oven-drying. Solids content is expressed in percentage.

A.2 Gravimetric (w) and Volumetric Water Content (θ)

For the calculation of gravimetric and volumetric water contents, the ASTM D2216-19 procedure was followed. Both properties can be calculated as:

$$\theta = \frac{V_w}{V_t} \times 100 \quad (\text{A.2})$$

$$w = \frac{M_w}{M_s} \times 100 \quad (\text{A.3})$$

where V_w and V_t is the volume of water in the tailings and the total volume of the material, respectively, M_w is the evaporated mass calculated by extracting the mass of solids from the initial total mass, and M_s is the mass of solids (tailings and bitumen) left after oven-drying.

A.3 Specific Gravity (G_s)

The specific gravity of unamended FFT can be determined using the ASTM standard of ASTM 854-10. This property can be expressed by the following equation:

$$G_s = \frac{\rho_s}{\rho_w} \quad (\text{A.4})$$

where ρ_s is the density of soil solids and ρ_w is the density of water at a temperature at 4°C.

Usually, distilled water at this temperature is selected as the standard liquid.

A.4 Atterberg Limits

The liquid limit of fine-grained soils can be determined by either using Casagrande's liquid limit device or fall-cone tests, which is often preferred over Casagrande's cup method because it provides repeatability and less significant variation with different operators. For the Determination of this Atterberg limit of slurries, the fall-cone device is favoured. For the Determination of Atterberg limits, the ASTM D4318-10 test was conducted.

(Feng, 2000) and (Feng, 2001) proposed a linear relationship to determine the plastic limit (PL_{100}) of fine-grained soils from the fall cone test results.

$$PL_{100} = c(2 \text{ mm})^m \quad (\text{A.5})$$

where c is the water content at the penetration depth of 1 mm, and m is the absolute slope of the best-fit line. Parameters c and m can be determined by performing the fall-cone tests on samples with various water contents and analyzing the results. The logarithmic water content vs. logarithmic of fall-cone penetration is plotted, and a best-fit linear line is drawn. This linear relationship is extended backwards (for a British Standard fall-cone), and the intercept of the best-fitted line and the corresponding water content on the axis at the

penetration of 2 mm would represent the plastic limit of the soil.

The plasticity index can be calculated by subtracting the plastic limit from the liquid limit of the sample, which demonstrates the plastic properties while the soil is transitioning from a semi-solid state to the liquid state.

A.5 Void ratio (e)

ASTM D7263-09 standard test is conducted to determine the void ratio of the tested soils, as expressed in the following equation:

$$e = \frac{V_v}{V_s} \tag{A.6}$$

where V_v is the volume of voids in soil (either filled with air or water), and V_s is the volume of solids. For saturated soils, all the voids are filled with water; hence this ratio becomes the volume of water to the volume of soil particles in the material. However, for unsaturated soils, these voids are partially filled with air.

A.6 Particle Size Distribution

In order to determine the particle size distribution of fine-grained soils, a combination of wet sieving and sedimentation (hydrometer) test is utilized (ASTM D7928-16). This combination provides a comprehensive range particle size analysis of the fine-grained portion of the tested soils.

A.7 Total Bulk Density

The standard ASTM test (D7263-09) was performed to determine this geotechnical property, as expressed in the following equation:

$$\rho = \frac{M_s + M_w}{V_t} \quad (\text{A.7})$$

where M_s and M_w are the weight of soil particles and water, respectively, and V_t is the total volume of the soil.

A.8 Clay Content

To determine the clay content of the FFT, the methylene blue index test (a modified version of ASTM C837-99, developed by Sethi (1995)) is performed on unamended, 7-day old and 42-day old samples. Methylene blue is a cationic dye, and it absorbs strongly to the clay surfaces displacing the ions present on the surfaces (i.e. Na^+ , Ca^+ , K^+ and Mg^{2+}). The percentage of clay in fluid fine tailings can be determined by the amount (millilitres) of the methylene blue solution added to the FFT sample during the test. This amount is absorbed by the sample and can be expressed in meq/100 g (milliequivalents of methylene blue per 100 grams of the sample). It was estimated by multiplying the amount of methylene blue index (in millilitres) utilized to titrate 100 grams of a sample by the molarity of methylene blue used (Kaminsky, 2014). Once this coefficient is established, an empirical formula is used to determine the percentage of clay portion, proposed by Sethi (1995):

$$\%clay = \frac{MBI \frac{meq}{100g} + 0.04}{0.14} \quad (\text{A.8})$$

A.9 Bitumen Content

The dean-Stark distillation extraction method (ASTM D95-05) is employed to determine the bitumen content of the unamended FFT. It was expressed using the following equation:

$$\text{Bitumen content} = \frac{M_b}{M_t} \times 100 \quad (\text{A.9})$$

where M_b is the mass of bitumen in the sample (in grams), and M_t is the total mass of FFT (including water, bitumen, solids and other minerals in grams).

Appendix B Dosage Optimization results for Polymer A3338 and Polymer B

B.1 Optimized Results using Shell FFT using A3338

For polymer amended FFT, the flocculation and dewatering efficiency depends on several factors such as polymer properties (i.e. molecular weight, ionic content, ionization degree, dosage, charge density, the nature of the functional groups), the intensity of mixing and the rate of polymer addition, tailings properties (such as solids content, tailings properties, mineralogical composition, particle size and surface charge, pore water chemistry etc.) (Vedoy & Soares, 2015). A series of laboratory-scale screening tests are implemented to determine the performance of different polymers or optimal polymer dosage for full scale or field-scale implementation. A number of commonly used screening tests have been performed in the laboratory to determine the optimum polymer dose of A3338, including;

- i. the settling rate,
- ii. capillary suction test time (CST),
- iii. net water release,
- iv. developed torque during mixing, and
- v. the zeta potential reading in the first two days.

The change in the height and the percentage settlement is demonstrated in Figure B-1. Their final conditions at 120 hours (5 days) are also presented in Figure B-2.

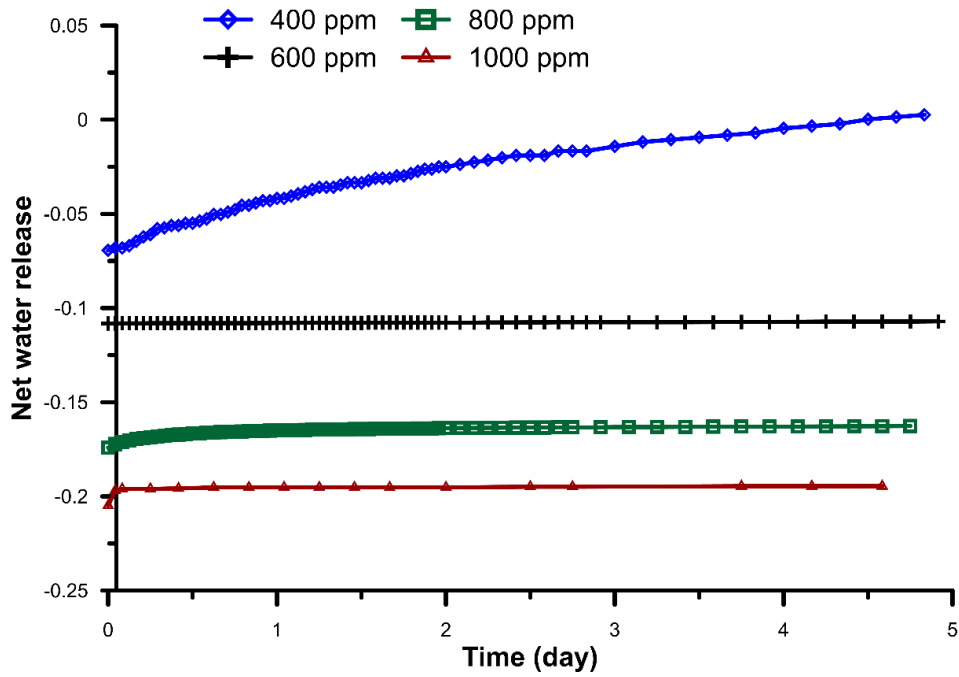
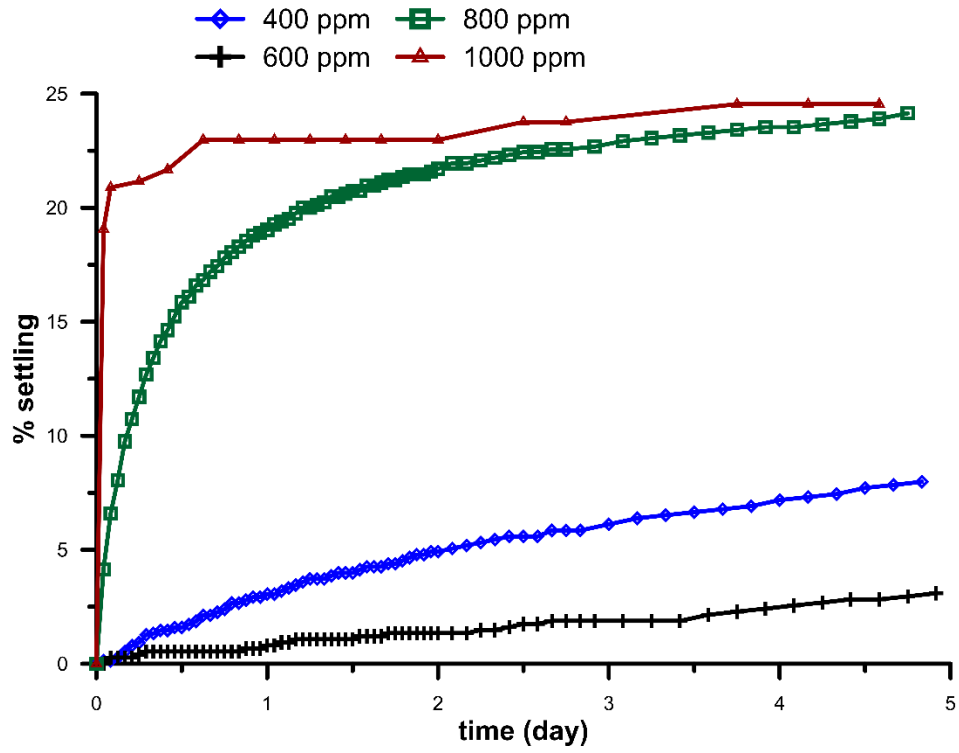


Figure B-1: Settlement analysis for different dosages

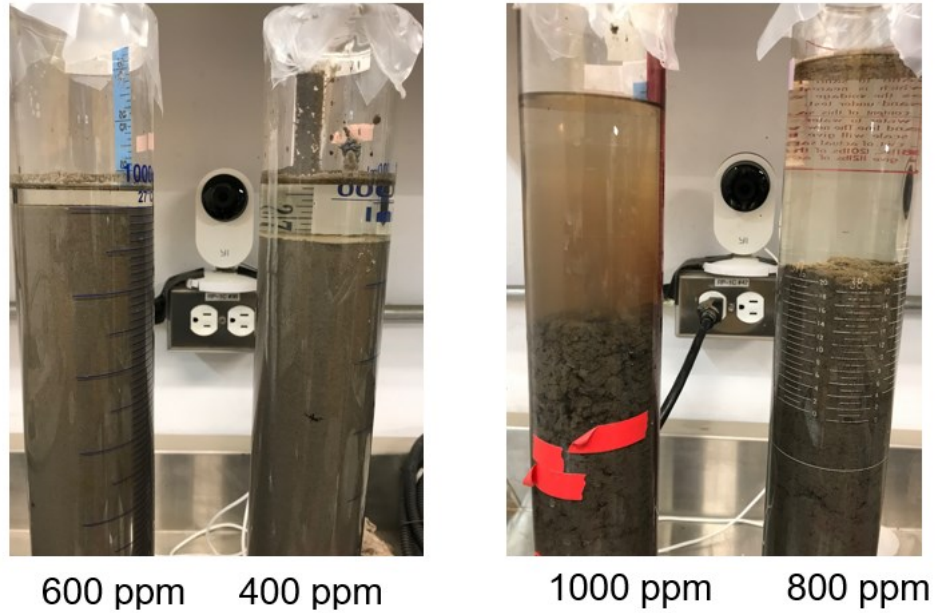


Figure B-2: Final height in the columns at the end of 5 days

Zeta-potential of the amended-FFT samples is determined for the first two days of the experiment, presented in Figure B-3. A higher zeta-potential reading indicates that the electrostatic repulsion between the particles is stronger. Therefore, the particles are in a more dispersed state, the colloidal dispersion is more stable, and it will resist aggregation. As expected, lower dosages measure higher zeta potentials, but the 600 ppm FFT sample recorded a higher value than the lowest dosage. This is probably because the 400-ppm sample is better flocculated. The same results are also demonstrated at the torque development vs. time and CST time plots as well.

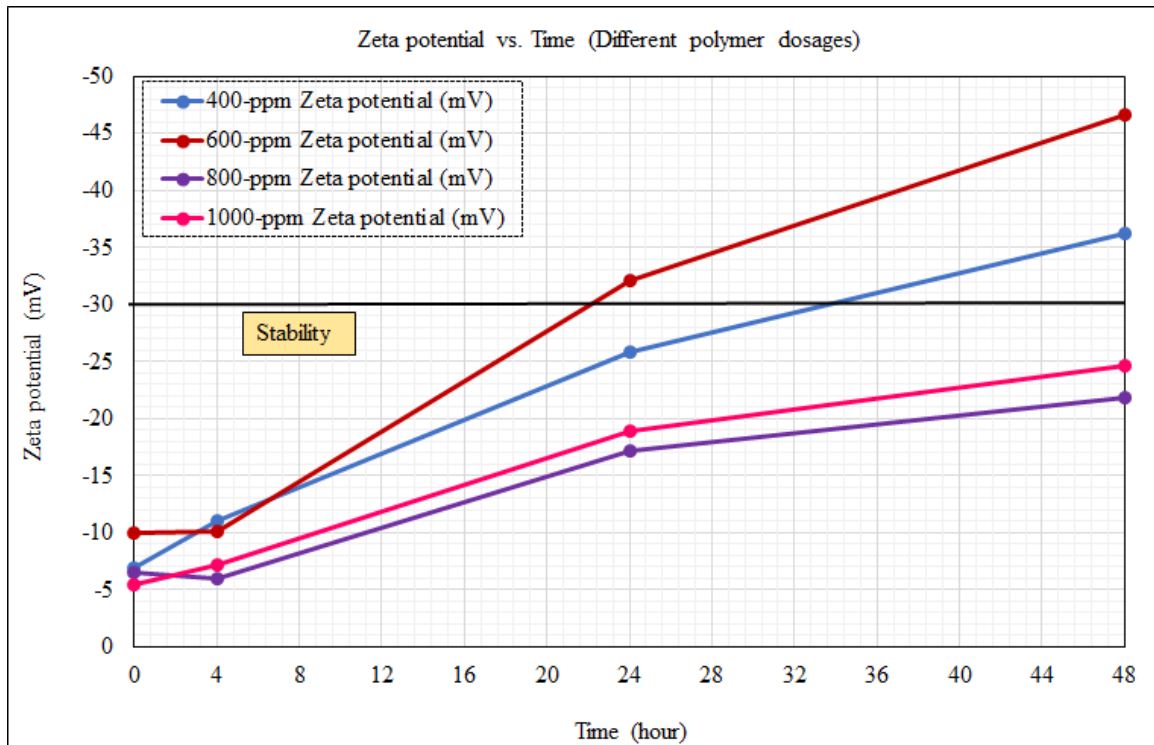


Figure B-3: Zeta-potential increase within 48 hours

The relationship between the torque force developed during flocculation in a Couette rheometer and the quality of the flocculation is proposed by Aldaeef and Simms (2019) for a quality control technique for improved flocculation of FFT. The peak torque forces are reached after 15-25 seconds after the polymer injection. These maximum values are believed to be associated with the formation of larger flocs since the rheometer needs to exert higher power to shear larger flocs. The development of the peak torque values is presented in the following figure for all polymer dosages. In addition, recorded CST time vs. dosage vs. maximum developed torque is introduced in Figure B-5. (P. Wells, Revington, & Omotoso, 2011). Capillary suction time tests measure the water release, and it is used to evaluate the flocculation and dewatering performances of the polymer-amended FFT samples. CST is found to be inversely proportional to the amount of water

released, such as higher CST values indicate poor flocculation and vice versa. The lowest recorded CST time was obtained from 800-ppm sample as well as the maximum torque development observed for this sample. Therefore, it is believed that 800-ppm amended FFT sample achieved the best flocculation and is the optimum dosage.

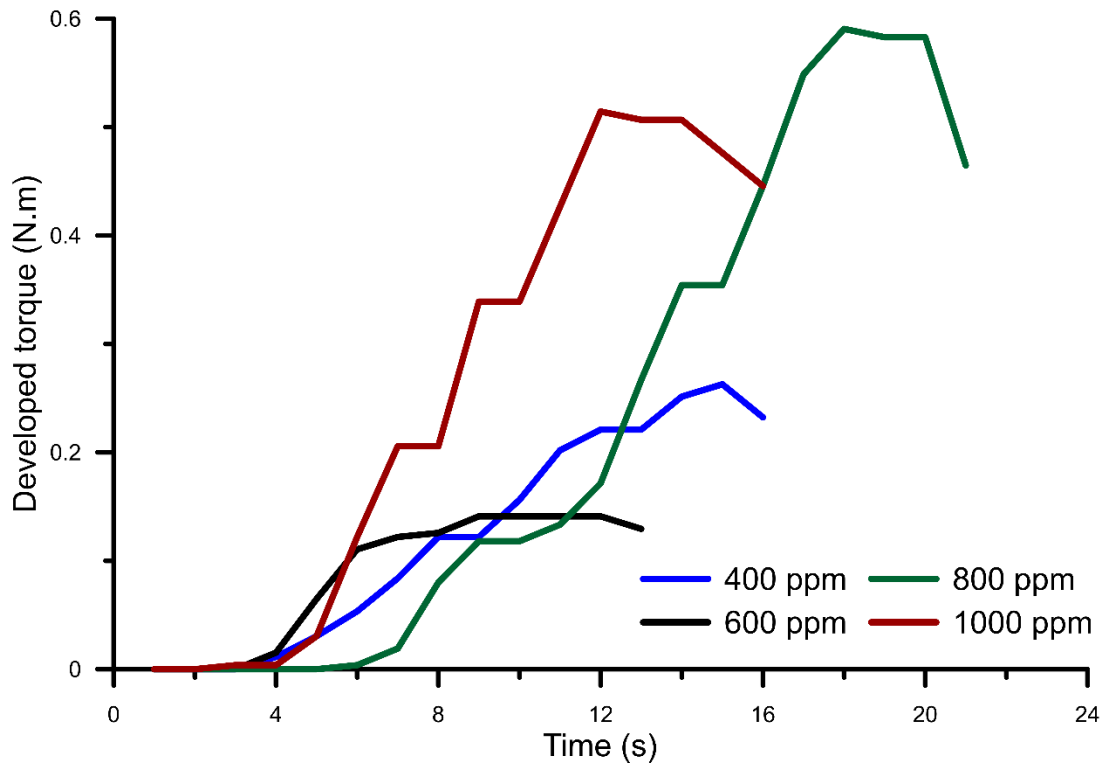


Figure B-4: Developed torque during mixing

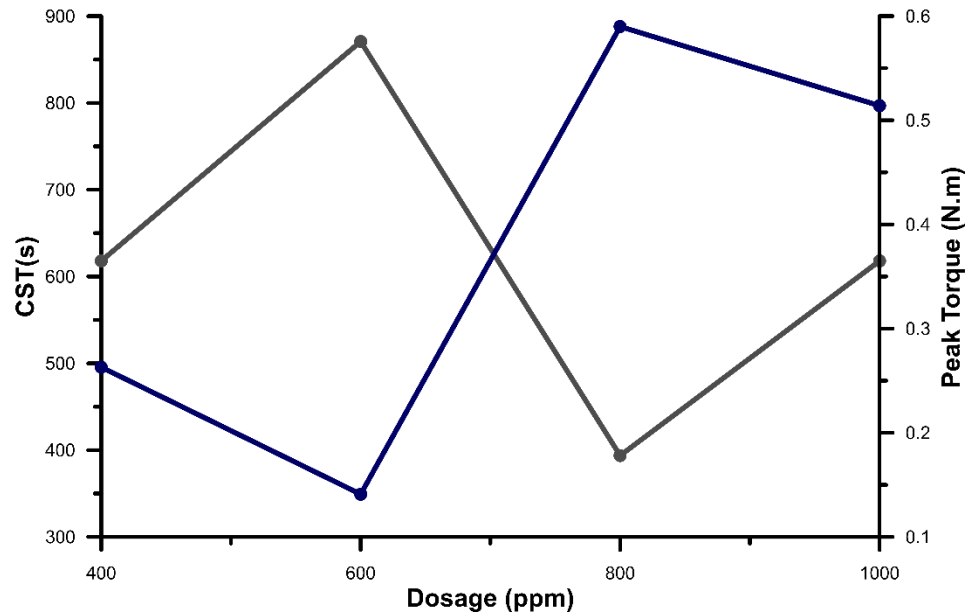


Figure B-5: CST time and developed torque vs. polymer dose

The tailings are pumped or transported through pipelines, and they need to possess fluid-like flow behaviour during this process. When they are deposited, this flow-like behaviour needs to cease so that stacking can start. Therefore, tailings exhibit both elastic and viscous behaviour, or elasticity, as they go through this transition between fluid-like to solid-like behaviour. This transition occurs when the yield stress of the material is exceeded. Both the elastic modulus (G') and the viscous modulus (G'') are viscoelastic properties of the tailings, and they can be determined as a function of the oscillatory stress from the oscillatory rheometry tests (Nasser & James, 2008). Elastic or small strain shear modulus (G') represents the elastic behaviour of the material corresponding to small, temporary and reversible deformation. When the material is subjected to small strain shear, the elastic deformation will take place within the material's elastic limit. Once that applied force is removed, the material regains its original configuration or shape. However, once a certain stress level is exceeded, the deformation is irreversible. The elastic modulus or G'

can be described as:

$$G' = \frac{\tau_c}{\gamma_c} \quad (\text{B.1})$$

where τ_c is the shear stress, and γ_c is the shear strain.

To determine the viscoelastic properties of non-Newtonian fluids, such as tailings, amplitude sweep tests are conducted. During this experiment, the material is sheared at a constant oscillation frequency (10 rad/s) with shear stress or increasing shear strain, and the transformation between elastic-plastic-viscous states can be identified as the material deforms irreversibly (Markgraf, 2006). The following figure demonstrates the development in G' and G'' for all four-dosages from 0-72 hours. In the beginning, G' is higher than G'' , elastic behaviour dominates in this region and passes the point where G' becomes equal to G'' ; the structure collapses, and the soil exhibits irreversible deformation. The intersection of G' and G'' curves provides the yielding point. This yielding stress increased with dosage, and maximum G' and G'' values increased with time for each dosage, as demonstrated in Figure B-6.

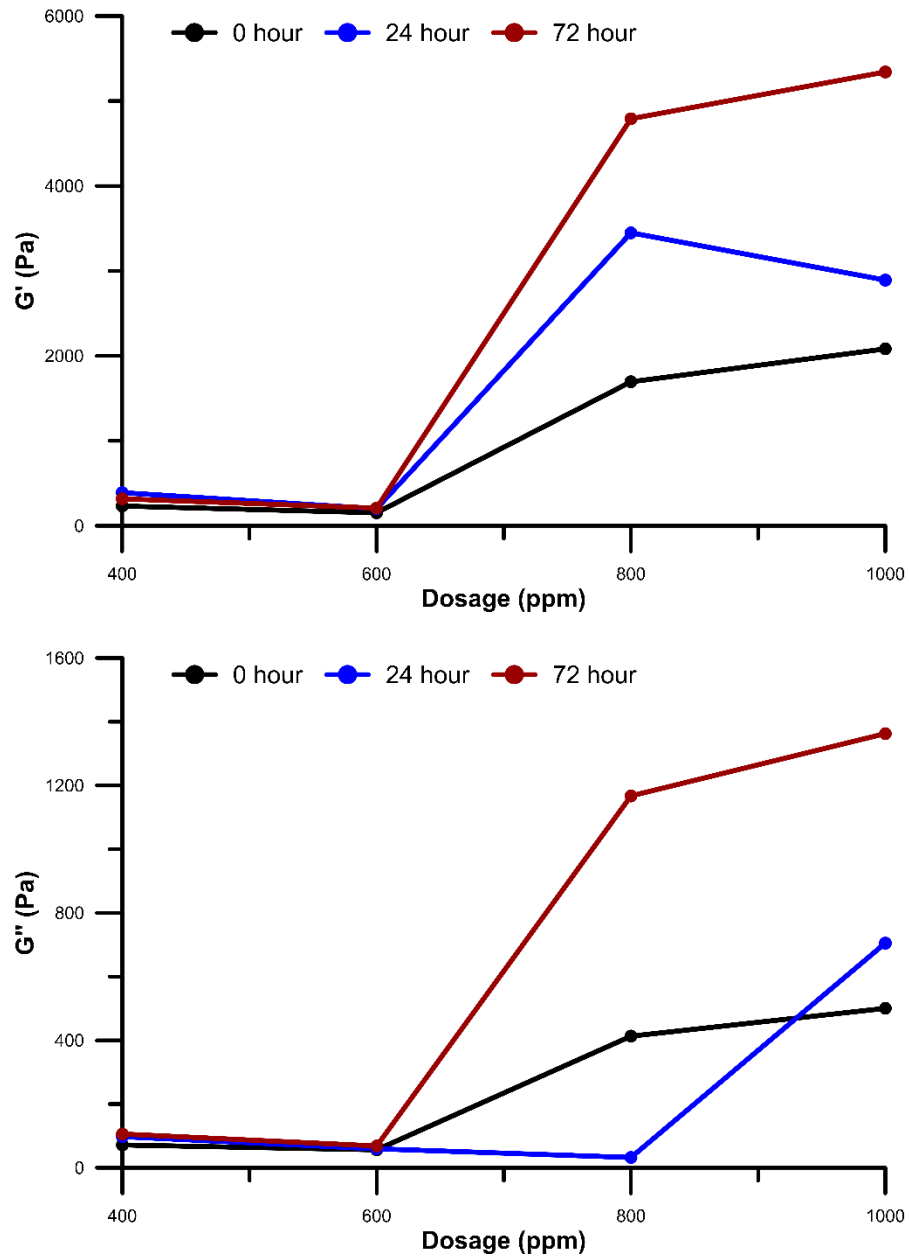


Figure B-6: Developed elastic and viscous modulus at different dosages

After comparing all the results, 800 ppm dosage provided the best dewaterability performance overall, followed by the amended FFT sample with 1000 ppm dosage. These two dosages are selected for further evaluation in the prototyped self-weight consolidation column, and the results are discussed in Chapter 7.

B.2 Optimized Results using Syncrude FFT using Polymer B

The same protocol has been followed while selecting the optimum dose for Polymer B with Syncrude FFT. The samples were prepared closer to the dosage reported by the University of Alberta. The settling and the net water release from the tailings are presented in Figure B-7. From looking at that plot only, 0 ppm and 2000 ppm performed compared to most of the other dosages. However, settling behaviour is not the only factor when it comes to determining dewatering and flocculation efficiency. Figure B-8 demonstrates the undrained shear strength development within a 35-day time frame, and the results clearly indicate that there's no strength development within the soil at those dosages. As a result, dosages over 2000 ppm are considered for the self-weight consolidation column tests.

It is also important to point out that the dosages for Polymer B are significantly higher; as a result, the volume of polymer stock utilized to prepare the samples at higher dosages are quite large. The settling for 10,000 ppm dosage is very high, which can be observed in Figure B-7, but the amount of added polymer stock solution is also very high at this dosage. Hence, lower dosages with better dewatering behaviours are considered for this study, and overall, 4000 ppm dosage provided better results compared to 6000 and 8000 ppm dosages.

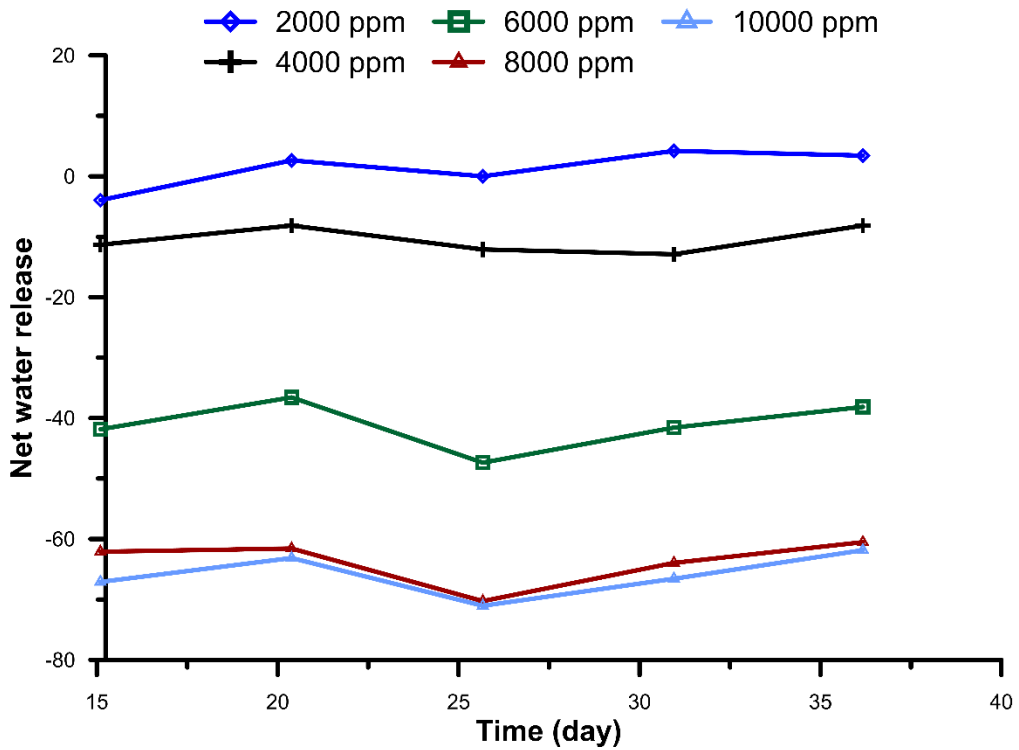
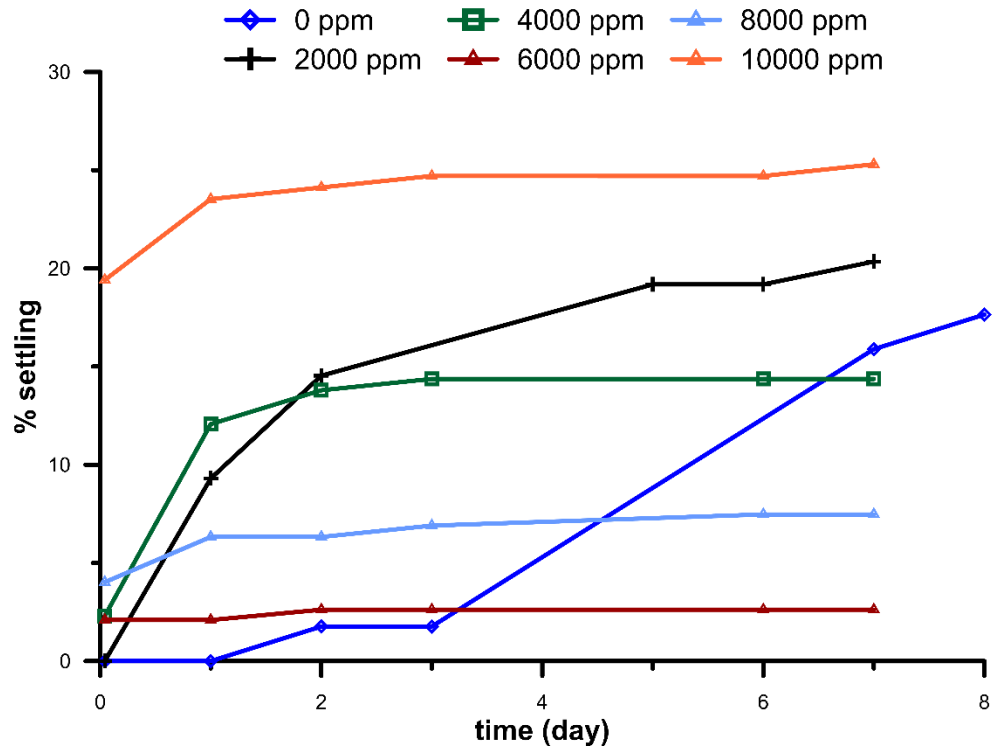


Figure B-7: The settling rate and net water release at different dosages for Polymer B

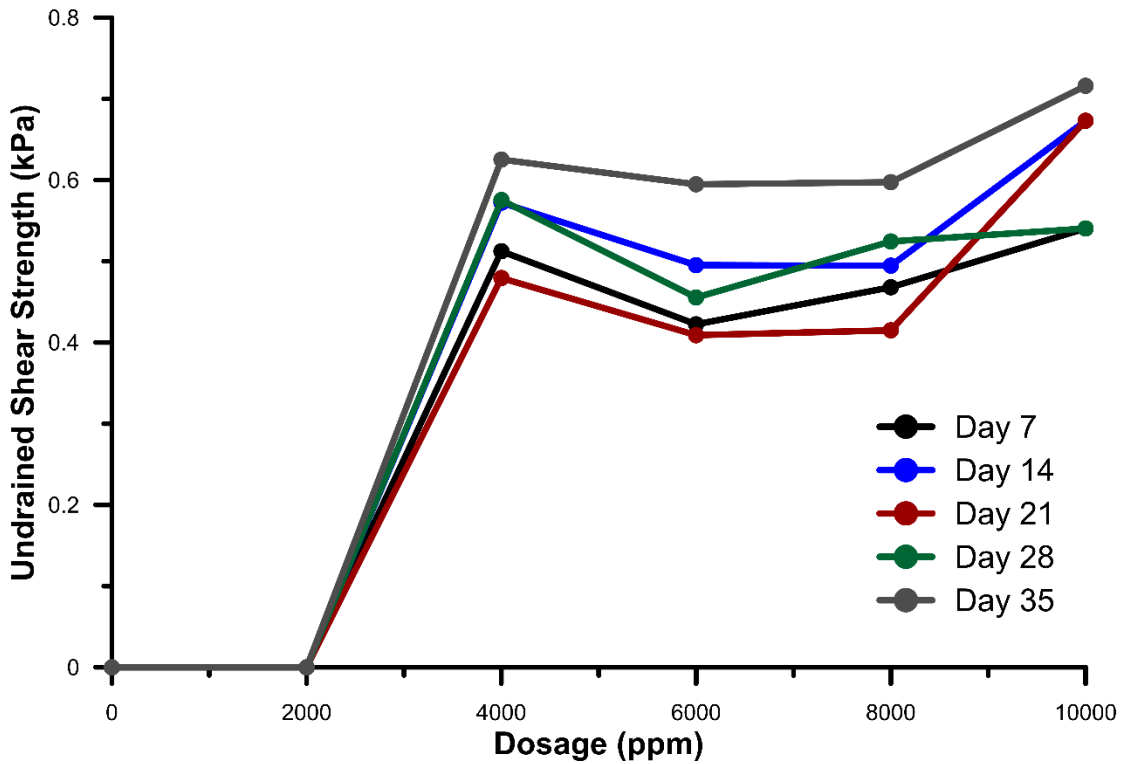


Figure B-8: Undrained shear strength development comparison on at different dosages

Capillary suction time and the peak torque developed during mixing at each dosage are presented in Figure B-9. CST values indicate how good the flocculation is in the prepared sample and how fast it will release water; hence shorter amount of time is better in terms of their dewatering behaviour. For dosages 4000 and higher, CST values become significantly smaller. This fast initial dewatering can also be observed in Figure B-7. In comparison, the maximum torques are developed at 8,000 and 10,000 ppm dosages. It is important to point out that compared to higher dosages prepared using flocculant A3338, Polymer B developed smaller peak torques during mixing.

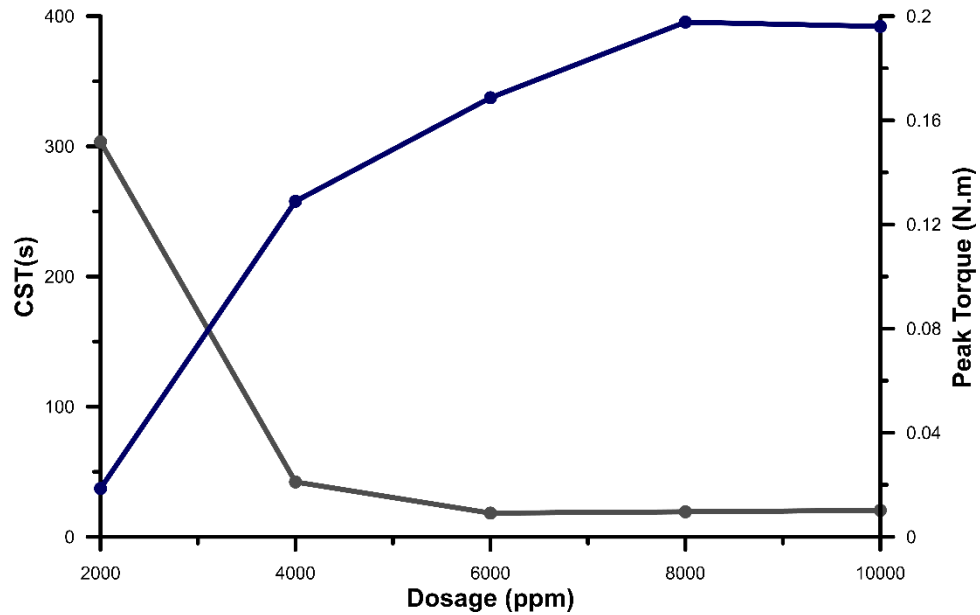
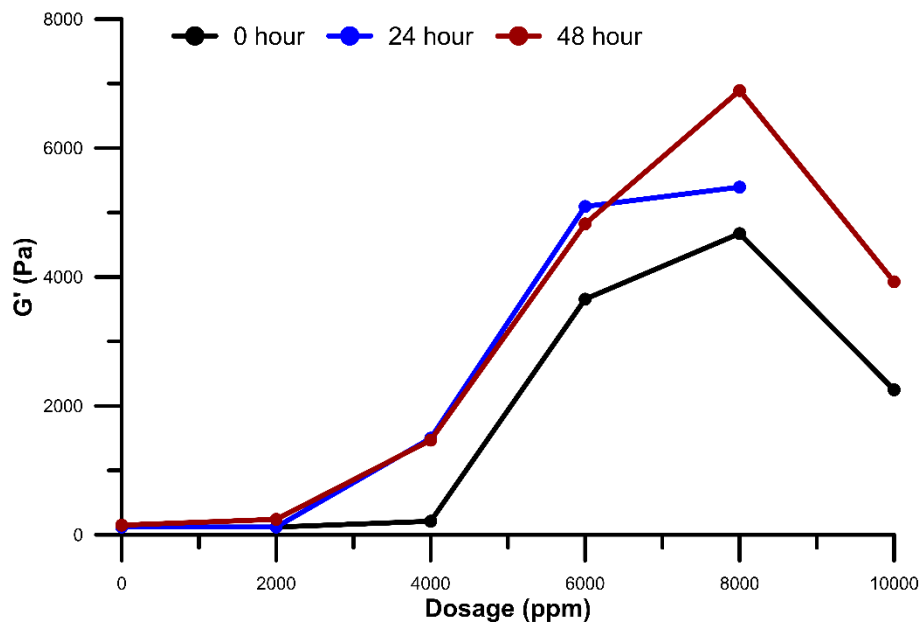


Figure B-9: Dosage vs CST vs. Peak torque developed during mixing

The elastic and viscous modulus is determined at every 0, 24 hours and 48 hours time frames. Similar to the previous tests with flocculant A3338, maximum G' and G'' values increased with dosages until 8,000 ppm dosage, and they decreased for the highest dosage.



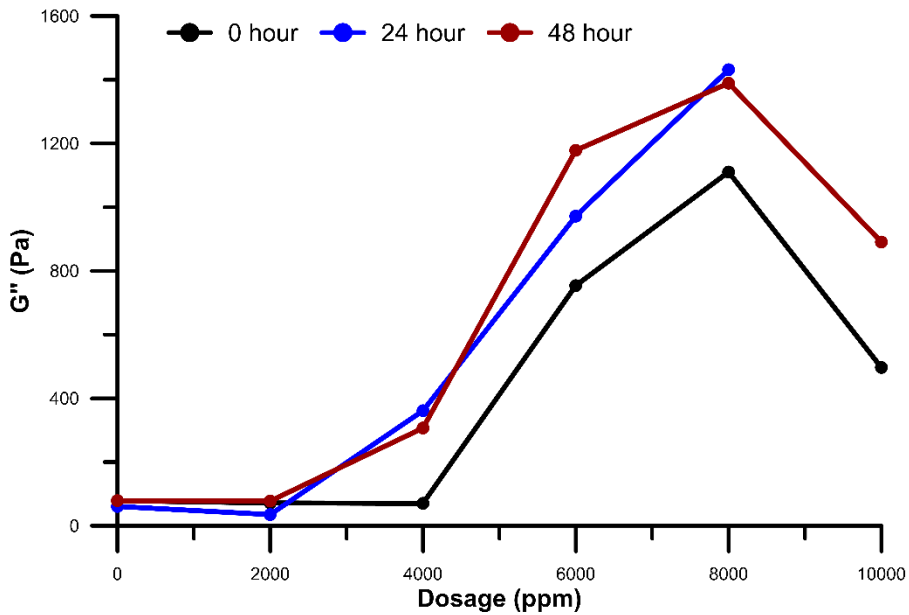


Figure B-10: Developed elastic and viscous modulus for amended FFT sample using Polymer B

When all these laboratory-scale screening tests are analyzed, the results indicate that the highest dosage would provide better dewaterability performance. However, the amount of polymer stock solution to prepare this sample is very high, which can explain the significant amount of water released from this sample when compared to other samples. 6,000 and 8,000 ppm dosages might have provided higher elastic and viscous modulus, but their settling behaviour and developed undrained shear strength results were poorer compared to the 4,000 ppm dosage sample. Considering the volume of polymer stock solution added to the samples and all of the results from the screening tests, the 4,000 ppm dosage sample provided the best performance, and it is selected for further analysis of its hydraulic properties in the prototype column.

Appendix C Estimating effective stress- void ratio equation for fine-grained soils using simple correlation relationships

The estimation of consolidation properties (compressibility and permeability relationships) using easily measured predictors for various types of fine-grained soils are studied in this thesis. The results from the prediction of $k-e$ relationship are presented in Chapter 4; whereas the prediction of the compressibility curve is discussed in this section.

Similar to the format of Chapter 4, all existing compressibility correlations collected from the literature and are summarized in Table B-1. Nagaraj and Murthy (1983), Nagaraj and Srinivasa Murthy (1986), Nagaraj et al. (1993), Sharma and Bora (2015), and Nagaraj et al. (1994), Morris et al. (2000), Carrier III et al. (1983) and Morris (2003) provide equations in which LL is the governing parameter, and the correlation is given in terms of a logarithmic relationship effective stress and void ratio.

Other equations incorporate the original water content through the use of LI: Carrier III et al. (1983) and re-evaluated by Carrier and Beckman (1984) for slurried mine wastes, proposed a power relationship between liquidity index, activity, and the effective stress. A similar relationship is later proposed by Morris et al. (2000) for mine tailings and by Sharma and Bora (2015) for fine-grained clay samples. Berilgen et al. (2006) proposed a stress-deformation relationship based on the equation presented initially by J.-C. Liu and Znidarčić (1991) correlating the effective stress-void ratio relationship to plasticity and liquidity indexes for dredged materials. A similar relationship is also proposed by Chandra Paul and Azam (2013) for fine-grained tailings using the plasticity index of the material.

	Correlation Relationship	Materials	Reference
(1)	$\frac{e}{e_L} = 1.099 - 0.2237 \log \sigma'$	Normally consolidated clays	Nagaraj and Murthy (1983)
(2)	$\frac{e}{e_L} = 1.22 - 0.2343 \log \sigma'$	Normally consolidated clays	Nagaraj and Srinivasa Murthy (1986)
(3)	$\frac{e}{e_L} = 1.25 - 0.28 \log \sigma'$	Normally consolidated clays	Nagaraj et al. (1993)
(4)	$\frac{e}{e_L} = 1.23 - 0.276 \log \sigma' + 0.041 \log \left(\frac{\sigma'}{\sigma} \right)$	Over-consolidated clays	Nagaraj et al. (1994)
(5)	$LI = 17.66 \sigma'^{-0.288} - 0.223$	Clayey & slurried mineral waste	Carrier III et al. (1983)
(6)	$LI' = \frac{LI}{0.963 + 0.808 (act)^{-1}}$ $LI' = 0.953 \left(\frac{\sigma'}{P_{atm}} \right)^{-0.143} - 0.610$	Remoulded Clays	Carrier and Beckman (1984)
(7)	$\frac{e}{e_L} = 1.549 - 0.3427 \log \sigma'$	Mine Tailings	Morris et al. (2000)
(8)	$LI = 2.409 \sigma'^{-0.423} + 0.299$		
(9)	$LI' = 1.562 \sigma'^{-0.198} - 0.165$		
(10)	$\frac{e}{e_L} = 2.478 \sigma'^{-0.112} - 0.802$	Dredged Materials	Morris (2003)

(11)	$e = A(\sigma' + Z)^B$ $A = 2.68 \exp(0.008PI)$ $B = (1 + e_0)(0.008 \ln(PI) - 0.054)$ $Z = (1 + e_0) \exp(1.97 - 3.91 \ln(LI))$	Dredged Materials	Berilgen et al. (2006)
(12)	$e = A\sigma^B$ $A = 0.065(PI + 21.5)$ $B = -0.004(PI + 22.8)$	Various fine-grained soils; including clays, dredged soils and oil sands tailings	Chandra Paul and Azam (2013)
(13)	$LI = 1.42 - 0.506 \log \sigma'$	Normally	Sharma and Bora
(14)	$\frac{e}{e_L} = 1.2315 - 0.2933 \log \sigma'$	consolidated clays	(2015)

Table C 1: Summary of correlation relationships for the effective stress-void ratio

Selecting the correct correlation between effective stress-void ratio is essential for the determination of consolidation behaviour of the materials. Especially for fine grained soils it's more difficult and challenging, as the material goes through large deformation, the final profiles can be greatly contrasting to the initial profiles. In order to foresee the long-term behaviour and making the appropriate selection on the design for storage and reclamation, determining the consolidation behaviour plays an important role.

Performance comparison of predictive models in Table B-1 are presented here for each types of fine-grained soils. Each method was tested against each class of soils or tailings, and the closest comparisons are shown in the following sections. Most of the results are presented in terms of the cumulative distribution function of the log of ratios between measured and predicted hydraulic conductivity data. The cumulative distribution plots demonstrated the probability of a variable to fall less than or equal to a given value. The

ratio of measured to predicted values is demonstrated in the horizontal line in logarithmic form and the probability of presented in the vertical line, which falls between 0 to 1. A perfect match would be a straight vertical line at 0 on the x-axis (indicating that the predicted values are equal to the measured data), methods that would provide a good fit on average would be centered around the same vertical line. Methods that replicate the trend well but not the absolute value would be relatively vertical but centred on a different value on the x-axis. Some data are presented in terms of measured versus predicted e or k to provide a better feel of the comparison.

C.1 Clays

The performance comparison for compressibility estimations for clays is presented in the following figure. The best performing equations are from Morris (2003) and Nagaraj et al. (1993); Nagaraj and Murthy (1983), Nagaraj and Srinivasa Murthy (1986), Nagaraj et al. (1994). The second relationship proposed by Sharma and Bora (2015) also provided relatively good performance; however, the data was more dispersed.

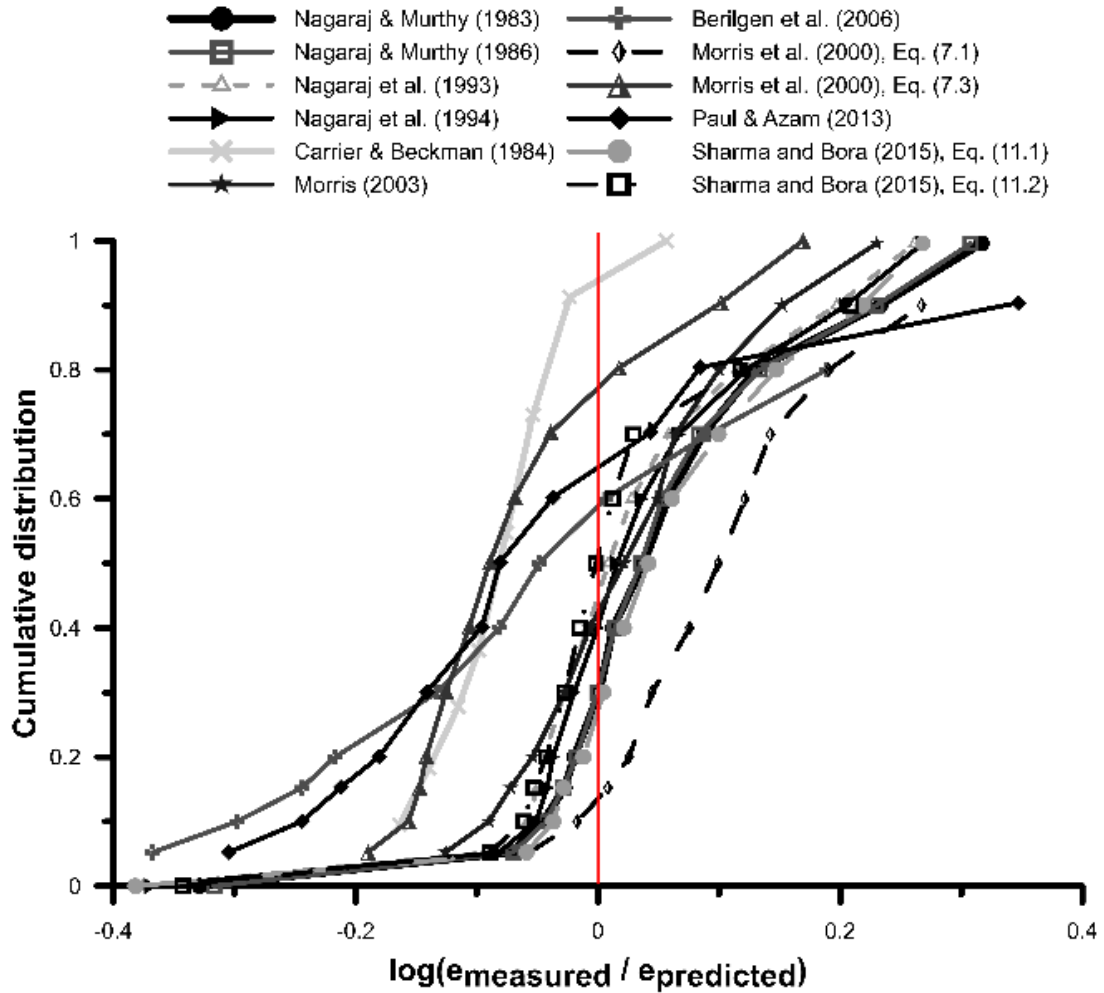


Figure C-1: Performance of compressibility equations for clayey soils

Using the experimental data, improved compressibility correlations were proposed for each type of soil by optimizing the fitting parameters of the successful methods. For clays, a modified form of Morris (2003), Equation 10, provided the best fit. The performance of the best-fitted regression model against the data sets is presented in Figure C-2. Note the modification is in the values of the exponent and the intercept of the original Morris (2003) equation.

Clays

$$\frac{e}{e_L} = 4.97\sigma^{1-0.062} - 2.927 \quad R^2 = 0.9074 \quad (15)$$

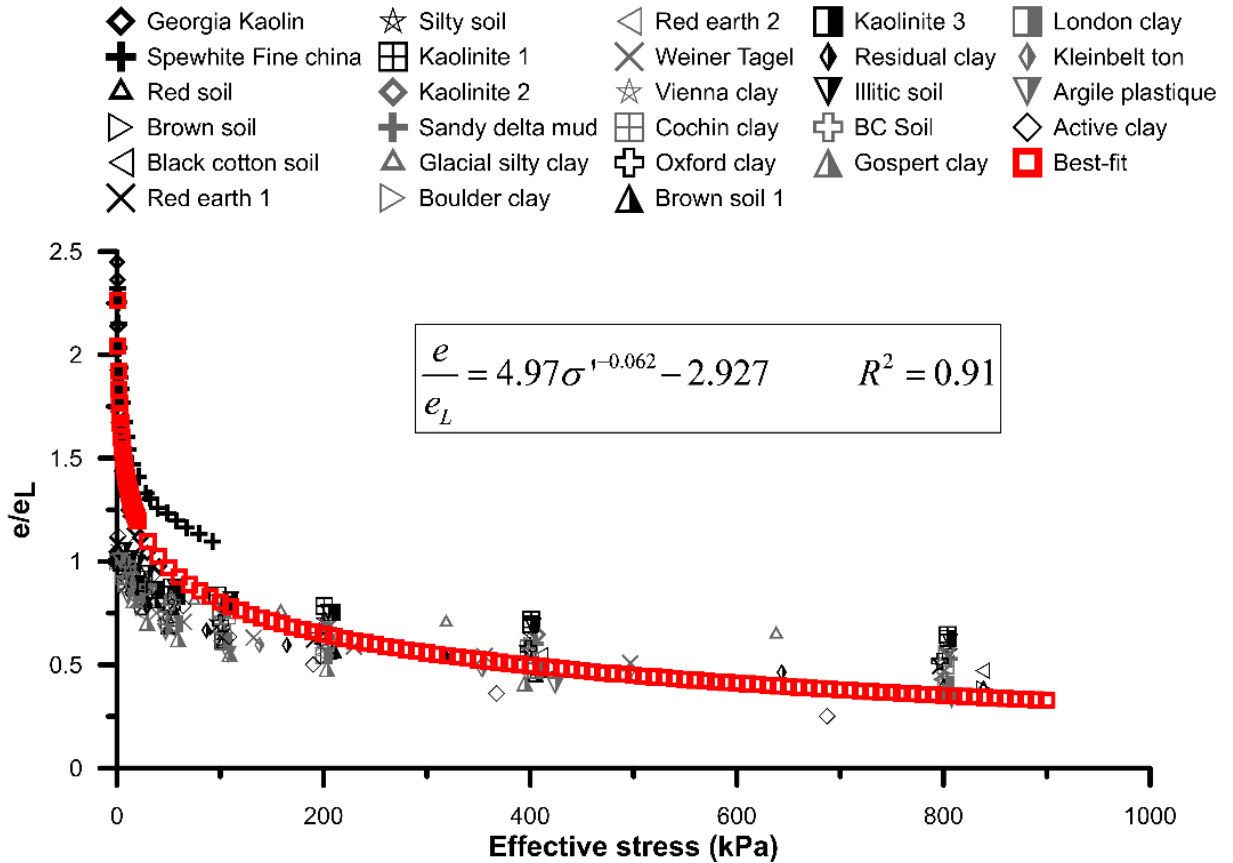


Figure C-2: Best-fit compressibility model optimized to clay data sets

C.2 Dredged Materials

The performance of the compressibility models for dredged materials, using 22 data sets collected from the literature, is shown in Figure C-3. Equations proposed by Nagaraj et al. (1993), Sharma and Bora (2015) and Carrier III et al. (1983) provided the best predictive capacity for estimating the compressibility of dredged soils. Unfortunately, most of the data sets acquired were missing the information of % finer than 2 μ m; therefore, for some of the methods using that predictor (such as Carrier and Beckman (1984) and Morris et al. (2000), the analyzed data were limited.

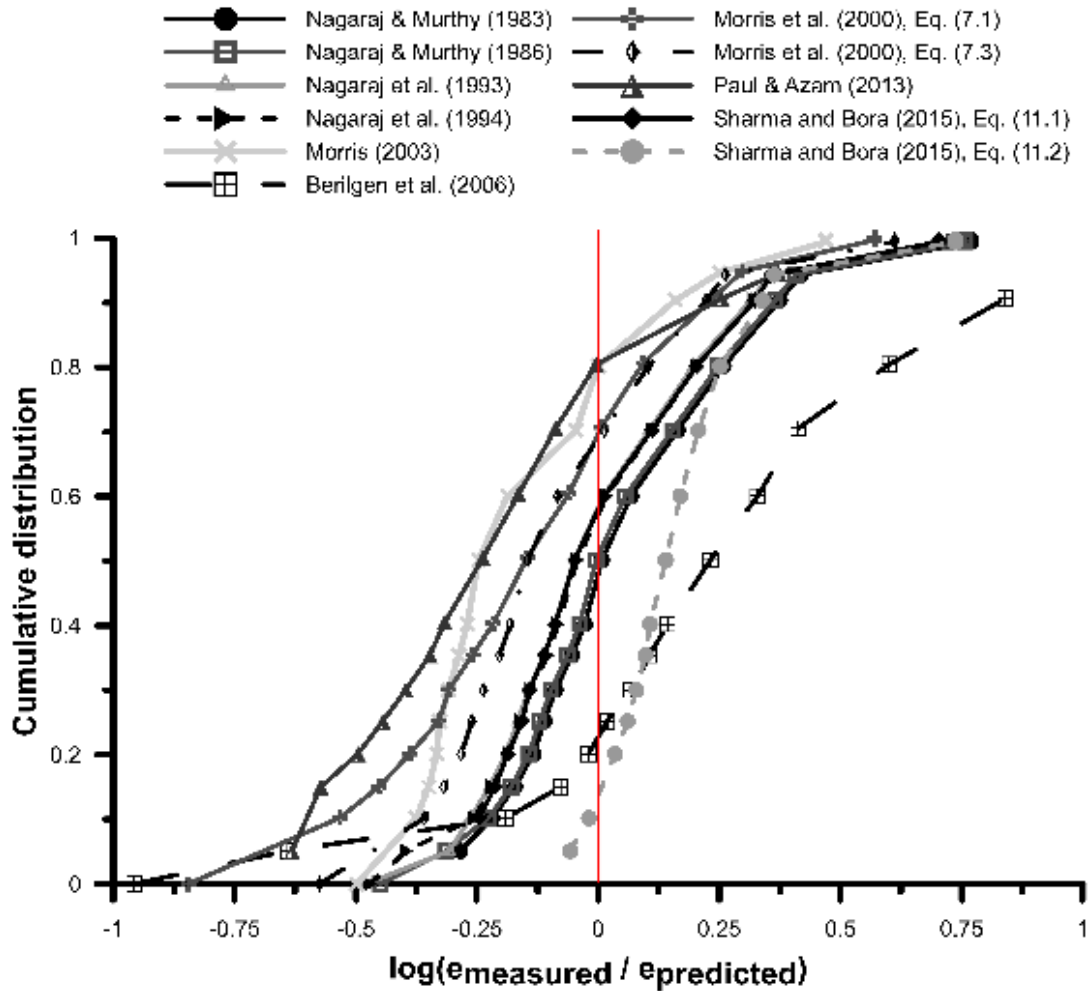


Figure C-3: Performance of the compressibility models for dredged soils

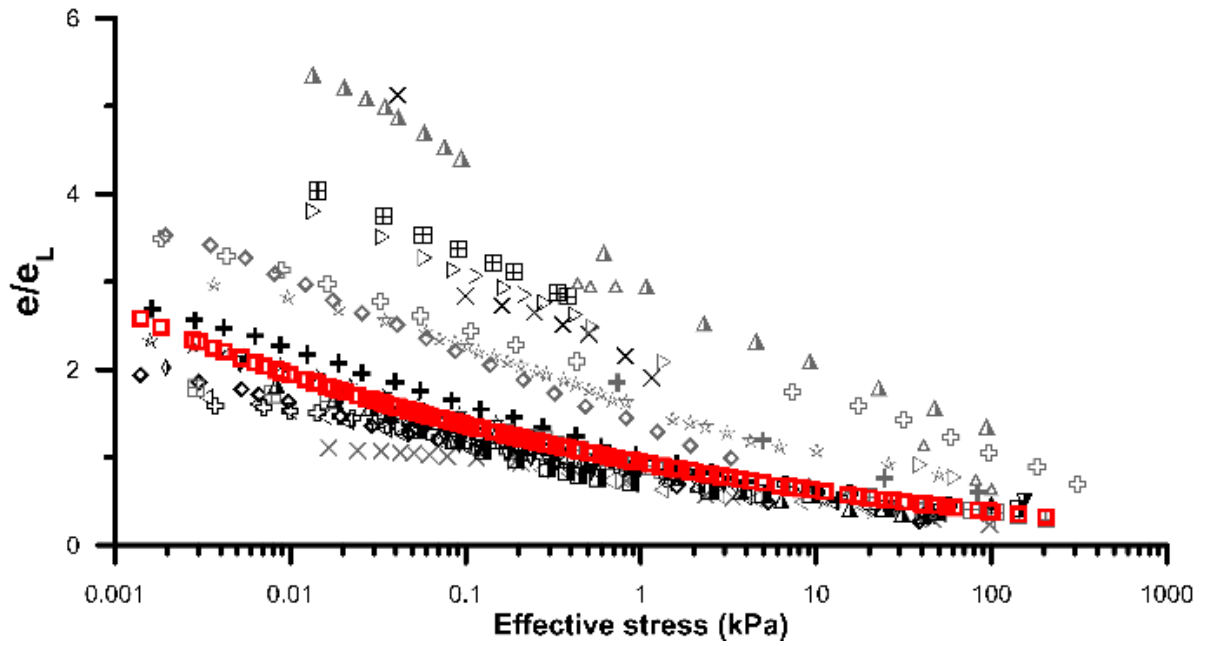
An improved model of Nagaraj et al. (1993) or Sharma and Bora (2015)'s equation are presented in Equations 13 and 14 to estimate effective stress-void ratio relationship. Similar to clayey soils, the void ratio at the liquid limit was utilized to estimate the compressibility of dredged soils. Also, the modified version of Carrier III et al. (1983)'s model using LI as it's correlator is presented in Equation 17. The comparison of the proposed model to estimate the ratio of void ratio to void ratio at the liquid limit for dredged soils is presented in Figure C-4.

Dredged Materials

$$\frac{e}{e_L} = 1.269\sigma'^{-0.1261} - 0.3276 \quad R^2 = 0.98 \quad (16)$$

$$LI = 2.089 - 1.05 \log \sigma' \quad R^2 = 0.99 \quad (17)$$

- | | | | | |
|------------------|---------------------|---------------------|-----------------|---------------|
| ◇ Lower Passaic | ☆ Red hook | ▷ Alibey green clay | ⊕ Craney Island | ▽ Duwamish |
| ⊕ Port Elizabeth | ⊞ Dutch kills | ◁ Kings Bay 1 | ▲ US Metals 2 | ⊕ Black rock |
| ▷ US Metals 1 | ◇ Port Authority | × Kings Bay 2 | ■ New Haven | ▲ Kings Bay 3 |
| ◁ Seguine Point | ⊕ Halic clay | ☆ Cape Canaveral | ◇ Stamford | □ Best-fit |
| × Earl Navy | △ Alibey black clay | ⊞ Drum Island | | |



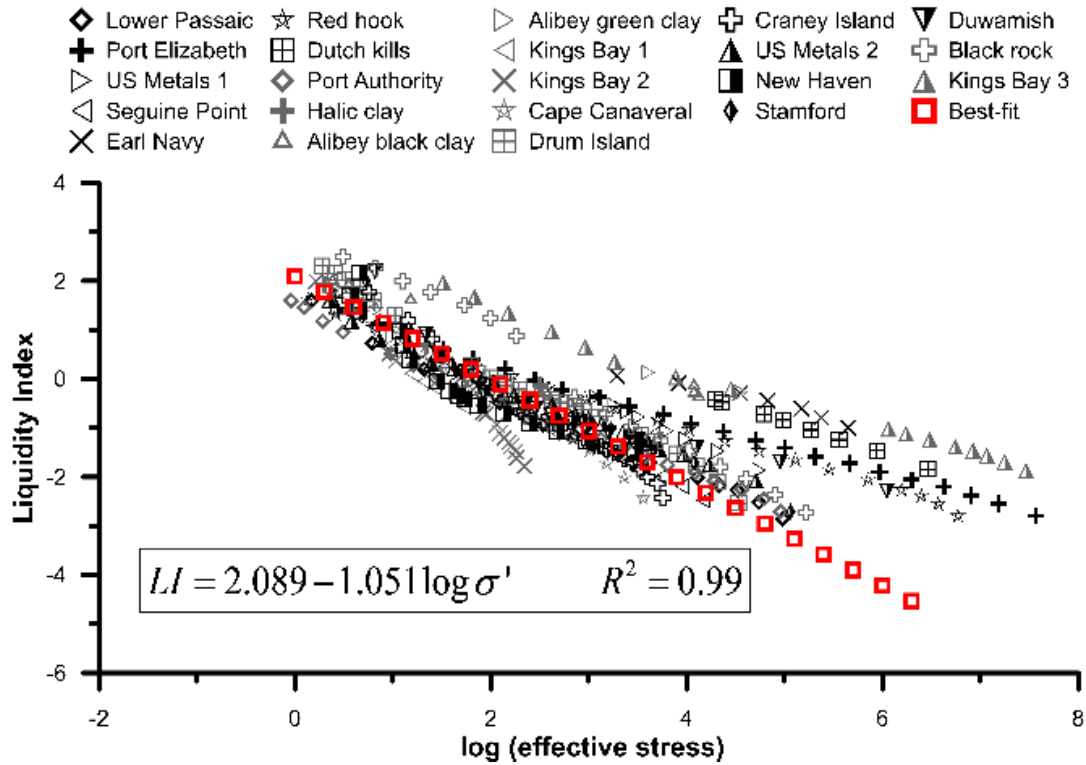


Figure C-4: Best-fit compressibility model optimized for dredged soil data sets

C.3 Oil Sands Tailings

The performance comparison for compressibility of oil sands tailings demonstrated that Morris (2003) and Berilgen et al. (2006) have the best predictive capacity compared to the other methods for both untreated and treated oil sands tailings samples respectively. The methods proposed by Carrier III et al. (1983) outlined the lower boundary for both types of tailings, and the methods provided good estimate trends include Chandra Paul and Azam (2013) and the second and the third equations proposed by Morris et al. (2000).

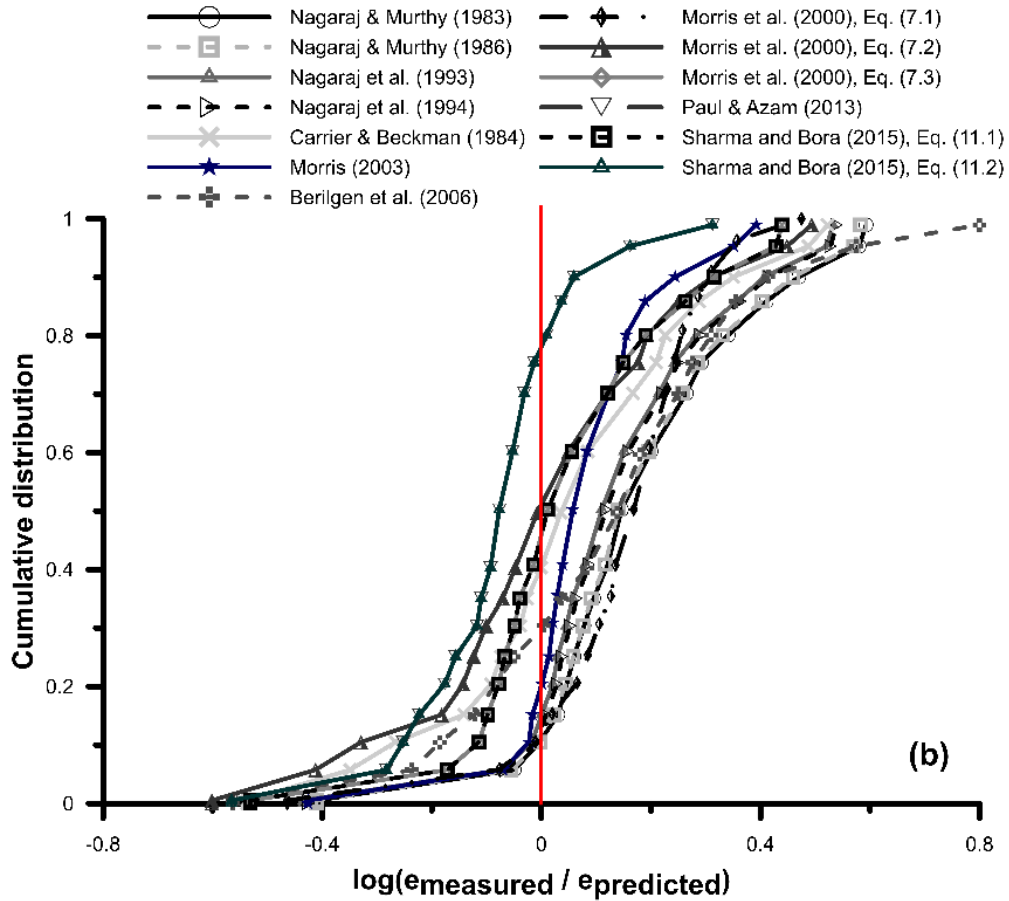


Figure C-5: Performance of compressibility equations for oil sands tailings

Similar to clayey soils, the model proposed by Morris (2003) provided the best predictive capacity, as mentioned. The modified equation based on that model is presented in Equation 18. Also, the application of the proposed model against the oil sands tailings data sets is presented in Figure C-6.

$$\begin{array}{l}
 \text{Oil} \quad \text{Sands} \quad \frac{e}{e_L} = 3.299\sigma^{-0.1601} - 0.8346 \quad R^2 = 0.97 \\
 \text{Tailings}
 \end{array} \quad (18)$$

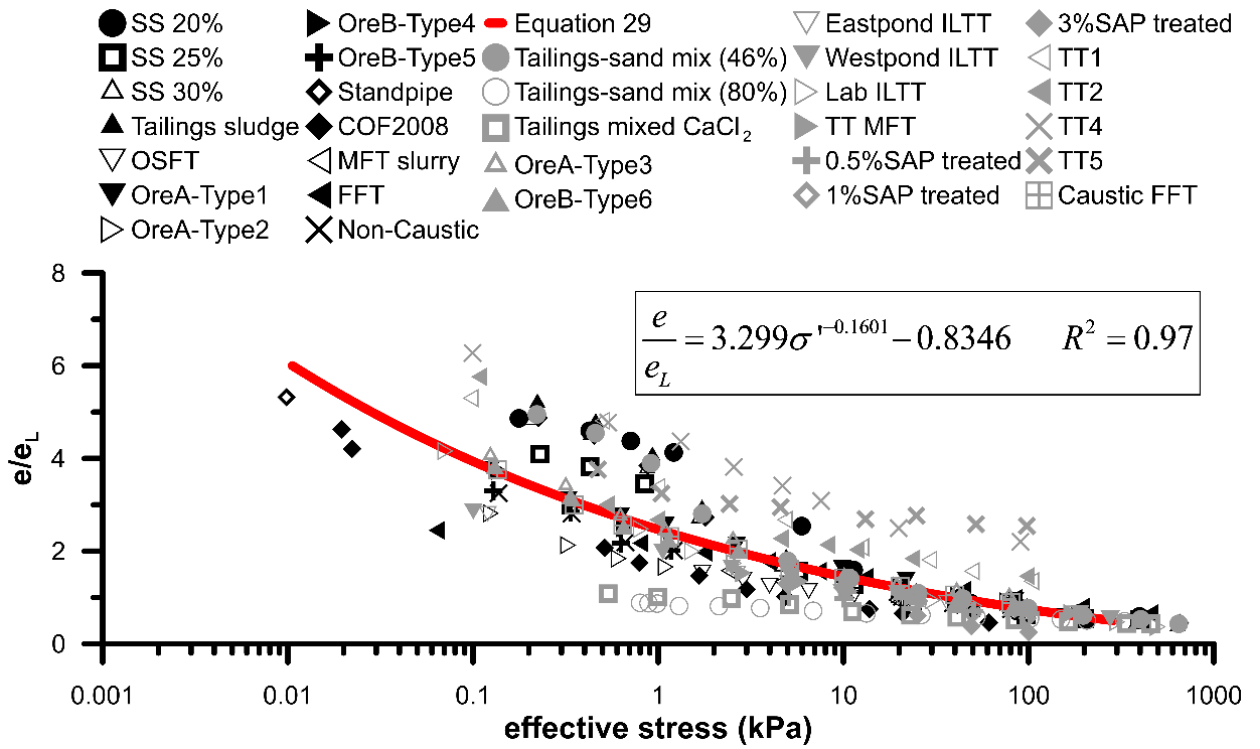


Figure C-6: Best-fit compressibility model optimized for oil sands tailings

Appendix D Arduino and MATLAB Scripts

This appendix contains the partial MATLAB script written for cumulative distribution analysis described in Chapter 4, and the Arduino Code written for the automation of linear actuator (presented in Chapter 5).

D.1 Cumulative Distribution Analysis – MATLAB Script

```
%read the data from the excel sheet
filename = 'probdist.xlsx';
sheet=1;
columnA = xlsread(filename,sheet,'A:A');columnB = xlsread(filename,sheet,'B:B');
columnC = xlsread(filename,sheet,'C:C');columnD = xlsread(filename,sheet,'D:D');

pd = makedist('Normal',0,1);
data1= cdf(pd,columnA);data2= cdf(pd,columnB);
data3= cdf(pd,columnC);data4= cdf(pd,columnD);

h =histogram(columnA,20,'DisplayStyle','stairs')
h1=cdfplot(columnA);
columnA_Xdata = h1.XData;
columnA_Ydata = h1.YData;
hold on;
h2=cdfplot(columnB);
columnB_Xdata = h2.XData;
columnB_Ydata = h2.YData;
hold on;
h3=cdfplot(columnC);
columnC_Xdata = h3.XData;
columnC_Ydata = h3.YData;
hold on;
h4=cdfplot(columnD);
columnD_Xdata = h4.XData;
columnD_Ydata = h4.YData;
hold on;

find mean and standard deviation
M1 = mean(columnA);S1 = std(columnA);
M2 = mean(columnB);S2 = std(columnB);
M3 = mean(columnC);S3 = std(columnC);
M4 = mean(columnD);S4 = std(columnD);
```

D.2 Automation System – Arduino Code

```

const int direct = 7;
const int power = 6;//assign relay INx pin to arduino pin

void setup() {

pinMode(direct, OUTPUT);//set relay as an output
pinMode(power, OUTPUT);//set relay as an output
}

void loop() {
  //going up
  digitalWrite(direct, LOW); //set the direction first
  delay(1000); //delay 1 second to make sure i activates t_total=1 s.

  //ready to move and read the first reading!

  //first position setup
  digitalWrite(power, HIGH);//power 12V source for 1.1 seconds t_total=2.2 seconds
  delay(1100);
  digitalWrite(power, LOW);
  delay(57900); //discontinue power for 57.9 seconds t_total=60 s.

  //second position
  digitalWrite(power, HIGH);//power 12V source for 1.1 seconds t_total=1.1 seconds
  delay(1100);
  digitalWrite(power, LOW);
  delay(58900); //discontinue power for 58.9 seconds t_total=60 s.

  //third position
  digitalWrite(power, HIGH);//power 12V source for 1.1 seconds t_total=1.1 seconds
  delay(1100);
  digitalWrite(power, LOW);
  delay(58900); //discontinue power for 58.9 seconds t_total=60 s.

  //fourth position
  digitalWrite(power, HIGH);//power 12V source for 1.1 seconds t_total=1.1 seconds
  delay(1100);
  digitalWrite(power, LOW);
  delay(58900); //discontinue power for 58.9 seconds t_total=60 s.

  //fifth position
  digitalWrite(power, HIGH);//power 12V source for 1.1 seconds t_total=1.1 seconds
  delay(1100);
  digitalWrite(power, LOW);
  delay(58900); //discontinue power for 58.9 seconds t_total=60 s.
}

```

```
//sixth position
digitalWrite(power, HIGH);//power 12V source for 1.1 seconds t_total=1.1 seconds
delay(1100);
digitalWrite(power, LOW);
delay(58900); //discontinue power for 58.9 seconds t_total=60 s.
```

```
//seventh position
digitalWrite(power, HIGH);//power 12V source for 1.1 seconds t_total=1.1 seconds
delay(1100);
digitalWrite(power, LOW);
delay(58900); //discontinue power for 58.9 seconds t_total=60 s.
```

```
//eight position
digitalWrite(power, HIGH);//power 12V source for 1.1 seconds t_total=1.1 seconds
delay(1100);
digitalWrite(power, LOW);
delay(58900); //discontinue power for 58.9 seconds t_total=60 s.
```

```
//ninth position
digitalWrite(power, HIGH);//power 12V source for 1.1 seconds t_total=1.1 seconds
delay(1100);
digitalWrite(power, LOW);
delay(58900); //discontinue power for 58.9 seconds t_total=60 s.
```

```
//change direction of the sensor - going down
digitalWrite(direct,HIGH); //turn the direction t_total=1 s.
delay(1000);
```

```
digitalWrite(power, HIGH);///power 12V source for 13 seconds t=13 seconds
//delay(10000);
delay(13000);
digitalWrite(power, LOW);///discontinue power for 46.0 s. t_final=60 s
//delay(46000);
//delay(646000);
delay(1246000);
```

Appendix E Calculation of k - e relationship from settlement curve for flocculated FFT at 800 ppm dosage

This technique has been developed by Shunchao Qi et al. (2020), and applied to one of the experiments conducted in this thesis. The k - e curve is presented in the form of $k = Me^P$. For the case of simulations of 1D consolidation in a column with one-way drainage, the authors discovered two important features of the predicted settlement curve.

1. The shape of the settlement curve is independent of M , but controlled by the P value, and
2. If P is fixed, changing M value only shifts the curve to left and right.

Total of 5 steps are followed to determine the M and P values. Step 1 is conducting at least 3 simulations with different P values. The same M value can be selected and even higher M values could be utilized to reduce the simulation time. Three simulations using different P values are presented below.

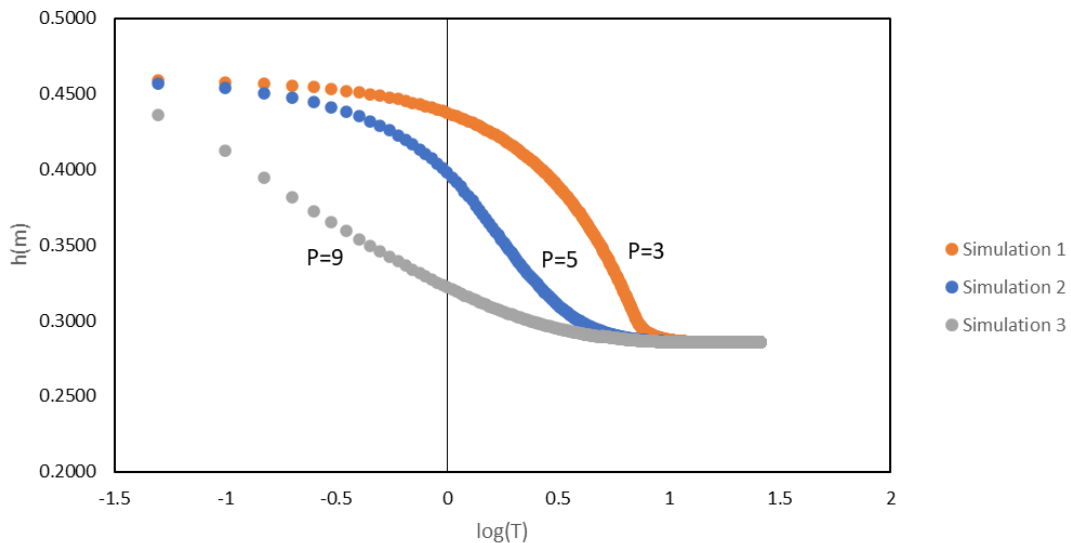


Figure E-1: Three simulations using three P values

At the second stage, select random 5 heights and note the corresponding $\log T$ values from each simulation. Using these values, the Var parameter can be calculated. For example, at a height of 0.4 m, the $\log T$ values are -1, 0 and 0.5 from predicted curves with P values 9,5 and 3.

$$Var = \frac{\sum_{i=1}^n (X_i - \bar{X})^2}{n}$$

$X_i = \log(T_i)$ at i^{th} selected height
 \bar{X} mean value of selected X_i

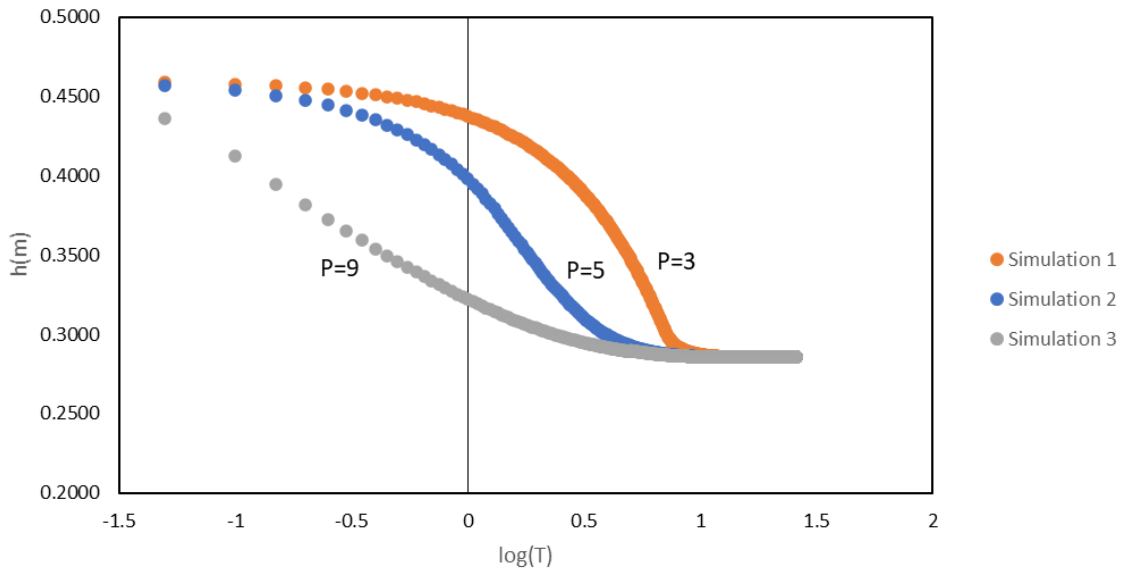


Figure E-2: Calculation of Var parameter

Once the Var value is calculated for each predicted settlement curve, plot P vs Var parameter to the equation on the slide and determine α , β and π values (Step 3) using the equation provided below.

$$Var = \frac{\sum_{i=1}^n (X_i - \bar{X})^2}{n}$$

$$Var = \alpha P^\beta + \pi$$

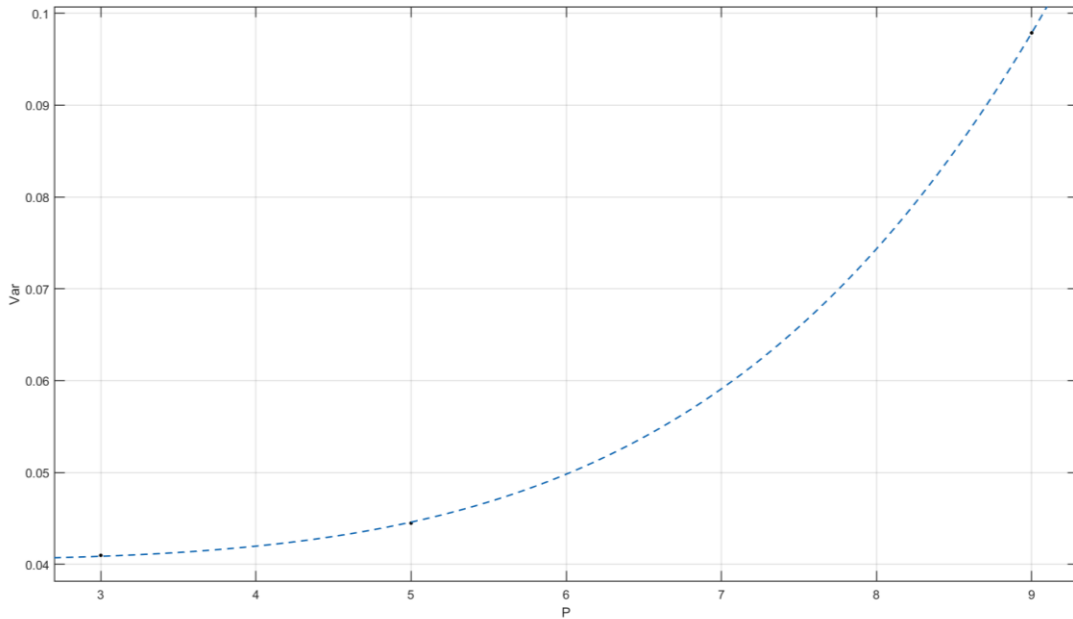


Figure E-3: P vs. Var for this case

Which are calculated as:

$$Var = 4 \times 10^{-7} P^{6.1} + 0.4$$

Once those parameters are determined, calculate Var value, the same method in step 2, but this time using the measured settlement curve instead of hypothetical simulations (Step 4).

The optimal P value is determined then, which is calculated as 9.92 for this test, run another simulation with these parameters and an arbitrary M_0 value (using the following equation, Step 5). A fairly small M_0 value is selected, because the P value was very high. Then calculate the average horizontal distances between the measured and the predicted

curve to calculate D value in the equation. The optimal M value can be back-calculated, which is calculated as 2×10^{-13} for this experiment.

$$\log\left(\frac{M}{M_o}\right) = \bar{D}$$

$$P = 9.92$$

$$M_o = 1 \times 10^{-13}$$

$$M = 2.05 \times 10^{-13}$$

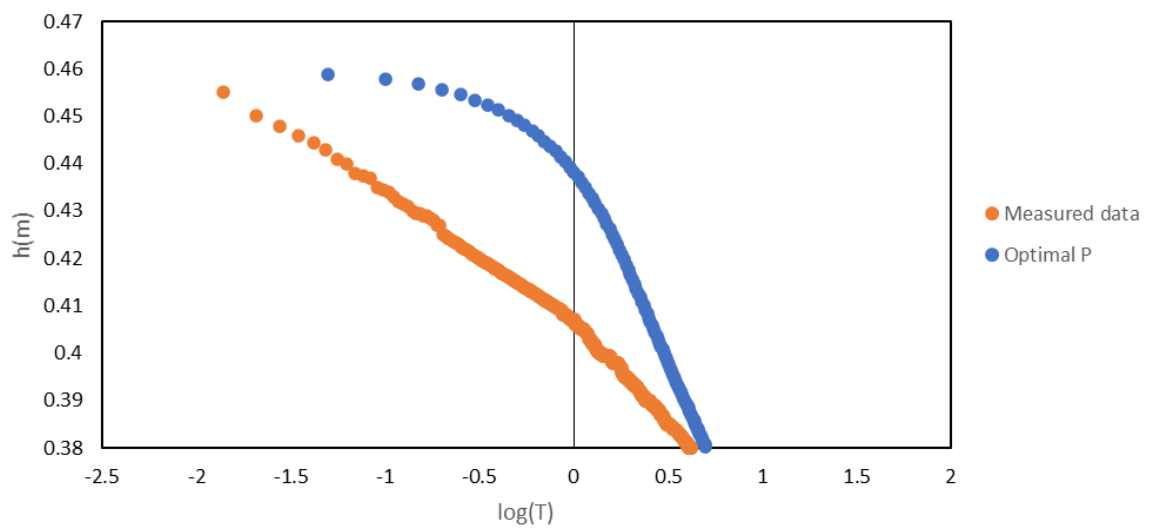


Figure E-4: Measured data points vs. predicted settlement curve with Optimal P value